

Bangor University

DOCTOR OF PHILOSOPHY

Understanding the Influence of Wood Species on Resin Modification and Property Enhancement in Resin modified Wood.

Kupfernagel, Carlo

Award date:
2024

Awarding institution:
Bangor University

[Link to publication](#)

General rights

Copyright and moral rights for the publications made accessible in the public portal are retained by the authors and/or other copyright owners and it is a condition of accessing publications that users recognise and abide by the legal requirements associated with these rights.

- Users may download and print one copy of any publication from the public portal for the purpose of private study or research.
- You may not further distribute the material or use it for any profit-making activity or commercial gain
- You may freely distribute the URL identifying the publication in the public portal ?

Take down policy

If you believe that this document breaches copyright please contact us providing details, and we will remove access to the work immediately and investigate your claim.

Download date: 03. May. 2024



PRIFYSGOL
BANGOR
UNIVERSITY

**Understanding the Influence of Wood Species on Resin
Modification and Property Enhancement in Resin
modified Wood.**

Carlo Kupfernagel

BioComposites Centre

Bangor University

Thesis submitted for the degree of Doctor of Philosophy

January 2024

Authors Declaration

I hereby declare that this thesis is the results of my own investigations, except where otherwise stated. All other sources are acknowledged by bibliographic references. This work has not previously been accepted in substance for any degree and is not being concurrently submitted in candidature for any degree unless, as agreed by the University, for approved dual awards.

I confirm that I am submitting the work with the agreement of my supervisors.

Yr wyf drwy hyn yn datgan mai canlyniad fy ymchwil fy hun yw'r thesis hwn, ac eithrio lle nodir yn wahanol. Caiff ffynonellau eraill eu cydnabod gan droednodiadau yn rhoi cyfeiriadau eglur. Nid yw sylwedd y gwaith hwn wedi cael ei dderbyn o'r blaen ar gyfer unrhyw radd, ac nid yw'n cael ei gyflwyno ar yr un pryd mewn ymgeisiaeth am unrhyw radd oni bai ei fod, fel y cytunwyd gan y Brifysgol, am gymwysterau deuol cymeradwy.

Acknowledgements

Firstly, I want to acknowledge my superb team of supervisors: Dr Morwenna Spear, Prof Graham Ormondroyd, and Dr Andrew Pitman. Without them, I couldn't have finished this thesis. Our endless conversations in online meetings (thanks to Covid) early during the PhD inspired me to read everything I could find about wood modification, especially during those monotonous lockdown days. And once the labs opened again after the pandemic, it was difficult to get me back out. They always gave me the freedom to pursue my own ideas and made sure that they provided me with the right keywords to keep me on track and held me back when necessary. Thanks to their knowledge, their passion for science, and their patience, I was able to learn more than I thought I'd ever do. I couldn't have wished for better supervisors.

Then, of course, I must thank my partner, Bianka, and our daughter, Rosa, for filling my life with so much joy. You have given me the strength to embark on this life-changing journey, and you never fail to cheer me up when life is tough. Words cannot express how grateful I am to have had you by my side during this time. I know that we will never forget our years in North Wales. Thank you for everything.

Funding was never an issue during this time, and I must thank Penny Dowdney and the KESS 2 team for this. Without their support on the admin side, I couldn't have finished this thesis either. Also, I would like to acknowledge them for organizing a great selection of doctoral workshops.

Jenny and Josh, I would like to thank you for our entertaining coffee breaks that helped to get through even the longest days in the office. A PhD is simply more fun when you have good friends in the office next door. On the same note, I am grateful to the rest of the team in the BioComposites Centre for providing a pleasant work environment, helping me out in the labs, and taking me to Friday lunches in the Pub!

But I also received much help from outside the BioComposites Centre. Dr Daniel Yelle from the Forest Products Laboratory collaborated with me on the cell wall dissolution and solution-state NMR work in this thesis. I would like to acknowledge him for taking the time to help me with the sample preparation and explaining the details of this fascinating method.

Mohammed Rahman, Dr Rosalie Cresswell, and Prof Steven Brown from the Physics department at Warwick University helped me substantially with the solid-state NMR work in this thesis. I want to thank them for running my samples and helping me with the interpretation of the solid-state NMR data. A sentence that stuck is 'Relaxation times are simple to measure but difficult to interpret'. I can't judge how simple it is to measure them, but they are certainly hard to interpret!

Also, a great thanks to all my friends in Bangor who made my weekends much more enjoyable and took me climbing everywhere across North Wales. I will miss those Snowdonia mountains!

Und zuletzt möchte ich mich von tiefsten Herzen bei meinen Eltern und meiner ganzen Familie bedanken, die mich während dieser Zeit zu selten gesehen haben. Trotzdem habe ich von euch nie etwas anderes als Unterstützung erfahren. Danke.

The Universe is under no obligation to make sense to you.

— Neil deGrasse Tyson

Abstract

Wood has played a crucial role in human history, evolving from its early use as a building material in pre-historic times to contemporary wooden skyscrapers. Its advantages are remarkable, offering a sustainable supply well into the future when managed responsibly.

Despite these benefits, the timber industry faces challenges, including conflicting interests among stakeholders and the impacts of global warming on forests. Coniferous forests, vital for softwood production, are under increasing pressure, with shifts in climate favouring more temperature-resistant species. This results in a growing demand met by a limited or decreasing wood supply, necessitating a significant increase in the service life of wood products.

To address the challenges in outdoor wood applications, where service life is often limited by biotic factors, conventional wood preservation methods that are based on metal salt solutions or creosote have been dominant in the past and present. However, these conventional preservatives are subject to increasingly strict regulation due to their fungicidal nature. Novel wood protection methods, categorised as wood modification, are gradually gaining ground. This includes thermally treated wood, acetylated wood, and wood treated with thermosetting resins like low-molecular-weight thermosetting phenol urea formaldehyde (PUF) resin, which is the focus of this thesis.

The research in this thesis, initiated by a collaboration with *Lignia Wood Company Ltd.* in 2020, originally aimed to explore aspects of upscaling their commercial wood modification process. However, a shift in focus occurred after the industrial partner went into administration in 2021, leading the research towards more fundamental aspects of wood modification.

The thesis comprises nine chapters, beginning with an introduction and literature review. It characterises wood species and the resin used in Chapters 3 and 4. Chapter 5 compares the modification of different wood species with PUF resin, revealing improved dimensional stability, although the efficiency varies based on factors like wood density and chemical composition. The primary focus in Chapters 5 and 6 was on the anti-swelling efficiency (ASE) as the main quality criterion for evaluating modified wood.

Chapter 6 explores process parameters in the modification process, highlighting the influence of curing time, resin concentration, and resin alkalinity in different wood species. It also emphasises the importance of resin diffusion into cell wall micropores during the drying stage, a concept that is further detailed in later chapters.

Chapters 7 and 8 delve into chemical interactions between wood and PUF resin, exploring curing reactions, retardation factors, and resin-wood interactions at different length scales. These chapters utilise techniques such as differential scanning calorimetry (DSC) and nuclear magnetic resonance (NMR) spectroscopy.

Finally, Chapter 9 provides a comprehensive summary, critically discussing the main results, proposing alternative experiments, and exploring potential future developments.

Contents

Authors Declaration	I
Acknowledgements.....	II
Abstract.....	IV
Contents.....	V
Table of Figures.....	XIII
Table of Tables	XXI
Abbreviations.....	XXIV
List of related Publications	XXVI
List of Hypotheses	XXVII
1. Introduction	1
2. Literature Review	3
2.1. Wood Properties	3
2.1.1. Macroscopic Properties	3
2.1.1.1. Growth of the Tree.....	3
2.1.1.2. Sapwood and Heartwood	3
2.1.1.3. Earlywood and Latewood	4
2.1.2. Microscopic Properties	5
2.1.2.1. Softwood Cells	5
2.1.2.2. Hardwood Cells	6
2.1.2.3. Pit Structure and Function.....	6
2.1.2.4. Structure of the Cell Wall	7
2.1.3. Chemical Composition and Nanostructure of Wood	8
2.1.3.1. Cellulose	8
2.1.3.2. Hemicellulose	9
2.1.3.3. Lignin	11
2.1.3.4. Nanostructure of Cell Wall Polymers	12
2.1.3.5. Micropores in the Cell Wall	14
2.2. Wood Modification.....	15
2.2.1. The Scope of Various Wood Modification Systems	15

2.2.2.	Impregnation Modification	16
2.2.2.1.	General Aspects	16
2.2.2.2.	Changes in Cell Wall Structure.....	18
2.2.2.3.	Property Improvement	18
2.2.2.4.	Commercialisation	20
2.2.3.	Acetylation	21
2.2.3.1.	General Aspects	21
2.2.3.2.	Changes in Cell Wall Structure.....	21
2.2.3.3.	Property Improvement	21
2.2.3.4.	Commercialisation	22
2.2.4.	Thermal Modification.....	23
2.2.4.1.	General Aspects	23
2.2.4.2.	Changes in Cell Wall Structure.....	23
2.2.4.3.	Property Improvement	24
2.2.4.4.	Commercialisation	24
2.3.	Phenol Urea Formaldehyde Resin	25
2.3.1.	Raw Materials and Production.....	25
2.3.2.	Laboratory Methods for Thermosetting Resins	27
2.3.3.	Chemical Reactions of Phenolic Resin.....	28
2.3.4.	Chemical Interactions between Phenolic Resin and Wood Polymers.....	30

3.	Chemical Characterisation of selected Softwood and Hardwood Species	32
3.1.	Introduction to Chapter 3	32
3.2.	Materials	33
3.2.1.	Wood Samples	33
3.3.	Methods	33
3.3.1.	FTIR-ATR Spectroscopy – Sample Collection	33
3.3.2.	FTIR-ATR Spectroscopy – Statistical Methods	34
3.3.3.	Isolation of Wood Constituents using Wet Chemistry	35
3.3.3.1.	Solvent Extraction with Toluene-Methanol-Acetone (4:1:1)	35
3.3.3.2.	Holocellulose	35
3.3.3.3.	Cellulose and Hemicellulose	35
3.3.3.4.	Klason Lignin	36
3.3.3.5.	Acid-Soluble Lignin	36
3.3.4.	Acid-Base Titrations of Hot-Water Wood-Extracts	36
3.3.5.	Acid-Base Titrations of Cold-Water Suspensions	37
3.3.6.	Solution-State NMR Spectroscopy – Wood Extractives Analysis	38
3.4.	Results and Discussion	39
3.4.1.	Wood and Wood Constituents studied by FTIR-ATR Spectroscopy	39
3.4.2.	Quantification of Wood Constituents using Wet Chemistry Methods	44
3.4.3.	The Alkaline Buffer Capacity of Wood Extracts and Suspensions	45
3.4.3.1.	Method Comparison of Hot-Water Extracts and Cold-Water Suspensions	45
3.4.3.2.	Long-Term Alkaline Buffering Capacity	46
3.4.3.3.	Species Comparison using Hot-Water Wood Extracts	47
3.4.4.	Wood Extractives Analysis using Solution-State NMR Spectroscopy	48
3.5.	Conclusions from Chapter 3	51

4.	Characterisation of Phenol Urea Formaldehyde Resin	53
4.1	Introduction to Chapter 4	53
4.2	Materials	55
4.2.1	Phenol Urea Formaldehyde Resin	55
4.3	Methods	55
4.3.1	Water Tolerance, pH value, Solids Content – Resin Quality Control	55
4.3.2	DSC – Sample Collection	56
4.3.3	DSC – Kissinger Method	56
4.3.4	FTIR-ATR Spectroscopy – Sample Collection	57
4.3.5	Solution-Sate NMR Spectroscopy – Resin Analysis	57
4.3.6	DVS – Hygric Properties of cured Resin	57
4.3.7	SEM-EDX – Imaging and Elemental Composition	58
4.4	Results and Discussion	58
4.4.1	The Curing Reaction of Resin studied by DSC	58
4.4.2	The Curing Reaction of Resin studied by FTIR-ATR Spectroscopy	61
4.4.3	Uncured and Partly Cured Resin studied by NMR Spectroscopy	64
4.4.4	The Hygric Properties of Cured Resin studied by DVS	66
4.4.5	The Elemental Composition of Cured Resin studied SEM-EDX	67
4.4.6	Resin cured in an open and closed System studied by SEM	68
4.5	Conclusions from Chapter 4	69

5.	Wood Modification with Phenol Urea Formaldehyde Resin: The Effect of Wood Species Selection	70
5.1.	Introduction to Chapter 5.....	70
5.2.	Materials.....	72
5.2.1.	Wood Samples and Resin.....	72
5.3.	Methods	72
5.3.1.	FTIR-ATR Spectroscopy – Sample Preparation and Statistics	72
5.3.2.	Light Microscopy – Sample Preparation	72
5.3.3.	Safranin Staining – Sample Preparation	73
5.3.4.	Light Microscopy – Image Acquisition	73
5.3.5.	SEM – Image Acquisition.....	73
5.3.6.	ASE Analysis – Resin Treatment of Small Blocks	73
5.3.7.	ASE Analysis – Cyclic Swelling and Drying of Small Blocks	74
5.3.8.	ASE Analysis – Soaking Solution Analysis.....	74
5.3.9.	ASE analysis – Calculations	75
5.3.10.	ASE analysis – Statistics.....	76
5.4.	Results and Discussion.....	77
5.4.1.	The Surface Chemistry of Modified and Unmodified Wood studied by FTIR-ATR Spectroscopy	77
5.4.2.	The ASE of various Wood Species after the same Resin Treatment	79
5.4.2.1.	Density, Liquid Resin Uptake, Bulking Coefficient and Microscopic Observations	79
5.4.2.2.	Swelling Coefficient	87
5.4.2.3.	Anti-Swelling Efficiency	88
5.4.2.4.	Swelling Coefficient in Water and Liquid Resin	89
5.4.2.5.	Total Swelling of Modified and Unmodified Wood	90
5.4.2.6.	Water Uptake during ASE Tests.....	91
5.4.2.7.	Mass Loss during ASE Tests	92
5.4.3.	The Soaking Solution from ASE Tests.....	93
5.4.3.1.	pH value, Solid Residue, and UV Absorbance at 272 nm	93
5.4.3.2.	Solution-State NMR.....	95
5.4.4.	Discussion of Factors that Influence the ASE of a Wood Species	97
5.5.	Conclusions from Chapter 5	99

6.	Wood Modification with Phenol Urea Formaldehyde Resin: The Influence of Processing Conditions	101
6.1.	Introduction to Chapter 6	101
6.2.	Materials	103
6.2.1.	Wood Samples and Resin	103
6.3.	Methods	103
6.3.1.	ASE Analysis – Resin Treatment of Small Blocks	103
6.3.2.	ASE Analysis – Design of Experiments	103
6.3.2.1.	Curing Time	103
6.3.2.2.	Resin Concentration	104
6.3.2.3.	Resin Alkalinity	104
6.3.2.4.	Resin Cell Wall Diffusion	104
6.3.3.	ASE Analysis – Statistics	106
6.3.4.	Multivariate Analysis of FTIR spectra – Predicting the WPG with a PLS model	106
6.4.	Results and Discussion	107
6.4.1.	The Effect of Curing Time	107
6.4.2.	The Effect of Resin Concentration	108
6.4.3.	Multivariate Analysis of FTIR Spectra – Predicting the WPG with a PLS Model	111
6.4.4.	The Effect of Resin Alkalinity	112
6.4.5.	The Effect of Cell Wall Diffusion	114
6.5.	Conclusions from Chapter 6	117

7.	Chemical Interactions between Wood and Phenol Urea Formaldehyde resin	118
7.1.	Introduction to Chapter 7.....	118
7.2.	Materials.....	120
7.2.1.	Wood Samples, Extractives, isolated Cell Wall Polymers, and Resin.....	120
7.3.	Methods	120
7.3.1.	DSC – Sample Preparation	120
7.3.2.	DSC – Sample Collection and Analysis	121
7.3.3.	Solution-State NMR – General Notes about the Sample Preparation	121
7.3.4.	Solution-State NMR – Ball Milling.....	121
7.3.5.	Solution-State NMR – Solubilisation of Wood in DMSO-d ₆ and Pyridine-d ₅	121
7.3.6.	Solution-State NMR – Spectra Acquisition Parameters	121
7.4.	Results and Discussion.....	122
7.4.1.	The Curing Reaction of Resin in the Presence of Wood and Wood Constituents studied by DSC	122
7.4.2.	Chemical Interactions between Wood and Resin studied by whole Cell Wall Dissolution in Combination with Solution-State NMR.....	126
7.4.2.1.	Modified and Unmodified Wood	126
7.4.2.2.	The Resin Fraction in Modified Wood	128
7.4.2.3.	Study of Covalent Bonds between Resin and Wood	129
7.5.	Conclusions from Chapter 7	131

8.	Cell Wall Diffusion in Phenol Urea Formaldehyde Resin Modified Wood	132
8.1.	Introduction to Chapter 8	132
8.2.	Materials	133
8.2.1.	Wood Samples and Resin	133
8.3.	Methods	134
8.3.1.	Resin Treatment and ASE Tests	134
8.3.2.	SEM – Imaging	134
8.3.3.	Thermoporosimetry – Isothermal Method	134
8.3.4.	Thermoporosimetry – Dynamic Method	136
8.3.5.	Solid-state NMR Spectroscopy and Relaxation Time Analysis	136
8.4.	Results and Discussion	137
8.4.1.	Resin Treatment and ASE Tests	137
8.4.2.	Scanning Electron Microscopy	138
8.4.3.	Thermoporosimetry	139
8.4.3.1.	Isothermal Method	139
8.4.3.2.	Dynamic Method	141
8.4.4.	Solid-State NMR	142
8.4.5.	Solid-State Nuclear Magnetic Relaxation Time Analysis	144
8.4.5.1.	T_1 (^1H) Relaxation Times	144
8.4.5.2.	$T_{1\rho}$ Relaxation Times	146
8.4.5.3.	T_1 (^{13}C) Relaxation Times	148
8.4.6.	Discussion of Solid-State NMR Results	149
8.5.	Conclusions from Chapter 8	152
9.	Discussion	154
9.1.	Significance of this Thesis	154
9.2.	Critical Review of Methodology	157
9.3.	Outlook and Possible Future Developments	161
	List of References	163
	Appendix	177

Table of Figures

Figure 2-1 The hierarchical structure of wood is characterized by a multi-level organisation. Timber is composed of various tissues, each consisting of different cell types, cell wall layers, and ultimately polymers. Image adopted from Chen et al. ¹⁹ (2020).	3
Figure 2-2 Three-dimensional microscopic structure of softwood (left) and hardwood (right) ²⁷ . Softwoods contain mainly tracheid cells and parenchyma cells, while hardwoods contain additional cell types such as vessels.	5
Figure 2-3 Cellulose repeat unit (cellobiose) is comprised of two glucopyranose units that are displaced at an angle of 180° to each other. Different ring positions are indicated by C1 – C6. Intramolecular hydrogen-bonds are indicated by dashed lines.	8
Figure 2-4 Glucomannan chemical structure in softwoods. The polymer backbone consists of alternating glucose and mannose units. Galactose side chains are introduced at the C6 position of mannose units. R = CH ₃ CO or H. ²⁷	10
Figure 2-5 Softwood xylan structure. The polymer backbone consists of β-(1-4) linked D-xylopyranose residues. Glucuronic acids residues are introduced at the C2 or C3 position. Furanose side chains may be linked to the backbone at C3. ²⁷	10
Figure 2-6 Lignin precursors in the biosynthesis of the tree are based on phenylpropane. Coumaryl, coniferyl, and sinapyl alcohol constitute the basis of lignin synthesis. Enzymatic polymerization yields the final lignin structure, where the precursors are linked by various forms of ether or methylene bridges.....	11
Figure 2-7 Spatial structure of the microfibril. Microfibrils consist of a crystalline core (domain 1), covered by amorphous cellulose (domain 2). Xylan and glucomannan (GGM) in 2-fold screw formation may bind to the same microfibril. Xylan that is bound to the hydrophilic microfibril surface converts cellulose domain 1 chains to a domain 2 conformation. Microfibrils are mediated by 3-fold xylan and glucomannan (matrix). Lignin occurs mainly in the periphery of the microfibril and interacts with both xylan and GGM. ³⁸	13
Figure 2-8 (a) Five commonly observed modes of action in different wood modification systems. (b) Summary of mechanisms active in various types of wood modification. Impregnation modification with low molecular weight PF resin uses the mechanisms lumen filling, cell wall filling, and degradation of the cell wall. Adapted from Ormondroyd et al. (2015).	15
Figure 2-9 Process steps in a typical impregnation modification with thermosetting resin. Unmodified wood is impregnated with an aqueous resin solution, which is followed by a drying and diffusion step, during which solvent water evaporated and resin monomers diffuse further to the cell wall, and finally cure in situ through the application of elevated temperatures ¹⁵	17
Figure 2-10 Acetylation is a well-established chemical wood modification. The reaction occurs between hydroxyl-groups in wood and acetic anhydride where R is -CH ₃ . The reaction with other anhydrides is possible but not commercially viable	21
Figure 2-11 Highway bridge certified for 65 t load. Construction is made of acetylated glue laminated timber. Sneek, Netherlands. ³¹⁸	22
Figure 2-12 Chemical structure of phenol urea formaldehyde resin. Self-condensation of phenolic units and co-condensation of phenolic and urea units occurs via methylene bridges in alkaline conditions.	26

Figure 2-13 (a) Formation of resonance stabilised phenolate ions from phenol under alkaline conditions, Nucleophilic addition of phenolate ion to formaldehyde in the ortho position (b) and para position (c). ¹⁹⁷	28
Figure 2-14 Crosslinking reaction of phenolic resin. (a) methylene bridge formation in free phenolic ring position, (b) methylene bridge formation via hydroxymethyl groups, (c) ether bridge formation in pH neutral conditions.	29
Figure 2-15 Theoretical framework of the catalytic self-condensation mechanism which is induced by the polarisation of the hydroxymethyl group and the phenoxy groups through hydrogen-bonding with wood carbohydrate	30
Figure 3-1 Example compounds that illustrate the common extractive types ²⁷ in wood and likely auto-hydrolysis products ²²⁶ . The extractive fraction in both hardwoods and softwoods is highly variable, comprising thousands of compounds. This illustration aims to highlight chemical features present in some of these groups.	33
Figure 3-2 FTIR-ATR spectrometer used in this thesis. A section of a small block is cut from the centre of the sample and presented directly to the surface of the ATR crystal.	34
Figure 3-3 Wood chemistry methods used to quantify the main cell wall polymers of eleven wood species. The milled wood powder was extracted with a solvent. The solvent was analysed in NMR test and the extractive-free wood was subjected to further testing in order to determine the holocellulose, alpha-cellulose and Klason-lignin contents. Each of these fractions was analysed by FTIR-ATR.	35
Figure 3-4 Sample preparation for the isolation of wood polymers, (a) wood solvent extractives after rotary evaporation, (b) a-cellulose in sinter crucible, (c) holocellulose preparation with NaClO ₂ in hot water bath, (d) Klason lignin preparation in 72% sulphuric acid, (e) Klason lignin preparation under reflux.....	36
Figure 3-5 Bruker 400 MHz Ultrashield+ NMR spectrometer used for solution-state NMR studies in this thesis.	38
Figure 3-6 FTIR-ATR spectra of isolated cell wall polymers (cellulose, hemicellulose, lignin) of beech wood and Radiata pine. Beech and Radiata pine serve as examples for typical hardwood and softwood species.	39
Figure 3-7 FTIR-ATR spectra of beech and Radiata pine as examples for typical hardwood and softwood species displayed between 1900 – 700 cm ⁻¹	39
Figure 3-8 HCA dendrogram for FTIR spectra in reflectance mode (left) and absorbance mode (right). Assignment of four main clusters (A - D) are made in the reflectance plot. The contents of each cluster are described below the dendrogram, and outliers are indicated by the striped area.	41
Figure 3-9 FTIR-ATR spectrum of tulipwood and Radiata pine, showing differences that are typical for hardwoods and softwoods.	42
Figure 3-10 Principal component analysis (PCA) outcome for eleven unmodified wood species. Score plots (a, c) illustrate wood species with similar chemical compositions positioned in close proximity to each other. Loading plots (b, d) indicate which wavenumber are responsible for variation in the dataset. PCA results from spectral data in reflectance mode (a, b) are different those obtained in absorbance mode (c, d).	43
Figure 3-11 (left) Effect of latency time on the pH of beech water extract and beech water suspension. The pH value of the suspension decreases over time, while pH of the extract remains on a constant level. (right) Effect of particle size on ABC in beech wood suspension during titration with NaOH. Suspensions with smaller particles display a higher ABC. 45	

Figure 3-12 Alkaline resin and acidic wood substrate interact over long time periods during the modification process. (a) Long-term alkaline buffering capacity of hot-water extract. (b-d) Long-term alkaline buffering behaviour of cold-water suspension with different particle sizes over the course of 24 days. Titrations were performed on the same sample every 3 - 4 days.	46
Figure 3-13 Comparing the hot water extracts of different wood species reveals some variability between species. Softwoods are shown on the left and hardwoods on the right.	47
Figure 3-14 Example of a ^1H - ^{13}C -Heteronuclear Single Quantum Coherence (HSQC) spectrum of SYP solvent extractives with an approximate assignment of the regions in the spectrum.	49
Figure 3-15 ^1H - ^{13}C -Heteronuclear Single Quantum Coherence (HSQC) spectra of SYP, lime, and sycamore extractives that were extracted with either organic solvent (top row) or water (bottom row).	50
Figure 4-1 Phenol Urea Formaldehyde (PUF) resin is a mixture of molecules with different properties. The chemical structure of main constituents in PUF resin including abbreviations used throughout this thesis are presented in the figure.	53
Figure 4-2 (a) Urea forms reactive intermediates (U_{HM}) but the self-condensation of hydroxymethylated urea (U_{HM}) with itself is restricted in alkaline environment. (b) Co-condensation with U_{HM} is kinetically favoured over self-condensation of PF_{HM} with itself.	54
Figure 4-3 The colour of the studied PUF resin changes with the pH value. PUF resin adjusted to different pH values by adding either acetic acid (99% w/w) or potassium hydroxide pellets. From left to right: pH 4.68, pH 6.3, pH 9.5 (default), pH 10.26.	55
Figure 4-4 (left) High-pressure crucible and open crucible next to a one penny coin for scale. (right) Wood section inside the pressurised crucible before it is sealed.	56
Figure 4-5 Example Kissinger plot. Three data points describe a linear regression line from which the activation energy (E_{A}) and the pre-exponential factor (Z) can be derived. The Kissinger plot is used for the analysis of DSC experiments in this thesis.	57
Figure 4-6 Example DSC scans of PUF resin in closed system. PUF resin with a solid content of 50% and pH 10.26. Heating rates of $1^\circ\text{C}/\text{min}$, $5^\circ\text{C}/\text{min}$, and $10^\circ\text{C}/\text{min}$ were used.	59
Figure 4-7 Example DSC scan of freeze dried PUF resin in an open system. The signals of heat flow and mass change are displayed in the same colour for the same sample. Heating rates of $1^\circ\text{C}/\text{min}$ (in black), $5^\circ\text{C}/\text{min}$ (in red), and $10^\circ\text{C}/\text{min}$ (in blue) were used.	60
Figure 4-8 FTIR-ATR spectrum of freeze-dried uncured PUF resin and cured PUF resin. Heat curing causes multiple changes in the resin chemistry, most prominently the depletion of the hydroxymethyl groups shown by the peak at 991 cm^{-1}	62
Figure 4-9 FTIR-ATR spectra of uncured PUF resin at different pH values. Resin was not freeze dried. The pH value affects various aspects of the resin structure.	63
Figure 4-10 FTIR-ATR spectrum of PUF resin cured at different pH values. The ratio of self-condensation and co-condensation is affected by the pH value.	63

Figure 4-11 FTIR-ATR spectra of PUF resin cured in an open system (atmospheric pressure) and in closed system (high pressure crucible). Resin cured in the closed systems is not fully crosslinked.	64
Figure 4-12 (a) ¹³ C-DEPTQ spectrum of uncured PUF resin dissolved in DMSO-d ₆ . Spectrum of partly cured PUF resin in DMSO-d ₆ after 30 min at 150°C (b) and after 60 min at 150°C (c).	65
Figure 4-13 ¹ H- ¹³ C-HSQC spectrum of partly cured (60 min at 150°C) PUF resin dissolved in DMSO-d ₆	66
Figure 4-14 DVS sorption isotherm of PUF resin cured for different durations at 150°C. The maximum moisture content decreases with longer curing time. Even fully cured PUF resin is slightly hygroscopic.....	66
Figure 4-15 Hysteresis between sorption and desorption for PUF resin cured for different durations at 150°C.	67
Figure 4-16 SEM-EDX analysis shows the elemental composition of the cured PUF resin. (a) SEM image showing the two point scan locations with arrows. (b) EDX spectrum of the cured resin showing the relative elemental composition. .	68
Figure 4-17 (a) SEM images of PUF resin cured at 150°C in an oven (open system). (b) PUF resin after a DSC run up to 250°C in high pressure crucibles (closed system). 1 – sharp edge of crushed resin structure, 2 – smooth surface of crushed resin structure, 3 – even surface of resin hemisphere that was pressed against the metal surface of the crucible during the DSC scan.	68
Figure 5-1 (a) Cone-shaped samples used for reflected light microscopy and SEM observation. The left sample was glued on larger block to facilitate microtome cutting. (b) Wood sections used for transmitted light microscopy. Top sections are stained with safranin.....	72
Figure 5-2 (a) Vacuum impregnation of small blocks with liquid PUF resin. Ballast keeps the samples submerged as the vacuum is drawn. (b) Modified wood samples during cyclic water storage.	74
Figure 5-3 Outcome of principal component analysis of FTIR-ATR spectra in reflectance mode showing the (a) score plot with four main clusters in each quadrant and the (b) loading score plot for PC1 and PC 2 on the right.....	77
Figure 5-4 Outcome of principal component analysis of FTIR-ATR spectra in absorbance mode showing the (a) score plot with four main clusters. Modified softwoods and hardwoods are poorly separated. (b)The loading plot for PC1 and PC 2 on the right.....	78
Figure 5-5 The carbonyl peak shifts to lower wavenumbers after PUF modification indicating changes in the hemicelluloses fraction. The difference in wavenumbers is displayed numerically.	79
Figure 5-6 Anatomical difference between low-density and high-density wood species. Low-density species contain a greater void volume and have thinner cell walls compared to high-density species. Example micrographs of (a) willow and (b) beech wood in the transverse section at 150x magnification. Detector for Back Scattered Electrons (BSE) was used.....	80
Figure 5-7 Relationship between liquid resin uptake (LU) and the oven dry unmodified density of different wood species that were impregnated with PUF resin in an identical treatment. A greater void volume in low-density species allows a higher liquid uptake compared to high-density species.	81
Figure 5-8 Resin deposits in the cell lumen can be observed in light and electron microscopy. (a-b) Show reflected light microscopy directly on the surface of small blocks. (c-f) Show transmitted light microscopy of sections prepared with a microtome. Prior to sectioning, these samples were embedded in methacrylate resin. (g-h) Show the longitudinal-	

tangential plane in SEM images. A detector for Back Scattered Electrons (BSE) was used. (a) poplar, (b) Radiata pine latewood, (c) beech, (d) Radiata pine, (e) lime, (f) poplar, (g) Radiata pine, (h) SYP. All samples are modified.	83
Figure 5-9 Additional micrographs of modified and unmodified wood. (a) Shows transmitted light microscopy image of modified tulipwood in the transverse section. (b-d) Show reflected light microscopy directly on the surface of small blocks. (b) modified Radiata pine, (c) unmodified Radiata pine, (d) unmodified poplar. (e-h) Show SEM images with BSE detector. (e) modified beech in TL plane, (f) modified willow in TL plane, (g) modified beech in transverse section, (h) modified sycamore in transverse section.	84
Figure 5-10 Safranin staining of thin wood sections can be used to measure the cell wall penetration of resin indirectly. Modified wood appears less intensely stained compared to unmodified wood. (a) Modified beech wood in the transverse section displays nearly no stain uptake in the earlywood (EW) and minimal uptake in the latewood (LW). (b) Unmodified beech in the transverse section displays a homogeneous magenta stain.	85
Figure 5-11 (a) Modified tulipwood in the transverse section. (b) Unmodified tulipwood in the transverse section.	86
Figure 5-12 Modified tulipwood in the transverse section. Magenta colour in the lumen indicates leaching of stain from the wood. Thus, cleaning the section in methylated spirit did not sufficiently remove excess safranin stain. (1) Area where cell walls are not stained. (2) Area where cell walls appear stained. (3) Ray cells that appear stained.	86
Figure 5-13 Comparison of water-induced swelling (S_{control}) and resin-induced swelling (S_{resin}) of modified groups. Species on the y-axis are arranged by decreasing density. S_{resin} is approximately equal to S_{control} for most species.	89
Figure 5-14 Comparison of total water-induced swelling (TS) between unmodified controls and modified wood during the first soak cycle. TS encompasses the swelling through water and cell wall bulking in modified wood. Species on the y-axis are arranged by decreasing density.	90
Figure 5-15 (a) Water Uptake in modified and unmodified control groups during the second soak cycle. If the weight of resin is included in the calculation, modified wood has a lower water uptake than unmodified wood. (b) Water uptake excluding the weight of resin in the calculation. If the resin weight is excluded, modified wood has a higher water uptake than unmodified wood. Species on the x-axis are arranged by increasing density.	91
Figure 5-16 (a) Water uptake over the course of three soak cycles in modified wood. Most species display an increasing water uptake. (b) Water uptake over course of three soak cycles in unmodified wood. Most species display a constant water uptake.	92
Figure 5-17 ^1H - ^{13}C -HSQC NMR spectra showing the partly cured PUF resin in DMSO- d_6 (left), the hot-water extract of beech wood in D_2O (centre), and the ASE soaking solution of modified beech wood in D_2O (right)	95
Figure 5-18 ^{13}C DEPTQ NMR spectra of ASE soaking solution beech and Radiata pine treated with different concentration of PUF resin in D_2O	96
Figure 5-19 Correlation between selected wood properties and the anti-swelling efficiency achieved after the treatment with PUF resin. Trends are displayed for softwoods and hardwoods. Top R^2 -value represents hardwoods and bottom R^2 -value represents softwoods. SYP is classified as an outlier in the sub-plot showing lignin content against ASE.	97
Figure 6-1 Cell wall diffusion mechanism of resin molecules as described by Tanaka et al. ⁸⁸⁻⁹¹ . PUF resin and water are equally distributed between cell wall and cell lumen after impregnation. Free water in lumen evaporates faster than	

bound water in the cell wall introducing a concentration gradient. PUF resin starts diffusion along this concentration gradient from the lumen to the cell wall.	102
Figure 6-2 Set up of cell wall diffusion experiments. Specimens were placed in a sample holder over saturated salt solution to adjust the RH in the sealed plastic container. Containers were moved between different temperatures.	105
Figure 6-3 The mass relative to oven dry state decreases with curing time at 150°C. The modified wood samples (left) show different rates depending on the wood species. (right) Pure PUF resin shows a higher loss in relative mass compared to unmodified wood.	108
Figure 6-4 A potential general relationship may exist between the performance of timber (e.g., BU, Smod1, Smod2) and resin concentration. The findings in this chapter indicate that various wood species exhibit distinct optimum concentrations, beyond which properties do not further improve and instead deteriorate. This optimum concentration might be linked to the density of a wood species and the saturation point of the cell wall.	110
Figure 6-5 The gravimetric water uptake in the second soak cycle of ASE tests. The water uptake decreases with a higher resin concentration in all samples.	111
Figure 6-6 Partial least square (PLS) model that predicts the WPG from the FTIR-ATR spectra of Radiata pine and beech wood with high accuracy. (a) and (c) show the comparison of predicted and gravimetrically measured WPG values. (b) and (d) show the spectra of corresponding training sets at different resin concentrations.	112
Figure 6-7 The statistical effect of four investigated factors (RH_{diff} , RH_{dry} , $time_{diff}$, and T_{diff}) on the results from ASE tests (BU, S_{mod1} , and S_{mod2}). The apparent effect on the WPG is included to show how much each factor might be influenced by differences in the WPG between test groups.	116
Figure 7-1 High-pressure crucible next to a one penny coin and wood section inside the pressurised crucible before it is sealed.	120
Figure 7-2 Sample preparation for solution-state NMR. (a) Ball-milled wood powder (approximately 30 mg) is filled in 5 mm NMR tube. (b) Solvent is added to the tube resulting in an inhomogeneous gel. (c) Gel is homogeneous after mechanical mixing and sonication.	122
Figure 7-3 (a) Thermogram of PUF resin mixed with either cellulose, lignin, or holocellulose showing heat flow against sample temperature. (b) Deconvoluted thermogram shows a new signal in resin mixed with holocellulose at 208°C. The cell wall polymers were isolated from tulipwood. The heating rate was 20°C/min.	125
Figure 7-4 1H - ^{13}C -HSQC NMR spectrum of (a) modified lime and (b) poplar wood with the assignments of chemical structures. (c) Common structures in lignin. (d) Common structures in PUF resin.	127
Figure 7-5 Partial 1H - ^{13}C HSQC NMR spectrum of partly cured PUF resin, modified lime, and modified poplar in the methylene bridge region. Structures PUF _A and PUF _B indicate novel methylene bridges that were not previously observed in the pure PUF resin. PUF _A and PUF _B might correspond to methylene bridges of resin interacting closely with the wood polymer surface.	129
Figure 7-6 Partial ^{13}C DEPTQ NMR spectrum of modified and unmodified lime and poplar wood in the ester bond region of the spectrum. No novel ester bonds could be detected.	130

Figure 8-1 DSC crucibles used for thermoporosimetry next to a one penny coin. Water-soaked solid wood samples were sealed in the crucible using sealing tool.135

Figure 8-2 Relative mass (a) and volume (b) throughout the diffusion and drying stages. The relative mass refers to the cured state and can easily be converted to the moisture content. The relative volume refers to the oven dry unmodified state to better illustrate the initial similarity after impregnation and how both groups separate over the course of the process. The x-axis indicates the day (1 – 7) on which volume and mass were measured.138

Figure 8-3 Scanning electron microscopy images of Wood A and B in different stages of the modification process. Views are on the tangential-longitudinal plane. Sections were prepared using a dry cut to avoid leaching of resin which might have occurred if samples were softened in water in a wet cut.138

Figure 8-4 Micropore size distribution determined in DSC scans for unmodified controls, cured wood A, and cured wood B. Error bars indicate standard deviation of three replicates. D is the diameter of micropores assuming a cylindrical shape. Micropores with a diameter larger than 400 nm are shown on a separate axis.....140

Figure 8-5 ^1H (500 MHz) ^{13}C CP MAS (12.5kHz) NMR spectra of unmodified tulipwood and pure heat cured PUF resin with peak assignments. AC indicates O – acetyl group in hemicellulose, C1 to C6 indicate cellulose ring positions in domain 1 (D1) or 2 (D2), Ar indicates aromatic ring carbons, Ar-Ph indicates phenoxy carbons, o-p and p-p indicate methylene bridges in ortho-para and para-para constellation, Ar-CH₂-N indicates methylene bridges of co-condensed urea and phenol, Ur indicates the urea carbonyl signal. The number of co-added transients for each experiment ranged from 812 to 1024.142

Figure 8-6 ^1H (500 MHz) ^{13}C CP MAS (12.5kHz) (a) NMR spectra untreated control and modified Wood A and B before and after heat cure. (a) comparison of uncured and cured Wood A and Wood B. Dashed lines indicate spectra of resin impregnated but uncured samples. Plain lines represent spectra of heat cured wood samples. (b) close-up of the C4 signal which is divided in a C4^{D1} (89 ppm) and C4^{D2} signal (84 ppm), (c) close-up of the C2, C3, C5 signal, (d) close-up of the C6 signal which is divided in a C6^{D1} (66 ppm) and C6^{D2} (62 ppm) signal, The number of co-added transients for each experiment ranged from 812 to 1024.....143

Figure 8-7 ^1H (500 MHz) T_{1ρ} of unmodified control, uncured, and cured samples of Wood A and B. Each sub-plot shows T_{1ρ} for the resolved ^{13}C peaks in the ^{13}C CP MAS NMR spectrum (see Figure 8-5). The unmodified control was tested at two moisture contents to account for the effect of water in the cell wall. All uncured samples were tested at ambient condition and all cured samples were tested at dry conditions. The chemical shift at 21 ppm represents the hemicellulose methyl acetate group, 57 ppm represents the lignin methoxy group, shifts between 106 – 65 ppm represents holocellulose, and chemical shifts between 161 – 130 ppm represent PUF resin relaxations. Note that for illustration reasons, the lignin signals of unmodified wood at 136 ppm and 153 ppm are included in the panels 130 ppm and 161 ppm, which are the prominent signal in modified wood.....146

Figure 8-8 In the hydrated state, the microfibril consists of cellulose surrounded by a matrix of hemicellulose and lignin, with water molecules tightly bound at the cellulose-xylan interface. Dehydration causes matrix collapse, leading to size shrinkage and closer proximity of lignin to cellulose. Upon rehydration, the microfibril expands, but certain changes persist: the xylan-cellulose interface remains unrehydrated, some cellulose retains a non-domain 2 conformation, a

fraction of galactoglucomannan (GGM) molecules becomes more mobile, and arabinose side chains show increased order. Image from Cresswell ⁴⁰ et al. (2021).	147
Figure 8-9 ¹³ C (125 MHz) T ₁ (¹³ C) of unmodified control, uncured, and cured samples of Wood A and B. Each sub-plot shows T ₁ (¹³ C) for the resolved ¹³ C peak in the ¹³ C CP MAS NMR spectrum (see Fig. 3). The unmodified control was tested at two moisture contents to account for the effect of water in the cell wall. All uncured samples were tested at ambient condition and all cured samples were tested at dry conditions. The chemical shift at 57 ppm represents the lignin methoxy group, chemical shifts between 62 ppm and 75 ppm represent holocellulose. Chemical shifts between 160 – 105 ppm did not give credible results and are therefore not included. Missing values are indicated by a X-symbol...	148
Figure 8-10 (a) The microfibril in different stages of the resin treatment. In the dry unmodified state, the microfibril and microfibrils are illustrated according to recent literature ^{38,40} . (b) Upon resin impregnation, both water and resin molecules create micropore spaces between the microfibrils. One fraction of the water is close contact with the microfibril surface, while another fraction is not closely associated with it. These water populations have been called NFBW and FBW in Chapter 8.4.3. Similarly, it is proposed that resin occurs in at least two distinct populations. Resin in direct contact with the microfibril disturbs hydrogen-bonding between water and cellulose causing T ₁ (¹ H) to increase and the NFBW content to decrease. The disruption of hydrogen-bonding at the microfibril interface might cause some cellulose chains to change from domain 1 to domain 2. The other fraction of resin located in the micropores is responsible for micropore blocking. Resin in micropores is more closely associated with matrix hemicellulose and lignin. (c) After heat curing, the resin induces a cell wall bulking effect.	150
Figure 8-11 The main difference between Wood A and Wood B could be the relative content of both resin populations, where Wood A contain more resin that is in direct contact with the microfibril, and Wood B contains more resin in micropores that is more associated with matrix hemicelluloses and lignin. Atmospheric conditions applied to Wood A have promoted the diffusion to the microfibril surface and subsequent curing in this location. Conditions applied to Wood B have potentially favoured resin agglomerations in the micropores.	151

Table of Tables

Table 2-1 The wood cell wall is comprised of distinct layers with varying properties and chemical composition. Selected properties of these layers are shown. MFA – Microfibril angle, MF – microfibril content, PW – Primary cell wall, SW – Secondary cell wall, SW1, SW2, SW3 – sub-layers within the secondary cell wall. ^{20,27,28}	8
Table 2-2 Frequent types of linkages in lignin and their percentages in hardwoods and softwoods.....	12
Table 3-1 Assignment of FTIR absorption bands from the literature. Cell wall polymers are indicated in bold script i.p. – in plane vibration, o.o.p. – out of plane vibration.	40
Table 3-2 Chemical composition of observed wood species determined by wet chemistry methods. Cluster refers to HCA classification in Figure 3-8. ExtrS - solvent extractive content in 4:1:1 solution. ExtrW - hot water extractives content. α -C - alpha-cellulose fraction. He-C - hemicellulose fraction. KL - Klason lignin fraction. ASL - acid soluble lignin fraction.	44
Table 3-3 The initial pH value of the hot water extracts in different species and the alkaline buffer capacity per gram of wood as well as per batch of 10 treated wood samples.....	48
Table 3-4 Grouping of eleven wood species according to hierarchical cluster analysis (HCA) of FTIR-ATR spectra and general properties that can be assigned to timbers in these clusters.	52
Table 4-1 Kinetic properties of the PUF-curing reaction in high pressure crucibles at different pH value and solids content calculated using the methods of Kissinger and Arrhenius.	59
Table 4-2 Kinetic properties of the PUF-curing reaction in open pan calculated using the Kissinger and Arrhenius methods.	61
Table 4-3 Assignment of wavenumbers in PUF resin according to literature. i.p. – in plane vibration, o.o.p. – out of plane vibration.....	62
Table 5-1 A summary of ASE studies comparing different timbers modified with thermosetting resins: s.c. - solids content of resin. MW - molecular weight. WPG – weight percentage gain. BU – bulking coefficient.....	71
Table 5-2 Average values for modified test groups. ρ_{control} – oven dry density before modification, ρ_{mod} – oven dry density after modification, LU – liquid resin uptake before curing, WPG – weigh percentage gain after curing, BU – bulking coefficient, S_{control} – swelling coefficient of unmodified wood, S_{mod} – swelling coefficient post-modification. Both S_{control} and S_{modified} refer to the first swelling cycle. ASE 1 – anti-swelling efficiency during the first soaking cycle, ASE 2 – anti-swelling efficiency during the second soaking cycle. Standard deviations are in parenthesis.	80
Table 5-3 Total mass loss (ML_{total}) in % over the course of the ASE experiment. Average values of ten. Standard deviation in parenthesis.....	93
Table 5-4 pH value of the ASE soaking solution in modified and unmodified control groups over the course of three soak cycles. Missing values are indicated by a hyphen.	93
Table 5-5 Solid residue of the ASE soaking solution in modified and unmodified control groups over the course of three soak cycles. Missing values are indicated by a hyphen.....	94
Table 5-6 UV absorbance at 272 nm of the ASE soaking solution in modified and unmodified control groups over the course of three soak cycles. Missing values are indicated by a hyphen.	95

Table 6-1 Half-factorial experiment plan used to investigate the effect of cell wall diffusion in ASE test. The control group was modified according to the standard procedure in Chapter 5.3.6 without a separate diffusion step.	105
Table 6-2 Average values for test groups treated with 20% resin concentration and cured for 8 h, 24 WPG – weigh percentage gain after curing, BU – bulking coefficient. Standard deviations are in parenthesis.	107
Table 6-3 Average values for test groups modified at the resin concentrations 20%, 30%, 40%. ρ_{control} – oven dry density before modification, ρ_{mod} – oven dry density after modification, LU – liquid resin uptake before curing, WPG – weigh percentage gain after curing, BU – bulking coefficient, $S_{\text{mod}1}$ – swelling coefficient post-modification after first soak cycle, $S_{\text{mod}2}$ – swelling coefficient post-modification after second soak cycle. Standard deviations are in parenthesis.....	109
Table 6-4 Average values for test groups modified at the resin pH 9.16, pH 9.45, pH 9.87. ρ_{control} – oven dry density before modification, ρ_{mod} – oven dry density after modification, LU – liquid resin uptake before curing, WPG – weigh percentage gain after curing, BU – bulking coefficient, $S_{\text{mod}1}$ – swelling coefficient post-modification after first soak cycle, $S_{\text{mod}2}$ – swelling coefficient post-modification after second soak cycle. ML_{total} – total mass loss over three cycles of water soaking. Standard deviations are in parenthesis.....	113
Table 6-5 Process conditions used and average values for test groups modified with different drying schedules in a half-factorial design to study cell wall diffusion. RH_{diff} – relative humidity in the separate diffusion step, RH_{dry} – relative humidity in the drying step at 50°C, t – time of the separate diffusion step, T_{diff} – Temperature in the separate diffusion step, ρ_{control} – oven dry density before modification, ρ_{mod} – oven dry density after modification, LU – liquid resin uptake before curing, WPG – weigh percentage gain after curing, BU – bulking coefficient, $S_{\text{mod}1}$ – swelling coefficient post-modification after first soak cycle, $S_{\text{mod}2}$ – swelling coefficient post-modification after second soak cycle. Standard deviations are in parenthesis.	114
Table 7-1 Review of possible chemical interactions between phenol urea formaldehyde resin and wood.....	119
Table 7-2 Kinetic parameters determined in differential scanning calorimetry showing the effect of the presence of solid wood on the curing reaction. The WPG varied across species due differences in the liquid uptake during impregnation.	123
Table 7-3 Kinetic parameters determined in differential scanning calorimetry showing the effect of water extractives (ExtrW) and solvent extractives (ExtrS) on the curing reaction. Results for pure resin are included for better comparison (see chapter 4).	123
Table 7-4 Kinetic parameter determined in differential scanning calorimetry for isolated cell wall polymers mixed with PUF resin. The pH value in the table refers to a suspension of the cell wall polymer in water.	124
Table 7-5 Integrated peak areas measured in 1H-13C HSQC NMR spectrum. Values refer to average of two replicates. Values are normalised to lignin methoxy signal at 56 ppm.	128
Table 7-6 The peak locations of resin specific signals in pure resin and modified wood. Conformational effects in modified wood might change the chemical shift by 1 – 1.5 ppm.....	129
Table 8-1 The effect of different diffusion and drying conditions on the performance of Wood A and Wood B in ASE tests during the 1 st cycle water soaking. Standard deviation in parenthesis.....	137

Table 8-2 Average values of water ratio (WR), non-freezing bound water (NFBW), freezing bound water (FBW), total cell wall water (TCW), bulk water (BW), and micropore blocking efficiency (MBE) determined by the isothermal DSC method. Standard deviation in parenthesis.	140
Table 8-3 Average values of water ratio (WR), non-freezing bound water (NFBW), freezing bound water (FBW), total cell wall water (TCW), bulk water (BW), and micropore blocking efficiency (MBE) determined by the dynamic DSC method using the heating rates 1°C/min, 5°C/min, 10°C/min. Standard deviation in parenthesis.	141
Table 8-4 The effect of different diffusion and drying conditions in Wood A and Wood B on their performance in ASE tests.....	144
Table 8-5 Proton spin-lattice relaxation times T_1 (^1H) and ratio of integrated areas under the peaks representing the cellulose domain 1 (89 ppm) and domain 2 (84ppm) signals in wood. MC is the gravimetric moisture content before the measurement.	145

Abbreviations

Abbreviation	Definition
ABC	alkaline buffer capacity
AFM	atomic force microscopy
ASE	anti swelling efficiency
ASTM	American standard testing method
BU	bulking coefficient
BW	bulk water
CP	cross polarisation
DEPTQ	distortionless enhancement by polarization transfer
DMA	dynamical mechanical analysis
DMDHEU	1,3-dimethylol-4,5-dihydroxyethyleneurea
DSC	differential scanning calorimetry
DVS	dynamic vapour sorption
EDX	energy dispersive x-ray analysis
EMC	equilibrium moisture content
F	formaldehyde
FA	furfural alcohol
FBW	freezing bound water
FSP	fibre saturation point
FTIR	Fourier transformed infrared
GGM	galactoglucomannan
GPC	gel permeation chromatography
GS	gas chromatography
HM	hydroxymethyl group
HM-P	hydroxymethyl-phenol
HPLC	high pressure liquid chromatography
HSQC	heteronuclear single quantum coherence
L	longitudinal
LCC	lignin carbohydrate complex
LU	liquid resin uptake
MALDI-TOF	matrix assisted laser desorption/ionisation – time of flight
MAS	magic angle spinning
MC	moisture content
MF	melamine formaldehyde
ML	middle lamella
ML _{total}	total mass loss during ASE tests
MOE	modulus of elasticity
MOR	modulus of rupture
MS	mass spectroscopy

MW	molecular weight
NFBW	non-freezing bound water
NMR	nuclear magnetic resonance
OD 0	oven dry unmodified state
OD 1	oven dry modified state
OD 2 / OD 3	oven dry state after the 2 nd and 3 rd soak cycle
P	phenol
PF	phenol formaldehyde
PUF	phenol urea formaldehyde
PW	primary cell wall
R	radial
RH	relative humidity
SANS	small angle neutron scattering
SAXS	small angle x-ray scattering
$S_{control}$	swelling coefficient of unmodified wood
SEM	scanning electron microscopy
S_{mod}	swelling coefficient of modified wood
S_{mod2} / S_{mod3}	swelling coefficient of modified wood after the 2 nd and 3 rd soak cycle
S_{resin}	swelling by resin during impregnation
SW	secondary cell wall
T	tangential
TCW	total cell wall water
TS	total swelling
UF	urea formaldehyde
UV	ultraviolet
v/v	volume on volume
w/w	weight on weight
WAXS	wide angle x-ray scattering
WPG	weight percentage gain
WS 1 / WS 2 / WS 3	water-soaked state during the 1st, 2nd, and 3rd soak cycle
WU	water uptake during soaking

List of related Publications

Peer-reviewed Articles

Kupfernagel, C., Spear, M.J., Pitman, A.J., Ormondroyd G.A. Wood modification with phenol urea formaldehyde (PUF) resin: the influence of wood species selection on the dimensional stability. *Eur. J. Wood Prod.* **81**, 5–19 (2023). <https://doi.org/10.1007/s00107-022-01893-5>

Under review

Kupfernagel, C., Spear, M.J., Yelle, D.J., Pitman, A.J., Dimitriou, A., Ormondroyd G.A. Wood modification with PUF resin: chemical interactions between wood and resin and their impact on the anti-swelling efficiency.

Kupfernagel, C., Rahman M., Thompson R., Spear M.J., Pitman A.J., Brown S.P., Ormondroyd G.A. Cell wall diffusion in resin modified wood studied on different levels of scale.

Conference Proceedings

Kupfernagel, C., Spear, M.J., Pitman, A.J., Ormondroyd G.A. Wood Modification with Phenol Urea Formaldehyde Resin: The Role of Micropore Blocking in Beech and Poplar Wood. In *Timber 2023*, London, (2023).

Kupfernagel, C., Spear, M.J., Pitman, A.J., Ormondroyd G.A. The curing reaction of Phenol Urea Formaldehyde Resin in the Presence of different Wood Species. In *International Panel Products Symposium*, Llandudno, (2023).

Kupfernagel, C., Rahman M., Thompson R., Spear M.J., Pitman A.J., Brown S.P., Ormondroyd G.A. Cell wall diffusion of low molecular weight PUF resin studied by liquid- and solid-state NMR. In *18th Annual Meeting of the Northern European Network for Wood Science and Engineering*, Göttingen, (2022).

Kupfernagel, C., Spear, M.J., Pitman, A.J., Ormondroyd G.A. Wood modification with Phenol-Formaldehyde-Resin and the effect of selected process variables. In *Timber 2022*, London, (2022).

Kupfernagel, C., Spear, M.J., Pitman, A.J., Ormondroyd G.A. Wood modification with Phenol-Formaldehyde-Resin and its influence on the dimensional stability of homegrown and imported hardwoods. In *17th Annual Meeting of the Northern European Network for Wood Science and Engineering*, Kaunas, (2021).

List of Hypotheses

The efficiency of the resin modification process depends on the choice of wood species.

Chemical and non-chemical interactions between wood and resin influence the efficiency of the resin modification process.

Process conditions in the impregnation, drying, and heat curing stages of the resin modification process impact on the properties of the resin modified wood.

1. Introduction

Throughout history, wood has always been invaluable to mankind as a material. From its first evidenced utilisation as a building material 1.5 million years ago¹, to wooden skyscrapers that are now constructed world-wide² – the advantages of wood are astonishing. Compared to non-renewable materials, the supply of timber is warranted well into the far future, provided that timber production and forest management occur in a sustainable manner and that the annual harvest rate does not exceed the annual growth rate. Taking sustainable management into account, the European forests are still producing enough timber every second to build a family home³. Compared to petroleum or mineral-based materials, wood in service constitutes an increasingly important carbon repository, because the carbon from the modern atmosphere is captured in the wood during its use⁴. Increasing the share of wood in construction would thus have multiple advantages in terms of climate change mitigation⁵. Wood products require relatively low processing energy and have a high strength-to-weight ratio². On a global scale, forests are distributed more evenly than other material resources, which facilitates the development of short supply chains and equal industrial opportunities for third world countries. Furthermore, by-products of the timber industry, such as lignin, are poised to play a vital role in the development of a new circular bioeconomy^{6,7}.

Despite these advantages, the timber industry encounters various challenges. Forest resources frequently become the focal point of conflicting priorities among different interest groups, including stakeholders in material production, biorefinery, bioenergy, as well as those dedicated to nature preservation and recreation⁷. Additional hurdles are linked to global warming, as extreme weather events (e.g., drought, wildfires, storms) and biotic disturbances (e.g., insects, pathogens) are becoming more frequent⁸. Especially coniferous forests, the primary habitats for industrially significant softwoods, are facing increasing pressures⁹. Their ecological niche is expected to be occupied by more temperature-resistant species that thrive in the changing climate, such as beech and oak, for which current industrial processes are not optimised¹⁰. The trends described above converge in an increasing demand, which is met by a limited or decreasing supply of wood from the forests. One consequence is that the service life of wood products must increase significantly. Therefore, different sectors must advance and adapt at the same time. Designers need to reconsider their products, architects must incorporate the reuse of building materials, regulators must endorse corresponding policies, consumers' choices must adjust, and innovative technologies must be implemented.

In outdoor applications of wood, the service life is often limited by biotic factors, such as wood destroying fungi or insects, but can be enhanced by technological means¹¹. For a long time, the durability issues of wood in demanding applications have been addressed using copper-chrome-arsenate or creosote-based preservatives^{12,13}. These compounds increase the durability of wood using a fungicidal mode of action, which increasingly restricts their use within close human contact¹⁴. While conventional wood preservation with fungicides is still the dominant approach, novel technologies are slowly gaining ground¹⁵. These alternative wood protection methods, using a non-fungicidal mode of action, are frequently summarised as wood modification^{11,15,16}. Commercially available modifications include thermally treated wood, acetylated wood, and wood treated with thermosetting resins. Wood modification with low-molecular weight thermosetting phenol urea formaldehyde (PUF) resin is the subject of this thesis.

The work on this thesis started in 2020 as part of a collaboration with *Lignia Wood Company Ltd.* who were producing PUF modified wood on a semi-commercial scale in the United Kingdom at the time. With the nature of this research being applied rather than fundamental, it was originally intended to investigate certain aspects of the upscaling process. However, these aspirations had to be adjusted after the industrial partner went into administration in 2021. Adapting to the new situation, the focus shifted towards the fundamental aspects underpinning the successful wood modification and away from the specific process used by *Lignia Wood Company Ltd.*

This thesis is divided into nine chapters including this introduction. After reviewing the relevant literature in Chapter 2, the various wood species and the resin used throughout the whole thesis are characterised in Chapters 3 and 4. The main quality criterion for evaluating modified wood in Chapter 5 and 6 is the anti-swelling efficiency (ASE), which describes the improvement of dimensional stability after a resin treatment.

In Chapter 5, the modification of seven hardwoods and four softwoods with the same PUF resin is compared in one consistent method. The primary result of this chapter is that the dimensional stability of all wood species can be improved by the resin treatment, however, the efficiency in doing so depends on various factors, including the density of wood and its chemical composition. While all wood species in Chapter 5 seem suitable for upscaling, certain exclusion criteria related to their treatability and drying properties in plank dimensions may necessitate evaluation at a pilot-scale production level, aspects not explored here given the use of relatively small samples in the laboratory.

Chapter 6 focusses on the process parameters considering the properties of the resin as well as the atmospheric conditions in the drying and heat curing stages. In terms of resin properties, it was found that a higher alkalinity is generally disadvantageous in the treatment, whereas the resin concentration must be adapted for each individual wood species to obtain optimum results. Chapter 6 also establishes the importance of resin diffusion into the cell wall micropores during the drying stage (i.e., cell wall diffusion), which is later studied in more detail.

Chapter 7 delves into the chemical interactions between wood and PUF resin, employing differential scanning calorimetry (DSC) and solution-state nuclear magnetic resonance (NMR) spectroscopy. The chapter revealed that compared to neat resin, the curing reaction in the presence of wood is significantly slower. The retardation varies among wood species and is linked to the neutralisation of the resin's alkaline catalyst by wood constituents (mainly hemicelluloses) and to the microscopic resin location within the wood (i.e., inside or outside the cell wall), causing steric hindrance effects. Moreover, the formation of covalent bonds between wood and resin, observed in previous studies, could not be verified by solution-state NMR.

Chapter 8 explores resin-wood interactions at different length-scales and builds upon the previously established phenomenon of resin cell wall diffusion during the drying stage of the treatment. It is demonstrated that the relative humidity and temperature applied in the drying stage significantly influence the cell bulking coefficient, swelling coefficient, and leaching of substances from modified wood. To gain a better understanding of resin cell wall diffusion, the micropore structure was studied using thermoporosimetry, and the molecular motions of wood polymers were investigated through solid-state NMR spectroscopy and relaxation time analysis.

Chapter 9 serves as a comprehensive summary, critically discussing the most crucial results from all results chapters. It also delves into alternative experiments and potential future developments, bringing this thesis to a conclusion.

2. Literature Review

2.1. Wood Properties

2.1.1. Macroscopic Properties

From a materials science perspective, wood is a natural composite made up of three polymer types (i.e., cellulose, hemicelluloses, lignin) that are organised on a microscopic level to form cell wall layers. The cell wall layers are organised into different cell types, which form various kinds of macroscopic wood tissue. This hierarchical structure can be found in many natural materials other than wood (e.g., bamboo, bone)¹⁷ and it is the reason why macroscopic properties of a natural material cannot be decoupled from its microscopic or even molecular arrangement^{18,19}.

The hierarchical structure of wood is illustrated in Figure 2-1. The macroscopic wood tissue typically shows a division of work and is therefore described according to the three principal functions: conduction of water, storage of nutrients, and mechanical support of the tree. Additional types of tissue such as excretion tissues (e.g., epithelial cells) and specialised tissues, such as tension wood in deciduous species and compression wood in coniferous species, may also be present²⁰.

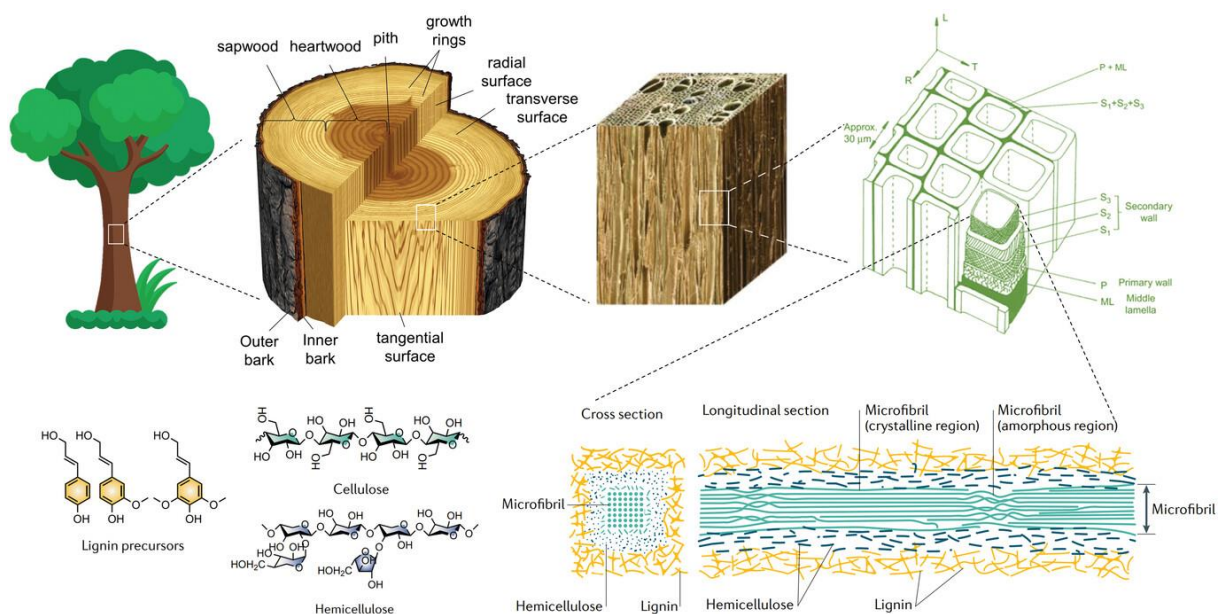


Figure 2-1 The hierarchical structure of wood is characterized by a multi-level organisation. Timber is composed of various tissues, each consisting of different cell types, cell wall layers, and ultimately polymers. Image adopted from Chen et al.¹⁹ (2020).

2.1.1.1. Growth of the Tree

The growth of the tree occurs in the cambium, a small layer of living cells responsible for producing the secondary xylem (i.e., inner parts of the tree) and the secondary phloem (i.e., bark). A cambial initial cell always divides in a manner so that phloem cells emerge on its outward-facing surface, and the xylem cells emerge on its inward-facing surface. The cambial initial may divide in the tangential or radial direction, allowing even thickness growth in all directions. Once the cell is formed, lignification takes place, embedding similar cells adjacent to each other to form a certain type of tissue.²⁰

2.1.1.2. Sapwood and Heartwood

The outer region of the xylem contains the sapwood, which is defined as the portion of the tree that contains living cells and reserve materials like starch²¹. Sapwood contains a low proportion of extractives, since its primary functions are the conduction of water from the roots to the crown and the storage of reserve materials in the parenchyma cells²². The relative amount of sapwood in the stem varies between different timbers and even within one species, it depends

on the age, location, and the amount of foliage of the tree^{20,22}. Regarding wood in service, the sapwood is generally more susceptible to biodeterioration by insects and microorganisms.

Heartwood is defined as the inner layers of wood, which, in the growing tree, has ceased to contain living cells, and in which the reserve materials (e.g., starch) have been removed or converted to extractives²¹. Heartwood serves the living tree by optimising the sapwood volume, conserving resources, and providing mechanical support²².

The conversion from sapwood to heartwood may occur in trees of a certain age and is accompanied by the aspiration of bordered pits in softwoods. From a biochemical perspective, the heartwood formation causes a shift from aerobic to anaerobic respiration²². This leads to the accumulation of carbon dioxide, ethylene gases, and to enzymes converting storage material into extractives^{23,24}.

In some species the heartwood may be distinguished from the rest of the tree by its darker colour. This colouration is the product of mostly phenolic extractives that diffused into the cell wall²⁵. Within these trees the heartwood might develop regularly (i.e., obligatory coloured heartwood) or irregularly (i.e., facultative coloured heartwood). In other species the heartwood retains the same colour as the sapwood (i.e., light-coloured heartwood) or develops only in very old sapwood (i.e., trees with retarded heartwood formation)²⁶. Obligatory coloured heartwood has altered properties compared to the sapwood. It is denser, more durable, has a lower equilibrium moisture content (EMC) and is less permeable than sapwood. However, this is not necessarily true for the other groups of heartwoods²⁰. Examples of wood species with different forms of heartwood are listed below:

- obligatory coloured heartwood (pine, larch, Douglas fir, oak, locust tree),
- facultative coloured heartwood (beech, ash, alder, birch, maple),
- light coloured heartwood (spruce, fir, beech, lime wood),
- retarded heartwood formation (aspen, birch, alder, maple).

In some trees, a narrow, pale-coloured transition zone can be observed at the border to the sapwood. The transition zone often contains living cells but no starch. It is impermeable to fluids and usually has a lower EMC than the sapwood. This zone should not be mistaken for the intermediate wood, which is defined as a layer between sapwood and heartwood in some species, transitional in colour and general character (e.g., in ash, elm).^{20,21,24}

2.1.1.3. Earlywood and Latewood

Over the course of one year, trees in the temperate climate zone exhibit a growth period and a rest period. The beginning of the growth period during spring is marked by the mobilisation of stored resources when the cambium slowly resumes activity. During this time, both the cambium and the parenchyma cells are highly active, and reserve materials are transported throughout the tree. At the end of the growth period, the cambium ceases activity and reserve materials are stored in the sapwood²⁰. During the rest period, the cambium is inactive.

Tissue formed in the beginning of the growth period is called earlywood, and tissue formed towards the end is known as latewood. Growth rings become visible if both types of tissue differ in their physiological and morphological properties. In softwoods, these differences are manifested in the thickness of cell walls and the dimensions of cells in earlywood and latewood. While the outer diameter of cells formed in hardwood throughout the year is similar, the arrangement and distribution of vessel cells may differ^{20,27}. Based on the appearance of hardwoods in the cross section, one distinguishes timbers that are:

- ring porous (e.g., chestnut, ash, elm, locust),
- half ring porous (e.g., walnut tree, cherry tree), and
- diffuse porous (e.g., maple, birch, poplar, alder).

In ring porous hardwoods, the large earlywood vessels are arranged as a ring at a certain perimeter and with a distinct boundary to the latewood. In half ring porous timbers, the vessel diameter gradually decreases from the earlywood to the latewood. Diffuse porous hardwoods show almost no change in vessel diameter across the growth ring²⁰.

2.1.2. Microscopic Properties

2.1.2.1. Softwood Cells

In the history of evolution, softwoods developed earlier than hardwoods. A comparison of their microscopic structure is shown in Figure 2-2. Softwoods are composed of only two major cell types, namely tracheid cells (or fibres) and parenchyma cells. The water-conducting tissue comprises longitudinal and radial tracheids. Parenchyma tissue includes longitudinal and ray parenchyma as well as epithelial cells. Resin canals that are often present in softwoods are not classified as cells but intercellular spaces.^{20,27,28}

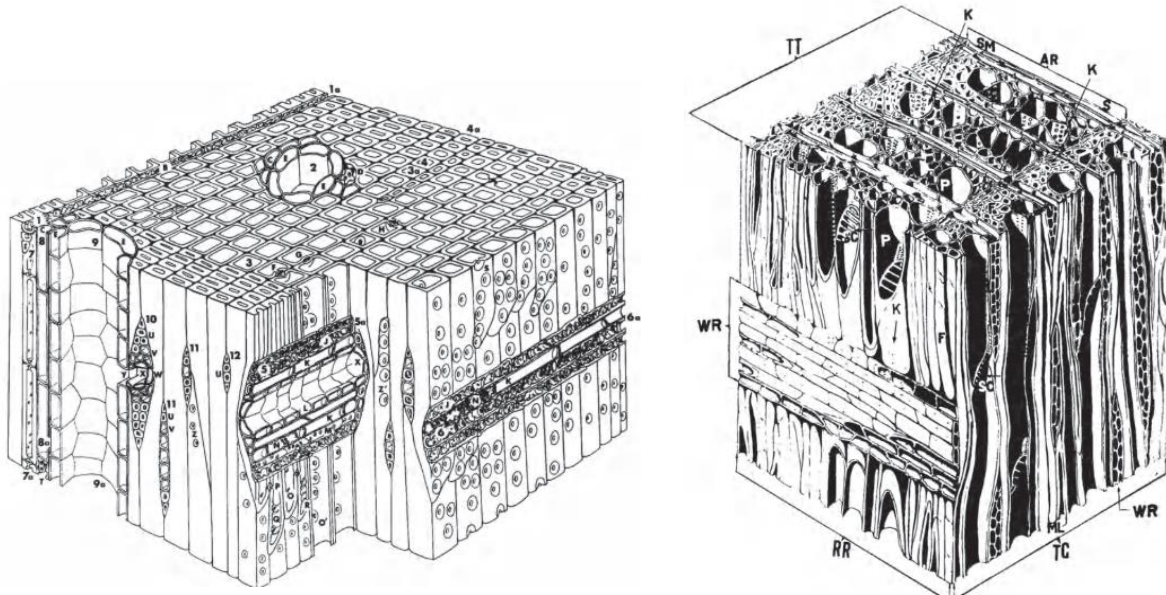


Figure 2-2 Three-dimensional microscopic structure of softwood (left) and hardwood (right)²⁷. Softwoods contain mainly tracheid cells and parenchyma cells, while hardwoods contain additional cell types such as vessels.

Tracheids account for 90 – 95% volume fraction of the stem²⁷. Thin-walled earlywood tracheids are responsible for water transport, whereas thick-walled latewood tracheids provide mechanical support to the tree. Tracheid cells are typically 2 – 4 mm long, 0.02 – 0.04 mm wide, and have a cell wall thickness between 4 – 8 μm²⁷. Longitudinal and ray parenchyma are living cells that are responsible for the storage of nutrients. They account for 5 – 10% volume fraction of the stem. Typical ray parenchyma cells are 0.01 – 0.16 mm long and 2 – 50 μm wide²⁷. Ray parenchyma cells arranged in narrow bands across the stem form ray tissue or rays. Softwood rays that exclusively consist of parenchyma cells are called homo-cellular (e.g., in fir or yew). Rays that comprise ray parenchyma and ray tracheids are called hetero-cellular (e.g., in pine, spruce, larch, Douglas fir).

Although rays account only for a relatively small fraction of the whole stem, their effect on the permeability of the wood can be significant, especially when treating large specimens. Resin canals are faced by epithelial cells that secrete oleoresins into the canals. The arrangement of resin canals in the cross section depends on the species. Pines contain more and larger canals than spruce for example²⁷.

2.1.2.2. Hardwood Cells

Cells in hardwoods are more specialised than those in softwoods. The support tissue in hardwoods consists of fibres. Hardwood fibres may occur as libriform fibres with simple pits, fibre tracheids with bordered pits, or in a few species as vascular tracheids (e.g., in *Fagaceae* and *Myrtaceae*)²⁰. Together, fibres make up between 20 – 70% of the volume fraction in hardwoods^{20,28}. Hardwood fibres have an elongated and thick-walled morphology in both early and latewood. Generally, they are slightly shorter and have smaller pits than their softwood equivalents, which makes them less permeable^{27,28}.

Vessel cells, which are unique to hardwoods, are responsible for the water conduction. Vessel cells transport a large amount of water during the leafing in spring. They consist of relatively short, thin-walled cells with open ends that are placed on top of each other. Thus, they build up tubes that may extend several meters throughout the stem to form an interconnected network. In diffuse porous hardwoods the vessels account for 20 – 60% of the volume fraction, with diameters ranging from 20 – 100 μm . In ring-porous hardwoods the volume fraction of vessels is smaller, with 5 – 25% and vessel diameters vary considerably between 50 – 400 μm in earlywood and between 10 – 50 μm in latewood²⁸. Vessels, characterised by numerous bordered pits, are generally highly permeable to adjacent tissues.

Some species (e.g., white oak, chestnut, black locust) may develop tyloses in the vessels after heartwood formation. While these structures protect the living tree from wood-destroying fungi, they also render the wood completely impermeable, causing challenges during kiln drying and impregnation processes. Tyloses grow from adjacent parenchyma cells through the pit openings into the vessels. Some tropical hardwoods may also contain mineral deposits within the vessels.^{20,29}

In hardwoods, parenchyma cells are present in both longitudinal and ray parenchyma forms. Longitudinal parenchyma cells occur more frequently in hardwoods compared to softwoods, constituting up to 18% of the volume fraction²⁸. Ray tissue in hardwoods is exclusively made up of ray parenchyma cells. Rays account for 5 – 35% volume fraction in the stem. Parenchyma cells are linked to each other via simple pits and to vessels and fibres via half-bordered pits. The ray tissue is rather impermeable, although in some cases it can provide a pathway for radial liquid transport²⁸. In some species (e.g., in beech) large rays are a frequent onset point for cracks that develop during kiln drying³⁰.

2.1.2.3. Pit Structure and Function

Wood cell walls are regularly interrupted by perforations called pits. Although various types of pits exist in different cells, their primary function is always the transport of water and nutrients from one cell to another. Adjacent pits of two neighbouring cells form a pit pair which encloses a cavity called the pit chamber. This perforation is transversed by the pit membrane (or margo) – a porous structure consisting of a middle lamella in between two primary cell walls. In some softwoods the margo contains an impermeable thickening called torus. Softwoods and hardwoods generally contain three types of pit pairs^{20,27,28}:

- simple pits (connecting parenchyma cells with each other),
- half-bordered (connecting parenchyma cells with tracheids, vessels, or fibres), and
- bordered pits (connecting water-conducting cells like tracheids, vessels, or fibres with each other).

In earlywood tracheids of softwoods, the radial face contains more bordered pits (approx. 200) than in the latewood (approx. 50)²⁷. The tangential face contains generally fewer and smaller pits than the radial face. The bordered pit chamber can be between 6 – 30 μm in diameter. The margo has a permeable structure containing gaps with a diameter between 0.02 – 4 μm . The margo is made up of microfibrillar strands that are radiating from the torus to the border.²⁸

The membrane in simple and half-bordered pit pairs has a thickness of 1.2 – 1.8 μm and is therefore much thicker than the membrane in bordered pit pairs (i.e., 0.1 – 0.5 μm) causing a higher resistance to fluid flow²⁸. Half-bordered pits take different forms in the radial plane depending on the wood species (e.g., window, lenticular, or slit-like). This appearance of half-bordered pits influences the permeability and drying properties of a wood species²⁸.

Pit aspiration is the result of heartwood formation or kiln drying. It occurs when the torus, which is completely impermeable, is pressed against the pit border blocking the aperture. Aspirated pits are fixated by hydrogen-bonds and sometimes encrusted by extractives. The proportion of aspirated pits in Radiata pine was shown to be low in the sapwood but increases steeply in the transition zone and the heartwood³¹. Latewood pit membranes are more rigid and therefore less susceptible to aspiration than earlywood membranes. The lower degree of pit aspiration results in a higher permeability of latewood compared to earlywood of pines^{28,32}.

Hardwood pits are not bordered and contain a plain margo without any torus or fibrillar features. While the thickness of the margo in hardwoods is similar to softwoods, gaps in the membrane are one order of magnitude smaller, i.e., 5 – 170 nm.²⁸

2.1.2.4. Structure of the Cell Wall

The cell wall comprises distinct layers with varying properties and chemical compositions. Approaching from the cell lumen, these layers are called secondary wall (SW), primary wall (PW), and middle lamella (ML). Selected properties of these layers are summarised in Table 2-1. Some wood species have a warty layer (W), which is situated on the inside of the cell lumen. This is an amorphous layer which occurs in all softwoods and some hardwoods²⁷. The SW is the largest layer in the cell wall and is made up of three sub-layers itself (SW1, SW2, SW3). Accounting for only a small fraction, SW1 and SW3 constitute the inner and outer sub-layers, which sandwich the SW2 in the secondary wall.

The SW2 is the thickest layer in the cell wall and contains highly-order microfibrils which are arranged at a high microfibril angle (MFA) with respect to the cell axis. SW2 contains the highest total amount of cellulose and lignin, thus, its structure and composition influence macroscopic wood properties (e.g., swelling coefficient, mechanical strength). The thickness and microfibril angle of SW2 vary significantly between earlywood and latewood, as shown in Table 2-1.^{20,27,28}

The PW is a thin layer with a high lignin content and random orientation of microfibrils. Together with the ML it is sometimes referred to as the compound middle lamella (CML). The ML has the highest lignin concentration and contains small amounts of pectic substances. Due to its relatively small size between 3 – 4 μm , it only accounts for 25% of total lignin in the wood²⁷. The middle lamella functions as an interface which binds adjacent cells together. The cell wall structure, as mostly described in textbooks, often refers to the softwood tracheid because softwoods are more frequently used in construction and their relatively simple composition facilitates basic research³³.

Table 2-1 The wood cell wall is comprised of distinct layers with varying properties and chemical composition. Selected properties of these layers are shown. MFA – Microfibril angle, MF – microfibril content, PW – Primary cell wall, SW – Secondary cell wall, SW1, SW2, SW3 – sub-layers within the secondary cell wall.^{20,27,28}

Cell Wall Layer	Thickness in μm	MFA in $^\circ$	No. of Lamellae	MF in %	
ML	0.2 – 1.0	-	-	-	
PW	0.1 – 0.2	random	-	10	
SW1	0.2 – 0.5	50 – 80	3 – 4		
SW	SW2	1(EW) – 8 (LW)	10(LW) – 30 (EW)	30(EW) – 150 (LW)	90
	SW3	0.1	50 – 90	6	

2.1.3. Chemical Composition and Nanostructure of Wood

2.1.3.1. Cellulose

Cellulose, despite its simple chemical composition, exhibits varied properties influenced by factors such as crystalline state, molecular weight, and the presence or absence of water. The repeating unit, cellobiose, comprises two β -D-glucopyranose residues displaced at a 180° angle (Figure 2-3). The glucopyranose residues are linked via glycosidic bonds between their C1 and C4 carbon, as shown in Figure 2-3. This conformation gives rise to a twofold screw structure allowing a high degree of linearity, which is maintained by two types of intramolecular hydrogen-bonds (O2-H...O6 and O3-H...O5)^{34,35}.

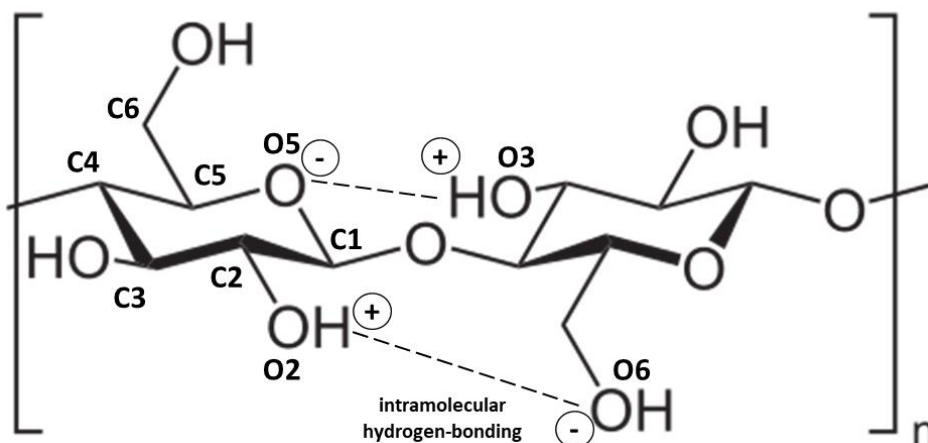


Figure 2-3 Cellulose repeat unit (cellobiose) is comprised of two glucopyranose units that are displaced at an angle of 180° to each other. Different ring positions are indicated by C1 – C6. Intramolecular hydrogen-bonds are indicated by dashed lines.

Cellulose forms linear chains with an average degree of polymerisation of around 10,000 in higher plants²⁷. Adjacent cellulose molecules align to form microfibrils (or elementary fibrils) through intermolecular hydrogen bonds between hydroxyl groups at C3 and C6^{27,34,35}. Microfibrils, consisting of 18 to 80 cellulose chains³⁶, exhibit a lateral dimension ranging from 3 nm x 3 nm to 8 nm x 8 nm. The nature of the microfibril arrangement depends on the type of plant or even on the location within the same plant. Multiple microfibrils combine to create a macrofibril (see Figure 2-7), which, in turn, contributes to the formation of a cell wall layer.

It is widely accepted that two populations of cellulose exist in the cell wall. Historically, these populations have been termed crystalline and amorphous cellulose, with the crystalline part constituting the core of the microfibril and the amorphous part on its surface.

While it is possible to chemically engineer cellulose so that it becomes completely amorphous or crystalline³⁷, recent advances in solid-state NMR *in situ* investigations^{38–40} of the cell wall propose a different terminology for the two cellulose populations in solid wood—cellulose domain 1 and domain 2. Cellulose domain 1 is mainly thought to be glucan chains in the core of the microfibril (historically crystalline cellulose), while cellulose domain 2 is primarily located on the surface of the microfibril (historically amorphous cellulose)³⁸. This thesis employs both historical and recent terminology depending on the context. The ratio of cellulose domain 1 to domain 2 (i.e., crystallinity) ranges from 40 – 95% in higher plants^{27,34}.

Next to solid-state NMR, the polymorphism of cellulose has been studied by x-ray diffraction⁴¹ or polarised FTIR⁴². So far, there are four known crystalline structures with different x-ray diffraction patterns (i.e., Cellulose I, II, III, and IV). The transformation between crystalline forms is possible in some cases and may have certain advantages, such as increased reactivity. Cellulose I, which is the dominant type in nature, occurs in two conformations called cellulose I_α and cellulose I_β. Higher plants contain mostly Cellulose I_β, whereas bacteria and algae produce a mixture of both types³⁴.

Since all hydroxyl-groups in cellulose are positioned equatorially, the sides of the chain are hydrophilic, whereas the top and bottom are hydrophobic³⁸. In microfibrils, the hydrophobic surfaces are stacked on top of each other, and hydrogen-bonds are formed between the sides. This assembly results in hydrophilic equatorial surfaces, with a relatively small proportion of hydrophobic surface at the corners of the microfibril⁴³. The corners play a crucial role in enzymatic degradation, as fungal cellulases bind specifically to these surfaces⁴⁴.

Intramolecular hydrogen bonds can be replaced by hydrogen-bonds with water. In this case, water molecules readily penetrate the surface regions of the microfibril, causing the structure to swell and forming new hydrogen bonds. Within the microfibril, only the equatorial surface is accessible to water molecules, while the core region remains inaccessible. On the microfibril surface, the O2-H...O6 bond is more easily disturbed by water than the O3-H...O5 bond⁴⁵.

The structure of the microfibril and macrofibril undergoes changes when water is absorbed from the atmosphere. X-ray scattering techniques (WAXS/SAXS) in combination with molecular dynamics simulations have demonstrated this phenomenon in a recent study⁴⁶. The size of the microfibril and its lattice spacings undergo changes within the range of 0 – 15% moisture content, but not beyond this point. Above 15% moisture content, the distance between different microfibrils starts to increase, while it remained constant below this threshold. At a macroscopic level, these changes result in the swelling and shrinking of the wood⁴⁶.

2.1.3.2. Hemicellulose

Hemicelluloses are heteropolysaccharides composed of a variety of sugar residues. Hemicelluloses are generally amorphous compounds with a much shorter chain length than cellulose, typically having a degree of polymerisation between 100 – 200. Generally, a linear polymer backbone is equipped with frequent side chains and branches. Composition and structure differ greatly between softwoods and hardwoods. Hemicelluloses are typically studied after alkali extraction of holocellulose, which can influence the available information about them^{27, 34, 47}. More recent studies are focussing on *in situ* investigations^{38, 39}.

Hardwood hemicelluloses consist predominantly of O-acetyl-4-O-methylglucurono-β-D-xylan, usually referred to as xylan. This fraction makes up 15 – 30% of dry mass in hardwoods. The xylan backbone is composed of β-(1-4) linked D-xylopyranose residues, which are frequently acetylated at the C2 and C3 position (7 acetyls per 10 residues).

To a lesser extent the hardwood xylan backbone is substituted with 4-O-methylglucuronic acid residues at the C2 position (1 glucuronic acid per 10 residues). Small amounts of galacturonic acid and rhamnose are also incorporated in the end chain structure of xylan⁴⁸. Recent studies suggest that hardwood xylan exists in two forms, one more linear and one more branched⁴⁹. The bond between xylose units is easily cleaved by acids, whereas the bond to glucuronic acid is more stable. Acetyl groups are easily cleaved by alkali, acid, or even hot water and form acetate salts or acetic acid^{27,50}. Glucomannan is a minor fraction of hardwood hemicelluloses. It makes up less than 5% of hardwood dry mass. Unlike softwood glucomannan, it is not acetylated^{27,34}

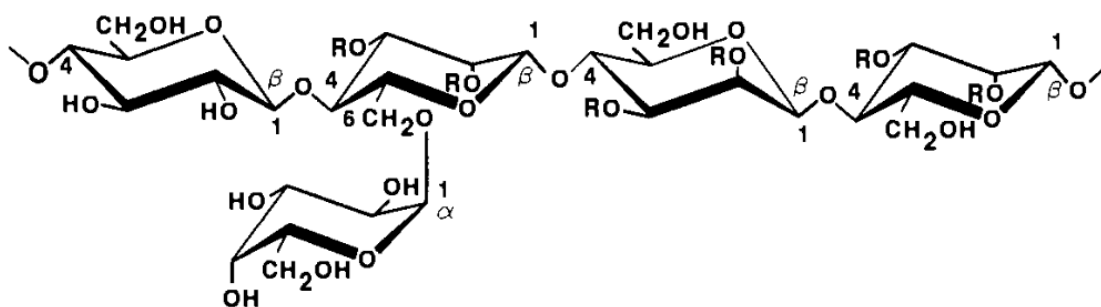


Figure 2-4 Glucomannan chemical structure in softwoods. The polymer backbone consists of alternating glucose and mannose units. Galactose side chains are introduced at the C6 position of mannose units. R = CH₃CO or H. ²⁷

Softwoods contain both glucomannan (20 – 25%) and xylan (5 – 10%). The polymer backbone consists of alternating D-glucose and D-mannose units in a ratio of 1:3, as illustrated in Figure 2-4. Glucomannan contains single unit side chains of D-galactose residues which are linked to mannose units via (C1-O6) bonds. This link is especially prone to acid hydrolysis. Glucomannan containing a high amount of galactose is referred to as galactoglucomannan (GGM). Glucomannan in softwoods is acetylated at the C2 and C3 position (3.5 acetyls per 10 residues).

Softwood xylan or arbinoglucuronoxylan contains twice as many glucuronic acid residues as in hardwoods (Figure 2-5). Moreover, there are arabinofuranose residues linked to the polymer backbone via (X1-O3) bonds. On average there 1.3 furanose residues per 10 xylan units. Softwood xylan is not acetylated ^{27,34}

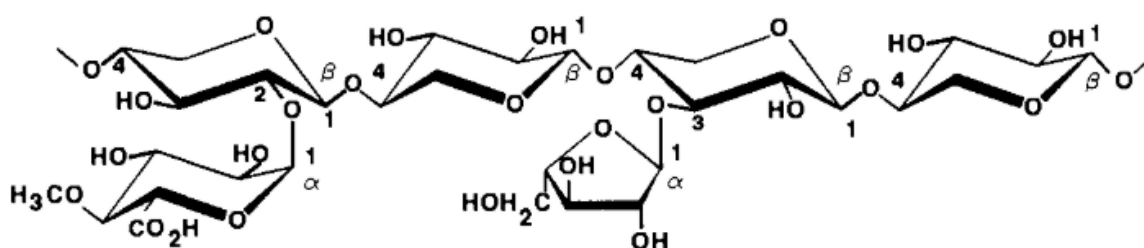


Figure 2-5 Softwood xylan structure. The polymer backbone consists of β -(1-4) linked D-xylopyranose residues. Glucuronic acids residues are introduced at the C2 or C3 position. Furanose side chains may be linked to the backbone at C3. ²⁷

The distribution of hemicelluloses varies between the individual cell wall layers. In hardwoods, the xylan concentration increases from the lumen towards in the PW. In softwoods, the xylan and glucomannan concentrations are highest in the SW3 layer²⁷. Additionally, the hemicelluloses content varies between different cell types, e.g., softwood xylan is more abundant in ray tissue than in tracheids. Other amorphous carbohydrates in wood include pectic substances that are highly branched polysaccharides, such as rhamnogalacturonan, arabinan, or arabinogalactan which occur mainly in the compound middle lamella and are usually not considered hemicelluloses^{27,34}.

2.1.3.3. Lignin

Lignin is a hydrophobic, highly branched, and aromatic cell wall polymer. It is often seen as the matrix material of the cell wall, responsible for developing compressive strength in wood. Microfibrils are encased in a lignin matrix and adjacent cells are glued by the lignin of the middle lamella. Unlike cellulose, lignin is a highly polydisperse polymer, with a wide distribution in the molecular weight. The weight-average molecular weight (M_w) of lignin was found to be around 20,000 g/mol in wood.^{34,47}

The Klason-method, based on acid hydrolysis of carbohydrates, is the most common determination method for lignin. However, various other forms of lignin that are based on ball milling (milled wood lignin), enzyme digestion (cellulotic enzyme lignin), or lab synthesis from model compounds (released suspension culture lignin) are available for different purposes. Softwood contains between 26 – 32% Klason-lignin and up to 40% in compression wood. The Klason-lignin content in hardwood ranges between 20 – 25%. Moreover, a notable fraction of hardwood lignin is acid-soluble and therefore not included in the Klason-lignin fraction. This acid soluble lignin fraction can be determined by UV-spectroscopy.^{34,47}

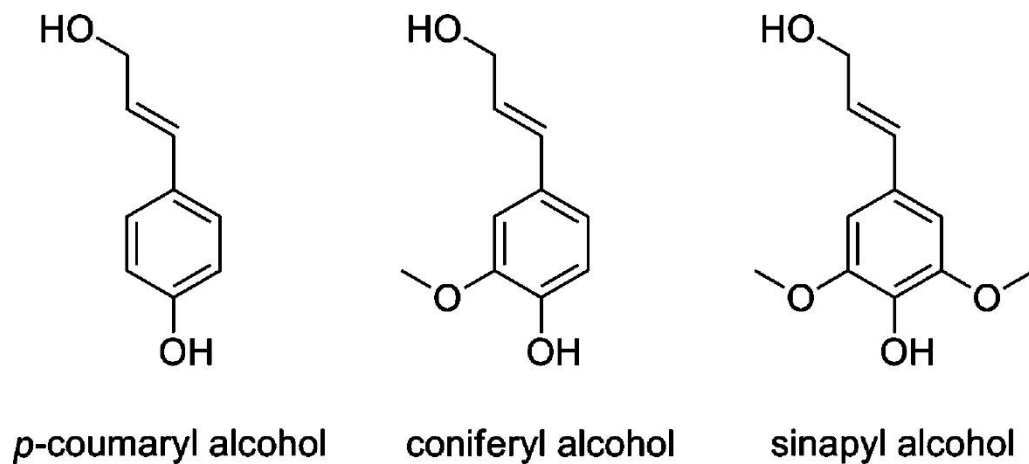


Figure 2-6 Lignin precursors in the biosynthesis of the tree are based on phenylpropane. Coumaryl, coniferyl, and sinapyl alcohol constitute the basis of lignin synthesis. Enzymatic polymerization yields the final lignin structure, where the precursors are linked by various forms of ether or methylene bridges.

The structural unit in all types of lignin is phenylpropane, which contains a phenolic ring and an aliphatic side chain. During biosynthesis of lignin, monomeric lignin precursors are formed from D-glucose via complex enzymatic reactions, known as the shikimate-pathway²⁷. Depending on the number of methoxy groups attached to one phenolic ring, these monolignols are known as coniferyl alcohol (G), sinapyl alcohol (S), and p-coumaryl alcohol (H), as shown in Figure 2-6.

The polymerisation of monolignols occurs via addition of phenoxy radicals, which gives rise to a variety of dimers. After reaching a tipping point, the reaction mechanism shifts to an endwise polymerisation, joining up loose ends and leaving just a small number of unreacted sites in the condensed lignin²⁷.

Structural units in lignin are connected by one of three possible ether linkages, or by one of four possible C-C linkages. Table 2-2 summarises the different types of bonds in lignin, showing pronounced differences between hardwoods and softwoods. Due to the higher number of available methoxy groups, hardwood lignin is dominated by ether linkages. Softwood lignin (G-type) is the condensation product of coniferyl alcohol and small amount of p-coumaryl alcohol. Hardwood lignin (GS-type) is a co-polymer of equal parts of coniferyl and sinapyl alcohol, and small amount of p-coumaryl^{27,34}.

Lignin and hemicellulose units connected by covalent bonds are called lignin-carbohydrate-complexes (LCC). Most of softwood lignin and around 47 – 66% of hardwood lignin units are incorporated in LCCs⁵¹. While there are several possibilities, the most common linkages in wood involve ester bonds with xylan or benzyl ether bonds through arabinofuranose units.

Table 2-2 Frequent types of linkages in lignin and their percentages in hardwoods and softwoods.

Lignin Dimer	Type of Linkage	Proportion in %	
		Hardwoods	Softwoods
β -aryl-ether	β -O-4	60	< 50
α -aryl-ether	α -O-4	7	2 – 8
phenylcoumaran	β -5	6	9 – 12
biphenyl	5-5	5	10
diarylether	4-O-5	7	4
diarylpropane	β -1	7	7
link through side	β - β	< 3	< 3

2.1.3.4. Nanostructure of Cell Wall Polymers

The properties of the cell wall arise from the interaction among its polymers, rather than being determined by the averaged characteristics of each individual polymer. Traditionally, this interaction is conceptualised as a microfibril that is coated by an amorphous layer of hemicelluloses and embedded in a lignin matrix⁵². In recent years, this model was refined by researchers who observed additional nuances in the orientation, freedom of movement, and *in situ* interactions of cell wall polymers, which are delineated in the following.^{42,53–57}

Major advances have been made using a dynamic Fourier transformed infrared (FTIR) method which allows the *in situ* study of a polymers response to a loading force^{42,53,54}. Cellulose is the main load-bearing component in the cell wall responding to loads both parallel and perpendicular to the cell main axis. Therefore, microfibrils may extend in a net-like or lenticular manner around the axis of the fibre⁴². Cellulose is a hydrophilic and stiff polymer, whereas lignin is rather hydrophobic and pliant. Both polymers rely on the mediating function of hemicelluloses, which are attached to the surface of microfibrils by hydrogen-bonds, providing a stable but flexible linkage⁵⁸. The backbone of glucomannan is orientated parallel to the microfibril showing a high affinity to it. Xylan orientates largely perpendicular to the microfibril and is less intimately associated with it⁴². For the same reason, glucomannan is chemically harder to separate from cellulose than xylan⁵⁹.

Lignin, long considered completely isotropic, has recently been shown to possess a preferred orientation in the cell wall. Aromatic rings of lignin are orientated in plane with the SW2-layer. The main axis of the lignin structural unit, reaching from the phenolic part through the propane backbone, is orientated parallel to the fibre direction. This orientation results from the growth of the cell wall, where monomeric lignols fill the templates formed by holocellulose.⁵³

The interaction of polymers in the hardwood cell wall is different than in softwoods, as dynamic FTIR studies suggest the presence of two types of xylan here⁴⁹. One highly branched type of xylan is associated mainly with the lignin fraction and may be lost during the delignification process. The other more linear form of xylan is associated with cellulose and may serve a similar function to that of glucomannan in the softwood cell wall.⁴⁹

A new level of detail has been obtained in solid-state NMR studies using mainly softwoods that were grown in a ¹³C-enriched atmosphere^{38,60}. In the model emerging from these studies, the microfibril consists of a cellulose domain 1

core (8 cellulose chains) which is sheathed by 10 cellulose domain 2 chains, as shown in Figure 2-7. Xylan exists in a 2-fold screw and in a 3-fold screw conformation in the cell wall³⁹. The 2-fold screw conformation results from an evenly substituted backbone with glucuronic residues being six xylan units apart. This 2-fold screw structure has one practically unsubstituted face, which binds to the hydrophilic surface of the microfibril via hydrogen-bonds. Xylan in a 3-fold screw cannot directly bond to the microfibril surface and acts as matrix material (see Figure 2-7).

In contradiction to previous assumptions, glucomannan and xylan chains are hydrogen-bonded to the surface of the same microfibril. Moreover, it appears that hydrogen-bonds between xylan and the hydrophilic microfibril surface convert the C6 carbon of a surface cellulose chain to a domain 1 conformation. In other words, the crystalline microfibril core may be extended to the surface, and xylan in the 2-fold screw conformation may be in direct contact with cellulose domain 1³⁸. Xylan in 3-fold screw conformation represents the minor fraction and is probably linked to another polymer or unlinked, serving as a matrix material.

As shown in Figure 2-7, several microfibrils with a diameter of 3 – 4 nm are integrated in a macrofibril with a diameter of approximately 30 nm. Microfibrils are mediated by single chains of 3-fold screw xylan and highly branched glucomannan. Lignin, in its oriented structure, occurs mainly on the periphery of the macrofibril. Lignin forms covalent bonds with hemicelluloses and is associated with the hydrophobic surface of the elementary fibril.³⁸

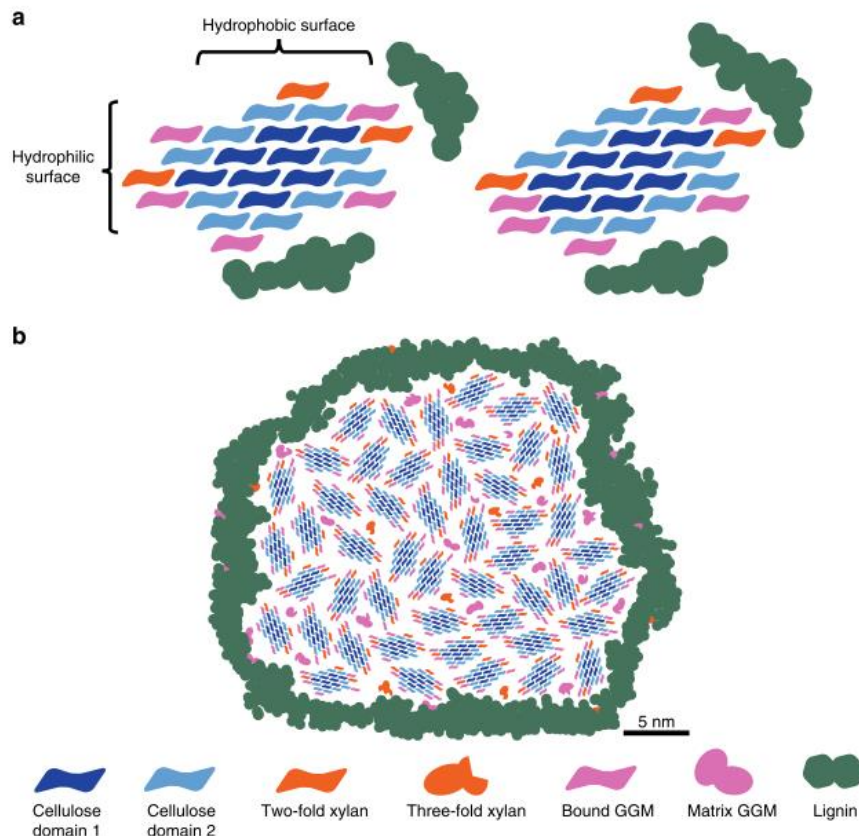


Figure 2-7 Spatial structure of the macrofibril. Microfibrils consist of a crystalline core (domain 1), covered by amorphous cellulose (domain 2). Xylan and glucomannan (GGM) in 2-fold screw formation may bind to the same microfibril. Xylan that is bound to the hydrophilic microfibril surface converts cellulose domain 1 chains to a domain 2 conformation. Microfibrils are mediated by 3-fold xylan and glucomannan (matrix). Lignin occurs mainly in the periphery of the macrofibril and interacts with both xylan and GGM.³⁸

2.1.3.5. Micropores in the Cell Wall

Micropores are elongated voids that extend between microfibrils and macrofibrils inside the cell wall⁶¹. The terminology in this context requires consideration. On the one hand, the IUPAC system⁶², which is intended for physisorption-based methods, classifies micropores as smaller than 2 nm, mesopores between 2 – 50 nm, and macropores with a width larger than 50 nm. However, in the hierarchical wood structure, it appears more feasible to distinguish the micrometre-scale voids inside the cell (i.e., lumen) from the nanometre-scale voids inside the cell wall. Therefore, in the context of wood science, the latter is often referred to as micropores, regardless of the IUPAC classification.

Cell wall micropores are often considered to form an interconnected network of cylindrical-shaped voids with diameters between 2 – 4 nm as reported by Hill (2006)¹¹, whereas other studies sometimes refer to larger dimensions^{63,64}. Other materials contain differently-shaped micropores with different properties⁶¹. Within the cell wall, the micropore size distribution differs between individual cell wall layers⁶⁵, e.g., the SW1 and SW3 layers contain larger micropores than the SW2.

Micropores are sometimes referred to as transient pores because they expand upon water absorption and collapse upon desorption. The study of pore size distribution is therefore often connected to the study of wood-water interactions. Thus, it is useful to distinguish between the methods that are measuring the cell wall in a water-saturated state (e.g., solute exclusion⁶⁶, thermoporosimetry⁶⁴, low-field NMR⁶⁷) and those that measure the cell wall in dry state (e.g., physisorption with nitrogen or krypton⁶⁸, mercury intrusion⁶⁹).

Recent studies are even questioning the existence of micropores in the cell wall, i.e., both in the dry and saturated state⁶⁸. While these results contradict many preceding studies and must be verified by additional research, it is certain that every method used to determine micropores and cell wall water content exhibits an intrinsic bias. Low-field NMR was shown to systematically overestimate the cell wall water content, solute exclusion generates highly-deviating results, and thermoporosimetry makes assumptions on the contact angle of water inside the cell wall and on the shape of micropores, both of which are unknown⁶⁷. Similarly, pore size distributions determined by physisorption assume certain mathematical models, which have been developed for inorganic materials and have therefore been suggested to be not applicable to wood⁶⁸. Moreover, nitrogen sorption tends to overestimate the surface area of wood due to interactions with hydroxyl-groups on the wood surface⁶⁸.

In this thesis, the emphasis will be on thermoporosimetry utilising DSC data to study the pore size distribution and wood-water interactions. Thermoporosimetry exploits the relationship between pore size and melting point depression of water^{61, 63,70–73}. According to the Gibbs-Thomson equation, water situated in smaller pore spaces has a lower melting point⁶¹. Thermoporosimetry distinguishes between non-freezing bound water (NFBW) which is directly adsorbed to the surface of wood polymers forming a thin layer, freezing bound water (FBW) which is situated in micropores and therefore subject to the Gibbs-Thomson equation, and bulk water (BW) which is located in the cell lumens where physio-chemical interactions with the wood are small, resulting in BW having the same melting point as normal water⁶⁴. Both isothermal and dynamic DSC scans can be used for thermoporosimetry^{64,71}.

Micropore blocking in wood modification is crucial for enhancing biological durability⁶⁶ and dimensional stability⁷⁴. Previous studies have demonstrated that impregnation with 1,3-dimethylol-4,5-dihydroxyethyleneurea (DMDHEU) primarily influenced micropores larger than 60 nm⁷¹, and thermal modification decreased the micropore volume possibly through lignin flow into micropore spaces⁶³.

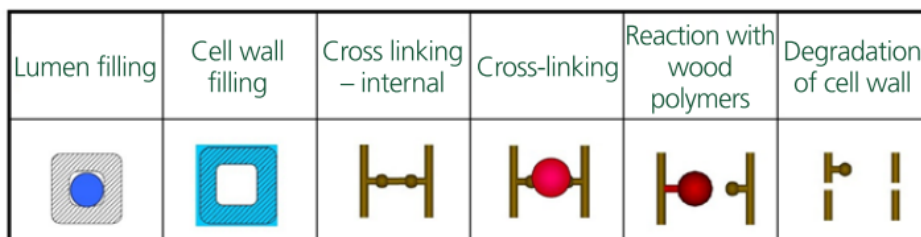
2.2. Wood Modification

2.2.1. The Scope of Various Wood Modification Systems








The environmental benefits of wood as building material have been heavily promoted in recent years with many governments supporting wood construction and the development of new bio-based products. From an environmental standpoint, timber should be processed as little as possible to maintain its carbon sink function⁷⁵. However, to extend the number of possible applications for wood, one must overcome certain undesirable properties inherent to this natural material (e.g., lack of durability in outdoor applications).

Established treatments for wood requiring high durability include the impregnation of biocidal preservatives¹³. Oil-based preservatives (e.g., creosote) were used during the past 200 years to protect wood in marine environments and railway sleepers. Water-based preservatives (e.g., copper-chrome based) are favoured in applications with greater human contact. With an annual production volume of 21 million m³ in the US alone, these preservative treatments account for the vast majority wood protection methods¹⁵. However, due to environmental concerns and tougher policy regulations, such as the regulation (EC) No 1907/2006 (REACH) or the Biocidal Products Regulation (EU) No 528/2012 (Council of the European Union 2006, 2012), there is a need for alternative wood protection methods.

Sandberg et al.¹⁶ (2017) describe several reasons that have favoured the development of wood modification techniques during the past two decades. These reasons include: (i) the change of wood properties due to different silvicultural practices, (ii) interest of wood producers adding value to sawn timber, and (iii) EU policies supporting the development of a sustainable society. Due to reason (iii), the interest in life cycle assessments of wood products including modified wood has seen a recent increase^{75,76}.



(a)

Modification method	Commercial	Principle
Heat treatment	X	
Acetylation (Accoya)	X	
Melamine resin	(X)	
DMDHEU (Belmadur)	X	
Furfurylation (Kebony)	X	
Silicone/Silane	(X)	
Oil/wax/paraffins	X	

(b)

Figure 2-8 (a) Five commonly observed modes of action in different wood modification systems. (b) Summary of mechanisms active in various types of wood modification. Impregnation modification with low molecular weight PF resin uses the mechanisms lumen filling, cell wall filling, and degradation of the cell wall. Adapted from Ormondroyd et al. (2015).

Wood modification generally describes a process after which the properties of the product stay permanently altered over the course of its service life. If the durability is improved, the mode of action must be non-biocidal¹¹. In many cases wood modification changes the wood-water interactions, often enhancing the dimensional stability, which provides another important advantage over conventional preservatives^{11,16}.

Changes in the wood cell wall structure are schematically illustrated in Figure 2-8. One may distinguish between chemical, thermal, and physical modification processes, and, depending on their interaction with the cell wall, between active and passive modifications. Active modifications change the chemical constitution of the cell wall leading to different properties, whereas passive modification changes the overall properties but not the chemistry of the cell wall.¹¹

Furthermore, the term wood modification may include many techniques which aim to improve other properties than the biological durability, such as surface hardness^{77,78}, wear and weathering resistance, aesthetics, or acoustic properties⁷⁹ of wood products. Research where wood is the raw material for highly functional composites is often adjacent to wood modification. Such materials may include transparent wood¹⁵, triboelectric wood nanogenerators⁸⁰, or high strength composites with a wood matrix⁸¹. For the sake of better distinction, one could summarise these processes as functionalised wood.

In the following section, the focus will be on the commercially more advanced wood modification systems, such as acetylation, thermal modification, and low molecular weight thermosetting resin modification. Their basic properties and active modes of action shall be outlined briefly.

2.2.2. Impregnation Modification

2.2.2.1. General Aspects

Impregnation modification is based on the impregnation of wood with a bulking agent (i.e., thermosetting resin molecule) that is small enough to enter the cell wall. In contrast to chemical modifications (e.g., acetylation) this bulking agent is not required to react with the wood, although it must be fixed in the cell wall to lock it in a permanently swollen state (i.e., cell wall bulking). Certain chemicals like polyethylene glycol (PEG) may enter the cell wall, but are not fixed and therefore easily leached upon water contact⁸². Suitable bulking agents are water-soluble, polar monomers, which, together with the solvent swell the cell wall. Fixing is then typically achieved by *in situ* polymerisation, rendering the chemical insoluble in water and leading to an entanglement in the cell wall structure¹¹. Any reagent intended to react with or within cell wall polymers must be able to access micropores spaces between them (see 2.1.3.5).

The resin modification process shown in Figure 2-9, which is the main topic of this thesis, comprises three separate process steps, including the (i) pressure impregnation, (ii) drying stage at low temperatures, and (iii) heat curing stage at elevated temperatures. The pressure impregnation is governed by a variety of factors (e.g., fluid properties, applied pressure), all of which can be optimised, but the treatability of wood is crucial since anatomical features that prevent free liquid flow (e.g., aspirated pits, tyloses, `wet pockets`) are difficult to address by technological means. Therefore, impregnation modification requires either a permeable wood species⁸³, a pre-treatment which improves treatability¹³, or sample dimensions where treatability ceases to be a limiting factor (e.g., veneers)⁸⁴. In the context of veneers or surface modifications of solid wood, plasma treatments could become an alternative to lengthy vacuum-pressure cycles, as they increase the surface energy of wood, which improves the resin uptake during a simple immersion period at atmospheric pressure⁸⁵.

The drying step aims to reduce the moisture content to minimise internal stresses that would otherwise occur in the heat curing stage. Hence, the primary goal is to remove the solvent water from the wood. One side-effect that comes with it is the diffusion of bulking agent from the cell lumen to the cell wall (i.e., cell wall diffusion). This is an important mechanism, since resin located inside the cell wall is far more effective than resin located in the cell lumen^{86,87}.

To some extent, cell wall diffusion already takes place in the impregnation step, but the removal of water in the drying step introduces a concentration gradient between the cell wall and the cell lumen which causes further cell wall diffusion^{88–91}. Zheng et al.⁹² (2018) showed that the relative humidity in the drying stage had a significant impact on the degree of cell wall diffusion in melamine formaldehyde (MF) impregnated wood, where high-humidity drying schedules were generally more beneficial than low humidity ones. Other studies suggest the opposite trend⁹³. Cell wall diffusion is discussed in more detail the Chapters 6 and 8 of this thesis.

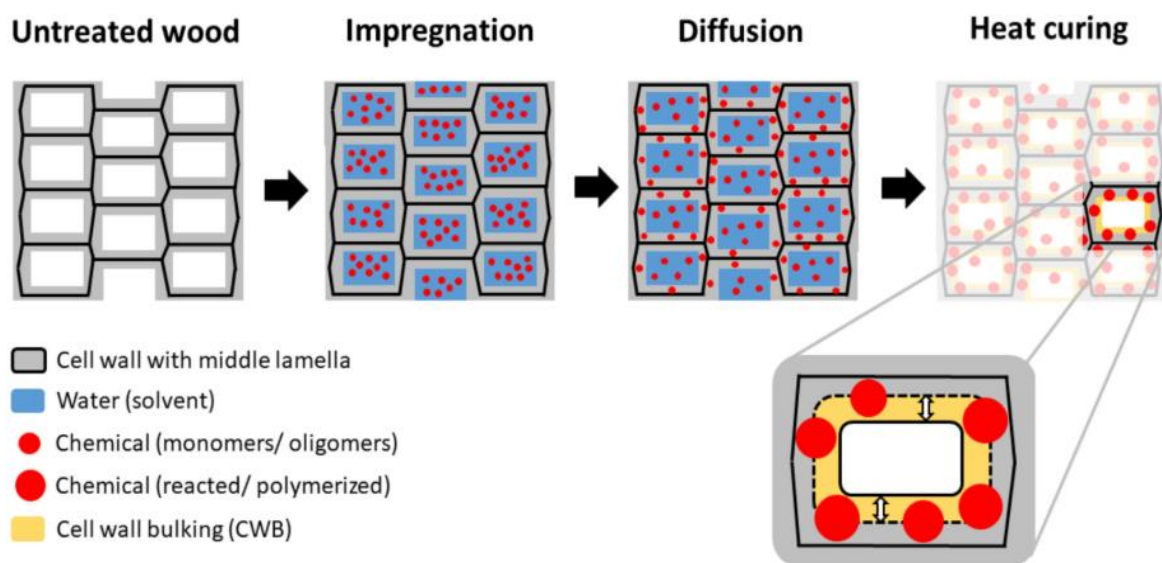


Figure 2-9 Process steps in a typical impregnation modification with thermosetting resin. Unmodified wood is impregnated with an aqueous resin solution, which is followed by a drying and diffusion step, during which solvent water evaporated and resin monomers diffuse further to the cell wall, and finally cure *in situ* through the application of elevated temperatures¹⁵

Heat curing takes place at elevated temperatures (approx. 150°C) to initiate the *in situ* cross linking reaction of the resin in the cell wall, after which the resin becomes irreversibly fixed in the wood structure¹¹. Heat curing on a laboratory scale can be done in a conventional lab oven and in dry conditions, but commercial wood modifiers must invest in specialised equipment, due to effects at planks scale that complicate this process step. The exact process parameters used by a company are confidential, but two general strategies have been observed.

For one, the *Kebony* and formerly *Lignia* processes use a system where the curing stage is performed in a closed reactor, using a pressure of up to 12 bar, which prevents water evaporation^{16,94}. This serves multiple purposes since the liquid water acts as a heat transfer medium and moisture gradients across the plank cross sections are avoided.

Another process variation used in the industry⁹⁵ (e.g., *Belmadur*) and frequently described in the literature^{93,96–98} is sometimes called wet curing. In this case, freshly impregnated wood with a high moisture content is heated in a superheated steam atmosphere under normal pressure, hence, drying and curing are combined in one process step. The use of steam guarantees good heat transfer and minimises the internal stress development. Wet curing helps to maintain a uniform resin content throughout larger specimens. The concepts of dry curing and wet curing are worth exploring at this point.

As the name suggests, dry curing takes place in a dry atmosphere (e.g., in a laboratory oven), where water evaporates from the sample and causes macroscopic resin migration from the sample core to the crosscut end grain area. This leads to an uneven resin distribution even within a single sample⁹⁹. In wet curing, water is not allowed to evaporate as the temperature increases, hence, resin migration to the surface of a plank-sized specimen is limited, and crosslinking takes place in the presence of water. In other words, the resin is immobilised before it can migrate to the sample surface. However, wet curing was found to result in lower cell wall bulking compared to dry curing, which was previously ascribed to more severe cell wall degradation in the presence of steam⁹⁶. Alternative explanations for this phenomenon will be addressed later in this thesis.

2.2.2.2. Changes in Cell Wall Structure

The cell wall bulking effect of resin is certainly the most notable feature in impregnation modification. In this context it is important to point out that the bulking coefficient (BU) is an external measure. The volume gain of the cell wall is not equal to the external volume gain measured by a calliper (i.e., BU), because upon cell wall bulking the cell wall swells into the lumen, hence the lumen volume is not constant.¹⁰⁰

The general mechanism by which impregnation modification (and others e.g., acetylation) improve the dimensional stability is the reduction of cell wall moisture variability¹⁵. Locking the cell wall in a swollen state causes spatial confinement which restricts the uptake of cell wall water to a minimum⁷⁴. The blocking of micropores, too, plays an integral role in the moisture exclusion and durability of impregnation modified wood⁶⁶. Other phenomena, such as the coating of the internal lumen surfaces with higher molecular weight resin might have a positive side effect but, ultimately, such coatings are easily bypassed by water molecules or breached by the hyphae of wood destroying fungi¹¹. Hence, the microscopic location of resin is far more important than the gross uptake that is often measured in kg/m³, which complicates the quality control in comparison to e.g., acetylated wood.

Emmerich et al.¹⁰¹ (2021) used chemically similar bulking agents with different affinities towards the cell wall to show the importance of resin cell wall depositions in durability tests. 1,3-dimethylol-4,5-dihydroxyethyleneurea (DMDHEU), which is a common treatment chemical, was compared against 1,3-dimethyl-4,5-dihydroxy-ethyleneurea (DMeDHEU), which is a similar compound with higher affinity to the cell wall. Having a similar molecule size and a lower WPG, the DMeDHEU treatment obtained an almost 100% higher BU and similar durability, solely due to the higher degree resin cell wall deposition. However, DMeDHEU is not well-fixed in the cell wall and largely lost during water storage.

The microscopic location of resin in the cell wall is studied by a number of techniques including energy dispersive x-ray detection (SEM-EDX)⁸⁶, atomic force microscopy (AFM)¹⁰², or ultraviolet (UV)-microscopy¹⁰³. For x-ray-based techniques, most resins must be brominated to increase their density and be able to detect their position in the cell wall^{86,104,105}. Some researchers observed a decreasing concentration of bulking agent from the lumen towards the middle lamella. The explanation is that resin starts migrating from the lumen inwards^{97,106–108}. Conversely, an equal number of studies found a homogeneous resin distribution throughout the cell wall or even a higher resin concentration in the middle lamella arguing that the lignin in the middle lamella has a higher affinity to some of the resins^{86, 103,109,110}.

2.2.2.3. Property Improvement

Ormondroyd¹¹¹ (2007) showed that Corsican pine treated with different thermosetting resins (e.g., UF, MF) became resistant towards various brown rotting and white rotting fungi above 30% WPG. For beech the threshold was 22% WPG. These thresholds were constant, regardless of the resin and fungi used. Grinins et al.¹¹² (2018) reported resistance

of PF treated birch veneer against *C. puteana* and *T. versicolor* at 6.6% WPG. Deka et al.¹¹³ (2002) found that wood treated with thermosetting resin became resistant towards termite attack above 30% WPG. Westin et al.¹¹⁴ (2006) compared differently modified timbers within field tests in the marine environment. Treatments with furfural alcohol (FA) at 29% WPG and MF resin at 23% WPG were shown to confer high resistance toward marine borers in wood.

While these threshold values, especially those obtained in field tests, are useful to some extent, they must be handled with care since they are based on the gravimetric resin uptake and on standards that have been developed for conventional preservative treatments (i.e., EN 113). Hence, the gravimetric uptake makes no statement about the microscopic resin location, and the non-biocidal mode of action preventing decay may not be reflected adequately by the test conditions in the according standard¹¹⁵. Ringman et al.¹¹⁶ (2014) summarised the five most common theories explaining how wood modifications limit fungal decay as follows:

- (i) fungal non-recognition of the substrate,
- (ii) blocking of easily accessible nutrients,
- (iii) physical blocking of wood micropores,
- (iv) alteration of wood hydroxyls prevents hydrolysis,
- (v) reduced cell wall moisture restricts diffusion of active substances in the cell wall.

While mechanism (i) can be largely ruled out, the consensus in the literature currently suggests that a reduced cell wall moisture content plays an integral role in wood protection. The mechanisms by which moisture is excluded from the cell wall of modified wood are discussed elsewhere in this literature review. Recent insights into the decay kinetics of modified wood, indicating a delay rather than prevention of decay¹¹⁵, hint at the importance of slowly-proceeding diffusion mechanisms¹⁵. Hence, while the role of moisture exclusion is acknowledged, it remains elusive how this protects the wood from decay.

An important role could be the retardation in the diffusion of decay initiators, such as Fenton's reagent in case of brown rots^{115,117}. Moreover, the presence of an interconnected network of hemicelluloses undergoing a moisture-induced glass transition could be relevant, as this transition coincides with the moisture range where decay occurs⁵⁷. This model rejects the idea of connected water pathways being responsible for diffusion processes in wood with a moisture content between 15 – 30%. Instead, it is proposed that moisture-induced relaxations render the hemicelluloses rubbery, with their high mobility enabling the transport of metal ions through the cell wall¹¹⁸. If a wood modification restricts the relaxation process of this interconnected hemicelluloses network, active fungal substances would be excluded.

Considering the enhancement in the dimensional stability, a general rule of thumb is that a lower molecular weight (MW) leads to a higher dimensional stability and durability¹¹⁹. Furuno et al.⁸⁶ (2004) observed 65% ASE in sugi wood (*Cryptomeria japonica*) treated with a low MW PF resin (290 g/mol) compared to only 26% ASE in wood treated with slightly higher MW resin (470 g/mol).

The efficiency of the treatment typically increases with the resin concentration, since more micropores can be filled by resin molecules⁸⁷. However, there is a limit to the improvement, either because the cell wall saturates above a specific resin concentration or due to a shortage of available solvent water to swell the micropore network⁹⁰. Grinins et al.¹²⁰ (2019) found that the ASE of birch veneer improved up to 20% resin concentration. A higher concentration had no further effect on the ASE or BU¹²⁰.

Biziks et al.¹²¹ (2019) showed that the BU of beech wood increased up to 27% PF resin concentration. The BU in the same study increased with a decreasing MW. Wang et al.¹²² (2019) noticed improvements in the ASE of PF treated Masson pine up to a resin concentration of 30%.

The hardness of resin treated wood is significantly higher compared to most other modifications, but the ability of the material to accumulate plastic deformation disappears. This leads to a general decrease in impact toughness, fatigue strength, and work in bending, which is often proportionate to the reduction in swelling^{123–125}.

2.2.2.4. Commercialisation

Many bulking agents are described in the literature, although only some of them are suitable for upscaling. The early work from the Forests Products Laboratory in Madison, Wisconsin focused on low molecular weight PF, UF, and dimethyl urea resin and found water soluble PF resin most promising¹²⁶. From this work the two veneer-based products *Impreg* (i.e., impregnated with PF) and *Compreg* (i.e., impregnated and densified) emerged. Compreg products were used during the second world war to manufacture aircraft propellers, and even today, there are Compreg products available for multiple niche application (e.g., *Permal*¹²⁷, *CK-Composites*¹²⁸).

Until recently, *Lignia Wood Company Ltd.* produced PF treated solid wood for flooring, cladding, decking, and joinery applications. The dimensional stability, durability, hardness, and weathering resistance of these products improved significantly compared to unmodified wood, so that *Lignia* wood was marketed as substitute for high quality tropical hardwoods¹²⁹. The main wood species used by *Lignia Wood Company Ltd.* was Radiata pine, although research was undertaken to diversify the raw materials supply.

Wood modification with FA was studied since the 1960s and has been commercialised as *Kebony* and *Nobelwood* during the early 2000s. FA is derived from sugar cane bagasse, which is a by-product from sugar production. The wood species used for *Kebony* include Radiata pine, Southern Yellow pine, maple, and Scots pine¹⁶. The production volume in 2021 was 31,000 m³.¹³⁰

DMDHEU originates in the textile industry but its suitability for wood modification was confirmed during the 1990s¹³¹. DMDHEU acts as a crosslinker between cellulose chains, but the cell wall bulking effect is the mode of action primarily responsible for dimension stabilisation and durability. Sustained research led to the pilot scale production of the product *Beladur* (by BASF) in 2016, however, market introduction has failed. One limiting factor are the formaldehyde emissions, therefore, research now continues towards low-emission alternatives¹³¹. In the field of wood functionalisation, a combined treatment of delignification followed by compression and DMDHEU impregnation was used to produce mouldable composites with a wet strength of up to 60 MPa.⁸¹

A recently developed technique, which is concurrently studied by two research groups at Goettingen University (i.e., *SorCa*) and Norwegian Institute of Bioeconomy (i.e., *CIOL*) uses a bulking agent based on sorbitol and citric acid¹³². These chemicals are non-toxic and comparably cheap, making them suitable for upscaling and commercialisation. The reaction mechanism is not yet fully understood. For one, it is possible that citric acid forms covalent bonds with wood, especially with the hemicelluloses fraction. Wood polymers may also be crosslinked by the sorbitol and citric acid esters. On the other hand, sorbitol and citric acid may react without the involvement of wood polymers, in which case the treatment would be solely based on the cell wall bulking effect.

Combined treatments are another possibility to enhance material properties even further. The combination of thermal modification and resin modification gave rise to the product *TESUMO* in Germany. This product is primarily intended for yacht decking and should act as an alternative for teak wood. Several other combined modifications are currently under investigation, but none them are commercially viable yet^{111, 124,133–136}.

2.2.3. Acetylation

2.2.3.1. General Aspects

Acetylation is the best-known chemical wood modification and commercially available products like *Accoya* and *Tricoya* are well-established on the market. The first experiment involving acetylation of wood was reported by Fuchs (1928) in Germany, however, the dimensional stabilisation effect in wood was not recognised until the 1940s and 50s. Acetylation is the chemical reaction of wood hydroxyl-groups with acetic anhydride. This reaction yields an acetyl group and acetic acid as a by-product, as shown in Figure 2-10. It is a single replacement reaction, hence, no crosslinking or other reactions are involved.^{11,137}

2.2.3.2. Changes in Cell Wall Structure

In acetylated wood, the level of modification is expressed by the WPG and BU, which result from the acetyl group being heavier and larger than the hydroxyl-group that has been replaced¹³⁸. The effects of this replacement on the cell wall are twofold. For one, the cell wall bulking leads to the physical exclusion of water, which was shown to be the main driver for the reduction in water sorption and the improvement of durability^{138–140}. Secondly, the acetyl group is less polar than the hydroxyl-group, which affects the water sorption to a smaller extent^{140,141}.

Cell wall polymers differ in their affinity towards acetic anhydride. The reactivity decreases in the following order: amorphous cellulose, hemicellulose, lignin¹¹. The study of different molecular weight anhydrides has shown that the reduction in cell wall moisture content is a function of weight gain rather than hydroxyl-substitution^{138,140}. In other words, higher molecular weight anhydrides might substitute fewer hydroxyls than acetic anhydride, but these unreacted hydroxyls in the cell wall are rendered inaccessible to water because of the cell wall bulking effect^{74,142}. Hence, spatial confinement of wood polymers in the cell wall is crucial⁷⁴.

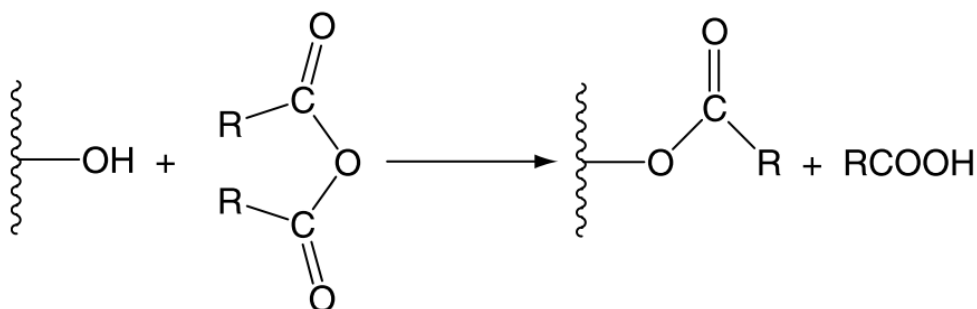


Figure 2-10 Acetylation is a well-established chemical wood modification. The reaction occurs between hydroxyl-groups in wood and acetic anhydride where R is -CH₃. The reaction with other anhydrides is possible but not commercially viable.

2.2.3.3. Property Improvement

Both ASE and BU increase in a linear fashion with the WPG of acetylated wood. At higher modification levels (i.e., WPG > 20%), the ASE improves more gradually¹⁴¹. Mechanical properties of acetylated wood are broadly comparable to those of unmodified wood. Typically, a slight increase in hardness is observed, while the MOE and MOR are often said to be unaffected¹³⁷. The reduction of EMC at a given RH benefits the mechanical properties. Cell wall degradation by acetic

acid and the lower potential of wood polymers to form hydrogen-bonds could be detrimental¹¹. Nevertheless, acetylated wood has been used for load bearing outdoor application, as shown in Figure 2-11.

The biological durability of acetylated wood was shown to be excellent towards brown rot and white rot fungi, termites, and marine borers^{114,137}. This applies for both laboratory and field tests. Until recently, it was assumed that certain decay thresholds in terms of WPG are set for different wood destroying organisms. For example, in pure culture tests it was observed that 10% WPG often sufficed to fully protect against white rots. The “full” protection against brown rots typically required 20% WPG¹¹.

These thresholds are based on standard procedures (i.e., EN 350) with an incubation time of 16 weeks. More recent studies have shown that the decay is not prevented, but greatly slowed down^{115, 117,143}. Fungal organisms are active in acetylated wood but need more time to initiate decay than in unmodified wood. Once initiated, decay proceeds at a similar rate and leads to a similar mass loss as in unmodified controls¹¹⁵. The decay is preceded by the loss of acetyl groups. Variability in decay behaviour between different labs may be caused by differences in wood species, and virulence of the culture¹¹.

2.2.3.4. Commercialisation

Koppers Inc. attempted to introduce acetylated wood in the 1960s but failed due to the economic climate at the time. *Daiken Wood Industry* uses acetylated wood for flooring products since the 1980s¹⁴⁴. *Eastman Chemical*, a major cellulose acetate producer, opened an acetylation plant in 2012 and sold their product *Perennial Wood* until 2014¹⁴⁵. The main product now is *Accoya* – acetylated solid wood – produced by *Accys Technologies* since 2007 in the Netherlands¹⁴⁶. The annual production volume in 2021 was 60,000 m³. The wood species treated include Radiata pine, alder, spruce, and Scots pine¹⁶. The production of *Tricoya* – medium density fibreboard (MDF) made from acetylated wood chips – is planned to be extended at a new site in Hull, UK.



Figure 2-11 Highway bridge certified for 65 t load. Construction is made of acetylated glue laminated timber. Sneek, Netherlands.³¹⁹

2.2.4. Thermal Modification

2.2.4.1. General Aspects

In thermal modification, wood is exposed to elevated temperatures, causing chemical changes that result in a darker colour and enhance biological durability as well as dimensional stability¹¹. Thermal modification is often perceived to be environmentally friendly because it does not require the use of chemicals.

Thermal modification is influenced by process variables, such as treatment time and temperature (i.e., 160 – 260°C), treatment atmosphere (e.g., air, vacuum, steam, N₂), the choice of an open or closed system, and size and species of wood samples.¹¹

The level of modification is often expressed by the dry mass loss resulting from hemicellulose degradation. This degradation is strongly affected by the selected process variables. The mass loss in hardwoods, closed systems, and treatments with high temperature is generally higher than in softwoods, open systems, and low temperature treatments¹¹. The level of modification can be assessed more accurately by the elemental composition¹⁴⁷.

The presence of oxygen favours oxidative processes in the wood, resulting in the loss of mechanical properties. Therefore, heat treatments differ primarily from each other in their oxygen exclusion strategy. Treatment media include steam, partial vacuum, inert gas, or vegetable seed oil. Heat treatments in the presence of steam are also called hydrothermal processes. The steam acts as heat transfer medium and protective layer against oxidation. Wet conditions accelerate the mass loss, initially increase cellulose crystallinity, and lead to a permanent reduction in hygroscopicity^{148,149}.

Treatments can be performed in an open or closed system. Green wood heated in a closed system generates superheated steam, and the pressure inside the reactor increases up to 13 bar. In an open system, the atmosphere can be exchanged and cleaned of degradation products (e.g., acetic acid). In the closed system these degradation products accumulate, accelerating certain degradation reactions.¹¹

2.2.4.2. Changes in Cell Wall Structure

Thermal modification reduces the equilibrium moisture content (EMC) at a given relative humidity (RH), typically including a permanent and a non-permanent component^{149,150}. The permanent reduction is attributed to the removal of hemicelluloses, whereas the non-permanent reduction is probably caused by drying stresses which are relaxed upon water soaking. Steam treatments seem to prevent the build-up of drying stresses, therefore the EMC reduction after such treatments is largely permanent¹⁴⁹. It is worth noting that the alteration of wood-water interactions occurs before any observable mass loss is detected¹⁵¹. Hence, hemicellulose degradation cannot be the only factor changing hygroscopicity.

The degradation of hemicelluloses in a thermal treatment is typically described as follows^{11,152,153}: acetyl groups are hydrolysed and form acetic acid, which promotes cleavage of the β -(1-4) glycosidic bond in amorphous polysaccharides. These amorphous polymers are broken down to monomers, which are dehydrated to furfural, hydroxymethylfurfural, and other monomeric compounds. Polysaccharide degradation products probably react with lignin. Hemicelluloses constitute a larger fraction in hardwoods, and are also more frequently acetylated than in softwoods¹⁵⁴. Therefore, the release of acetic acid and subsequent degradation are more severe in hardwoods¹¹.

During the initial stages of the treatment, the crystallinity index of the wood increases. This results not only from the loss of amorphous fractions, but also from the reorientation of cellulose in the presence of steam¹⁴⁸. Lignin is known to be the most thermally stable cell wall component. Nevertheless, it undergoes certain depolymerisation and repolymerisation reactions. Linkages at α -O-4 and β -O-4 are cleaved and form aldehyde units. Methoxy groups are cleaved from the aromatic ring and free up new reactive sites, which are then crosslinked via methylene bridges. Furan and other degradation products are involved in these crosslinking reactions¹⁵³.

2.2.4.3. Property Improvement

Dimensional stability in thermally modified wood results from (i) degradation products that bulk the cell wall and prevent water absorption, (ii) the decrease in hydroxyl-groups reducing overall hygroscopicity, (iii) crosslinking of lignin with itself and degradation products, and (iv) changes in the mobility of the polymer network¹⁵⁵. The dimensional stabilisation effect decreases throughout repeated cycles of wetting and drying. This is due to extractives and degradation products that bulk the cell wall initially but can be washed out in water¹⁵⁵. The ASE improves up to a mass loss of approximately 20%. A higher mass loss leads to no further improvements¹⁵⁶. Interestingly, the swelling in concentrated NaOH, pyridine, and morpholine was found to be unaffected by thermal modification¹⁵⁶.

In an attempt to understand the most influential factors during the process, Zhan et al.¹⁵⁷ (2021) compared 48 studies in a meta-analysis focussing on the ASE in thermal modification. Their results suggest that both the material properties (e.g., growth location, plantation, or natural growth) and the process conditions (e.g., time, peak temperature, heat transfer medium) significantly affect the ASE. The ASE in hardwoods, heartwood, and plantation timbers was highest. Regarding the process conditions, shorter treatment times (under 4 h), peak temperatures in the range of 150 – 180°C, and an initial moisture content of 13 – 16% appear to yield the highest ASE values.¹⁵⁷

The biological durability towards brown rots and white rots improves with thermal modification and full protection can be achieved in pure culture tests^{158,159}. However, as previously discussed for acetylation, the onset of decay in thermally modified wood is merely delayed and the rate at which decay occurs is slowed down rather than prevented. The relevant modes of action for thermally modified wood include loss of hemicellulose as an easily accessible nutrient, the reduction in EMC and number of hydroxyl-groups, a reduction in pH value, and possibly fungicidal degradation products trapped in the wood^{116,159,160}. Thermally modified wood is suitable for applications in use class 1, 2, and 3, hence cladding and decking above ground are the main applications¹⁶¹. It is not suitable for applications in ground contact¹⁶² and little protection is provided against soft rot fungi and wood destroying insects¹¹.

Thermal modification always results in a decrease of mechanical properties and particularly in the embrittlement of the material. Hence, the reduction of impact strength and tensile strength parallel to the grain is more severe than the decrease in hardness^{163–165}. Furthermore, chemical changes of the cell wall affect the surface energy. Therefore, an increased contact angle of water, a reduced capillary water uptake, and possible chemical interaction with degradation products must be considered in the use of coatings and adhesives^{151,166}.

2.2.4.4. Commercialisation

In recent decades, thermal modification has seen numerous commercialisations and the global production of thermally modified wood is ever growing¹⁶¹. With a total production volume of more than 500,000 m³ and more than 100 producers, mainly based in Europe, thermal modification is by far the most commercially advanced wood modification

at the moment^{15,167}. As thermal modification allows for a high level of variation in process conditions, there is not just one standardised process, instead, various systems coexist on the market.

The open and dry process is the most common variant because it allows the use of larger kilns. *Thermowood* in Finland was the first product to enter the market in the 1990s using a steam process. Companies like *Finnforest* or *Stora Enso* are producing under the *Thermowood* patent. Under this patent, wood is heated to temperatures between 150 – 240°C for 0.5 – 4 h in the presence of steam¹⁶⁸.

The Plato process, developed by *Shell* in the 1980s and now operated by *Plato Company* in the Netherlands, consists of four steps: (i) heating, (ii) drying, (iii) curing, (iv) conditioning¹⁶⁸. Wet wood heated in a closed system generates steam and pressures up to 12 bar. In the first step, phenols and aldehydes are released between 160 – 190°C for 4 – 5 h. Subsequent drying requires several days and curing of the released substances is achieved again between 170 – 190°C.^{153,168}

Inert gas processes, e.g., by *Balz Holz* in Switzerland, are operated in smaller kilns due to issues with gas consumption and air tightness¹⁶¹. In this variant of the process, pre-dried wood (MC 12%) is heated to 210 – 240°C¹⁶⁸.

Vacuum treatments prevent the accumulation of degradation products in the kiln. However, as both vacuum and dry wood are bad heat conductors, the vacuum method relies on contact plates for heat transfer, which requires a high manual workload in commercial production.

Until recently, *Menz Holz* produced thermally modified wood in Germany, employing a heat treatment with vegetable seed oils such as rapeseed, linseed, and sunflower. In this process, oxygen is displaced by the oil and a temperature of 200 – 220°C must be maintained in the core of the plank for 2 – 4 h. Oil heat treatments claim to maintain the stiffness of the material, although its strength is still reduced¹⁶⁸. Currently, oil-heat treated wood is produced by the Canadian firm *Qijuk*.

2.3. Phenol Urea Formaldehyde Resin

2.3.1. Raw Materials and Production

Phenol formaldehyde (PF) resin was the first polymer artificially synthesised by mankind. This was when Leo Hendrik Baekeland started producing so called *Bakelite* in the early 20th century. Due to its high chemical, moisture, and thermal stability, similar PF polymers are still used today in various applications across many industries, such as moulding compounds, thermal insulation, coatings, as a matrix material, or in light weight foams.^{169,170}

Pure phenol is a highly toxic, colourless solid which becomes liquid in the presence of small amounts of water. Unlike aliphatic alcohols, phenol is mildly acidic because of its resonance stabilised phenolate ion. Phenol is mainly used in the production of PF resins and bisphenol-A (BPA). The majority of phenol is produced from fossil fuels (e.g., coal, mineral oil,) in the cumene process¹⁷⁰. However, there are increasing efforts to devise PF resins from renewable sources like lignin or cashew nut shell oil^{171,172}.

Formaldehyde is a colourless gas with a melting point at –92°C. With a production volume of 20 million tonnes in the year 2019, it is one of the most produced organic chemicals worldwide. It is synthesised by the oxidation of methanol. More than half of the formaldehyde production is used in the synthesis of thermosetting resins for the wood products industry¹⁷⁰. However, formaldehyde is carcinogenic and therefore subject to increasingly strict regulations in the indoor environment.

Urea is a colourless, low-toxic solid, that is highly soluble in water. In the wood industry, urea is used to synthesise urea formaldehyde, and melamine formaldehyde resins. Urea can be added to other resins (e.g., PF) in order to lower costs, reduce viscosity, and as a formaldehyde scavenger¹⁷³. Phenol, formaldehyde, and urea are the raw material for the production phenolic resins.

Thermosetting PF resins (or resoles) are synthesised in an alkaline environment with a molar ratio of formaldehyde (F) to phenol (P) greater than 1. The solubility of resoles depends on the molecular weight and pH value. An alkaline catalyst, such as NaOH or KOH, often has the side-function of increasing the resin solubility in water. Liquid resoles are crosslinked through heat curing¹⁷³.

Thermoplastic phenolic resins that are synthesised with a molar ratio (F/P) smaller than 1 are called Novolacs. Novolacs are meltable solid thermoplastics which are used in the microelectronics and rubber industry. The curing of novolacs is initiated by an external formaldehyde source (e.g., hexamethylenetetramine or HEXA). Once cured, both resoles and novolacs have similar properties¹⁷⁴. However, novolacs are practically not relevant in the wood industry, so the focus will be on resoles in the following.

The production of resole type resin includes an alkaline catalysed addition reaction and a heat-driven condensation reaction. The manufacturing process is described in more detail elsewhere¹⁷³. Once cured, resoles are rigid solids with a dark reddish, milky white or pinkish colour, depending on their pH value¹⁷⁵. Resoles used as wood adhesives usually have a molar ratio (F/P) between 1.8 and 3.0, a solids content around 45 – 48%, a pH value of 10 – 13, and a viscosity of 300 – 900 mPa*s¹⁷³. Phenolic resins used for wood modification have a lower solids content (e.g., 15 – 30%), pH value (e.g., 9 – 10), and viscosity (e.g., 150 mPa*s)^{122,176,177}.

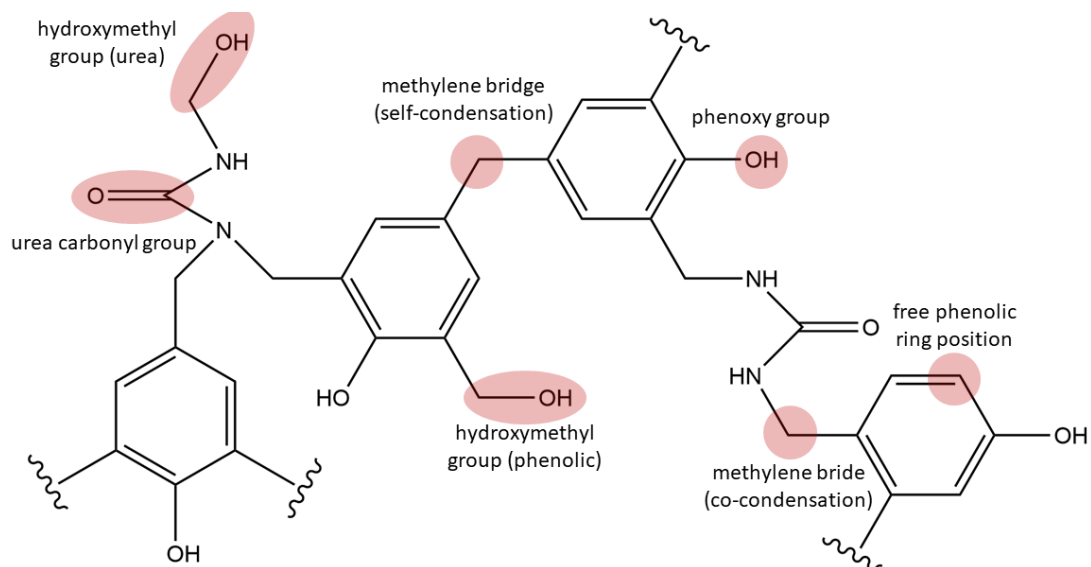


Figure 2-12 Chemical structure of phenol urea formaldehyde resin. Self-condensation of phenolic units and co-condensation of phenolic and urea units occurs via methylene bridges in alkaline conditions.

Compared to other wood adhesives, PF resin is typically associated with high bond strength, high cost, and long curing times. It is mainly used in structural and outdoor applications. UF resin which is low cost, fast-curing, but hydrolysis unstable, is preferably used for interior applications¹⁷³. There are various possible ways of combining the benefits of both in a PUF resin. One common approach is the mechanical mixing of urea into already synthesised PF resin¹⁷⁸. This has the benefit of reducing the viscosity, lowering manufacturing costs, and scavenging formaldehyde. Another

possibility is the co-condensation of phenol and urea units in the synthesis process. Co-condensed PUF resin has a faster curing time than PF resin alone¹⁷⁹. The synthesis may proceed in an alkaline or acidic environment^{180,181}. Urea and phenol structures may be linked via methylene and ether bridges as shown in Figure 2-12. The self-condensation of phenol structures is possible under alkaline and acidic conditions, however, urea self-condensation is restricted in an alkaline environment¹⁸².

2.3.2. Laboratory Methods for Thermosetting Resins

A thermosetting resin is characterised by parameters like solids content, viscosity, gel time, pH value, molecular weight, and curing temperature, among others. The following section aims to present relevant characterisation methods for some of these parameters.

Thermosetting resins are often a mixture of reactive monomers, oligomers of higher molecular weight, and unreacted raw materials. Information about the molecular size distribution are typically obtained by gel permeation chromatography (GPC) in which the sample runs through a porous gel (e.g., polystyrene or dextran based) and different molecular fractions are separated by size and polarity^{173,183,184}. High pressure liquid chromatography (HPLC) is favourable for separating low molecular weight compounds based on polarity, molecular size, or charge. HPLC was frequently used to study the early stages of PF resin synthesis^{185–187}. Further information about molecular size may be obtained from other techniques such as matrix assisted laser desorption/ionisation (MALDI-TOF) or NMR spectroscopy^{188,189}.

Crosslinking reactions of resin are often exothermic (i.e., generate heat) and endergonic (i.e., do not occur spontaneously but only at certain conditions). This curing behaviour is studied by thermoanalytical methods (e.g., DMA, DSC, TGA). Dynamic mechanical analysis (DMA) applies an oscillating force to a sample while it is heated or cooled across a temperature range and measures the proportions of elastic and viscous response of the sample. It directly shows the emergence of cohesive forces during resin curing¹⁹⁰. The mechanical curing measured by DMA is often completed before the chemical curing measured by differential scanning calorimetry (DSC)¹⁹¹. DSC allows quantitative calorimetric measurements by recording the heat flow into and out of the sample while it is heated, cooled, or held a certain temperature. The measurement is compared to an inert reference material allowing distinction between endothermic and exothermic events. DSC can be combined with TGA (thermogravimetric) analysis which measures the weight loss related to certain reactions. Similarly, if no weight loss occurs, exotherms or endotherms can be assigned to physical phase transitions (e.g., glass transition, melting). DSC–TGA analysis is often used to model the reaction kinetics such as activation energy or rate constant of resin curing^{70,192}. DSC analysis includes a variety of experiments like single-heating rate, multi-heating rate, or isothermal runs.

Structural analysis identifies chemical bonds in resin but can also show reactions taking place during curing. Various forms of spectroscopy (e.g., FTIR, NMR) are used for this task. Fourier Transform Infrared Spectroscopy (FTIR) measures the interaction of a sample with infrared light (i.e., wavenumber 400 – 4000 cm⁻¹). Light with this wavelength excites molecular vibrations (e.g., stretching, bending, rocking) causing an absorption for each molecular vibration present in the sample¹⁹³. FTIR spectroscopy is frequently used to study the curing reaction of resin or its interactions with wood^{194,195}.

NMR spectroscopy provides information about the chemical environment of a certain nucleus in a sample. In most organic substances the measured nucleus is ¹H or ¹³C. Usually their nuclear spins are in one of two possible energy states. In NMR experiments all nuclear spins are aligned in an equilibrium state after applying a static external magnetic

field B_0 . Another oscillating magnetic field B_1 is applied to move nuclear spins out of their equilibrium state. Depending on the chemical environment (e.g., in an aromatic ring, close to an electronegative atom, or in an aliphatic chain) the nucleus is differently shielded from B_1 by its own magnetic field. This shielding is expressed by the chemical shift, and the frequency of the nucleus is shown by the relative intensity of a peak¹⁹⁶. NMR detects chemical bonds in resin and wood with high accuracy and has been used to determine the crosslinking density after cure^{175,197}. This is defined as the ratio of methylene bridges to phenolic cores. The crosslinking density increases with molar ratio (F/P), curing temperature, and curing time. However, if the temperature is too high and curing times too long, the crosslinking density decreases as methylene bridges are decomposed¹⁷⁵.

2.3.3. Chemical Reactions of Phenolic Resin

During resin synthesis, the raw materials phenol (P) and formaldehyde (F) are converted to a resole type resin in two main reactions. (i) The first reaction (i.e., addition reaction) is the nucleophilic addition of F to the phenolate ion creating reactive hydroxymethyl phenols (HM-P) which is shown in Figure 2-13 (a)¹⁹⁸. (ii) The second main reaction (i.e., heat curing) is the condensation of HM-P with itself and with P via the formation of methylene and ether bridges as shown in Figure 2-14 (a-c)^{170,173}. The chemical formulation of the resin is adjusted in the synthesis process. It significantly affects the properties of wood products like the internal bond strength and formaldehyde emissions of fibre boards and particle boards¹⁹⁹. The resin formulation can even be optimised for different wood species¹⁹⁰. The role of urea (U) as a raw material is addressed in more detail in chapter 4 of this thesis.

The addition reaction is favoured by low temperatures and high alkali concentrations^{170,173}. The reaction mechanism is illustrated in Figure 2-13 (a-c). Alkaline conditions favour the formation of resonance stabilised phenolate/enolate ions with a significant negative charge at the *ortho* and *para*-positions of the phenolic ring (Figure 2-13 a). The nucleophilic addition (S_N2) of the phenolate anion onto F forms HM-P, either in the *ortho* (2-HM-P) or *para*-position (4-HM-P) as shown in Figure 2-13 (b-c). The conversion of HM-P to its highly reactive quinone form is also considered a relevant step in some cases^{194,198}.

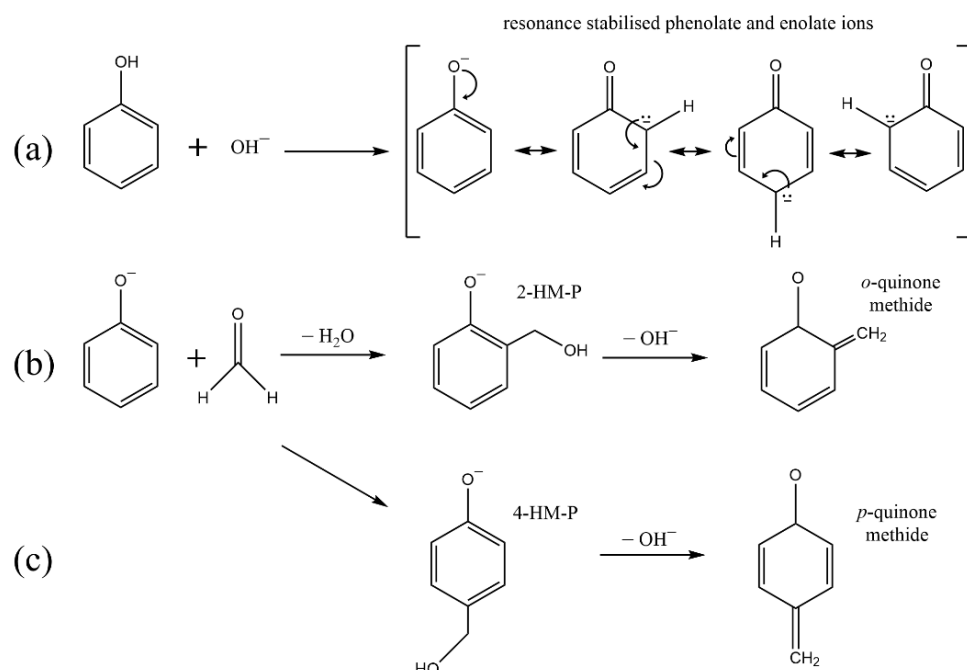


Figure 2-13 (a) Formation of resonance stabilised phenolate ions from phenol under alkaline conditions, Nucleophilic addition of phenolate ion to formaldehyde in the *ortho* position (b) and *para* position (c).¹⁹⁸

The monomer 2-HM-P is the first compound formed at low temperatures, with a higher rate constant than 4-HM-P because more free *ortho*-positions are available at this stage (i.e., 2 *ortho*, 1 *para* per phenol)¹⁸⁷. Grenier-Loustalot *et al.*²⁰⁰ (1996) reported a ratio of 2-HM-P to 4-HM-P of 1.8 during the early stages of the reaction. The *para*-position becomes a relevant reaction site later in the process when most *ortho*-positions have been substituted. Then, 2-HM-P and 4-HM-P reach maximum concentrations and begin to disappear while further F is added to the phenolic core^{187,201}. Di-hydroxymethylphenol (DHM-P) and 2,4,6-tri-hydroxymethylphenol (THM-P) are formed this way and begin to crosslink as soon as they are formed²⁰¹⁻²⁰⁴. Small amounts of free formaldehyde and phenol will always remain unreacted in the synthesis¹⁸⁶.

With the formation of the first HM-Ps, the condensation reaction starts a chain building process. In the resin synthesis, the reaction temperature is now increased until the mixture reaches the desired molecular weight which corresponds to the viscosity at this stage²⁰⁵. Then, the reaction vessel is cooled down to stop the crosslinking and the resin synthesis is completed. The final crosslinking takes place in the application of the resin¹⁷³.

The main chemical curing reactions available to PF resin are shown in Figure 2-14. Pathway (a) shows the electrophilic addition of a hydroxymethyl (HM) group to a free phenolic ring position releasing a water molecule. Pathway (b) shows the reaction of two HM-groups releasing water and formaldehyde. Pathway (b) is kinetically more favourable than pathway (a) making it the main reaction under alkaline conditions²⁰⁶. Pathway (c) shows the formation of ether bridges, which is favoured in a neutral environment but irrelevant under alkaline conditions. Ether bridges are converted to methylene bridges at high temperatures (> 160°C) releasing water^{175,194}. Emerging dimers are linked via *para-para* (*p-p*) and *ortho-para* (*o-p*)-methylene bridges. The *ortho-ortho* constellation is sterically hindered and does not form in the neat resin²⁰⁷. However, low molecular weight PF resin cured in the presence of wood may form *o-o*-methylene bridges¹⁹⁸.

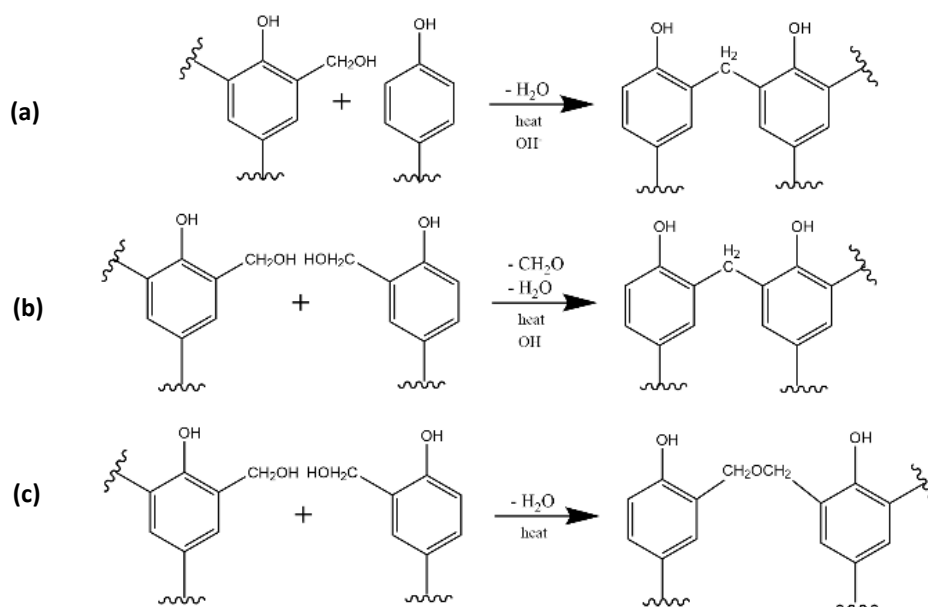


Figure 2-14 Crosslinking reaction of phenolic resin. (a) methylene bridge formation in free phenolic ring position, (b) methylene bridge formation via hydroxymethyl groups, (c) ether bridge formation in pH neutral conditions.

As the chain building proceeds, the PF-polymer undergoes multiple physical phase changes, namely gelation (i.e., liquid to rubbery), vitrification (i.e., rubbery to glassy), and crosslinking (i.e., reducing molecular mobility). Changes in the physical phase impact on the curing kinetics. In the beginning the curing system is governed by multiple simultaneous

reactions that, in summation, require a large activation energy. Beyond a certain degree of cure, larger polymers have formed, and the time required for diffusion to a reaction site becomes a significant factor. Hence, the overall rate constant becomes lower, and the activation energy decreases towards the end of the curing reaction. Therefore, one can divide the curing reaction into a kinetic regime in the beginning and diffusion regime in the end.¹⁹²

Alkali (e.g., NaOH, KOH) serves as a catalyst in resoles, but also improves the resin solubility, viscosity, and longevity¹⁷³. Negative effects of alkali used in wood panels include increased hygroscopicity, creep formation, and stains on the board¹⁷³. Interestingly, the relationship between alkalinity and reactivity of a PF resin is non-linear. Pizzi & Stephanou²⁰⁸. (1993) observed a maximum reactivity (i.e., minimum gel time) between pH 7 and 9. Retardation effects at higher alkalinity are explained by either (i) intramolecular chelate formation or (ii) quinone formation. The sodium chelate formation incorporates the 2-HM group and consequently reduces its reactivity²⁰⁹. In case (ii) it is assumed that quinone species are less reactive to form methylene bridges with each other. Hence, as the proportion of quinone species increases with pH value, the reaction rate drops²⁰⁸. The rate of the addition reaction is correlated to the ionic radius of the hydrated cation used in the catalyst. The conversion time of F decreases in the following order with the cation type²⁰⁰: Mg > Ca > Ba > Li > Na > K. Catalysts other than alkali include hydroxymethylurea, propylene carbonate, or ammonia^{210,211}.

2.3.4. Chemical Interactions between Phenolic Resin and Wood Polymers

The curing behaviour of PF resin is significantly affected by the presence of wood and wood extractives^{212–215}. The exact nature of this interaction remains unclear. The presence of wood may lower the activation energy required for resin cure by (i) catalytic self-condensation²¹² or by (ii) the formation of covalent bonds with lignin²¹⁶. If present, mechanism (ii) would have a comparatively small effect on the activation energy²¹⁶. Catalytic self-condensation, if present, would be induced by dipolar forces and hydrogen-bonds originating from cellulose. These secondary forces would polarise the C-atom of the HM-group and the O-atom of the phenolic hydroxyl-group, as shown in Figure 2-15. This way, methylene bridge formation might be accelerated. He & Riedl²¹² (2004), on the other hand, observed an increased activation energy for PF resin at pH 10 in the presence of wood. This was explained by wood lowering the pH value of the reaction system. Isolated cellulose with a neutral pH value did not affect the activation energy at all. Therefore, it remains questionable if catalytic self-condensation occurs.

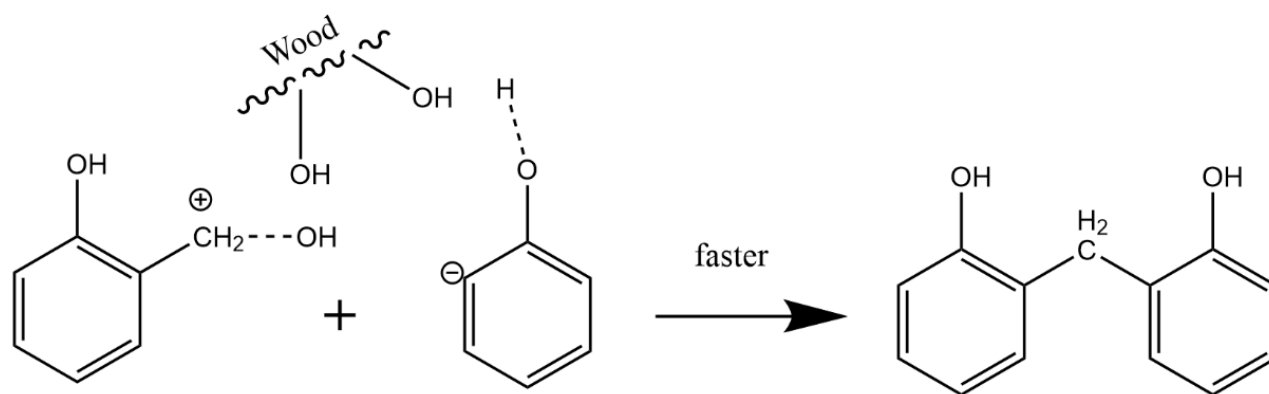


Figure 2-15 Theoretical framework of the catalytic self-condensation mechanism which is induced by the polarisation of the hydroxymethyl group and the phenoxy groups through hydrogen-bonding with wood carbohydrate²¹⁶.

As the reactivity of the resin depends on the pH value and wood is an acidic material, the alkalinity of the resin should be considered. He & Yan²¹³ (2005) compared two commercial PF resin with pH 11 and pH 13 and found that the presence of wood lowered the activation energy in both cases. PF resin appears to have the lowest activation energy around pH 10–11. Hence, if wood is added to a highly alkaline resin, it may accelerate cure by moving the reaction system towards the optimum pH value. However, if it is added to a mildly alkaline resin the curing reaction may be retarded by moving out of the optimum. Hence, changes in activation energy seem to be caused by changes in pH value rather than by catalytic self-condensation or covalent bonds with wood.

Water soluble wood extractives related to organic acids (e.g., gallic, citric, acetic acid) have been shown to lower the resin pH value and influence the curing rate as well²¹⁴. Other wood extractives may have different effects. Hydrophobic extractives (e.g., waxes, fatty acids) may impair the wettability of the wood surface. Pinosylvins and pinosylvins monoethylether, which readily occur in pine heartwood may act as formaldehyde scavengers²¹⁵. Any of these effects are more likely to affect the heartwood, which is rarely used for wood modification with thermosetting resins.

The wood cell wall is a microporous structure composed of polymers with varying polarity, crystallinity, and rheology²⁷. The precise incorporation of resin in this structure is a complex field of study. Early molecular dynamics studies have indicated that PF resin may be fixed in the cell wall through intermolecular hydrogen-bonds with cellulose. Therefore, covalent bonds are not required to develop good bond performance^{217,218}. This principle is still true today, however, more advanced techniques are available to detect even rare covalent bonds. Yelle & Ralph¹⁹⁸ (2016) utilised ¹H-¹³C-Heteronuclear Single Quantum Coherence (HSQC) NMR experiments to demonstrate that a small fraction of low molecular weight PF resin can react with G-lignin. The condensation reaction occurs at the unsubstituted *ortho*-position of G-lignin and requires free formaldehyde as a crosslinking agent. While some formaldehyde is formed in the curing reaction, the authors suggest that additional formaldehyde may be generated through the alkaline hydrolysis of lignin structures (e.g., β -aryl ether, phenylcoumaran). In addition to the formation of covalent bonds, the authors showed that steric hinderances in the cell wall affect the ratio of methylene bridges in *o-p* and *p-p* configuration significantly. These ratios are greatly different in neat resin, earlywood, and latewood. Moreover, the *o-o* configuration which does not occur in neat resin, was detected when resin was cured in wood.

Chemical imaging and x-ray based techniques are able to quantify the amount of resin in different locations of a treated plank and even individual layers of the cell wall^{92, 99,108}. Therefore, it is widely accepted that low molecular weight resin diffuses into the cell wall and cures *in situ*^{86,92}. It is, however, still unclear how resin is incorporated in the ultrastructure of wood. Small angle neutron scattering (SANS) has shown that resin migrates in the cell wall, where it is in close contact with microfibril surfaces, however, crystalline regions are inaccessible to PF resin²¹⁹.

Solid-state NMR and relaxation time studies, also suggest an intimate association of resin and wood polymers^{220–222}. Laborie²²⁰ (2002) found that amorphous and crystalline cellulose become phase separated after modification with low molecular weight PF resin. Thus, the molecular motions of both domains showed significant differences after modification. Furthermore, the partial removal of hemicelluloses from the cell wall seems to allow resin monomers to fill newly created pore spaces^{221,222}. These nanometre-scale interactions between resin and wood are investigated in chapter 8 of this thesis.

3. Chemical Characterisation of selected Softwood and Hardwood Species

3.1. Introduction to Chapter 3

The fundamentals of wood anatomy, chemistry, and cell wall ultrastructure have been described in the literature review. The experimental chapters that follow are concerned with variations of the wood modification process using low molecular weight phenol urea formaldehyde (PUF) resin. The various wood species, which are the raw material for this modification, are described in the present chapter in the unmodified state. Chemical characterisation methods including FTIR spectroscopy, determination of wood constituents, and extractives analysis will help to explain certain patterns in the behaviour of these species throughout all following experimental chapters.

The wood species selected for this work were initially chosen due to various factors. (i) Some timbers were selected due to their promising anatomical features, although they are rarely used commercially because of their limited availability or other shortcomings (e.g., willow, sycamore, lime). The main anatomical feature of these species is the high number of vessels, which are distributed evenly between latewood and earlywood (i.e., diffuse porous), indicating good treatability of larger specimens. (ii) Other timbers are of particular interest to the industry as they are fast-growing, readily available in clear (i.e., knot-free) lengths, and are known to have an excellent treatability (e.g., sapwood of Radiata pine, Southern yellow pine, tulipwood). These timbers were imported from overseas through commercial timber buyers. (iii) Yet another set of timbers was chosen exclusively due to their good availability across Europe (e.g., poplar, beech, birch, Scots pine).

The selection of species used in this thesis is diverse in terms of growing location (e.g., plantation or natural forest), drying history (e.g., kiln, air, unknown), age, and available sample size. It is crucial to recognise that the attributes of a wood species cannot be captured by a single plank of its timber. Therefore, the samples which have been used here display only a snapshot of possible wood properties. Fortunately, these samples are matched pieces that were always cut from the same plank of wood, which means that there is as little as possible within-species variation in this thesis. This way the performance of modified wood can be directly linked to the properties of the unmodified wood, which are determined in the current chapter.

In this chapter, FTIR spectroscopy in combination with cluster analysis (i.e., hierarchical clustering and principal component analysis) is used to obtain a general overview of the chemical properties in the selected wood species. Both cluster analyses are well-established for this purpose and have been used in the past to identify the species of unknown wood samples²²³. Classical wet chemistry techniques are used to isolate and quantify individual cell wall polymers⁴⁷. Acid-base-interaction between the alkaline PUF resin and the acidic wood samples were already mentioned in chapter 2.3.4. and will be investigated further in Chapter 7. As a prerequisite, the pH value and alkaline buffer capacity (ABC) of wood samples are determined in the present chapter by two different methods^{224,225}. Wood extractives and degradation products that might interact or interfere with the resin are studied by solution-state NMR spectroscopy. For reference, examples of common extractive types and likely degradation products are shown in Figure 3-1^{27,226}.

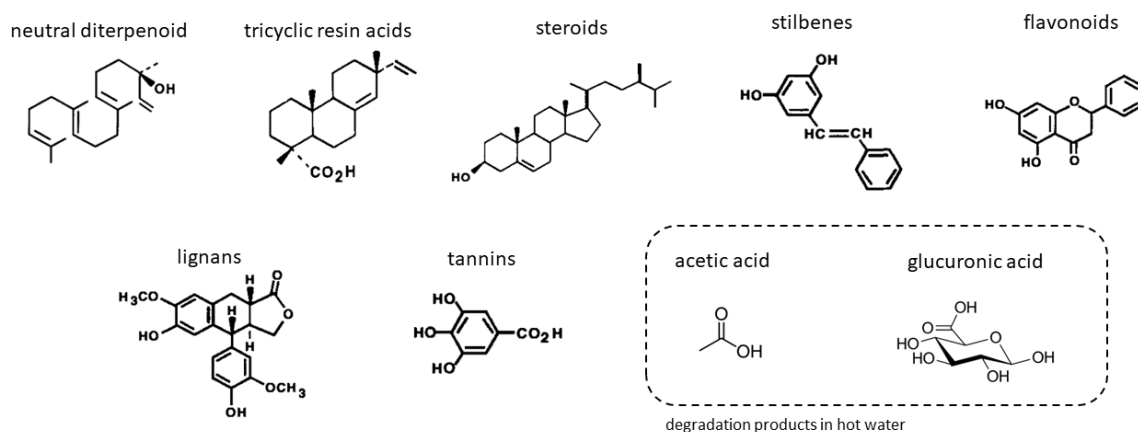


Figure 3-1 Example compounds that illustrate the common extractive types²⁷ in wood and likely auto-hydrolysis products²²⁶. The extractive fraction in both hardwoods and softwoods is highly variable, comprising thousands of compounds. This illustration aims to highlight chemical features present in some of these groups.

3.2. Materials

3.2.1. Wood Samples

Seven hardwoods and four softwoods were selected for this thesis. The hardwoods were European beech (*Fagus sylvatica*), silver birch (*Betula pendula*), sycamore (*Acer pseudoplatanus*), willow (*Salix alba*), common poplar (*Populus tremula*), European lime (*Tilia x europaea*) and tulipwood (*Liriodendron tulipifera*). The softwoods included Southern yellow pine (SYP, this is a commercial mix of four pine species: *Pinus palustris*, *P. elliotii*, *P. taeda* and *P. echinate*), Scots pine (*Pinus sylvestris*), Radiata pine (*Pinus radiata*) and *Pinus taeda*.

The *Pinus taeda* timber was procured from a single species plantation in Brazil for comparison with the mixed species SYP from North America. Some timbers were sourced commercially, with requirement for low heartwood content. Visual examination on receipt, and use of heartwood indicator solutions where relevant, confirmed that sapwood was used in this study. These timbers were stored at ambient conditions until further processing. As different methods require different types of wood sample, the following types of samples are used throughout this thesis:

- Wood powder was prepared using a cutting mill (*Retsch SM300*) with a sieve opening of 1 mm². The milled powder was fractionated by size, using sieves with the mesh numbers 44 and 60. The fraction that passed the former and was retained on the latter was used for analysis, unless stated otherwise.
- Small blocks were cut with good alignment of the grain and growth rings to the edges of the specimen. The dimensions were 20 mm (radial) × 20 mm (tangential) × 5 mm (longitudinal).

3.3. Methods

3.3.1. FTIR-ATR Spectroscopy – Sample Collection

A Nicolet 8700 FTIR (*Thermo Scientific*) with GladiATR vision (*Pike Technologies*) was used for the surface chemical analysis of small blocks of wood. The FTIR spectrometry was performed directly on the material surface using the attenuated total reflectance (ATR) mode, so the sample surface was presented to the aperture of the ATR (see Figure 3-2). Each spectrum was an average of 32 scans collected, over wavenumbers from 4000 to 400 cm⁻¹. To minimise the spectral noise and peaks relating to changes in atmospheric CO₂ and water vapour in the laboratory, background spectra were taken after every two spectra.

The FTIR spectra were taken after ASE tests, which are described in Chapter 5.3.7, hence the small blocks had been through three cycles of water soaking and oven drying before spectra were collected. This may have led to changes in wood chemistry compared to modified and unmodified samples that have not been leached. In future studies, the effect of leaching on FTIR spectra should be considered.

For the analysis in this chapter, four small blocks per test group were cut in half so that the centre area could be analysed. Two spectra were collected from each small block of wood, totalling eight spectra per test group. From these eight spectra, one average spectrum was calculated per test group. Average spectra were cropped between the wavenumbers 2500 cm^{-1} and 1900 cm^{-1} to exclude noise relating to CO_2 . Subsequently, the spectra were smoothed using a rolling average function of the instrument software.

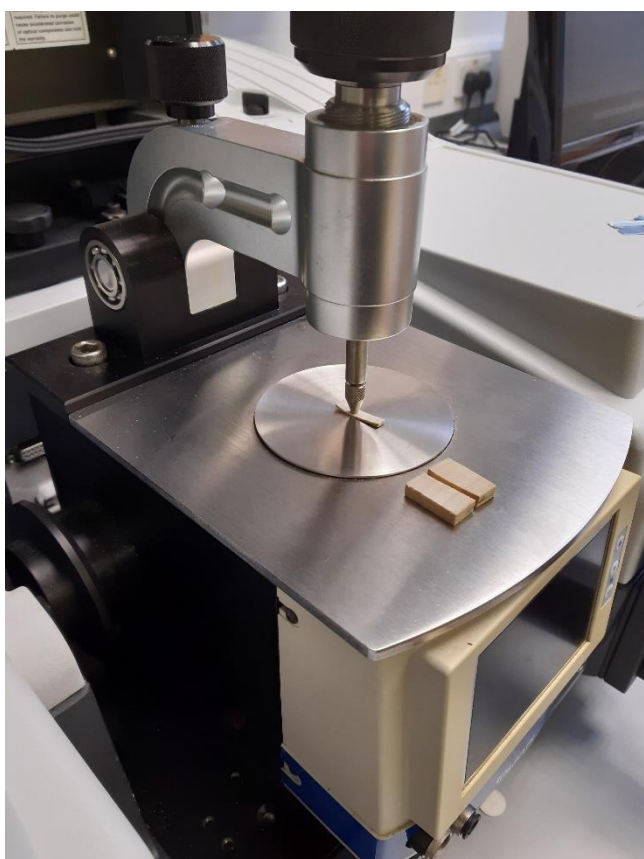


Figure 3-2 FTIR-ATR spectrometer used in this thesis. A section of a small block is cut from the centre of the sample and presented directly to the surface of the ATR crystal.

3.3.2. FTIR-ATR Spectroscopy – Statistical Methods

Principal component analysis (PCA) and hierarchical clustering analysis (HCA) were performed to investigate chemical differences among unmodified wood species. PCA is a statistical analysis method, used for reducing the dimensionality of complex datasets. The data is transformed into a new coordinate system, where most of the variation can be explained by just a few principal components (PCs). HCA is a cluster analysis, where each observation starts in its own cluster, and similarities between clusters are shown schematically, merging as one moves up the hierarchy. The R functions *prcomp()* and *hclust()* were used and spectra were normalised before the analysis. All analyses were performed using R Statistical Software (v4.1.2; R Core Team 2021).

3.3.3. Isolation of Wood Constituents using Wet Chemistry

3.3.3.1. Solvent Extraction with Toluene-Methanol-Acetone (4:1:1)

Oven dry wood powder (20 g) was placed in pre-weighed cellulose extraction thimbles. The thimble was placed in a Soxhlet apparatus. Toluene, acetone, and methanol were mixed under the volume ratio 4:1:1. A solvent volume of 250 ml was poured in a 500 ml round bottom flask which was then attached to the Soxhlet apparatus under reflux. The extraction time was 6 h. After extraction, the thimble containing extract-free wood powder was dried for 48 h at 105°C. Subsequently, the thimble was re-weighed, and the extractive content was calculated from the mass loss during extraction. All steps of the wet chemistry analysis are summarised in Figure 3-3 and picture of the sample preparation are displayed in Figure 3-4.

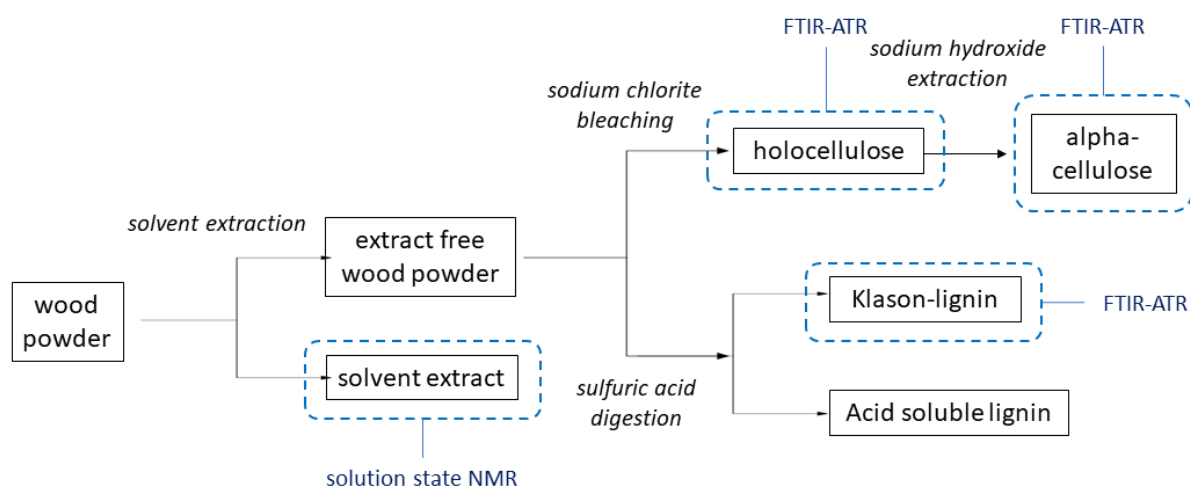


Figure 3-3 Wood chemistry methods used to quantify the main cell wall polymers of eleven wood species. The milled wood powder was extracted with a solvent. The solvent was analysed in NMR test and the extractive-free wood was subjected to further testing in order to determine the holocellulose, alpha-cellulose and Klason-lignin contents. Each of these fractions was analysed by FTIR-ATR.

3.3.3.2. Holocellulose

Oven dry, extract-free wood powder (1 g) was placed in a 250 ml Erlenmeyer flask, and the weight was noted. Volumes of 80 ml deionised water, 0.5 ml glacial acetic acid, and 10 ml sodium chlorite solution (15% w/w) were added. A 25 ml conical flask was inverted in the neck of the reaction vessel to retain the developing chlorine gas. The assembly was placed in a water bath set at 70 - 80°C for one hour. Subsequently, 0.5 ml of glacial acetic acid and 10 ml sodium chlorite solution were added. This was repeated three times with a total reaction time of 4 h. At the end of the reaction, the assembly was cooled down using an ice bath. The mixture was filtered through a pre-weighed sinter crucible and rinsed with cold deionised water, ethanol, and acetone. The crucible was dried at 50°C and re-weighed to estimate the fraction of holocellulose.²²⁷

3.3.3.3. Cellulose and Hemicellulose

Oven dry holocellulose (0.5 g) was placed into a 250 ml Erlenmeyer flask, and the weight was noted. A volume of 20 ml NaOH (17.5% w/w) was added, and the flask was sealed with parafilm. The mixture was agitated gently for 2 h at 20°C. Subsequently, the mixture was filtered through a pre-weighed sinter crucible and washed with NaOH and acetone. The crucible was dried at 105°C and then re-weighed to calculate the cellulose fraction. The fraction which dissolved in the alkaline solution was mainly hemicelluloses.

3.3.3.4. Klason Lignin

The lignin content was determined on a 1 g sample of extract free oven dry wood powder by acid hydrolysis of carbohydrates using the Klason-method. A volume of 20 ml of cold H₂SO₄ (72% w/w) was added to the extract free wood powder and each sample was triturated with a glass rod to ensure good mixing. After digesting for 2 h at 20°C, each product was quantitatively flushed from the beaker and rod into a 500 ml round bottomed flask, using 345 ml of deionised water. The mixture was heated under reflux for 4 h, then it was allowed to cool in a water bath. Subsequently, the mixture was filtered through pre-weighed glass filter paper (Whatman Grade GF/B - 12.5 cm) in a Buchner funnel using vacuum. The filter paper carrying Klason lignin was then dried at 105°C and re-weighed to estimate the lignin fraction.



Figure 3-4 Sample preparation for the isolation of wood polymers, (a) wood solvent extractives after rotary evaporation, (b) α -cellulose in sinter crucible, (c) holocellulose preparation with NaClO₂ in hot water bath, (d) Klason lignin preparation in 72% sulphuric acid, (e) Klason lignin preparation under reflux.

3.3.3.5. Acid-Soluble Lignin

A small fraction of lignin is acid soluble, especially in hardwoods. To determine its amount, the filtrate from the Klason lignin determination was analysed by UV-vis spectroscopy. A small aliquot of known concentration was diluted with three parts deionised water. Then the absorbance at wavelength 205nm was noted (UV_{205}). An absorptivity ϵ of 88 l/g*cm was assumed for all wood species²²⁸. The ASL fraction can be estimated with the following equation:

$$ASL \text{ in } \% = \frac{UV_{205} * V_{filtrate} * dilution}{\epsilon * m_{wood} * pathlength} * 100\%$$

The volume of the filtrate $V_{filtrate}$ was 365ml. The dilution is 4 and the pathlength through the cuvette is 1cm.

3.3.4. Acid-Base Titrations of Hot-Water Wood-Extracts

Acid-base titration were performed using either hot-water wood-extract, or a cold-water wood suspension. In the extract method, the procedure of Johns & Niazi²²⁴ (1980) was used. Dry wood powder (25 g) was mixed with 250 ml deionised water. The mixture was refluxed for 20 min. The hot extract was then allowed to cool and subsequently filtered through filter paper. Two 50 ml samples per species were prepared for the NaOH and H₂SO₄ titrations. The pH-

meter was calibrated to pH 4 and 7 using standard buffer solutions. Titration curves between pH 3 and pH 10 were determined by adding 1 ml increments of NaOH (0.02 N) or H₂SO₄ (0.02 N) to the extract and subsequently measuring the pH value. Close to the neutral range the volume of the added increment was reduced to 0.5 ml. During measurements the extract was agitated constantly. The pH value of the extract was calculated as the average of both initial pH value readings. The alkaline buffer capacity (ABC) per gram of wood powder was determined by the following calculation, where V_{NaOH} is the volume of titrant required to raise the starting pH value to an end point between pH 10 – 11, n is the normality of the titrant (0.02 N), ΔpH is the difference between starting and end point, and m_{powder} is 25 g.

$$ABC \left[\frac{mmol}{g} \right] = \frac{V_{NaOH} * n}{\Delta pH * m_{powder}}$$

Later in this thesis, resin treatments are performed in batches of 10 small blocks that are impregnated with a constant volume of 100 ml PUF resin. To calculate the ABC per batch, the mass of these ten small blocks (m_{batch}) is considered in the next equation:

$$ABC [batch] = ABC \left[\frac{mmol}{g} \right] * m_{batch}$$

The remaining extract solution, which was not used for ABC measurements was freeze-dried at –66°C and 13 mTorr to obtain samples of pure water-soluble extractives. The weight of the samples was noted before and after freeze drying to calculate the water-soluble extractive content of the sample. These extractives are used for solution-state NMR experiments in Chapter 3.4.4 and for DSC experiments in Chapter 7.4.1.

3.3.5. Acid-Base Titrations of Cold-Water Suspensions

The suspension method was performed at room temperature, with the wood substrate present at all times^{225,229,230}. Beech sapwood was the only sample measured with this method, because the objective of this section was to compare the different methods not the different species. The dry beech wood particles were prepared in three different particle sizes: those passing a 60-mesh sieve (i.e., small), those passing 44-mesh but not 60-mesh (i.e., medium), and solid wood cubes with the dimension 5 (r) x 5 (t) x 5 (l) mm that were cut from a larger plank using a band saw (i.e., large).

Wood particles (5 g) were mixed in a beaker with 100 ml deionised water under constant stirring. A latency time of 1 h was set between the preparation of the suspension and the measurement of titration curves. The pH value was monitored periodically throughout the latency time. Titration curves between pH 3 and pH 10 were determined by adding 1 ml increments of NaOH (0.1 N) or H₂SO₄ (0.1N) to the suspension. A 60 s wait was set between adding the titrant and measuring the pH value.

The long-term buffering was studied for both beech sapwood extracts and suspensions. Therefore, the beaker with the extract or suspension was sealed with parafilm and stored at room temperature for 3 days after the first titration. Subsequently, after 3 days waiting, the pH value of the samples had decreased below pH 8. Then the titration with NaOH was repeated. The beaker with the extract or the suspension was stored for alternating intervals of 3 and 4 days before each titration was repeated. The titration of the same sample was repeated every 3 or 4 days for 24 days.

3.3.6. Solution-State NMR Spectroscopy – Wood Extractives Analysis

Solution-state NMR spectroscopy was performed using a *Bruker 400 MHz Ultrashield+* spectrometer. The water in hot-water extracts was removed by freeze-drying and the solvent in solvent extracts was removed by rotary evaporation at 60°C. Water extractives (approx. 20 mg) were dissolved in 500 μl deuterium oxide (D_2O) and transferred to a 5 mm borosilicate NMR tube using disposable Pasteur pipettes. Solvent extractives were dissolved in a 2:1 (v/v) mixture of methanol- d_4 and acetone- d_6 .

Generally, solution-state NMR spectra in this thesis were collected in one of the following three modes: ^1H NMR, ^{13}C -DEPTQ NMR, and ^1H - ^{13}C -HSQC NMR. The acquisition parameters for each method are always the same, unless stated otherwise. ^1H NMR spectra were acquired with the pulse program zg30, D1 delay of 1 s, AQ of 4 s, and a spectral range from 0 to 10 ppm. The pulse program used for ^{13}C DEPTQ NMR experiments was deptqgsp.2. The number of scans was 1024, D1 delay of 2 s, AQ of 1.1 s, scanning a range between 0 and 250 ppm. DEPTQ mode implies that $-\text{CH}_2-$ and quaternary carbons are displayed as positive peaks whereas $-\text{CH}-$ and $-\text{CH}_3-$ carbons are displayed as negative peaks. The pulse program for ^1H - ^{13}C -HSQC NMR scans was hsqcedetgpsisp.2.3. The number of scans was 2, D1 1.91 s, AQ of 0.158 s, with a total scanning time of 20 minutes.



Figure 3-5 *Bruker 400 MHz Ultrashield+ NMR spectrometer used for solution-state NMR studies in this thesis.*

If methanol- d_4 was present as a solvent, the solvent peak was set to 3.31(σ_{H_1}) ppm and 49.00($\sigma_{\text{C}_{13}}$) ppm. If DMSO- d_6 was present as a solvent, the solvent peak was set to 2.5(σ_{H_1}) ppm and 39.52($\sigma_{\text{C}_{13}}$) ppm. Automatic phase correction, baseline correction, denoising, and smoothing was performed in MestreNova chemical software when necessary. The NMR spectrometer used for solution-state experiments is shown in Figure 3-5.

3.4. Results and Discussion

3.4.1. Wood and Wood Constituents studied by FTIR-ATR Spectroscopy

FTIR-ATR spectroscopy was used to display chemical differences between the eleven wood species selected for this thesis. Table 3-1 shows the assignments of FTIR wavenumbers as found in the literature. To confirm these assignments and to secure the quality of the chemical isolation methods used, the cell wall polymers of beech and Radiata pine are discussed prior to solid wood samples.

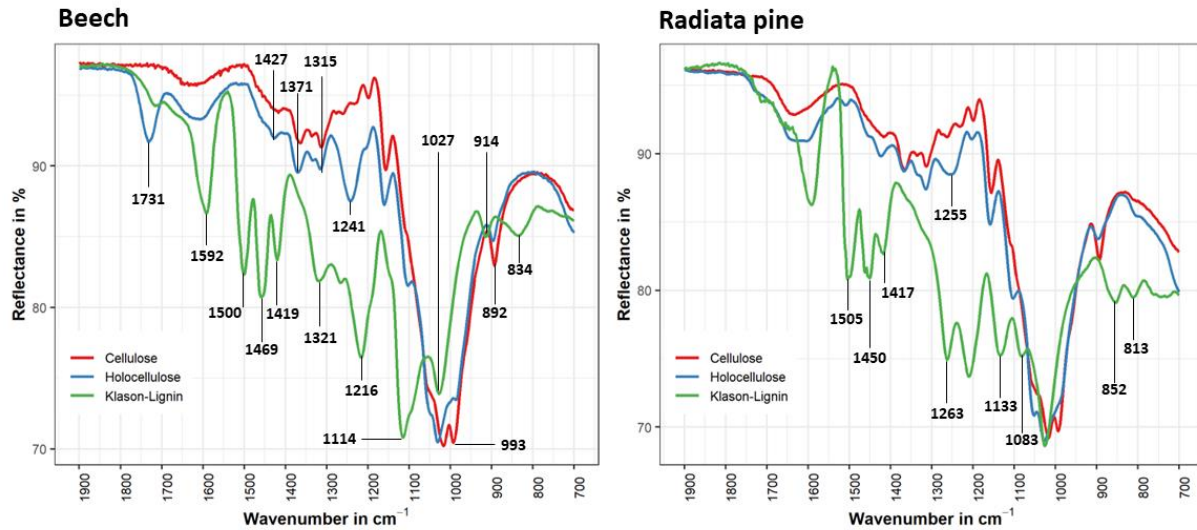


Figure 3-6 FTIR-ATR spectra of isolated cell wall polymers (cellulose, hemicellulose, lignin) of beech wood and Radiata pine. Beech and Radiata pine serve as examples for typical hardwood and softwood species.

Figure 3-6 shows the spectra of the main cell wall polymers for beech and Radiata pine with the assignment of the prominent absorption bands. The spectra in Figure 3-6 correspond well with those described in the literature and good separation of individual polymers can be attested. For beech as well as for Radiata pine, the main difference between cellulose and holo-cellulose is the carbonyl stretching at 1730 cm^{-1} and the C-O stretching at 1255 cm^{-1} or 1240 cm^{-1} , both assigned to hemicelluloses. Qualitative differences between softwoods and hardwoods are evident in the lignin fraction, where C-H deformations and C-O stretching occur at different wavenumbers and with different intensities. Additionally, the hemicellulose C-O stretch in hardwoods (1241 cm^{-1}) peaks at lower wavenumbers than in softwoods (1255 cm^{-1}).

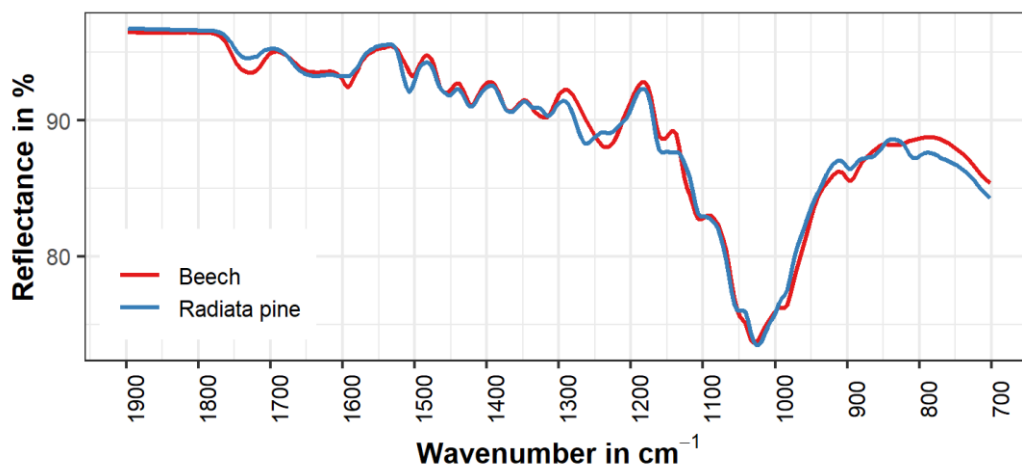


Figure 3-7 FTIR-ATR spectra of beech and Radiata pine as examples for typical hardwood and softwood species displayed between $1900\text{--}700\text{ cm}^{-1}$.

In solid wood, all three cell wall polymers are present, resulting in an overlap of the peaks as shown in Figure 3-6 above. Figure 3-7 displays the FTIR spectra of unmodified beech and Radiata pine, serving as examples of typical hardwood and softwood species. The figure reflects the well-known differences between softwoods and hardwoods in terms of hemicellulose and lignin structure²³¹. The carbonyl region at 1730 cm⁻¹ displays a more intense signal in hardwoods. The aromatic ring vibration peaks at 1511 cm⁻¹ in Radiata pine and at 1500 cm⁻¹ in beech. The C-O stretch of G-lignin, located at 1270 cm⁻¹ is intense in pine and absent in beech. Additionally, the aromatic C-H stretch at 811 cm⁻¹, indicative of G-lignin, is present in pine and absent in beech.

Table 3-1 Assignment of FTIR absorption bands from the literature. Cell wall polymers are indicated in bold script i.p. – in plane vibration, o.o.p. – out of plane vibration.

Wavenumber in cm ⁻¹	Indicative of Structure in Cell Wall Polymers
810	glucomannan in-phase ring stretching ^{212, 232} and aromatic C-H o.o.p. lignin ¹⁹³
855 - 866	aromatic C-H o.o.p. in G-lignin ^{212, 233}
870	glucomannan and cellulose deformation of equatorial C2-H ²³²
895	glucose ring stretch and C1-H deformation in hemicellulose ²¹² , and cellulose ^{233, 231}
1030	C-O deformation in aliphatic alcohols and ethers, symmetric C-O-C stretching of dialkyl ethers, aromatic C-H i.p. ^{212, 231, 234} cellulose, hemicellulose, lignin
1049	glycosidic linkages (C-O-C) in xylan ²³²
1106	cellulose not specified ²³²
1113	C-H i.p. deformation S-lignin ^{233, 235} (strong)
1140	C-H i.p. deformation G-lignin ^{233, 235} (medium)
1160 - 1168	C-O-C asymmetric stretch cellulose ^{212, 234} and hemicellulose ²³⁶
1205 - 1210	C-O-H i.p. bending at cellulose C-6 ²³⁴ , aryl aldehyde, lactones, phenolic hydroxyl ^{232, 235}
1225 - 1215	S-lignin C-O stretch ^{231, 235}
1240 - 1260	hemicellulose C-O stretch and O-H i.p. vibration ²³⁶
1265 - 1273	G-lignin and C-O stretch ^{231, 235}
1315	crystalline cellulose C-H2 wagging ^{42, 233} , C-O stretching in S-lignin ^{231, 235}
1335 - 1341	crystalline cellulose O-H i.p. bending ^{232, 233, 236}
1330 - 1340	S-lignin C-O stretch ²³⁶
1370 - 1378	symmetric C-H2 bending cellulose and hemicellulose ^{212, 231, 234}
1420 - 1430	lignin aromatic in-ring vibration ^{231, 235} and C-H and O-H bending cellulose ^{233, 236} (weak)
1460 - 1468	lignin aromatic in-ring vibration ^{231, 235}
1500 - 1515	lignin aromatic in-ring vibration SW (1510), HW (1505) ^{231, 237}
1600	lignin aromatic in-ring vibration, conjugation with carbonyl groups in hemicellulose ^{232, 231}
1635 - 1650	O-H bend in absorbed water ¹⁹³ and conjugated C=O ²³¹
1708 - 1715	C=O in carboxylic acids of lignin and hemicellulose ^{235, 238}
1730 - 1740	unconjugated C=O stretch in esters and aldehydes of hemicellulose ²³⁸ , HW (>1730) and SW (<1730) ²³¹

While spectra were collected for all species, cluster analysis has been used to show the major similarities and differences, and to identify trends among the eleven wood species. Both hierarchical cluster analysis (HCA) and principal component analysis (PCA) transform the spectral data in a manner that facilitated interpretation. However, it is important to note that the outcomes of cluster analysis, being a statistical approach, may be influenced by factors such as whether the spectra are collected in absorbance or reflectance mode and how they are processed. Such effects are considered before the outcomes of HCA and PCA are discussed in the following.

Generally, FTIR spectra were always acquired in attenuated total reflectance mode (ATR) due to the uncomplicated sample preparation, as opposed to data acquisition in transmittance mode, which involves the use of potassium iodide discs. Therefore, the default spectra are collected in reflectance mode.

Spectra in reflectance mode are primarily used to describe qualitative trends. A general drawback of ATR is that absorption bands located at smaller wavenumbers have more intense peaks than at higher wavenumbers, compared to the transmittance mode. This discrepancy arises because the penetration depth of the IR beam increases with lower wavenumbers¹⁹³. Software based ATR-corrections are available but have not been used in this work since these corrections are viewed critically by the scientific community. Instead, this thesis acknowledges a potential systematic bias in the ratio of absorption peaks when ATR is used.

The use of spectra in reflectance mode is unsuitable for quantitative purposes. However, quantitative statements can be made after transformation to absorbance mode and normalisation¹⁹³. Normalised spectra in absorbance mode are presented Appendix 1. It is worth noting that, a certain level of spectral resolution may be lost during the transformation, due to the logarithmic nature this conversion. Consequently, low intensity signals, which are important for the qualitative characterisation, may be underrepresented in the absorbance mode.

Figure 3-8 shows the results of the HCA for both reflectance and absorbance mode spectra. The dendrogram is the result of a hierarchical clustering computation in R-Studio, in which the spectra of unmodified wood were analysed. HCA generates a tree-like structure with the distance coefficient on the y-axis. Timbers with similar chemical features will have similar spectra, therefore, the distance coefficient at which objects start merging will be small²²³. This plotting method generates several clusters, which differ slightly between reflectance and absorbance mode.

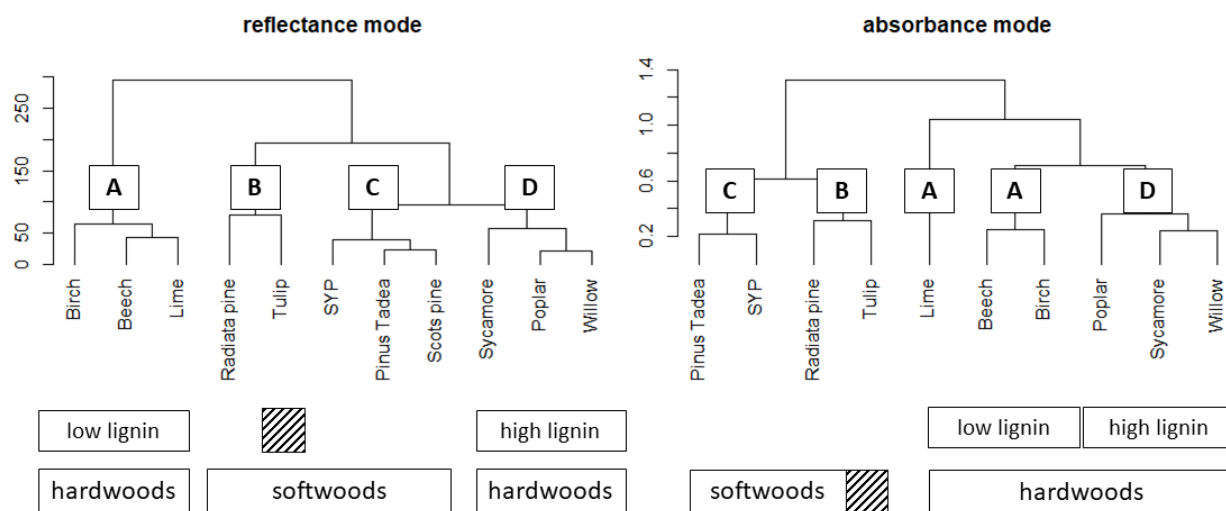


Figure 3-8 HCA dendrogram for FTIR spectra in reflectance mode (left) and absorbance mode (right). Assignment of four main clusters (A - D) are made in the reflectance plot. The contents of each cluster are described below the dendrogram, and outliers are indicated by the striped area.

Four main clusters are identified in the reflectance mode dendrogram (left). These clusters have been labelled A – D, and this assignment is maintained in the following discussion and later chapters. Cluster A contains hardwoods with a high hemicellulose and low lignin content, as will be shown in section 3.4.2. The clusters B and D include the softwoods, and apparently as an outlier – tulipwood. It is not clear why tulipwood is clustered together with the softwoods. From Figure 3-9, it is evident that tulipwood displays absorption bands that are typical for a hardwood.

Hence, the allocation of Radiata pine and tulipwood in the same cluster is regarded as an artefact and not further investigated. Cluster D contains hardwoods with a higher lignin and lower hemicellulose content. The hardwoods in clusters A and D differ not only by their lignin content, but also by their lignin structure, as will be demonstrated in chapter 7 through NMR results. Specifically, poplar in cluster D exhibits a notably higher ratio of G-type lignin to S-type lignin (G:S ratio) compared to lime wood in cluster A. Thus, it is assumed that the G:S ratio represents a general distinction between the timbers in clusters A and D.

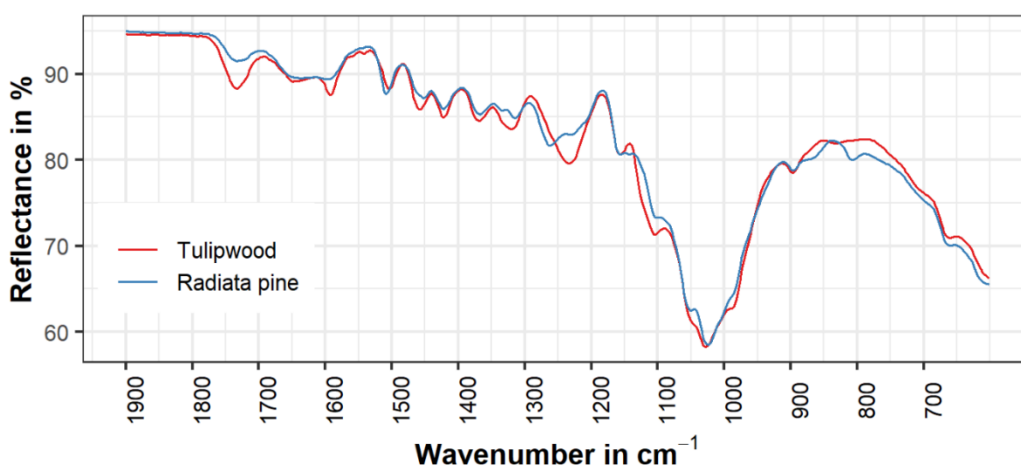


Figure 3-9 FTIR-ATR spectrum of tulipwood and Radiata pine, showing differences that are typical for hardwoods and softwoods.

HCA in absorbance mode (Figure 3-8 – right) distinguishes hardwood and softwood spectra more consistently than the reflectance mode, as the separation occurs at the highest distance coefficient. The softwoods are again grouped in clusters B and D and tulipwood is again incorrectly assigned in the same cluster as Radiata pine. Cluster A is split in two branches, indicating that lime wood has a distinct chemical composition to other hardwoods in this study. In fact, lime contains an especially high hemicellulose and low lignin content, which could be the reason for the separate allocation. Cluster D contains the same species in reflectance and absorbance mode but, the order at which species start merging differs at the lowest distance coefficient.

Figure 3-10 (a-d) shows results of the PCA analysis for spectra in reflectance mode (a-b) and absorbance mode (c-d). Figure 3-10 (a, c) show the PCA score plot, wherein clusters form in a manner similar to that observed in the HCA. This becomes especially prominent in 3-10 (c), where beech and birch (cluster A) are located at the bottom of the score plot, lime (cluster A) is on the far top right, cluster D species are in the centre, and cluster B and C species are found on the left side of the score plot. The axes of the score plot show how much variation can be explained by the principal components PC1 and PC2. In reflectance mode, PC1 explains 78.2% and PC2 14.2% variation in the data. In absorbance mode it is 58.7% for PC1 and 29.0% for PC2. The remaining variation is explained by PC3, PC4, and PC5, which are not displayed.

The loading plots Figure 3-10 (b, d) show which wavenumbers account for most of this variation. The main responsible wavenumbers in reflectance mode are labelled in Figure 3-10 (b). In reflectance mode, PC1 is strongly affected by wavenumbers 1733 cm^{-1} and 1236 cm^{-1} . The former wavenumber corresponds to C=O stretching in acetyl and carboxylic acid groups of hemicelluloses. The latter is indicative of C-O stretching in hemicellulose. PC2 is influenced by many wavenumbers typically assigned to the lignin fraction, such as 1511 cm^{-1} , 1459 cm^{-1} , 1267 cm^{-1} , 1230 cm^{-1} , and 1120 cm^{-1} (see Table 3-1). Wavenumber 1756 cm^{-1} , which strongly affects PC2, could indicate the presence of lactones²³⁸ in lime

wood and sycamore, since these two species have distinct negative PC2 values in Figure 3-10 (a). Lactones may be present in the form of extractives²³⁹. Hence, it appears that PC1 explains differences in the hemicelluloses and PC2 primarily differences in the lignin structure.

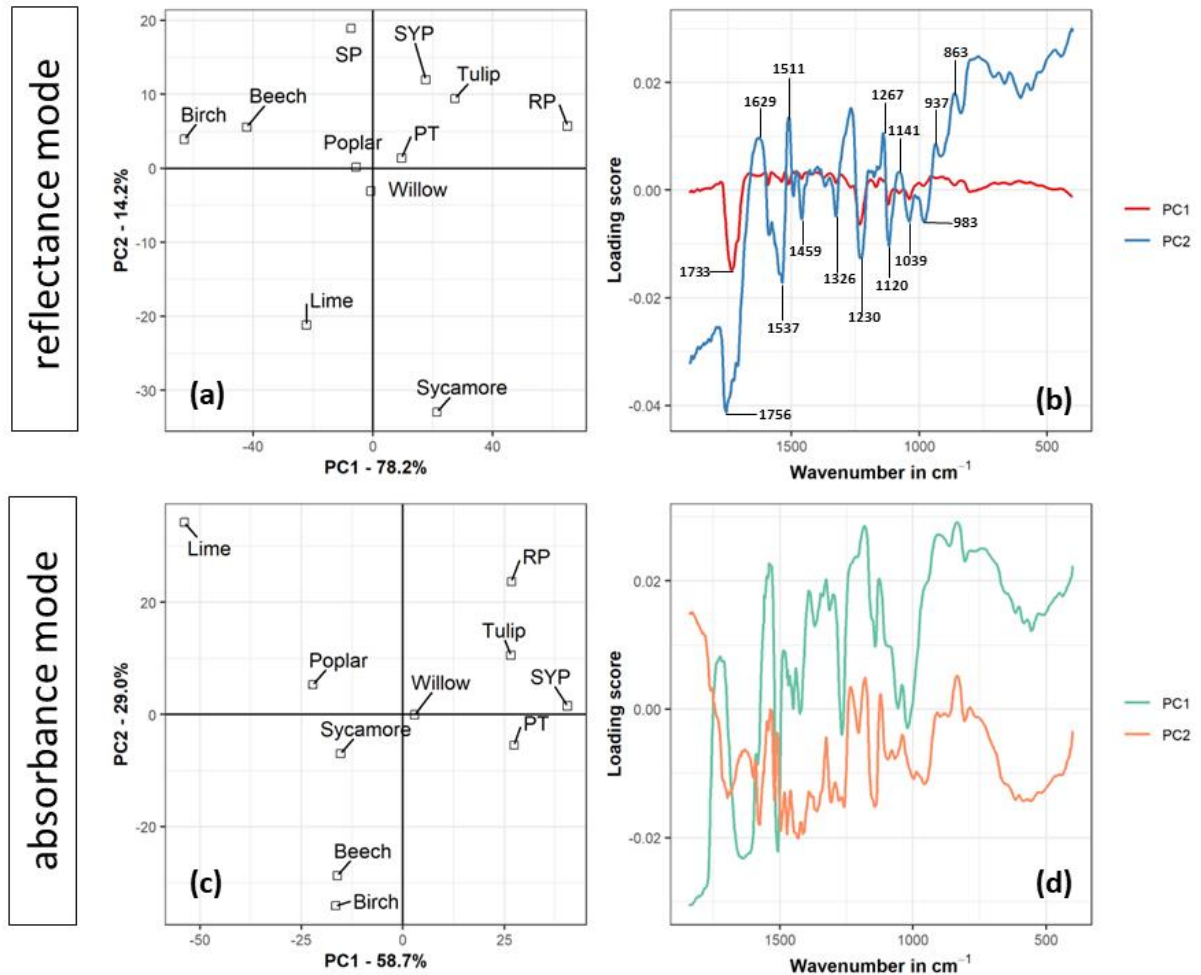


Figure 3-10 Principal component analysis (PCA) outcome for eleven unmodified wood species. Score plots (a, c) illustrate wood species with similar chemical compositions positioned in close proximity to each other. Loading plots (b, d) indicate which wavenumber are responsible for variation in the dataset. PCA results from spectral data in reflectance mode (a, b) are different those obtained in absorbance mode (c, d).

In absorbance mode, the loading plot appears to be more convoluted. PC1 contains absorption bands at 1730 cm⁻¹, 1540 cm⁻¹, 1508 cm⁻¹, 1392 cm⁻¹, 1326 cm⁻¹, 1180 cm⁻¹, 1128 cm⁻¹, 900 cm⁻¹, and 835 cm⁻¹. The main absorption bands for PC2 are at 1697 cm⁻¹, 1577 cm⁻¹, 1521 cm⁻¹, 1497 cm⁻¹, 1472 cm⁻¹, 1432 cm⁻¹, 1361 cm⁻¹, 1260 cm⁻¹, 1143 cm⁻¹, 997 cm⁻¹, and 956 cm⁻¹. Thus, certain loadings of PC1 and PC2 can be attributed to differences in the content and structure of lignin and hemicelluloses. However, the PCA in absorbance mode is also influenced by arbitrary wavenumbers that cannot be assigned to specific cell wall polymers (e.g., 1697 cm⁻¹, 1540 cm⁻¹, 1392 cm⁻¹). Increased loadings at these wavenumbers could indicate more subtle differences between the timbers or possibly artefacts arising from the computation.

3.4.2. Quantification of Wood Constituents using Wet Chemistry Methods

Established wood chemistry methods⁴⁷ were used to quantify the main cell wall polymers, as well as extractive content, in the selected timbers. The results presented in this section complement the previous FTIR observations, therefore the assignment of timbers to clusters A – D is continued here. Table 3-2 shows the percentage of the main cell wall polymers in all observed wood species and their extractive content in different solvents.

Carbohydrates and lignin were isolated using different methods, and imperfect separation or degradation of polymers during isolation resulted in the sum of wood constituents not totalling 100%. In the hardwoods, the sum of wood constitutions was overestimated by 2 – 8%, and in the softwood the sum was underestimated by up to 6%.

Table 3-2 confirms several well-established trends in wood chemistry. Specifically, it is evident that hardwoods exhibit a lower KL content (17.9 – 24.9%) than softwoods (26.4 – 31.6%), higher ASL content (2.1 – 3.2%) compared to softwoods (0.8 – 0.9%), and greater hemicellulose content (31.3 – 42.2%) than softwoods (23.1 – 26.9%).

Table 3-2 Chemical composition of observed wood species determined by wet chemistry methods. Cluster refers to HCA classification in Figure 3-8. ExtrS - solvent extractive content in 4:1:1 solution. ExtrW - hot water extractives content. α -C - alpha-cellulose fraction. He-C - hemicellulose fraction. KL - Klason lignin fraction. ASL - acid soluble lignin fraction.

	Cluster	ExtrS in %	ExtrW in %	α -C in %	He-C in %	KL in %	ASL in %	Ash in %
Beech	A	1.11	0.19	43.4	34.2	22.3	2.8	0.4
Birch	A	1.40	0.18	42.9	34.6	23.2	2.5	0.2
Sycamore	D	2.86	0.29	46.2	33.9	24.2	2.1	0.4
Lime	A	3.95	0.16	44.9	42.2	17.6	3.2	0.3
Tulipwood	B	0.88	0.15	43.9	35.8	21.9	2.8	0.4
Poplar	D	1.46	0.17	43.7	32.8	24.9	2.6	1.3
Willow	D	2.04	-	43.8	31.8	24.0	2.1	0.6
SYP	C	0.29	0.17	43.0	23.1	26.4	0.9	0.2
Scots pine	C	0.05	0.36	43.4	26.9	29.4	0.8	0.3
Pinus taeda	C	3.19	0.62	40.1	24.6	31.3	0.9	0.2
Radiata pine	B	0.05	0.26	40.2	23.9	31.6	0.8	0.3

Among the hardwoods, Table 3-2 validates certain trends that were indicated in the HCA analysis in section 3.4.1. Thus, hardwood species in cluster A have a higher hemicellulose content (34.2 – 42.4%) than hardwood species in cluster D (31.8 – 33.9%). Conversely, cluster D species display a higher lignin content (24.0 – 24.9%) than cluster A species (17.2 – 23.3%). Lime wood has an especially low lignin (17.6%) and high hemicellulose content (42.4%), which could also be indicative of tension wood, given the unknown exact origin of the samples.

Returning to the allocation of tulipwood and Radiata pine in cluster B, Table 3-2 clearly shows a different chemical composition in the two species, further confirming that this allocation is an artifact in the computation. Moreover, the values for ExtrS, ExtrW, and ash content display some variability between individual species, however, no trend can be observed either between hardwoods and softwoods or between clusters.

3.4.3. The Alkaline Buffer Capacity of Wood Extracts and Suspensions

3.4.3.1. Method Comparison of Hot-Water Extracts and Cold-Water Suspensions

The Alkaline Buffer Capacity (ABC) is a quantification of the alkali required to elevate the pH value of a solution to a predetermined endpoint. This becomes relevant when alkaline-catalysed resin interacts with an acidic wood substrate (see chapter 2.3.4). Methods used for measuring the pH value and ABC of wood are plentiful. These methods include hot water extractions^{224,240}, cold water extractions to avoid heat-induced hydrolysis²⁴¹, extraction with sodium acetate solution²⁴², measuring directly on the surface of solid wood²⁴³ or paper²⁴⁴, or using wood suspensions rather than extracts^{225,229,230}.

The following section outlines differences in two common methods: the hot-water wood extract method²²⁴ and the cold-water wood suspension method²²⁵. It is crucial to note that the hot water used for the extractions can introduce products of partial hydrolysis, along with water-soluble extractives²²⁶. This is considered reasonable for the studied wood modification process, where hydrolysis of wood constituents is likely to occur in the drying and curing stages of resin modification, requiring elevated temperatures in the range of 50 – 150°C.

Additionally, previous studies using hot-water extractives have demonstrated good correlations between the measured pH values of different wood species and their effect on the gel time of a resin^{224,245}. For the purpose of this method comparison, beech sapwood is used as a reference material.

In comparison to the extract method, the suspension method requires the consideration of additional factors. One such factor is the latency time, which refers to the duration between the mixing of wood and water and the subsequent pH measurement. As shown in Figure 3-11 (left), the pH value of the suspension consistently decreases during the initial hour after preparing the suspension. The pH value of the extract remains on constant over time. Therefore, acid-base titrations in the suspension were performed after one hour latency time when the pH value had stabilised.

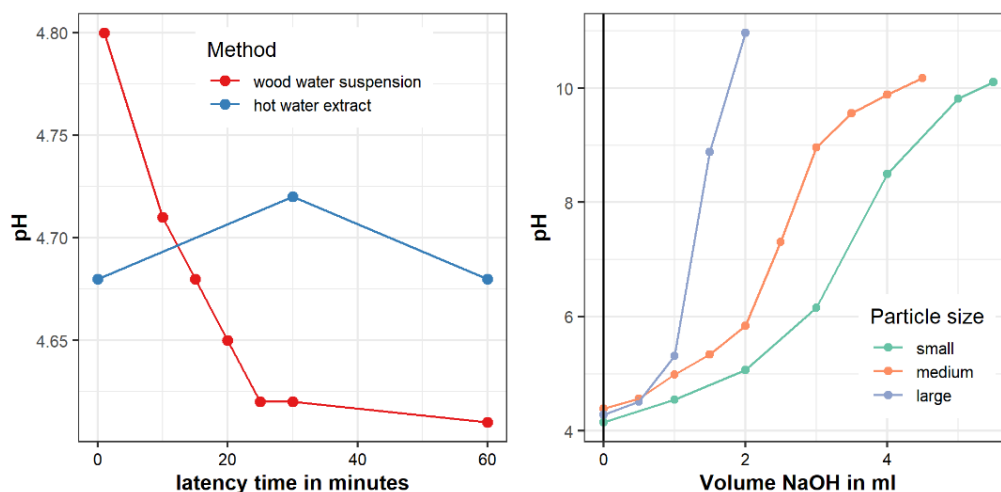


Figure 3-11 (left) Effect of latency time on the pH of beech water extract and beech water suspension. The pH value of the suspension decreases over time, while pH of the extract remains on a constant level. (right) Effect of particle size on ABC in beech wood suspension during titration with NaOH. Suspensions with smaller particles display a higher ABC.

Another crucial factor is the wood particle size in the suspension. Figure 3-11 (right) shows the effect of particle size during the titration with NaOH. Evidently, suspensions with smaller particle size require more NaOH to reach the endpoint at pH 10 and have therefore a higher ABC. This is due to the higher surface area, which enables the diffusion of acidic compounds from the wood to the water phase. The coarsest sample used in this test was made of small cubes of beech wood (5 x 5 x 5 mm³), which are thought to reflect the situation in solid wood most realistically. This group has

by far the lowest ABC, suggesting that the diffusion of acidic wood constituents requires a much longer time in the solid wood than in wood particles.

It becomes evident that the suspension method depends on many more variables than just the extraction method. The full titration curves of both methods (extract and suspension) are presented in Appendix 2. Although both titration curves have a similar shape and starting pH value, the suspension method required a higher titrant volume and concentration to reach the end point. Additionally, obtaining meaningful pH readings from the suspension proved challenging, due to a continuous buffering effect. In this case, the pH value decreases notably during measurement itself.

3.4.3.2. Long-Term Alkaline Buffering Capacity

In the context of the studied wood modification process, it is crucial to note that the freshly impregnated wood is soaked with resin and must be kiln dried for relatively long time periods, often exceeding 30 days⁹⁴. Given that the alkaline resin and the acidic wood substrate interact continuously during this time, it becomes necessary to also consider long-term buffering effects²²⁵.

Figure 3-12 (a) illustrates the long-term alkaline buffering behaviour of the beech water extract. Following the initial acid-base titration on day 0, the extract underwent subsequent testing on days 3, 4, and 5 thereafter. It is apparent from the figure that the pH value decreased from the endpoint of the initial titration (pH 10) to the starting point of the next titration on day 3 (pH 8). With each repetition of the procedure, the starting point gradually increased to pH 9 on day 5 and further to pH 9.5 on day 5.

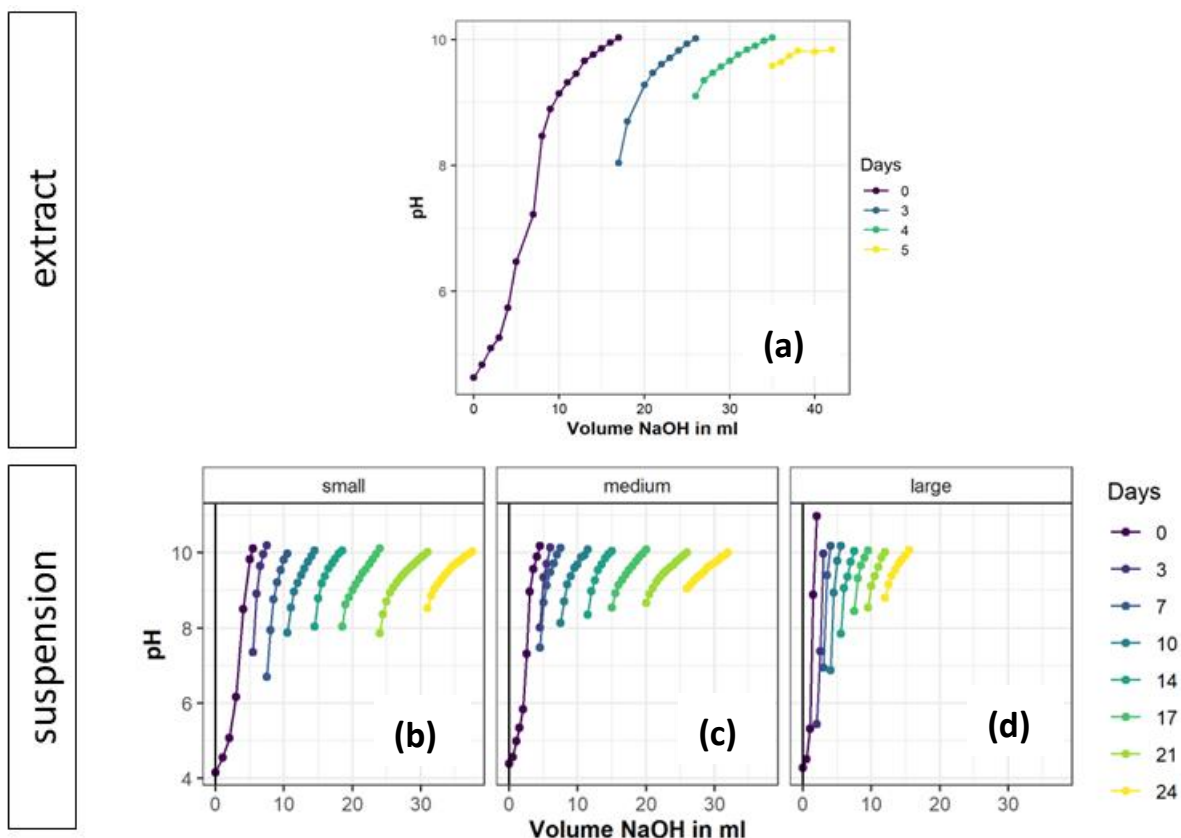


Figure 3-12 Alkaline resin and acidic wood substrate interact over long time periods during the modification process. (a) Long-term alkaline buffering capacity of hot-water extract. (b-d) Long-term alkaline buffering behaviour of cold-water suspension with different particle sizes over the course of 24 days. Titrations were performed on the same sample every 3 - 4 days.

Figure 3-12 (b – d) shows the long-term alkaline buffering behaviour of suspensions with different particle size. In this test, the titration with NaOH was reiterated every 3 – 4 days. After the first iteration, the pH value decreased from pH 10 to below pH 8, regardless of the particle size. This was the new starting pH for the next iteration. During the 24 days of the experiment, the starting pH value increased constantly for all particles sizes. However, the total titrant volume required was significantly higher in smaller particles (Figure 3-12 b). Compared to the extract, the suspension displays a more pronounced long-term buffering behaviour, demanding more alkali and exhibiting lower starting pH values on the subsequent testing days. Generally, these results correspond well with previous research in this field²²⁵. However, since the test was finished on day 24, it remains elusive how much alkali and time it would take to adjust the pH value of the suspension to a permanently set end point.

In previous literature, the long-term alkaline buffering behaviour was observed in wood suspensions²²⁵ and has been attributed to the gradual diffusion processes from the wood phase in suspension to the water phase. Consequently, it was surprising to observe a similar effect in the extractive, where the wood substrate is not present as a continuous source of buffering. This suggests that the long-term buffering effect is inherent to certain wood extractives or degradation products rather than solely associated with the wood substrate.

To conclude, the wood-water extract method simplifies certain aspects in the ABC measurement that are better represented by the suspension method, such as the effect of surface area in large particles and continuous buffering during the measurement. However, the suspension method relies on many additional variables (i.e., particle size, latency time), requires more chemicals, and yields more variable results due to continuous buffering effects. Therefore, the hot-water extract method is employed in the following section to compare multiple wood species.

3.4.3.3. Species Comparison using Hot-Water Wood Extracts

The hot-water extract method was selected to compare different timbers in this section. Titration curves of the different extracts are displayed in Figure 3-13 and the initial pH value as well as the ABC per gram and per batch of treated samples are shown in Table 3-3. The table shows that the pH value of the extracts ranged between pH 4.43 – 5.37 in the hardwoods and pH 4.27 – 4.89 in the softwoods.

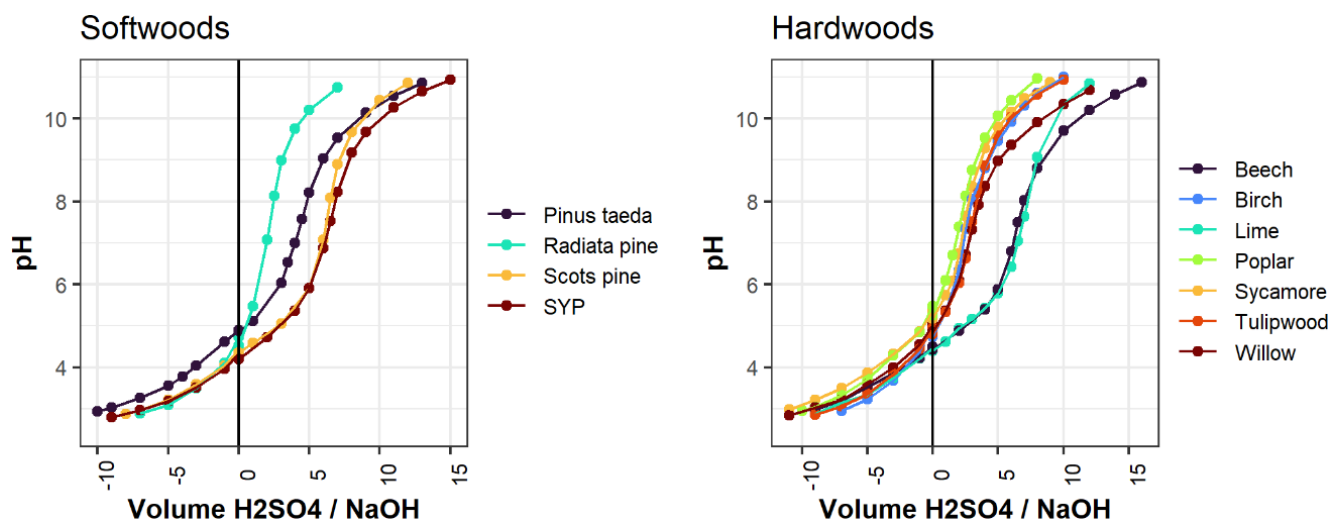


Figure 3-13 Comparing the hot water extracts of different wood species reveals some variability between species. Softwoods are shown on the left and hardwoods on the right.

From Figure 3-12 and Table 3-3, it is evident that Radiata pine exhibits the lowest ABC among the softwoods, followed by Scots pine, *Pinus taeda*, and SYP. Among the hardwoods, a clear separation is observed between lime and beech (with a high ABC) and all other hardwoods (with similarly low ABC values). As lime and beech were found to have a high hemicellulose content (Table 3-2), their higher ABC values could be explained by the auto-hydrolysis of acetyl-groups in hemicelluloses to acetic acid²²⁶. This implies that the ABC of the hot-water extract is mainly determined by the presence of degradation products, whereas water-soluble extractives seem to have a minor influence. This consideration is strengthened by the lack of a significant correlation between extractive content (both ExtrW and ExtrS, pH value, and ABC (Appendix 3)). The chemical composition of different extracts is discussed further in section 3.4.4.

Table 3-3 shows the ABC values per gram of material and per batch of treated wood samples. To investigate the relevance of acid-base interactions in the modification process, the ABC per batch of treated wood samples was compared with the amount of alkali in one batch of resin. As will be described in chapter 5, the resin volume used for impregnating 10 wood samples was consistently 100 ml, but the mass of treated wood varied with its density. This is considered with the ABC in mmol/batch. Each batch of wood was impregnated with 100 ml resin at 30% (w/w) solid content. According to the technical data sheet of the resin at 50% solid content, potassium hydroxide is present at a concentration of 1 – 2 % (w/w) as an alkaline catalyst.

Table 3-3 The initial pH value of the hot water extracts in different species and the alkaline buffer capacity per gram of wood as well as per batch of 10 treated wood samples.

Species	Cluster	pH value	ABC in mmol/g	ABC in mmol/batch
Beech	A	4.47	1.30	18.0
Birch	A	4.87	0.84	9.8
Sycamore	D	5.26	0.81	9.2
Lime	A	4.43	1.04	12.1
Tulipwood	B	4.88	0.85	6.4
Poplar	D	5.37	0.74	6.5
Willow	D	4.94	1.10	7.3
SYP	C	4.27	1.18	14.0
Scots pine	C	4.39	1.06	13.3
<i>Pinus taeda</i>	C	4.89	1.12	18.3
Radiata pine	B	4.63	0.72	6.1

Interestingly, the calculated values for alkali present in each resin batch (10.7 – 20.4 mmol/batch) and the ABC of wood per batch (6.1 – 18.3 mmol/batch) are in a similar range. Although such comparisons must be made with caution, it is likely that acid-base interactions occur. Moreover, differences among species might be significant in terms of the potential consumption of alkali. While the ABC measurements in Figure 3-13 are suitable to show differences between wood species, they do not fully capture the situation in resin impregnated wood.

3.4.4. Wood Extractives Analysis using Solution-State NMR Spectroscopy

The following section aims to better understand which compounds in wood might interfere with the resin curing reaction, e.g., through acid-base interactions or by the formation of covalent bonds with the resin. Therefore, the structure of wood extractives is characterised using solution-state NMR spectroscopy. It is noted that the extractives fraction of wood is structurally complex, and multiple compounds exist in a single wood species. Consequently, NMR spectroscopy can only provide a broad description of these complex mixtures of molecules.

Figure 3-14 shows an example ^1H - ^{13}C HSQC NMR spectrum of SYP solvent extractives with an approximate assignment of the spectral regions that are indicative of certain functional groups in the sample. More precise assignments of the peaks can be made by comparing them with the existing literature or by utilising the chemical shift prediction tool of a chemical analysis software like MestreNova. Additionally, it should be noted that the pulse sequence that was chosen for the NMR experiments in this section displays carbons of the type $-\text{CH}-$ and $-\text{CH}_3-$ in blue, while carbons of the type $-\text{CH}_2-$ are shown in red. Quaternary carbons are not displayed in the ^1H - ^{13}C HSQC NMR spectrum. The spectrum shows a peak for every ^1H attached to a ^{13}C nucleus. The x-axis represents the chemical shift of ^1H , while the y-axis corresponds to the chemical shift of ^{13}C .

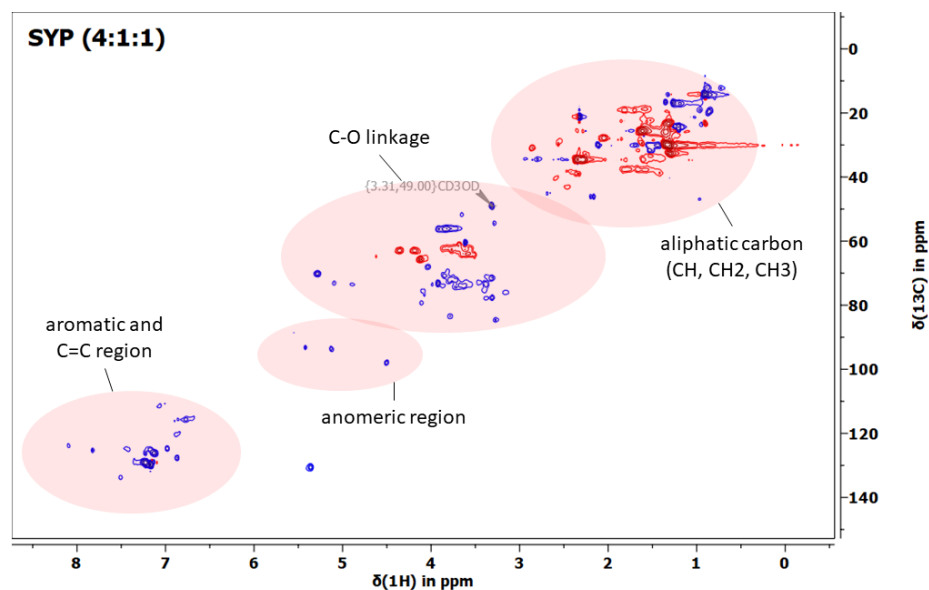


Figure 3-14 Example of a ^1H - ^{13}C -Heteronuclear Single Quantum Coherence (HSQC) spectrum of SYP solvent extractives with an approximate assignment of the regions in the spectrum.

Figure 3-15 shows a comparison of solvent extractives and hot-water extractives for SYP, lime, and sycamore. Red peaks in the aliphatic region (i.e., 2/30 ppm – 0.5/10 ppm) indicate saturated alkane chain elements that constitute the cyclohexane backbone of resin acids (see Figure 3-1). The region between 8/140 ppm – 5/100 ppm further indicates aromatic ring carbons found in many other types of extractives²⁷. In addition, the SYP solvent extractives show patterns indicative of carbohydrates, where red peaks between 4.5/65 ppm – 3.5/60 ppm correspond to exocyclic carbons, blue peaks between 4/80 ppm – 3.10/66 ppm to endocyclic carbons, and blue peaks between 92 – 97 ppm to anomeric carbons in a carbohydrate ring^{246–248}.

In polymeric carbohydrates, the anomeric carbon bears the glycosidic linkage and would show up in the region of 105 ppm^{38,249}. As no such signal is detected, the carbohydrates in the solvent extractives are likely monomers such as glucose.

For SYP, it is evident that most of the carbohydrate peaks are also present in the water extractives, while most of the aliphatic and aromatic signals disappear. Peaks at 5.28/70.1ppm and 4.88/73.6ppm disappeared as well. New peaks appeared at 3.49/66.2 ppm, 3.73/66.6 ppm, 5.07/92.7 ppm, 4.34/102.3 ppm, 4.46/104.12 ppm, and 4.56/100.33 ppm indicating new polymeric carbohydrates that are bearing a glycosidic bond (e.g., pectin, starch, xylan, mannan).

In conclusion, the solvent extractive of SYP seems to be a mixture of typical softwood extractives (e.g., stilbenes, lignans, flavonoids, resin acids) and some monomeric carbohydrates. The water extractive of SYP contains fewer non-polar extractives but more carbohydrates, which are probably polymeric. Appendix 4 shows that the HSQC spectra of different softwood species are similar, indicating chemically similar solvent extractives fractions.

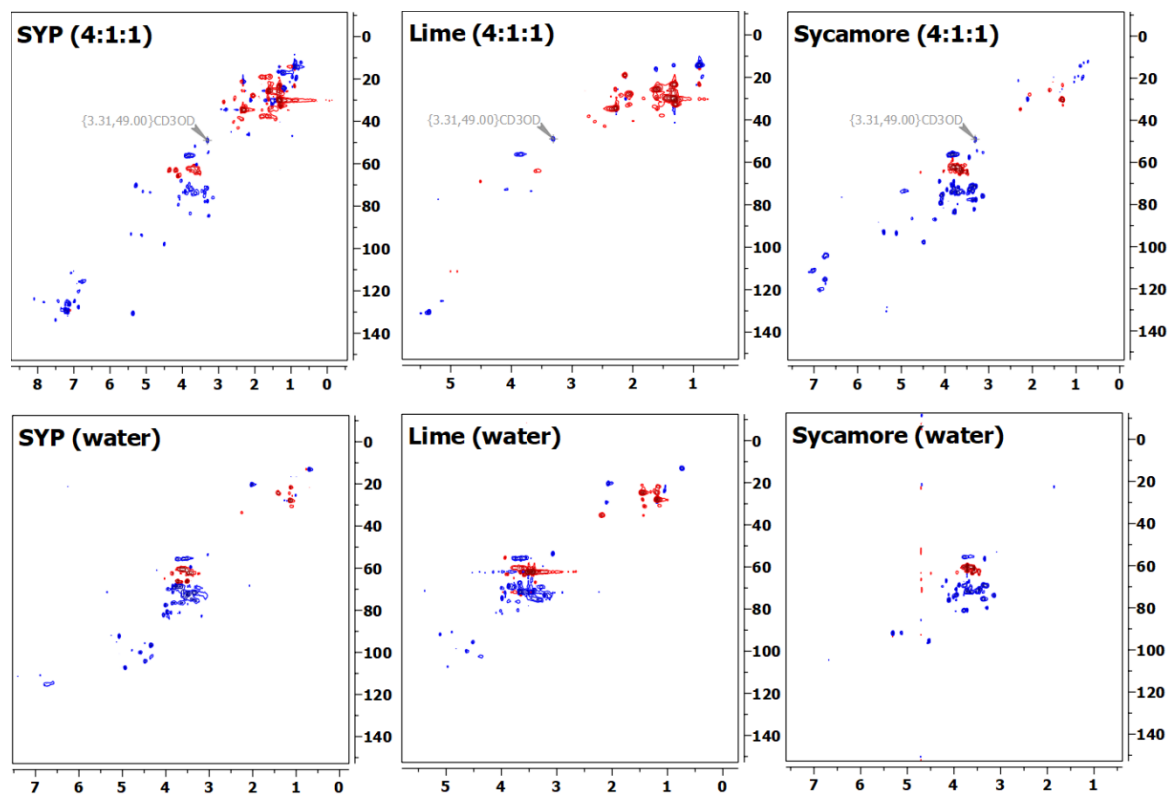


Figure 3-15 ^1H - ^{13}C -Heteronuclear Single Quantum Coherence (HSQC) spectra of SYP, lime, and sycamore extractives that were extracted with either organic solvent (top row) or water (bottom row).

Hardwood solvent extractives in Figure 3-15 are generally more variable, showing distinct HSQC spectra for each wood species (see also Appendix 5). In lime, this fraction is almost exclusively constituted of aliphatic chain elements, indicating the prevalence of hydrophobic compounds such as steroids, fats, or waxes. Water extractives of lime display completely different peaks that are more characteristic of carbohydrates. Solvent extractives of sycamore show patterns of carbohydrates as well as signals in the aliphatic and aromatic region, which indicate the presence of other typical hardwood extractives, such as steroids or fatty acids²⁷. In sycamore, both the solvent extractive and the water extractive display the same peaks in the carbohydrate region. However, aromatic and aliphatic signals are absent in the water extract, indicating that water dissolved only the polar sugar fraction and left the less polar compounds behind.

Acetic acid, indicated by a peak at 2.1/20.5 ppm, is present in all water extractives observed, but not in the solvent extractives. The acetic acid signal is intense in SYP and lime but subtle in sycamore. Since these are the same samples used in the ABC measurements in section 3.4.3.3, it is reasonable to assume the acetic acid concentration in the water-extract influences its ABC. However, quantification of acetic acid concentration by peak integration was not possible as no reference compound was present. Acetic acid is a degradation product of hemicelluloses that is formed via auto-hydrolysis in water. Other hydrolysis products, such as glucuronic acids²²⁶, formed through similar pathways in the presence of hot water, could also explain many of the carbohydrate signals observed in water extractives in this section.

To conclude, solution-state NMR studies have shown similar structures in the solvent extractives of softwoods, despite some differences in the sugar profile. Solvent extractives in softwoods are probably stilbenes, tannins, flavonoids, lignans, and resin acids, as expected. In hot water, however, the hydrophobic components are not extracted, and they are therefore not relevant in ABC measurements. Instead, the hot water extract mainly contains sugars, and the acidity originates from acetic acid and glucuronic acids.

Hardwood extractives are generally more diverse than those of softwoods. However, regardless of the composition that extractives have in organic solvent, water dissolves mainly the polar sugar fraction and the acetic acid that is present as a degradation product of hemicelluloses. Although the functional groups of these substances can be assigned with high accuracy, it is difficult to characterise mixtures with NMR spectroscopy. More information about the structure of wood extractives could be gathered in future studies using techniques such as gas chromatography-mass spectrometry (GC–MS). However, this is not the primary aim of this thesis.

3.5. Conclusions from Chapter 3

This chapter primarily revealed chemical differences between the eleven wood species that are used throughout this thesis. The cluster analysis of FTIR spectra identified four main groups of chemically similar timbers (clusters A – D). Species in the same cluster often showed similar properties in wet chemistry and ABC measurements, although exceptions were seen. Lime wood might constitute a separate cluster due to its distinct chemical composition. Radiata pine and tulipwood are assigned to the same cluster, although their chemical composition is clearly different. Nevertheless, it is practical to use cluster analysis assignments in the following. Table 4 shows a summary of properties. Further conclusions from this chapter are:

- Acid-base interactions between alkaline resin and acidic wood might be relevant during the studied modification process.
- Acetic acid and glucuronic acid derivatives influence the ABC of wood-water extract to a great extent.
- Long-term buffering is pronounced in both wood-water suspensions and extracts.
- Solvent extractives differ from hot-water extractives in most species.
- Solvent extractives of softwoods are chemically similar.
- Solvent extractives of hardwoods are variable.
- Hot-water extractives from all timbers are relatively similar and contain mainly carbohydrates and hydrolysis products such as acetic acid and glucuronic acid derivatives.

In the context of wood modification with PUF resin, it is essential to account for the variations in wood chemistry between different species. These differences must be taken into consideration when explaining variations in treatment efficiency among different types of wood.

Table 3-4 Grouping of eleven wood species according to hierarchical cluster analysis (HCA) of FTIR-ATR spectra and general properties that can be assigned to timbers in these clusters.

Cluster	Species	Wood Type	Carbohydrate Content	Acetyl Content	Lignin Content	G:S Lignin Ratio	Acidity of the Extract	
A	beech, birch, lime (?)	hardwood	high	high(?)	low	low(?)	more acidic	
B	tulipwood, Radiata pine	assignment not clear – regarded as an artefact introduced by clustering methods						
C	Scots pine, <i>Pinus taeda</i> , SYP	softwood	low	low(?)	high	high(?)	more acidic	
D	willow, poplar, Sycamore	hardwood	low	low(?)	relatively high	relatively high(?)	less acidic	

4. Characterisation of Phenol Urea Formaldehyde Resin

4.1 Introduction to Chapter 4

The fundamentals of PUF resin chemistry were discussed in the literature review Chapter 2.3. While most resole resins in the literature are used as adhesives, the resin used throughout this thesis has a different set of properties, such as a lower molecular weight and a lower pH value. Furthermore, it contains urea which is often neglected in the literature. The aim of this chapter is to characterise the properties of the resin, which is used throughout the experimental work in the following chapters. In this context properties that are relevant for the studied wood modification process are investigated, such as reaction kinetics, chemical structure, water absorption. This will improve the understanding of the studied modification process and enable further work in this thesis.

The reaction kinetics are studied by differential scanning calorimetry (DSC). Previous DSC studies used either open or closed crucibles for this analysis. Open crucibles allow the evaporation of water from liquid resin, which is a disadvantage, as it interferes with the signal for the exothermic curing reaction occurring in a similar temperature range. It was found, however, that open crucibles can still be used if the liquid resin is freeze-dried prior to the analysis²⁵⁰. Closed crucibles, in which water evaporation is completely prevented by high pressure, have proven more popular in the literature. However, they might not reflect the true curing conditions of application where the resin is cured under normal pressure^{206, 212,251}.

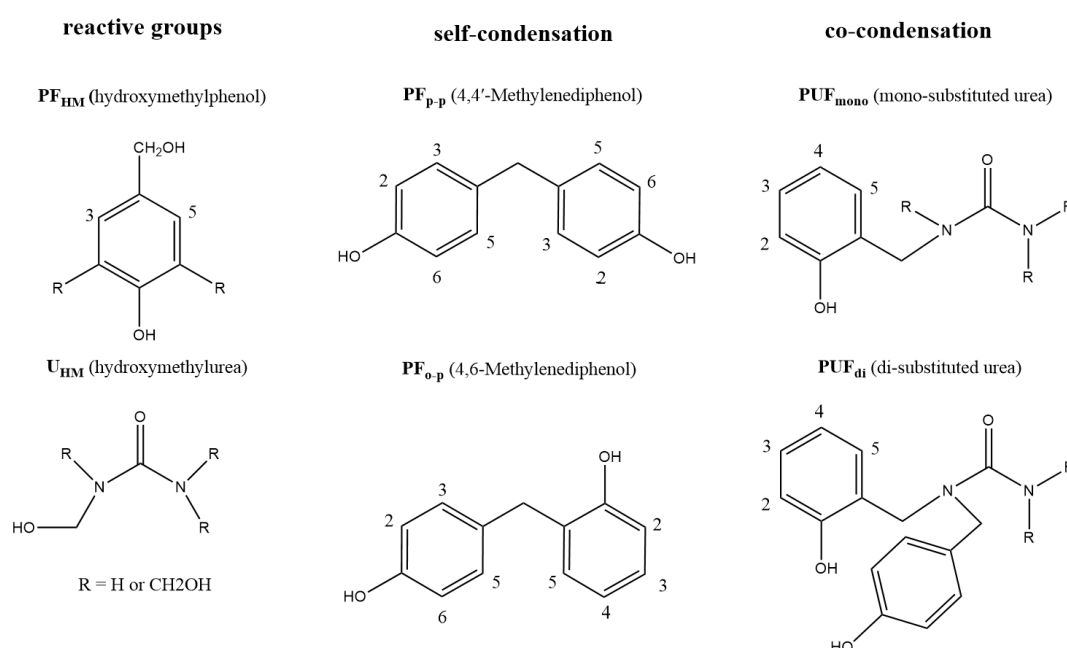


Figure 4-1 Phenol Urea Formaldehyde (PUF) resin is a mixture of molecules with different properties. The chemical structure of main constituents in PUF resin including abbreviations used throughout this thesis are presented in the figure.

The curing reaction of a resole resin in closed crucibles typically shows one or two exothermic peaks. Christiansen and Gollob²⁰⁶ (1985) observed two peaks in the range from 98 – 129°C and from 139 – 151°C, shifting with the molar ratios F/P and NaOH/P. The first peak was attributed to the initial addition of formaldehyde to free positions on the phenolic ring. The second peak was associated with the condensation reaction. Park *et al.*⁷⁰ (1999) made similar observations on powdered PF resin. Depending on the heating rate, the first peak varied from 120 – 142°C and second one from 153 – 165°C. However, Park *et al.*⁷⁰ argue that the first peak corresponds to the reaction of a high molecular weight fraction and the second peak to a low molecular weight fraction. Papadopoulou and Chrissafis¹⁷² (2011) favoured this explanation too.

The thermogram of a DSC scan provides information about the onset temperature and reaction enthalpy, however, much of the reaction kinetics can be derived from the relationship between heating rate and peak temperature for multiple runs with three or more heating rates^{192,252,253}. A well-established evaluation method in this context is based on the Kissinger-plot (see Figure 4-5). Three scans at different heating rates generate a straight line in this plot, where the slope of the trendline is used to calculate the activation energy and the intercept provides the pre-exponential factor. The rate constant of the curing reaction is then calculated using the Arrhenius law.

Figure 4-1 shows examples of the main constituents in the studied PUF resin. Reactive intermediates, which contain a hydroxymethyl group, are formed both by phenol (PF_{HM}) and urea (U_{HM}). In the curing reaction, these intermediates engage in self-condensation or co-condensation, as shown in the Figure 4-1. Notably, in an alkaline environment, urea can form reactive intermediates with formaldehyde, but these intermediates cannot crosslink with themselves¹⁸². This mechanism is summarised in Figure 4-2.

Self-condensation of PF_{HM} with itself and co-condensation of PF_{HM} with U_{HM} occur simultaneously. Co-condensation is kinetically favoured^{182,254} but may be limited by the amount of available U_{HM}. The formation of U_{HM} requires free formaldehyde, which is only available in trace amounts. Once free formaldehyde is depleted, the hydroxymethylation of urea (see Figure 4-2) stops and this pathway becomes unavailable. Free urea will remain unreacted and curing may continue via other pathways.

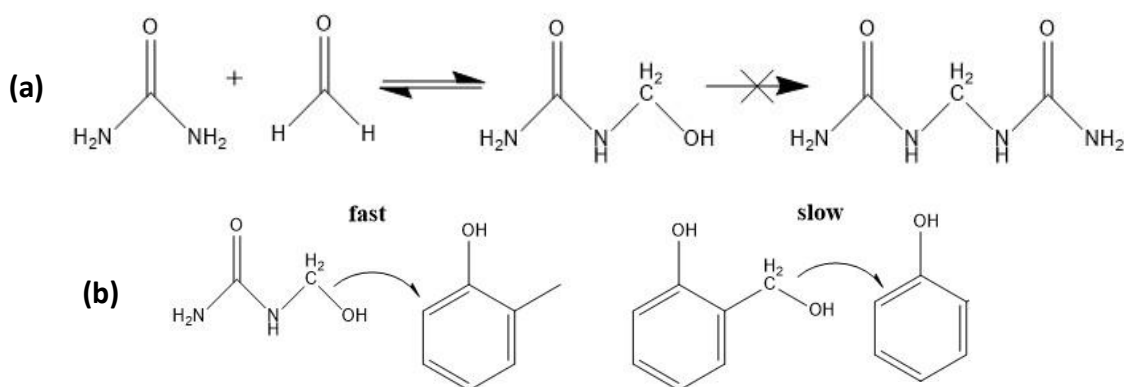


Figure 4-2 (a) Urea forms reactive intermediates (U_{HM}) but the self-condensation of hydroxymethylated urea (U_{HM}) with itself is restricted in alkaline environment. (b) Co-condensation with U_{HM} is kinetically favoured over self-condensation of PF_{HM} with itself.

Wood products can be negatively affected by the absorption of water from the atmosphere, impacting various properties. Wood modification with thermosetting resins aims to suppress water absorption by various mechanisms, such as the blocking of micropores¹¹¹. However, it should be noted that even cured thermosets absorb water from the atmosphere. Wimmer et al.²⁵⁵ (2013) compared the absorption behaviour of various commercial adhesive films such as phenol resorcinol formaldehyde (PRF), melamine urea formaldehyde (MUF), and polyurethane (PU) resin by using dynamic vapor sorption (DVS). Formaldehyde-based adhesives displayed especially high moisture uptakes, with up to 18% moisture content in PRF. The absorption behaviour of cured resins seems to be governed by the free volume available in the cured polymer, and by ionic groups incorporated in the polymer chain. Water absorption should be minimised, as high moisture contents negatively affect the hardness and MOE of the cured resin²⁵⁶.

4.2 Materials

4.2.1 Phenol Urea Formaldehyde Resin

Commercial PUF resin (*Prefere 5K600M*) containing potassium hydroxide catalyst (1 – 2% w/w), trace amounts of free formaldehyde, and free phenol was provided by *Prefere GmbH* (Germany). The molecular weight information as reported by *Prefere GmbH* are $M_n = 406$ g/mol and $M_w = 484$ g/mol. The resin was delivered with a concentration of 50% (w/w) and pH 9.5. Later this is referred to as default resin. It is noted that the potassium hydroxide concentration of 1 – 2% does not correspond with the measured pH value of 9.5. In pure water, such a concentration would correspond to pH value of 12.4 and 12.7, respectively.

In this Chapter, the resin concentration and pH value were altered (after delivery) to study their effect in the curing reaction. Figure 4-3 shows resin samples after changing their pH values. The pH value of two samples was lowered to pH 6.3 and pH 4.6 by adding acetic acid (99% w/w) dropwise. In one specimen, the pH value was raised to pH 10.2 by adding potassium hydroxide pellets (85% w/w). There was a notable change in colour as shown in Figure 4-3. One resin sample was diluted to 30% (w/w) by adding deionised water. For some DSC, FTIR-ATR, and NMR analysis the default resin was freeze dried at -65°C and 10 mTorr.



Figure 4-3 The colour of the studied PUF resin changes with the pH value. PUF resin adjusted to different pH values by adding either acetic acid (99% w/w) or potassium hydroxide pellets. From left to right: pH 4.68, pH 6.3, pH 9.5 (default), pH 10.26.

4.3 Methods

4.3.1 Water Tolerance, pH value, Solids Content – Resin Quality Control

The work in this thesis involved the use of multiple batches of the same resin. Upon delivery, the resin was stored in a cold room at 2°C without sunlight to minimise aging effects. To ensure consistent resin properties, quality control checks were conducted after the delivery of a batch and before its utilisation. The quality controls measures taken in this thesis include the monitoring of water tolerance, pH value, and solids content.

Water tolerance was measured according to EN ISO 8989 (1998). Therefore, a volume of 5 ml resin with 30% solid content was placed in 100 ml beaker. Under constant stirring, deionised water was added in 0.5 ml increments, using a burette. The titration end point was reached once the resin turned from clear to cloudy. According to EN ISO 8989, the water tolerance was calculated by referring the volume of added water to the volume of resin. The water tolerance upon delivery was between 1:10 and 1:20 and remained constant when the resin was stored in a cooled room at 2°C . When stored at ambient temperature, the water tolerance dropped rapidly within a couple of weeks.

The resin pH value was measured using a pH-meter (*Mettler*, FiveEasy) which was calibrated at pH 4 and 7 using standard buffer solution. The resin solid content was measured by placing approximately 5 g liquid resin in an oven at 103°C overnight to evaporate the water and induce resin cure. The solid content was calculated by referring the dry resin mass to the liquid resin mass.

4.3.2 DSC – Sample Collection

DSC was performed using a TGA/DSC STARe System (*Mettler Toledo*). To eliminate the noise caused by water evaporation, reusable high-pressure aluminium crucibles (ME – 51140404) were used for most measurements. This system can hold a pressure of up to 15 MPa. Crucibles were sealed with gold-plated membrane (ME – 51140403) and closed with a special sealing tool (ME – 51119915). The acceptable mass loss due to evaporation of surface moisture was 50 µg according to the manual. Scans showing significantly higher mass loss indicate that crucibles were not properly sealed. These scans were rejected and repeated.

Open aluminium crucibles (ME – 267363) were used for comparison with the closed system. In this case, freeze dried resin was used, that was stored in a desiccator over silica gel before the analysis. All samples were approximately 10 mg to ensure comparability. The temperature programme was run from 30°C to 250°C at the heating rates 5°C/min, 10°C/min, and 20°C/min for each sample to allow calculation of activation energy and pre-exponential factor (see 4.3.3). A constant N₂ flow of 50 cm³/min was ensured for all scans. Both crucible systems are displayed in Figure 4-4.



Figure 4-4 (left) High-pressure crucible and open crucible next to a one penny coin for scale. (right) Wood section inside the pressurised crucible before it is sealed.

4.3.3 DSC – Kissinger Method

The activation energy (E_A) and the pre-exponential factor (Z) of the resin curing reaction were calculated using the Kissinger method²⁵³. Therefore, the same sample was scanned at three different heating rates (β) as described earlier. The peak temperatures (T_p) of each scan were used the calculations which are outlined in the following.

Non-isothermal DSC makes certain assumption which must be met by the investigated reaction. Firstly, the reaction kinetics must follow an n^{th} -order mechanism in which the rate of conversion ($\frac{d\alpha}{dt}$) depends on a rate constant (k), on the conversion (or concentration) of reactants (α), and on the reaction order (n), which can be written as:

$$\frac{d\alpha}{dt} = k (1 - \alpha)^n$$

It is further assumed that the temperature dependence of (k) can be described Arrhenius law:

$$k(T) = Z \exp\left(-\frac{E_a}{RT}\right)$$

where R is the universal gas constant 8.145 J/K , and T is the temperature on the absolute scale. Kissinger argued that $n(1 - \alpha)^{n-1} = 1$ and independent of temperature. Using this assumption, one yields the following equation:

$$-\ln\left(\frac{\beta}{Tp^2}\right) = -\frac{Ea}{RTp} - \ln\left(\frac{ZR}{Ea}\right)$$

Plotting $-\ln\left(\frac{\beta}{Tp^2}\right)$ against $\left(\frac{1}{Tp}\right)$ for three different heating rates yields a Kissinger plot as shown in Figure 4-5, where the slope of the trend line is equal to $-\frac{Ea}{R}$ and the y-intercept equal to $-\ln\left(\frac{ZR}{Ea}\right)$. Once Ea and Z are determined, the rate constant can be calculated using Arrhenius law.

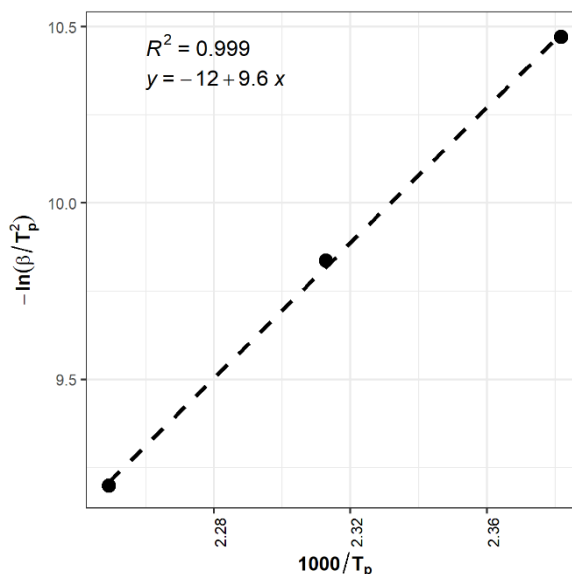


Figure 4-5 Example Kissinger plot. Three data points describe a linear regression line from which the activation energy (E_a) and the pre-exponential factor (Z) can be derived. The Kissinger plot is used for the analysis of DSC experiments in this thesis.

4.3.4 FTIR-ATR Spectroscopy – Sample Collection

The acquisition parameters of the FTIR–ATR scans are the same as in section 3.3.1, however, the sample preparation of the resin differs from the sample preparation of wood. Uncured resin was presented to the ATR crystal either in the liquid state at a concentration of 50% (w/w), or in the freeze-dried state to improve the quality of the spectrum. Cured resin was crushed to fine powder with a dismembrator (*Micro-Dismembrator U - Braun*), before it was analysed.

4.3.5 Solution-State NMR Spectroscopy – Resin Analysis

The method employed in this chapter is analogous to Chapter 3; however, there were variations in the resin sample preparation methods. The liquid resin was freeze-dried and subsequently re-dissolved in DMSO- d_6 before the analysis.

To study the early stage of the curing reaction, the liquid resin was placed in silicon cases and was transferred to an oven set to 150°C for either 30 min or 1 h. After this time, the solvent water has largely evaporated, hence, freeze drying was not necessary. The partly cured resin samples were re-dissolved in DMSO- d_6 and then analysed as previously described in Chapter 3.3.6.

4.3.6 DVS – Hygric Properties of cured Resin

Dynamic vapour sorption (DVS) was employed to investigate the hygric properties of cured resin. The DVS Advantage instrument (*Surface Measurement Systems Ltd.*) was used for all analysis. Resin samples (5 g, as supplied) were cured in an oven at 150°C for 1.5 h, 3 h, and 5 h to achieve different levels of crosslinking.

The now solid samples were crushed to a fine powder using a dismembrator. Approximately 10 mg of each sample was required for DVS analysis. The sample was suspended in a microbalance within a sealed thermostatically controlled chamber. A constant flow of gaseous nitrogen was passed over the sample at a set rate of 200 cm³/min, carrying a controlled quantity of water vapour. The relative humidity (RH) was increased from 0 – 95% by increments of 5% for the absorption phase. This schedule was reversed for the desorption phase. For each step, the same RH was maintained until the mass change of the sample was less than 0.002 %/min, before proceeding to the next set point. Mass readings were recorded every 20 s. Sorption and desorption isotherms as well as hysteresis curves were calculated from the DVS data.

4.3.7 SEM-EDX – Imaging and Elemental Composition

Resin samples cured in both open and closed systems during the DSC scan were examined through scanning electron microscopy (SEM) and energy dispersive X-ray (EDX) analysis. Therefore, the lid was removed, and the crucibles were directly attached to carbon tape on a stub for presentation to the electron beam. The resin cured in the open system was crushed with a rod to obtain a coarse powder. In contrast, the resin cured in the closed system resembled a paste containing solid resin grains and did not require crushing. All SEM images were taken with a scanning electron microscope (*Hitachi, TM4000*) using a beam acceleration voltage of 15 kV and a detector for backscattered electrons. The EDX spot scans were recorded with the AzTecEnergy program, using a recording time of 300 s.

4.4 Results and Discussion

4.4.1 The Curing Reaction of Resin studied by DSC

The following section deals with the calorimetric characterisation of the curing reaction. Different pH values of the resin are considered to identify mechanisms that may also be relevant when alkaline resin is mixed with acidic wood. The pH value affects the resin curing but also its appearance (see Figure 4-3). Decreasing the pH value results in a brighter colour and finally in an orange-yellowish tone. Increasing the pH value causes a darker colour. This effect is attributed to the different ionisation of the phenolate ion, an effect that is also commonly known from the pH indicator phenolphthalein. In previous correspondence with *Lignia Wood Company Ltd.*, it was noted that certain heartwood sections turned yellowish after modification⁹⁴. This may be one of the effects related to the resin pH value.

Figure 4-6 displays an example of a DSC scan for the same resin sample at pH 10.2 under three different heating rates. This scan, which was conducted in a closed system, exhibits one exothermic signal with a peak between 136 – 162°C, depending on the heating rate. The exothermic peak temperature increases with a faster heating rate, which is due to differences in the absolute energy flow into the sample over time²⁵⁷. If the sample is heated with lower heating rate, it is exposed to the same temperature for longer, compared to heating at a fast rate. Hence the reaction peaks at a lower temperature. The exothermic peak is assigned to all resin curing reactions, i.e., self-condensation and co-condensation.

Table 4-1 displays the main kinetic parameters for PUF resin at different pH values and concentrations and compares them to values found in the literature for PF resin. The default pH value of the resin used throughout this thesis is 9.5. This resin requires an activation energy of 76.8 kJ/mol, which is in a similar range to values measured by Park *et al.*⁷⁰ (1999), but slightly higher than the value measured by He & Riedl²¹² (2004). Differences in the resin formulations are the most likely reason for these variations.

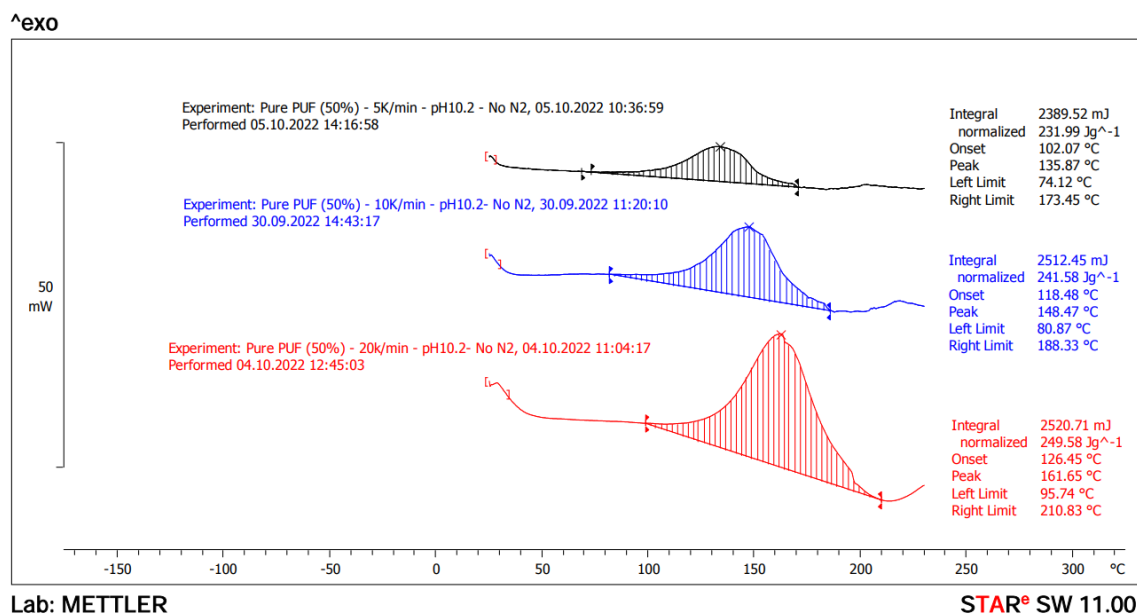


Figure 4-6 Example DSC scans of PUF resin in closed system. PUF resin with a solid content of 50% and pH 10.26. Heating rates of 1 °C/min, 5 °C/min, and 10 °C/min were used.

Previous studies often compare the activation energy of different samples but tend to neglect the pre-exponential factor, when using the Kissinger method. This can lead to false conclusions, as the activation energy alone is not a meaningful parameter. Such limitations become evident in Table 4-1, where the activation energy of acidified resin (pH 6.3) and the more alkaline resin (pH 10.2) decreases compared to the default resin, suggesting increased reactivity. To avoid false conclusion in this thesis, the pre-exponential factor was considered and the resin curing rate (k) was calculated for a typical curing temperature of 150°C using the Arrhenius law. A higher curing rate corresponds to a faster reaction and higher reactivity.

Table 4-1 Kinetic properties of the PUF-curing reaction in high pressure crucibles at different pH value and solids content calculated using the methods of Kissinger and Arrhenius.

Sample	pH	Solid Content in %	T _p in °C			R ²	E _A in kJ/mol	Z in s ⁻¹	k at 150°C in s ⁻¹
			5 °C/min	10 °C/min	20 °C/min				
Pure resin	9.5	50	136.52	148.94	160.96	0.9996	76.80	1.69E+09	0.56
Pure resin	9.2	30	137.82	150.13	161.43	0.9990	80.02	4.16E+09	0.55
Pure resin	6.3	50	149.32	168.08	180.53	0.9888	62.22	9.94E+06	0.21
Pure resin	10.2	50	135.87	148.47	161.65	1.0000	72.50	4.72E+08	0.53
He & Riedl ²¹²	10.5	52	130.00	140.30	159.40	0.9853	59.82	1.35E+07	0.56
Park et al. ⁷⁰	10.2	46	138.95	151.05	164.75	0.9998	73.53	5.48E+08	0.46

Table 4-1 illustrates that the highest curing rate ($k = 0.56 \text{ s}^{-1}$) is achieved under default conditions with resin at pH 9.5 and 50% (w/w) solids content. Acidifying the resin to pH 6.3 significantly reduces the rate from 0.56 s^{-1} to 0.21 s^{-1} . This deceleration is attributed to the neutralisation of the alkaline catalyst. While it is reasonable to assume that adding more alkali might increase the rate constant, this was not observed. In fact, a slight decrease was noted after raising the pH value from 9.5 to 10.2. Similar observations were made in previous studies. Pizzi & Stephanou²⁵⁸ (1993) found that the gel-time of PF resin, which is representative of reaction rate, had an optimum at around pH 7 – 9. Retardation effects at higher pH values were explained by either (i) chelate formation or (ii) quinone formation.

In case (i), the potassium chelate formation incorporates the *ortho*-hydroxymethyl group of PF_{HM}, reducing its reactivity²⁰⁹. For case (ii), it is assumed that quinone species are less reactive in forming methylene bridges with each other. Thus, as the proportion of quinone species increases with pH, the reaction rate drops²⁰⁸.

Moreover, it is possible that changes in pH value affect the reaction pathways, and different pathways may proceed at varying rates. One affected pathway could be the co-condensation between urea and phenol units¹⁸². Also, self-condensation of urea entities becomes possible in an acidic environment with resin at pH 6.3.

The resin was supplied at a concentration of 50% (w/w). However, for wood impregnations, it was diluted to achieve a lower solids content. Table 4-1 provides a comparison between the default resin at 50% and the diluted resin at 30% solids content. Both the activation energy and pre-exponential factor exhibit slight changes, however, the curing rate (k) is barely affected, suggesting that the reaction proceeds at a similar speed. Comparable results were observed in previous studies involving melamine formaldehyde resin⁹⁷.

Using high-pressure crucibles is the prevalent approach when studying the curing behaviour of thermosetting resins. However, one can argue that a pressurised system does not reflect the real-world conditions of resin during applications under normal pressure. In fact, the curing stage in wood modification can be performed in both a pressurised system and an open system^{16,94}. To study the curing reaction in an open system, freeze-dried resin was tested in standard aluminium crucibles allowing water evaporation. Thus, it is assumed that the only water released during the scan is water of condensation formed in the curing reaction.

Figure 4-7 shows an example thermogram of freeze dried PUF resin at pH 9.5 and 50% solids content in an open system and with variable heating rate. The heating rates of 1°C/min, 5°C/min, and 10°C/min are consistent with previous DSC work in this chapter. Additionally, the thermogravimetric (TG) curve is included in Figure 4-7, offering insight into the sample's mass change throughout the scan. Up to three endothermic signals are observed in each scan. The double peak between 120 and 144°C shows the most intense signal which coincides with an increasing rate of mass loss in the TG curve.

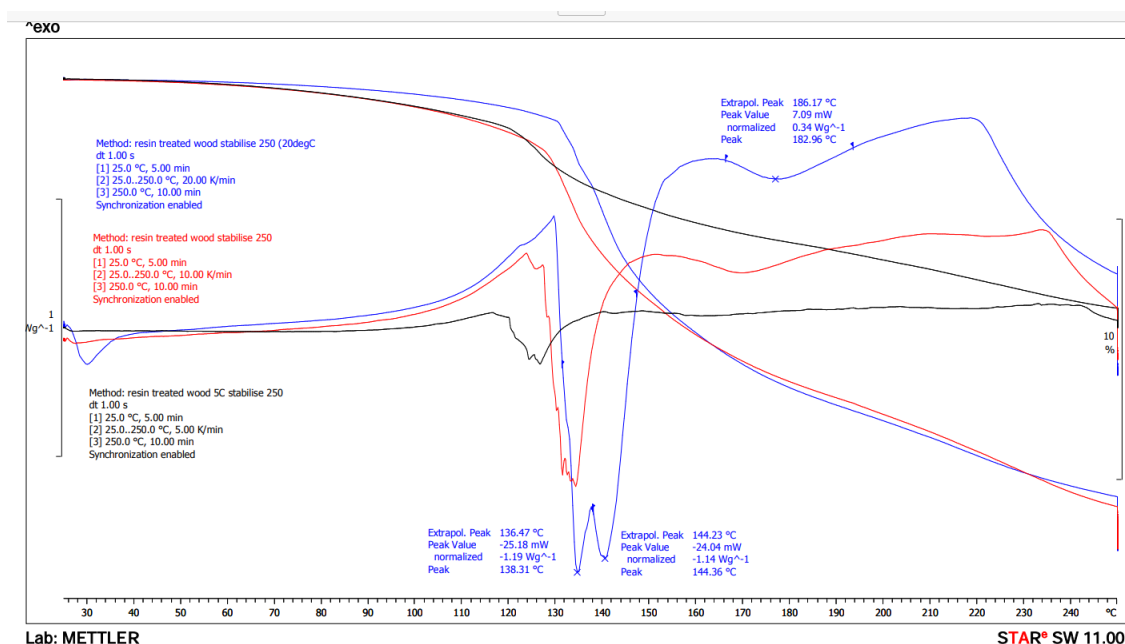


Figure 4-7 Example DSC scan of freeze dried PUF resin in an open system. The signals of heat flow and mass change are displayed in the same colour for the same sample. Heating rates of 1°C/min (in black), 5°C/min (in red), and 10°C/min (in blue) were used.

The slight weight loss (2 – 4%) occurring before the main endothermic event, as marked by the double peak, could indicate the desorption of moisture absorbed from the atmosphere while the open crucible was positioned in the autosampler of the calorimeter. The double peak, with peak I at lower temperature and peak II at higher temperature, is assigned to the curing reaction of the resin. A third endothermic peak with relatively low intensity is observed between 164 – 184°C depending on the heating rate. This Peak III could be associated with another curing or oxidation reaction in the resin, or it might be an artifact, given that it is less pronounced at lower heating rates. Consequently, our focus will be on Peaks I and II in the following analysis.

Table 4-2 shows the main kinetic parameters of the curing reaction in an open system. Interestingly, the curing rates associated with peak I and peak II are one order of magnitude higher than those observed in the closed system. One possible explanation can be formulated based on the law of mass action and Le Chatelier's principle. In the course of the curing reaction, gases such as water and formaldehyde are released, leading to an increase in the volume of the end products compared to the volume of the starting products. According to Le Chatelier's principle, such reactions are constrained by high pressures. Therefore, the curing reaction in the closed and pressurised system requires higher temperatures and proceeds at a lower rate compared to the open system.

Table 4-2 Kinetic properties of the PUF-curing reaction in open pan calculated using the Kissinger and Arrhenius methods.

Sample	T _p in °C			R ²	E _A in kJ/mol	Z in s ⁻¹	k at 150°C in s ⁻¹
	5 °C/min	10 °C/min	20 °C/min				
open pan - peak I	127.87	134.55	138.65	0.9888	166.16	2.62E+21	8.07
open pan - peak II	129.15	137.32	144.36	0.9984	120.10	1.72E+15	2.57
open pan - peak III	164.48	174.22	184.35	1.0000	108.70	3.21E+12	0.12

While it is reasonable to assume different reaction kinetics at different pressure, it is difficult to interpret the thermograms of open crucibles reliably. It cannot be conclusively demonstrated that the main double peak originates exclusively from water of condensation. Even if that were the case, a substantial overlap of endothermic and exothermic events is still apparent, as indicated by the shape of the thermogram in Figure 4-7. Therefore, the conclusions drawn from DSC scans in an open system remain tentative and high-pressure crucibles continue to be the preferred choice for further investigations in Chapter 7.

4.4.2 The Curing Reaction of Resin studied by FTIR-ATR Spectroscopy

While the previous section addressed the kinetics of the curing reaction, this chapter delves into the chemical composition and the changes in chemical composition during heat curing, utilising FTIR-ATR spectroscopy. In this context, the effects of different resin pH values and crucible systems (see 4.4.1) were compared. Table 4-3 shows the assignment of the main absorption bands in the spectrum of PUF resin. The table refers both to the uncured and the cured state of the resin. It should be noted that there is some overlap between peaks originating from phenolic and urea structures, but most bands are assigned with sufficient accuracy.

Table 4-3 Assignment of wavenumbers in PUF resin according to literature. *i.p.* – in plane vibration, *o.o.p.* – out of plane vibration.

Wavenumber in cm^{-1}	Indicative of structure in PUF resin
760 - 740	C-H deformation in ortho-substituted PF ¹⁹⁴ or N-H deformation in secondary amides ¹⁹³
890	2,4,6 – tri-hydroxymethylphenol ring ¹⁹³
1000	aliphatic C-O stretch of phenolic hydroxymethyl group ^{193, 259}
1165	phenolic C-O stretching ^{193, 259}
1250	asymmetric phenolic C-C-O stretching ²⁵⁹ and C-N stretching in primary amides ¹⁹³
1390 - 1315	phenoxy O-H deformation ^{193, 194, 259}
1470	phenolic in-ring vibration ^{193, 194, 259}
1482	C-H deformation of methylene bridges ^{193, 194, 259} in cured PUF resin
1550	phenolic in-ring vibration ¹⁹³
1600	phenolic in-ring vibration ^{193, 194, 259} and N-H deformation in primary amides ¹⁹³
1640	carbonyl C=O stretch in amides ¹⁹³
2900	CH ₂ stretching of methylene bridges in PUF resin ¹⁹⁴
3100	phenolic C-H stretching of unsubstituted aromatic ring ¹⁹⁴
3441 - 3307	phenolic O-H stretching - broad in uncured state, narrow in cured state ¹⁹³
3300 - 3150	solid amides ¹⁹³ N-H stretching
3500 - 3400	liquid amides ¹⁹³ N-H stretching

Figure 4-8 displays the FTIR-ATR spectrum of the default PUF resin in the wavenumber range of 1900 – 700 cm^{-1} both before and after heat curing at 150°C. Uncured resin was freeze dried to improve the quality of the spectrum. The effect of heat curing can be observed throughout the whole spectrum. The peak at 1604 cm^{-1} decreases after cure as N-H groups are crosslinked and form C-N bonds. These C-N bonds, which indicate co-condensation are shown as a shoulder at 1270 cm^{-1} in the spectrum of the cured resin. The peak at 1473 cm^{-1} , which in uncured resin is assigned to the phenolic in-ring vibration, becomes prominent in the cured resin, due to the formation of methylene bridges. The phenolic O-H deformation decreased after cure and moves to lower wavenumbers (from 1350 cm^{-1} to 1338 cm^{-1}). The hydroxymethyl signal at 991 cm^{-1} , which dominates the spectrum of the uncured resin, disappears completely after heat curing. The double peak at 779 cm^{-1} and 755 cm^{-1} , which is indicative of N-H deformations in the uncured resin, turns into a single peak at 763 cm^{-1} upon curing. After the crosslinking of N-H groups, this single peak now exclusively represents the C-H deformation of the phenolic ring.

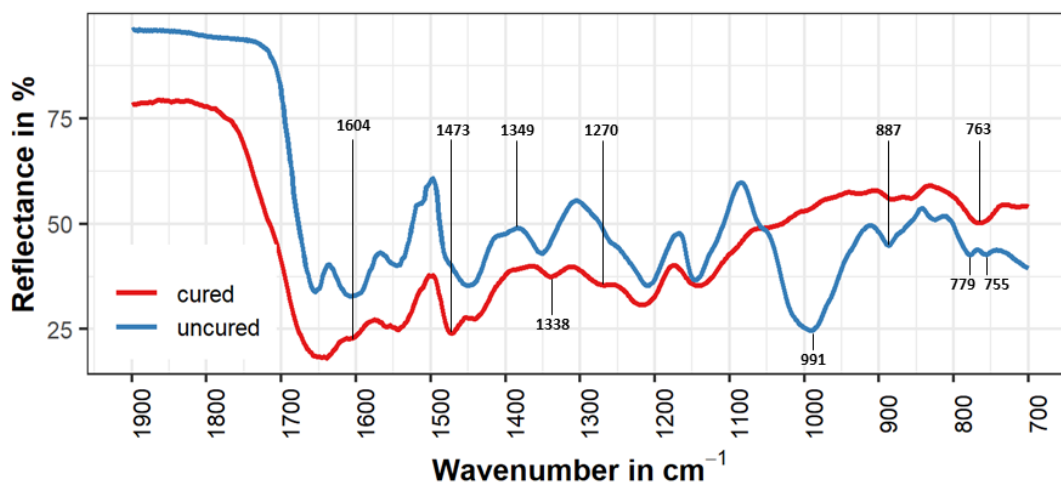


Figure 4-8 FTIR-ATR spectrum of freeze-dried uncured PUF resin and cured PUF resin. Heat curing causes multiple changes in the resin chemistry, most prominently the depletion of the hydroxymethyl groups shown by the peak at 991 cm^{-1} .

Figure 4-9 illustrated the spectrum of uncured PUF resin after adding acetic acid or potassium hydroxide to adjust the pH value, as described earlier in section 4.4.1. Figure 4-9 shows that the first aromatic in-ring stretch at 1546 cm^{-1} intensifies in the acidified resin. The second in-ring stretch around 1450 cm^{-1} moves to different wavenumbers, depending on the pH value. In the acidified resin, it moves to higher wavenumber and in the more alkaline resin to lower wavenumbers. The acidified resin shows an additional peak at 1403 cm^{-1} , which is absent in the other two samples. The 1270 cm^{-1} peak increases in both the acidified and the more alkaline resin. Figure 4-9 demonstrates that certain parts of uncured resin structure are affected by the pH value. In particular, the configuration of the aromatic ring and the interactions between phenol and urea seem to be affected. Earlier in this chapter, changes in pH have been linked to various mechanisms that could account for the observations in Figure 4-9, including chelate formation, quinone formation, or alterations in the ionization of the phenolic group.

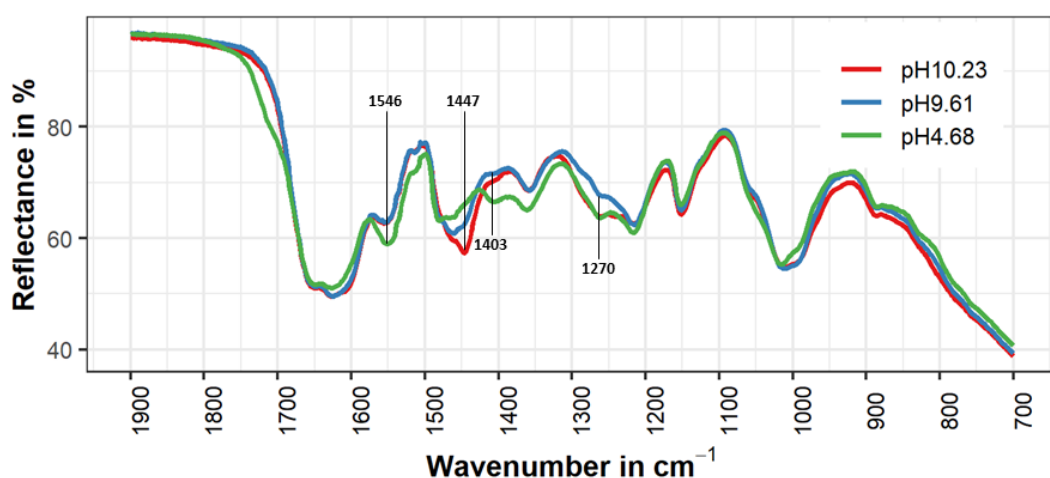


Figure 4-9 FTIR-ATR spectra of uncured PUF resin at different pH values. Resin was not freeze dried. The pH value affects various aspects of the resin structure.

Figure 4-10 shows the previously described samples at three different pH values after heat curing. Differences between the samples are even more pronounced than in Figure 4-9. The ratio of peaks at 1650 cm^{-1} and 1546 cm^{-1} changes notably with the pH value. In the default resin at pH 9.5, both peaks exhibit a similar intensity. In the more alkaline resin, the 1650 cm^{-1} peak dominates, while in the acidified resin the 1546 cm^{-1} peak becomes more intense. This observation suggests differences in the urea fraction of the resin (see Table 4-3).

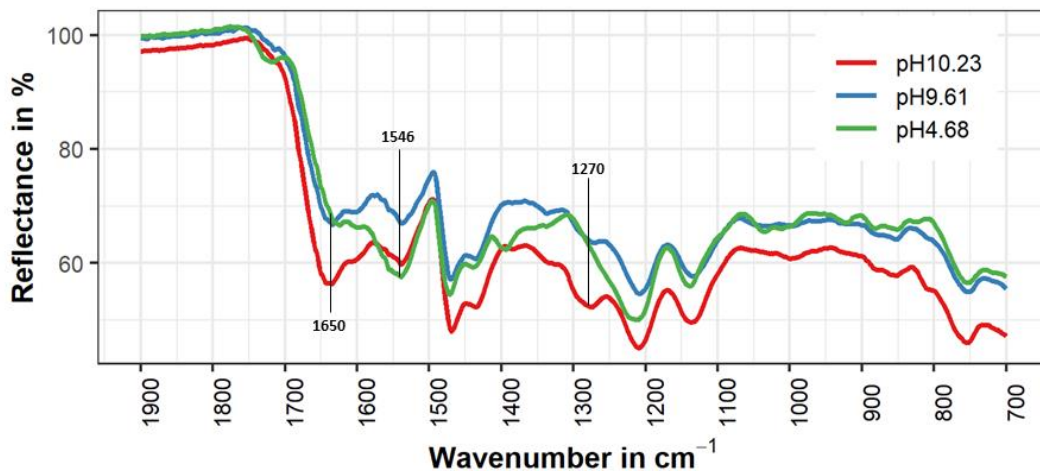


Figure 4-10 FTIR-ATR spectrum of PUF resin cured at different pH values. The ratio of self-condensation and co-condensation is affected by the pH value.

The shoulder at 1270 cm^{-1} intensifies in the alkaline resin and disappears in the acidified resin. This indicates that more alkaline conditions enable co-condensation, whereas acidification restricts co-condensation. Previously, it was assumed that co-condensation of urea and phenol fractions is limited by the amount of free formaldehyde available (see Figure 4-2). However, as the percentage of co-condensation appears to increase at higher pH values, there seem to be other factors involved. Possibly, the formaldehyde generated from the curing reaction, not previously considered, could play a role in the conversion of free urea to hydroxymethylated urea (U_{HM}) under the right conditions.

DSC scans in Chapter 4.4.1 have revealed different curing kinetics for the default PUF resin in an open and closed system. Figure 4-11 displays the FTIR-ATR spectra of resin samples obtained from the two crucible systems after the DSC scans (i.e., in the cured state). In the closed system, the methylene bridge signal at 1473 cm^{-1} is less intense, the phenolic O-H deformation at 1350 cm^{-1} is at higher wavenumbers, and the hydroxymethyl peak at 991 cm^{-1} is more intense compared to the closed system. Notably, the resin cured in a closed system displays patterns indicative of incomplete cure, whereas the same resin appears to be fully cured in the open system. As previously indicated, this difference could be explained with Le Chatelier's principle, which disfavours the reaction of resin in the closed system. This could result in a lower degree of crosslinking observed in Figure 4-11. Regardless of the explanation, Figure 4-11 shows that DSC scans in the closed system do not represent the complete curing reaction.

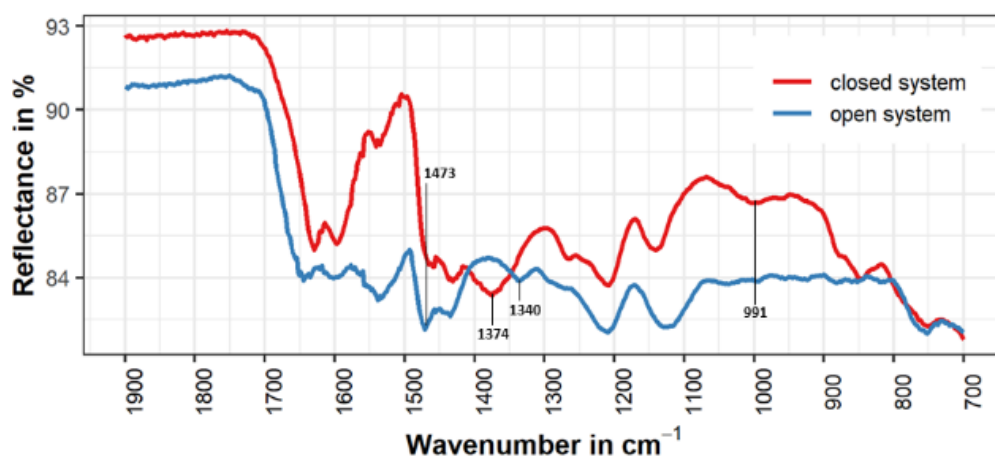


Figure 4-11 FTIR-ATR spectra of PUF resin cured in an open system (atmospheric pressure) and in closed system (high pressure crucible). Resin cured in the closed systems is not fully crosslinked.

4.4.3 Uncured and Partly Cured Resin studied by NMR Spectroscopy

Solution-state NMR spectroscopy was employed to further investigate the chemical structure of the uncured resin and to confirm previous observations from the FTIR section. In comparison to FTIR-ATR spectroscopy, a greater level of detail can be obtained with NMR. However, the analysis is limited to liquid and partly cured resin samples, because the fully cured resin cannot be tested in a solution-state NMR experiment. Partly cured samples could be investigated as long as they were soluble in $\text{DMSO-}d_6$.

Figure 4-12 shows the ^{13}C DEPTQ NMR spectra of uncured and partly cured PUF resin. The pulse sequence of the DEPTQ experiment displays carbons with a $-\text{CH}_2-$ configuration as positive peaks in the spectrum, whereas carbons with a $-\text{CH}-$ or $-\text{CH}_3-$ configuration are displayed as negative peaks. Methylene bridges and residual methanol are shown between 50 – 35 ppm. PF_{HM} groups are observed between 67 – 59 ppm and U_{HM} groups between 72 – 67 ppm. A peak at 83.7 ppm represents free formaldehyde in its oxymethylene form^{206,260}. The region between 132 – 110 ppm represents phenolic ring carbons. Peaks in the region of 116 ppm are assigned to free *ortho*-position.

A small negative peak at 121.3 ppm represents free *para*-position. The positive signals at 125.1 ppm and 128.5 ppm correspond to substituted *ortho*-positions. Negative peaks in the region of 131 – 127 ppm originate from unsubstituted *meta*-positions. The *meta*-position remains generally unsubstituted as it is sterically blocked¹⁷⁰. Peaks at 134.5 and 133.4 ppm are assigned to substituted *para*-positions^{179,260}. Phenoxy carbons are shown between 158 – 150 ppm depending on their molecular environment. A large singlet at 162.9 ppm represents free urea. Mono-, di-, and tri-substituted U_{HM} appears more upfield depending on the degree of substitution¹⁷⁹. The negative singlet at 167 ppm indicates the potassium formate ion (K⁺HCOO⁻), which results from the reaction of KOH and free formaldehyde²⁶¹.

To quantify the relevant functional groups in the resin, peak integration was performed for all signals in the ¹³C DEPTQ spectrum shown in Figure 4-12. The integrated peak values are shown in Appendix 6. Peak integration shows that the *p-p* configuration of methylene bridges is slightly favoured compared to the *o-p* configuration. Moreover, the *ortho*-substitution of PF_{HM} is 23% more frequent than *para*-substitution. The ratio of all reactive intermediates to all methylene bridges is 5.4:1. The ratio of free *para*-positions to free *ortho*-positions is 1:10. Unsubstituted urea is more abundant than mono-, di-, or tri-substituted U_{HM} and free formaldehyde. The ratio of free formaldehyde to free urea is 1:37. Hence, the formation of U_{HM} is limited by the amount of free formaldehyde in the resin. However, formaldehyde generated in the curing reaction might react with the unsubstituted urea to form U_{HM}.

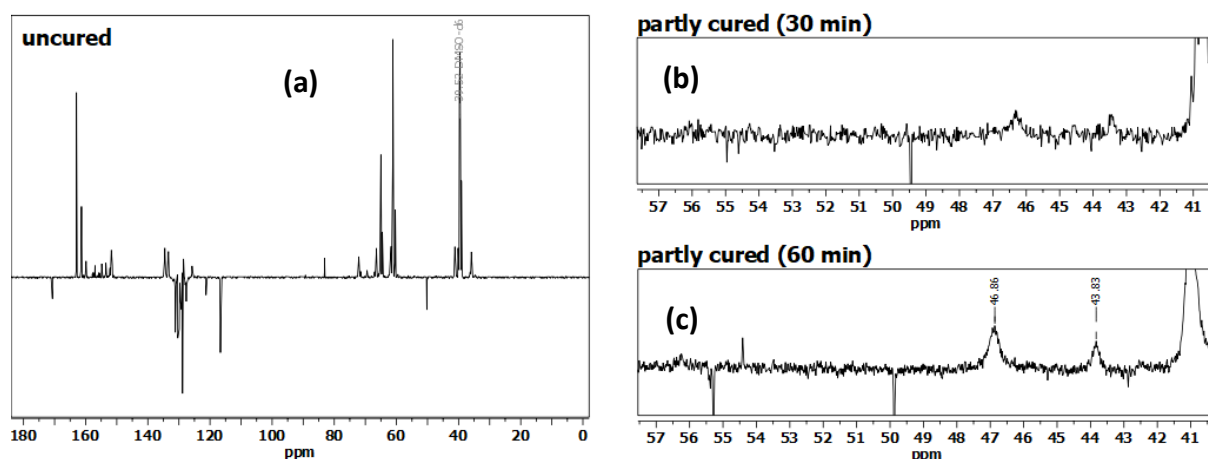


Figure 4-12 (a) ¹³C-DEPTQ spectrum of uncured PUF resin dissolved in DMSO-*d*₆. Spectrum of partly cured PUF resin in DMSO-*d*₆ after 30 min at 150°C (b) and after 60 min at 150°C (c).

Figure 4-12 (b-c) shows the range between 57 – 40 ppm in the ¹³C DEPTQ spectrum of the default PUF resin after curing for 30 – 60 min at 150°C. Evidently, new signals emerge at 55.29 ppm, 54.4 ppm, 46.86 ppm, and 43.83 ppm. The peaks at 46.86 ppm and 43.83 ppm can be assigned to co-condensation at the *ortho*- and *para*-position of the phenolic ring, respectively^{179,182}. These structures correspond to PUF_{mono} in Figure 4-1.

Figure 4-13 shows the ¹H–¹³C HSQC spectrum of the partly cured resin after 60 min and confirms the previous observations. Additionally, a new blue peak at 55.3/3.4 ppm is assigned to methoxymethane (CH₃O-CH₂OH) which occurs as an intermediate side product¹⁹⁹.

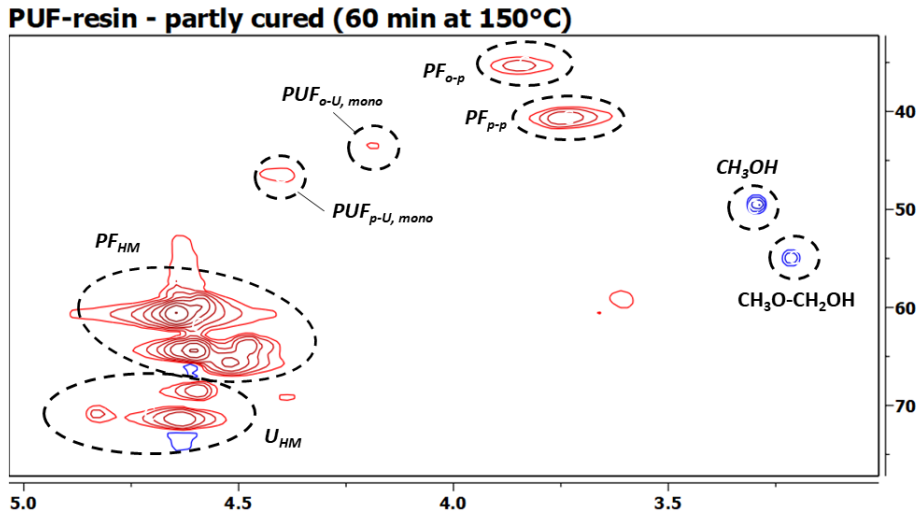


Figure 4-13 ^1H - ^{13}C -HSQC spectrum of partly cured (60 min at 150°C) PUF resin dissolved in DMSO-d_6 .

4.4.4 The Hygric Properties of Cured Resin studied by DVS

Wood modification with thermosetting resin is intended to limit the water uptake of the wood. Nevertheless, the thermosetting resin itself may still absorb small amounts of water from the atmosphere²⁵⁵. This section investigates resin-water interactions using DVS. The resin samples used in this section were cured at 150°C for either 1.5 h, 3 h, or 5 h in order to achieve a varying degree of cure.

Figure 4-14 shows the sigmoid-shaped sorption/desorption isotherms for cured PUF resin. Resin cured for 1.5 h absorbs more water, reaching a higher equilibrium moisture content (EMC) compared to resin that was cured for 3 h or 5 h. The discrepancy between the EMC values intensifies at higher relative humidity (RH). The maximum moisture content at 95% RH decreases with curing time: from 20.69% for 1.5 h, to 9.9% for 3 h, and 8.1% for 5 h. Thus, the hygroscopicity of the resin decreases with the degree of cure.

The most likely explanation is that the sorption behaviour correlates with the number of unreacted PF_{HM} and U_{HM} groups in the resin, since the hydroxymethyl group in these reactive intermediates is the most suitable absorption site in the

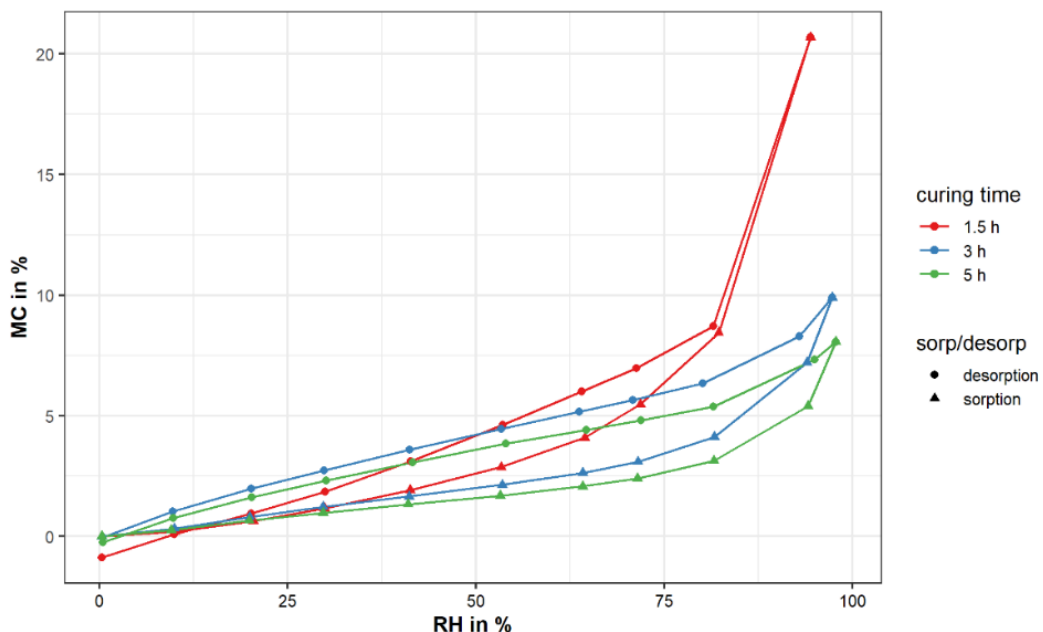


Figure 4-14 DVS sorption isotherm of PUF resin cured for different durations at 150°C . The maximum moisture content decreases with longer curing time. Even fully cured PUF resin is slightly hygroscopic.

resin²⁵⁵. With longer curing time, the degree of cure increases, resulting in reduced water absorption. Nevertheless, the resin assumed to be fully cured (5 h at 150°C) still exhibits water absorption.

This could indicate the presence of a small number of unreacted hydroxymethyl groups. Alternatively, this phenomenon could be attributed to the porous microstructure or to the hygroscopic nature of the KOH catalyst.

Hysteresis, indicating the variance between sorption (wetting) and desorption (drying), is evident in all samples presented in Figure 4-14. The extent of hysteresis across the entire relative humidity range is illustrated in Figure 4-15. Hysteresis is most prominent after 3 h and 5 h of curing time, and least after 1.5 h. Curing times of 3 h and 5 h yield similar hysteresis values at RH below 80%, with differences becoming more pronounced above this RH. Hysteresis in the second sorption/desorption cycles is generally smaller compared to the first cycle.

Various explanations for the hysteresis effect are found in the literature, including different concentrations of hydroxyl groups participating in the adsorption and desorption²⁶², the formation of metastable states of adsorbate in fixed pores²⁶³, and a moisture induced relaxation of glassy solids, resulting in different physical states during absorption and desorption²⁶⁴. In the resin, the molecular rigidity increases with the degree of cure. Therefore, during absorption, more energy would be required to stretch a rigid resin network compared to a more elastic one. This difference in rigidity could account for the higher hysteresis in fully cured resin.

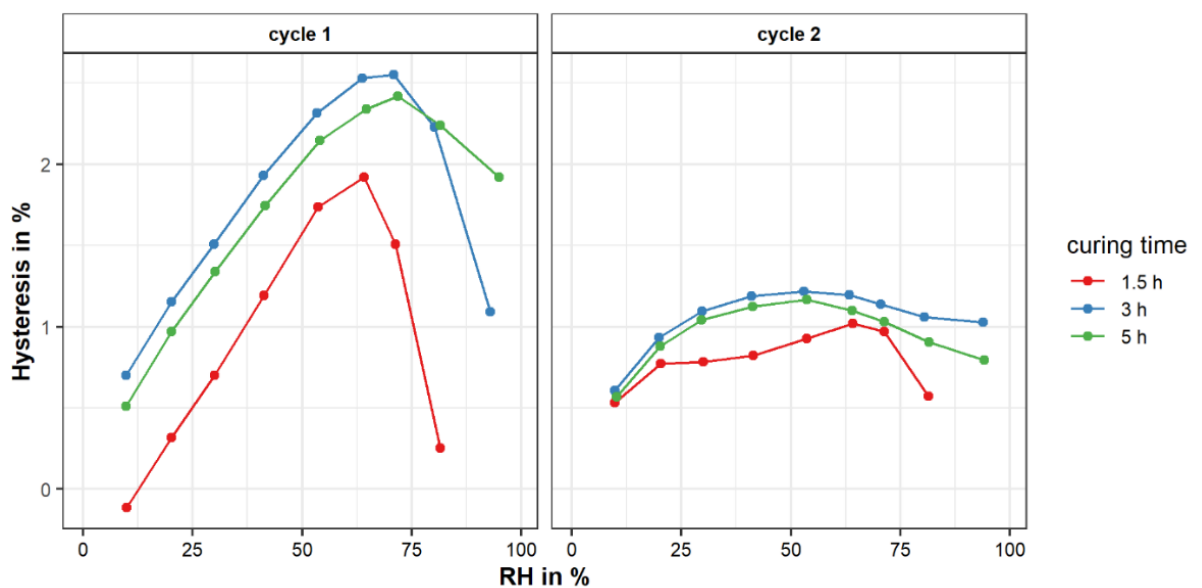


Figure 4-15 Hysteresis between sorption and desorption for PUF resin cured for different durations at 150°C.

4.4.5 The Elemental Composition of Cured Resin studied SEM-EDX

To complement other techniques in this chapter, the elemental composition of the cured resin was investigated using SEM-EDX point scans. Figure 4-16 (a) shows the two point scan locations in the SEM image. Figure 4-16 (b) displays the EDX spectrum of the sample. The average mass percentages of each element were measured as follows: carbon (60.13%), oxygen (22.03%), nitrogen (16.38%), and potassium (1.04%). Traces of sodium, aluminium, silica, and sulphur are not discussed here. The main nitrogen source in the resin is U_{HM} and free urea, and the potassium source is potassium hydroxide. Hence, Figure 4-16 (b) provides a good estimate about the relative abundance of each component.

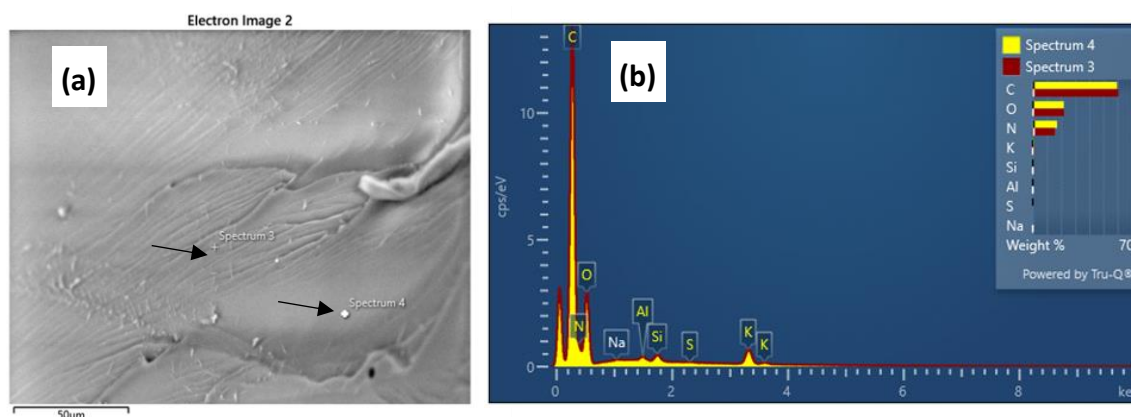


Figure 4-16 SEM-EDX analysis shows the elemental composition of the cured PUF resin. (a) SEM image showing the two point scan locations with arrows. (b) EDX spectrum of the cured resin showing the relative elemental composition.

4.4.6 Resin cured in an open and closed System studied by SEM

Chapter 4.4.1 and 4.4.2 have demonstrated that the kinetics and the type of bonds in the PUF resin depend on the crucible systems that was used for DSC scan. This section compares the morphology of resin from the two systems. After the DSC scan was complete, the crucible was directly transferred to the SEM analysis.

Figure 4-17 (a-b) shows the corresponding SEM images of resin cured in an open and a closed system. In the open system the resin forms a solid bulk structure which had to be crushed for SEM observations. The figure shows the fractures of the bulk structure after crushing. The fractures display sharp edges (1) and smooth surfaces (2). Resin cured in the closed system did not form a continuous bulk structure, so it was not necessary to crush it. Instead, opening the lid of the previously sealed DSC pan, revealed a material that was like a paste with solid grains in it. Water was still present in the pan, but the resin was no longer dissolved, after heat curing took place during the DSC scan. The image taken from the resin in the closed system shows that resin crosslinked in the form of sphere-like structures, which vary in diameter. Some of the larger hemi-spheres contain holes in their even surface (3). The even surface is the side, which pointed towards the crucible surface during the DSC scan. The agglomeration of resin to (hemi)spheres is typical for resins that begin to cure in the presence of water. As the molecular weight increases, the agglomerate becomes water insoluble and forms spheres. Their size depends on the temperature, curing time, and pH value of the system²⁶⁵.

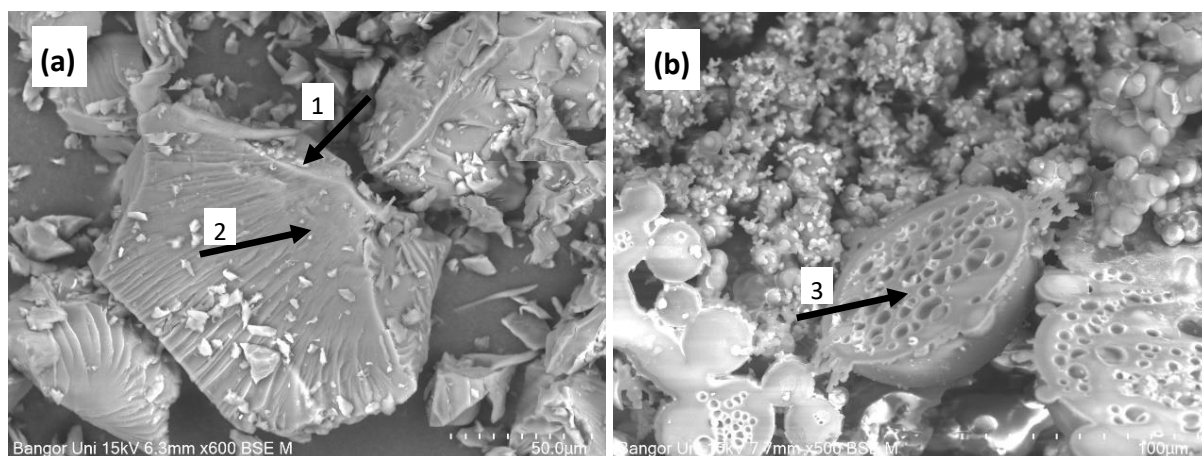


Figure 4-17 (a) SEM images of PUF resin cured at 150°C in an oven (open system). (b) PUF resin after a DSC run up to 250°C in high pressure crucibles (closed system). 1 – sharp edge of crushed resin structure, 2 – smooth surface of crushed resin structure, 3 – even surface of resin hemisphere that was pressed against the metal surface of the crucible during the DSC scan.

4.5 Conclusions from Chapter 4

The chemical composition of the PUF resin used in this thesis was confirmed, showing that the uncured resin contains mainly reactive intermediates (PF_{HM}) and a few self-condensed phenolic structures. Urea entities, which make up around 15 % w/w of the cured resin, are present in the form of reactive intermediates (U_{HM}) and free urea. Co-condensation of urea and phenolic entities occurs early in the curing reaction but becomes less important as U_{HM} is consumed. After this point, self-condensation of phenolic structures prevails. Effects of the resin pH value during cure were clarified, showing that:

- Lowering the pH value to a mildly acidic environment drastically reduces the reaction rate and restricts co-condensation.
- Increasing the curing pH value has little effect on the reaction rate but facilitates co-condensation.

Heat curing in an open system was compared to heat curing in a closed system, and it was found that:

- Under controlled conditions, the degree of cure is lower in the closed system.
- The reaction rate might be higher in the open system, but DSC scans of open crucibles are difficult to interpret.
- In the closed system, the resin forms microspheres due to the presence of water.

The water sorption behaviour of cured resin powder was studied in DVS studies, and it was found that:

- Cured PUF resin absorbs water from the atmosphere.
- The maximum absorption decreases with an increasing degree of cure.

The results of Chapter 4 focus on the pure PUF resin, without considering the presence of wood. Nonetheless, this Chapter bears significance for the wood modification process explored in this thesis. Specifically, it highlights the importance of considering the acid-base interactions between wood and resin in the subsequent chapters. Additionally, the pressure applied during the curing step affects the resin curing kinetics and should be taken into account in commercial processes. Moreover, it is important to ensure that the modified wood undergoes adequate curing, meaning it is exposed to sufficiently high temperatures for a suitable duration, in order to minimise the resin's hygroscopicity.

5. Wood Modification with Phenol Urea Formaldehyde Resin: The Effect of Wood Species Selection

5.1. Introduction to Chapter 5

The result Chapters 3 and 4 focussed on the properties of unmodified wood and neat PUF resin with both raw materials being studied in isolation. This chapter now investigates the combination of low molecular weight phenol urea formaldehyde (PUF) resin and wood in the according impregnation modification process. Many aspects of this modification process are well-understood amid frequent scientific publications and several successful commercialisations (see chapter 2.2.2.4.). However, despite an extensive literature search, no study that investigates the influences of different wood species in an impregnation modification process was found to have a satisfying level of detail. E.g., parameters like BU or ASE were not recorded in studies that compared different species (see Table 5-1). Therefore, it is the aim of this chapter to establish the influence of wood species in this process.

The eleven wood species described in Chapter 3.2.1 were all modified using an identical treatment method with the resin described in Chapter 4.2.1. The modified wood is studied by FTIR-ATR spectroscopy, microscopy, and most importantly by anti-swelling efficiency (ASE) tests. The ASE is used as the primary measure of quality control for modified wood in Chapters 5 and 6 of this thesis as it quantifies the improvement of dimensional stability, which is seen as a main property of the modified wood. A comparison of previously published ASE studies is provided in Table 5-1. Other improved properties of modified wood such as the biological durability, surface hardness, or fire resistance are also relevant, but have not been tested in this PhD project.

The ASE method is frequently used to study modified wood, and a variety of species has been investigated in the literature^{86, 96, 120,125,126}, however, it is often difficult to compare results due to variations in resin type (e.g., melamine formaldehyde, phenol formaldehyde, urea formaldehyde), resin properties (e.g., molecular weight, solids content, pH value) or variations in the method (e.g., sample dimensions, soaking time, use of high relative humidity cycles instead of soaking in water). Consequently, the effect that species differences have on the treatment cannot be derived from the existing literature.

To complement ASE tests, FTIR-ATR spectroscopy in combination with principal component analysis (PCA) is used to show the chemical differences between unmodified and modified wood species. Light microscopy and scanning electron microscopy (SEM) are used to study the morphology of modified wood at microscopic scale. Light microscopy in combination with safranin staining was used to study the cell wall penetration by resin¹²¹. The soaking solution generated from ASE tests is analysed by solution-state nuclear magnetic resonance (NMR) spectroscopy to study the leaching of resin in water and possible degradation products. NMR was used because the chemical shifts of resin are known from Chapter 4, so that resin leaching from the modified wood would be easy to identify in the soaking solution.

At the end of this chapter, an attempt is made to explain which factors contribute to the ASE value that a wood species can achieve. The density is likely to play a role in this, as it governs key parameters like the percentage liquid resin uptake. Wood anatomical features might play another, often overlooked, role, e.g., when different cell types take up dissimilar amounts of resin. The alkaline buffer capacity (ABC, see Chapter 3.4.3.3.) is also discussed in this context. Finally, the wood chemical composition, as determined in Chapter 3.4.2., is correlated with the ASE of the same timbers. Possible interactions between wood and resin will be investigated in more detail in Chapters 7 and 8.

Table 5-1 A summary of ASE studies comparing different timbers modified with thermosetting resins: s.c. - solids content of resin. MW - molecular weight. WPG – weight percentage gain. BU – bulking coefficient.

Species	Size r . t . l in cm	Resin Specifications			Modification Step			WPG in %	BU in %	ASE in %	Ref.
		conc.	MW	pH	imp.	diff/drying	cure				
<i>Acer saccharum</i>	7x 7x 180	20 (PF)	-	-	pressure imp. 14bar & 5h	diffusion 2d at ambient temp. drying 14d & <70°C,	heat cure with hot plate & 155°C	15.7	-	37 - 53	126
<i>Betula alleghaniensis</i>								23.8	-	42 - 59	
<i>Liquidambar styraciflua</i>								23.2	-	63.5 - 70	
<i>Liriodendron tulipifera</i>								30.8	-	52 - 61	
<i>Populus section Aigeiros</i>								31.5	-	57.5 - 63.5	
<i>Pseudotsuga menziesii</i>								11	-	13.5 - 50.5	
<i>Pinus ponderosa</i>								26.6	-	37.5 - 57	
<i>Picea sitchensis</i>								19.5	-	31 - 65	
<i>Anthocephalus cadamba Miq.</i>	1x 0.5x 8	30 (PF)	-	9.5	vacuum imp.	-	heat cure 100°C	33.7	14.45	68	176
<i>Cryptomeria japonica</i>	3x	30 (PF)	309 -	6.7 -	vacuum imp. 1h	diffusion submerged in resin 1 d	heat cure in oven & gradual from 60 to 180°C	-	-	60 (any pH)	86
	3x 0.5	30 (PF)	335	10.3				10	-	-	
<i>Paraserianthes falkata</i>	10x 6x 0.6	20 (PF)	300	5.5	vacuum imp. 12h repeat 7x	diffusion 2d & ambient, drying 50°C vacuum	subsequent densification and cure	48.9	5.2	-	266
<i>Shorea sp.</i>								72.4	7.8	-	
<i>Cryptomeria japonica</i>								43	8	-	
<i>Picea abies</i>								47	7.8	-	
<i>Pseudotsuga douglasii</i>								34.7	8.9	-	
<i>Ulmus sp.</i>								42.3	13.5	-	
<i>Fagus crenata</i>								33.7	12.4	-	
<i>Betula maximowicziana</i>								28.1	16.3	-	
<i>Pinus sylvestris</i>	2.5x 2.5x 1	30 (PF)	400	9.6	vacuum pressure imp. 12bar & 2h	-	drying & cure gradual from 20 to 103°C	50	~13	-	93
<i>Betula pendula</i>	2x 2x 2	5 - 15 (PF)	460	-	vacuum imp. 1h	diffusion submerged in resin 2h; drying gradual;	heat cure 140°C	6 (low conc) - 14 (high conc)	2.2 (low conc) - 5.2 (high conc)	30 (low conc) - 40 (high conc)	120
<i>Fagus sylvatica</i>	2.5x 2.5x 1	9 - 27 (PF)	297 - 854	-	vacuum imp. 45 min	diffusion submerged in resin 1h; drying gradual 25 to 103°C	heat cure 140°C	8 (any MW, low conc) - 23 (any MW, high conc)	6 (high MW, low conc) - 14 (low MW, high conc)	-	121
<i>Pinus massoniana</i>	2x 2x 2	15 - 30 (PF)	300	-	vacuum pressure imp. 8bar & 2h	drying at ambient	heat cure 130°C 2h	20 (low conc) - 38 (high conc)	-	26 (low conc) - 54 (high conc)	122
<i>Pinus sylvestris</i>	2.5x 2.5x 1	10 - 25 (MF)	840	10.1	vacuum imp. 1h	diffusion submerged in resin 1h	drying & heat cure gradual 25 to 103°C	14 (low conc) - 30 (high conc)	2.5 (low conc) - 5 (high conc)	-	96

5.2. Materials

5.2.1. Wood Samples and Resin

The eleven wood species described in Chapter 3.2.1 and the default PUF resin in Chapter 4.2.1 were used in this chapter. PUF resin with a pH of 9.5 and a solids content of 50% was diluted to 30% by adding deionised water prior to impregnation treatments. Sapwood specimens from each species were cut with good alignment of the grain and growth rings to the edges of the specimen, the dimensions were 20 (r) × 20 (t) × 5 (l) mm. These were stored at ambient conditions until further processing. Every unmodified and modified test group in this study consisted of 10 specimens from the same board.

Additionally, it should be noted that the materials section in this chapter overlaps with others. Solution-state NMR measurements were conducted on freeze-dried hot-water extractives (see 3.4.4), on freeze-dried PUF resin (see 4.2.1), and on the cold-water soaking solution of modified beech and Radiata pine samples (see 5.3.7). To account for the effect of different resin concentrations on leaching products, beech and pine samples that were treated with a resin concentration of either 20% (w/w) or 40% (w/w) were also used (see Chapter 6.3.2.2).

5.3. Methods

5.3.1. FTIR-ATR Spectroscopy – Sample Preparation and Statistics

The methods used for samples preparation and principal component analysis (PCA) in this chapter aligns with those reported in Chapter 3.3.2. The PCA presented here encompasses both modified and unmodified small blocks.

5.3.2. Light Microscopy – Sample Preparation

The small blocks were soaked in cold water for several days to soften them prior to microtome cutting. The water storage was often ineffective when cutting the rigid modified samples. Therefore, some samples were embedded in methacrylate resin (*Technovit 7100 – Taab Laboratories*) to facilitate sectioning. This was done by vacuum impregnating dry blocks with hydroxyethyl methacrylate (HEMA) for 24 h, which was subsequently polymerised at room temperature by adding hardener solution. Then, sections with a thickness of 25 – 35 µm were obtained using a microtome with reusable blades (*Jung K microtome Heidelberg 1928*). Some sections were then stained in safranin, others were directly dehydrated in methylated spirit (99% v/v) and mounted on a slide with glycerol. The sections were used for transmitted light microscopy and the remaining wood blocks with a smooth surface were used for reflected light microscopy and SEM observations. Figure 5-1 shows examples of the sample preparation that was done for microscopic observations.

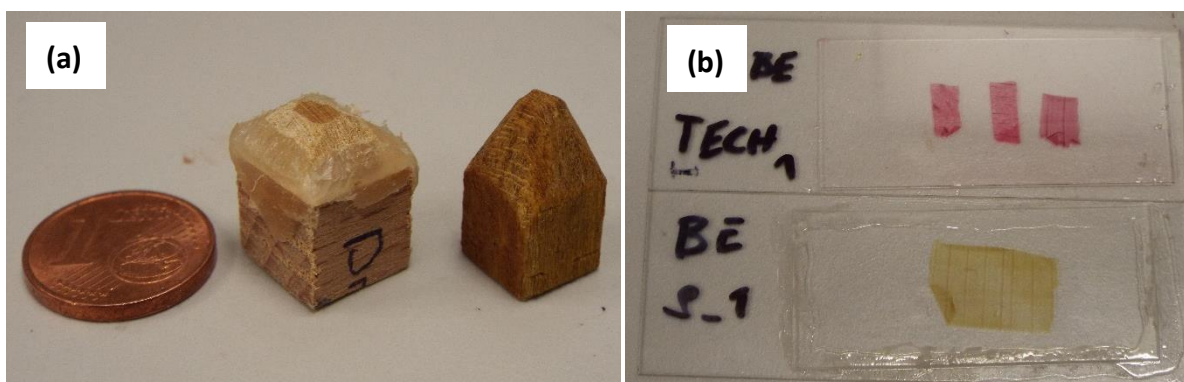


Figure 5-1 (a) Cone-shaped samples used for reflected light microscopy and SEM observation. The left sample was glued on larger block to facilitate microtome cutting. (b) Wood sections used for transmitted light microscopy. Top sections are stained with safranin.

5.3.3. Safranin Staining – Sample Preparation

Microtomed sections were carefully immersed in safranin solution diluted with water (0.1% v/v) for 10 min. Subsequently, the sections were dehydrated in methylated spirit with a concentration of 50% (v/v) in water followed by a second step at 99% (v/v) each for 2 min each. Dehydrated samples were then mounted using glycerol and covered with a cover slip.

5.3.4. Light Microscopy – Image Acquisition

Light microscopy both in transmitted light and reflected light mode was performed using an optical microscope (*DM6000 M – Leica*). Prior to observations a white reference was obtained using a white sheet of paper.

Two specimens (i.e., ASE blocks) were taken from each modified and unmodified wood species for microscopic investigations. These specimens were cut into 2 – 4 smaller blocks, which were used to observe the traverse, tangential-longitudinal (TL), and radial-longitudinal (RL) surfaces of the wood. The samples were first observed with a 5x objective to select general areas of interest. Subsequently, the objective was switched to 10x or 20x for more detailed observations. A minimum of 3 images was acquired for each sample and magnification.

5.3.5. SEM – Image Acquisition

Wood samples were prepared for scanning electron microscopy (SEM) by soaking small blocks in water overnight before smoothing the radial and transverse sections by making several 10 µm cuts with a rotary microtome. The blocks with smoothed surfaces were then dried and attached to carbon tape without further pre-treatment. All SEM images were taken with a scanning electron microscope (*Hitachi, TM4000*) using a beam acceleration voltage of 15 kV and a detector for backscattered electrons.

5.3.6. ASE Analysis – Resin Treatment of Small Blocks

The sample mass was measured with a 4 d.p. balance (*Ohaus Explorer Analytical*) and the surface area was measured with a digital calliper (2 d.p.) in the radial, tangential, and longitudinal directions of the specimen. To enable the distinction between various states of the experiment in the following sections, an abbreviation of the corresponding state is placed behind the process step. These abbreviations will also be used in the results section.

The oven dry mass and dimensions of unmodified test blocks were determined after drying at 105°C for 24 h (OD 0). Subsequently, samples were conditioned at ambient relative humidity and room temperature for 24 h prior to use. For the resin impregnation, samples were placed in a 250 ml beaker in a desiccator attached to a vacuum line (see Figure 5-2). A vacuum was drawn for 20 min prior to impregnation. Then, the resin was injected through a dropping funnel until all samples were fully submerged. Ballast was used above the samples to ensure they remained below the level of the fluid throughout the procedure. A volume of 100 ml resin was used for each impregnation. Still under vacuum, the samples were immersed for 20 min, before the vacuum was released. Subsequently, the treatment solution was drained off and samples were removed from the beaker, excess resin was blotted with tissue and the mass and dimensions were noted (Imp). The samples were now carefully dried at 50°C for 16 h to reduce the moisture content before cure. Heat curing took place at 150°C for a duration of 8 h. The mass and dimensions after cure were noted (OD 1).

5.3.7. ASE Analysis – Cyclic Swelling and Drying of Small Blocks

Sets of 10 modified and 10 unmodified control specimens were subjected to cyclic water soaking and oven drying. Oven dry mass and dimensions of control (OD 0) and modified groups (OD 1) were determined, as described previously. The water soaking was carried out by vacuum impregnating each test group with 100 ml deionised water, using a similar procedure to that described for resin treatment, within a beaker in a desiccator. The soaked samples remained submerged in water for 5 days at room temperature (see Figure 5-2). Subsequently, they were lightly blotted with a tissue to remove excess water before mass and dimensions were noted (WS 1). Water-soaked samples were then dried at 50°C for 16 h to eliminate moisture without initiating stresses in the samples, and then at 105°C for 24 h. The mass and dimensions were noted (OD 2) and the procedure was repeated until three wetting and drying cycles were completed.

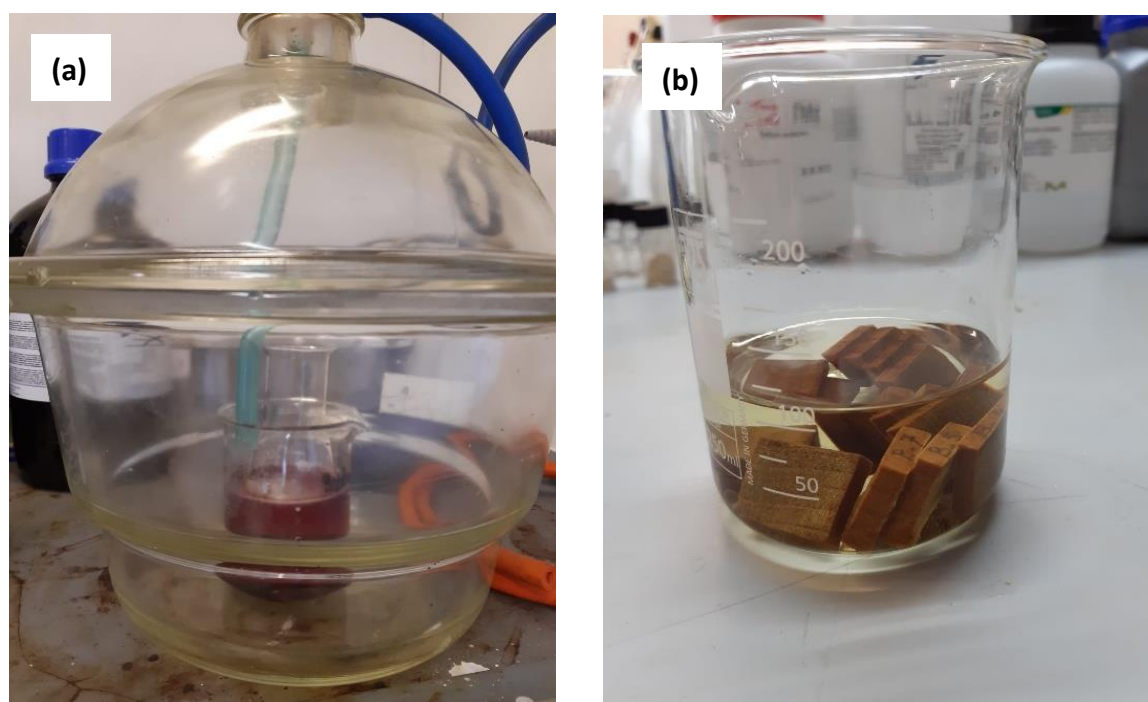


Figure 5-2 (a) Vacuum impregnation of small blocks with liquid PUF resin. Ballast keeps the samples submerged as the vacuum is drawn. (b) Modified wood samples during cyclic water storage.

5.3.8. ASE Analysis – Soaking Solution Analysis

After each soaking cycle, the percentage of leached substances was estimated by measuring the weight of the solid residue in solution after evaporation of water. The nature of leached substances was investigated by measuring the pH value and the UV absorbance at 272 nm of the leachate.

The soaking solution was transferred to a volumetric flask and diluted to a volume of 1 litre, to ensure the concentration and UV data could be used for quantitative comparison between each set of samples. The high level of dilution was necessary to obtain meaningful results in the UV measurements within the range of the UV spectrometer used. Approximately 20 ml of the diluted solution was poured in a glass vial of known dry mass for evaporation at 105°C. The solid residue SR [%] was determined by dividing the dry mass with the liquid mass. The solid residue in percent was then converted to a volumetric concentration SR $\left[\frac{g}{l}\right]$:

$$SR [\%] = \frac{m_{solid}}{m_{liquid}} * 100\%$$

$$SR \left[\frac{g}{l} \right] = SR [\%] * 10 \left[\frac{g}{l} \right]$$

A small aliquot of the diluted soaking solution was transferred to a quartz cuvette for UV absorption measurement at 272 nm. This wavelength is characteristic for aromatic compounds and displays the maximum absorption peak for phenolics²⁴⁷. Approximately 50 ml diluted soaking solution was transferred to a small beaker for pH-measurement. The pH-meter was calibrated with standard buffer solution at pH 4 and 7 prior to use. The procedure was performed for the test and the control group of every investigated species.

To analyse the chemical composition of the soaking solution in more detail, selected samples were freeze dried and re-dissolved in deuterium oxide (D₂O). The solution-state NMR analysis was then carried by the Chemistry department of Cardiff University. ¹³C NMR spectra and ¹H–¹³C HSQC NMR spectra were collected in a similar procedure to that described in Chapter 3.3.6.

5.3.9. ASE analysis – Calculations

The liquid resin uptake (LU) describes the mass change between the oven dry and the impregnated state during modification. The weight percentage gain (WPG) describes the dry weight gain achieved after cure. The bulking coefficient (BU) describes the dry volume gain after cure. They are calculated as follows:

$$LU = \frac{m_{Imp} - m_{OD 0}}{m_{OD 0}} * 100\%$$

$$WPG = \frac{m_{OD 1} - m_{OD 0}}{m_{OD 0}} * 100\%$$

$$BU = \frac{(r * t)_{OD 1} - (r * t)_{OD 0}}{(r * t)_{OD 0}} * 100\%$$

The water-induced swelling coefficient of unmodified control groups ($S_{control}$) relates to the swelling of oven dry unmodified wood (OD 0) and the swelling coefficient of the modified groups (S_{mod}) refers to the oven dry modified state (OD 1) during ASE tests. Within this study, the swelling coefficients were calculated on an area basis, to minimise error arising from longitudinal dimension data. They are calculated as follows^{11,267}:

$$S_{control} = \frac{(r * t)_{WS 1} - (r * t)_{OD 0}}{(r * t)_{OD 0}} * 100\%$$

$$S_{mod} = \frac{(r * t)_{WS 1} - (r * t)_{OD 1}}{(r * t)_{OD 1}} * 100\%$$

$$ASE = \frac{mean(S_{control}) - mean(S_{mod})}{mean(S_{control})} * 100\%$$

The resin-induced swelling coefficient (S_{resin}) of modified groups describes the volume gain during impregnation and relates to the oven dry state of unmodified state (OD 0). Hence, this is the volume gain after impregnation but before curing, where the samples are still wet. It is calculated as follows:

$$S_{resin} = \frac{(r * t)_{Imp} - (r * t)_{OD 0}}{(r * t)_{OD 0}} * 100\%$$

The total water-induced swelling coefficient (TS) describes the volume change from the oven dry unmodified state (OD 0) to the first water-soaked state (WS 1) in the ASE test for both modified and unmodified sample groups. In modified groups, this coefficient includes the permanent volume change by bulking. In unmodified control groups TS is identical with $S_{control}$. TS is calculated as follows:

$$TS = \frac{(r * t)_{WS 1} - (r * t)_{OD 0}}{(r * t)_{OD 0}} * 100\%$$

In unmodified wood, the water uptake WU_0 describes the mass gain from the first oven dry state OD 0 to the following water-soaked state WS 1 as a percentage. Equally, in modified wood, WU_1 describes that mass gain from the first modified dry state OD 1 to the following water-soaked state WS 1. The water uptake in the following cycles is calculated identically for unmodified and modified wood. They are calculated as follows:

$$\text{For unmodified wood: } WU_0 = \frac{m_{WS 1} - m_{OD 0}}{m_{OD 0}} * 100\%$$

$$\text{For modified wood: } WU_1 = \frac{m_{WS 1} - m_{OD 1}}{m_{OD 1}} * 100\%$$

$$\text{For both: } WU_2 = \frac{m_{WS 2} - m_{OD 2}}{m_{OD 2}} * 100\%$$

$$WU_3 = \frac{m_{WS 3} - m_{OD 3}}{m_{OD 3}} * 100\%$$

In modified wood, this calculation of WU_1 accounts for the mass gain of both water and resin, hence, this is the water uptake including the resin mass. To exclude the mass gain of resin in the calculation, WU_0 can also be calculated for modified wood samples and becomes the water uptake excluding the resin mass.

The mass loss during ASE tests ML_{total} compares the oven dry mass of the last cycle with the initial oven dry weight. In modified groups, the first cycle starts at OD 0 and in modified groups it starts at OD 1. It is calculated as follows:

$$ML_{total} = \frac{m_{OD 3} - m_{OD 0 \text{ or } 1}}{m_{OD 0 \text{ or } 1}} * 100\%$$

5.3.10. ASE analysis – Statistics

The experimental set-up consists of two variables. Variable one describes whether a test group is modified or unmodified. Variable two is the wood species. Every wood species was tested in a modified and unmodified state giving a total of 22 test groups each containing 10 specimens. All analyses were performed using R Statistical Software (v 4.1.2; R Core Team 2021). Boxplots used in several figures show the median value, standard deviation, as well as maximum and minimum values in each test group. Linear regression models have been calculated using the R functions `stat_regline_equation()` and `stat_cor()`. Two-way analysis of variance (ANOVA) was carried out to discern significant differences at a 95% level of confidence between swelling, total swelling, and total mass loss of modified and unmodified wood. Extreme outliers have been removed from the datasets prior to ANOVA analysis using the R function `identify_outliers()`. ANOVA was performed using the R functions `aov()`. A Tukey Honest Significance Differences (HSD) test was performed on the same data to identify significant differences within each wood species. The R function `TukeyHSD()` was used.

5.4. Results and Discussion

5.4.1. The Surface Chemistry of Modified and Unmodified Wood studied by FTIR-ATR Spectroscopy

The surface chemistry of wood undergoes several changes through treatment with PUF resin. Monitoring these changes is crucial for understanding the influence of different wood species with distinct chemical compositions in the modification process. In the following, FTIR-ATR spectroscopy, coupled with principal component analysis (PCA), is employed to study some of these changes. The PCA encompasses spectra from both modified and unmodified samples. Similar to the approach used in section 3.4.1. for unmodified wood exclusively, one PCA is conducted for spectra in reflectance mode, and another is performed for spectra in absorbance mode. Notably, the two methods yield slightly different results once again.

Figure 5-3 shows the outcome of a PCA in which the FTIR spectra in reflectance were compared. The score plot in Figure 5-3 (a) shows four distinct clusters separating modified versus unmodified samples horizontally along PC1, and hardwoods versus softwoods vertically along PC2. Samples that are not allocated in the correct cluster (i.e., beech, tulipwood, birch) are indicated in the Figure. Overall, the analysis predicts with reasonable accuracy whether a sample was a hardwood or softwood and whether it was modified or unmodified, which could be useful in a quality control context.

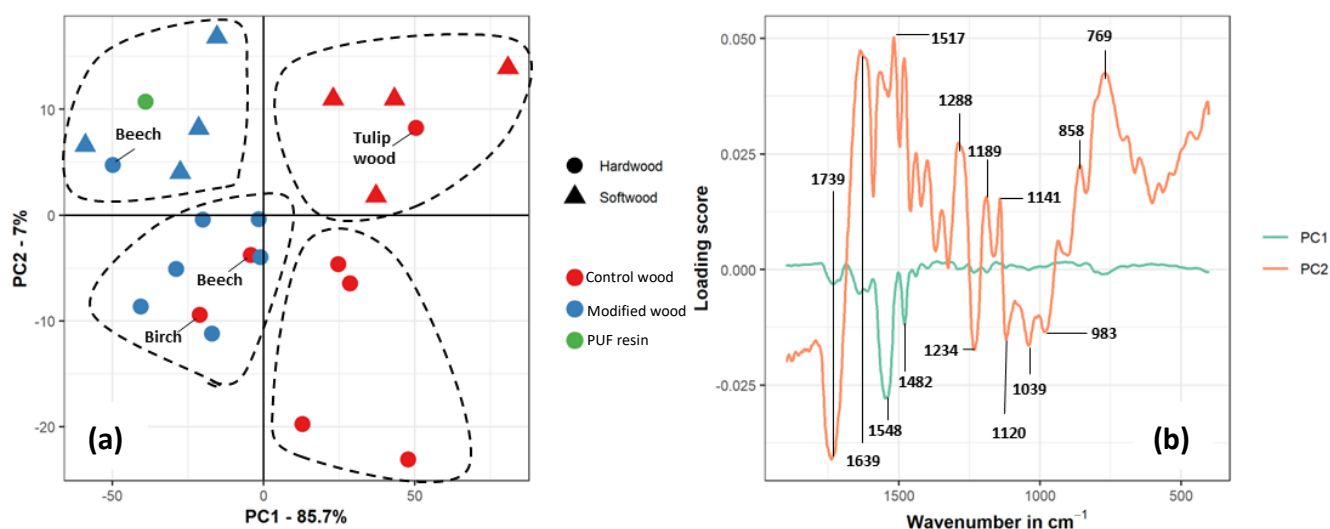


Figure 5-3 Outcome of principal component analysis of FTIR-ATR spectra in reflectance mode showing the (a) score plot with four main clusters in each quadrant and the (b) loading score plot for PC1 and PC2 on the right.

The loading plot in Figure 5-3 (b) shows that PC1, which accounts for 85.7% of the variation in the dataset, is influenced by absorption bands at 1640 cm^{-1} , 1548 cm^{-1} , and 1482 cm^{-1} . These wavenumbers have been assigned to the urea carbonyl stretch and to the phenolic in-ring stretch of the resin fraction (see section 4.4.2). But PC1 is also influenced by wavenumber 1730 cm^{-1} , which is assigned to the carbonyl stretch in the hemicellulose fraction. Hence, PC1 distinguishes between modified and unmodified samples based on the presence of resin and changes in the hemicellulose fraction.

The loading plot of PC2 in Figure 5-3 (b) is influenced by wavenumbers that explain the difference between hardwoods and softwoods (see Table 3-1). Primarily, these wavenumbers highlight differences in lignin composition, as shown by wavenumbers 1517 cm^{-1} , 1141 cm^{-1} , and 1120 cm^{-1} . Other variations could be attributed to hemicelluloses, as indicated by wavenumbers 1234 cm^{-1} and 983 cm^{-1} .

Figure 5-4 shows the outcome of a PCA in which the FTIR spectra in absorbance mode were compared. The score plot in Figure 5-4 (a) illustrates clear separation between modified and unmodified samples. The PCA in absorbance mode distinguishes accurately between unmodified softwoods and unmodified hardwoods, again except for tulipwood. However, the scores of modified softwoods and modified hardwoods overlap more than previously in the reflectance mode. Possibly, this is due to differences in the computation. In reflectance mode, PC1 and PC2 collectively account for 92.7% of the variation in the dataset. However, in absorbance mode, PC1 and PC2 explain only 88.9%. The residual variation is elucidated by PC3, PC4, and PC5, which are not displayed in the Figures. Thus, the observed variations between reflectance and absorbance mode could be attributed to computational effects.

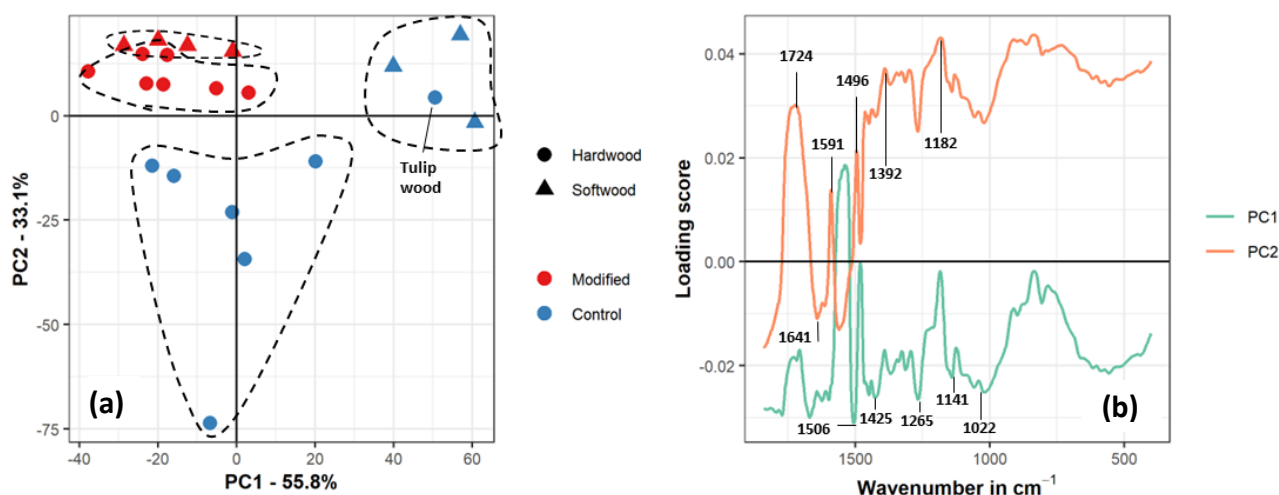


Figure 5-4 Outcome of principal component analysis of FTIR-ATR spectra in absorbance mode showing the (a) score plot with four main clusters. Modified softwoods and hardwoods are poorly separated. (b) The loading plot for PC1 and PC2 on the right.

The loading plot for the absorbance mode is shown in Figure 5-4 (b). The loadings of PC1 and PC2 are more convoluted than in reflectance mode, hence, it is less clear which differences the two principal components account for. Both PC1 and PC2 have an increased loading score at 1541 cm^{-1} , which has been assigned to the resin fraction (see 4.4.2). PC1, accounting for 55.8% of the variation, exhibits increased loading scores in wavenumbers corresponding to differences in softwood and hardwood lignin, such as 1506 cm^{-1} and 1265 cm^{-1} . PC2, representing 33.1% of the variation, includes wavenumbers assigned to both hemicelluloses (1724 cm^{-1}) and lignin (1591 cm^{-1} , 1496 cm^{-1}). However, many other wavenumbers characterising PC2 either overlap with resin bands or cannot be definitively assigned to a single component. In conclusion, the qualitative task of distinguishing softwoods from hardwoods and modified from unmodified samples is most effective in FTIR-ATR reflectance mode.

Figures 5-3 and 5-4 indicate that the modification affects the carbonyl region at approximately 1730 cm^{-1} , which includes peaks from different compounds in wood such as esters, carboxylic acids, ketones, and aldehydes, all of which peak at slightly different wavenumbers²³⁸. The O-acetyl group of the hemicelluloses is the most abundant carbonyl group in unmodified wood. After modification, the peak in the carbonyl regions shifts to lower wavenumbers, as illustrated in Appendix 7, but the extent of this shift varies between species. This shift indicates changes in one or more bonds in the region.

Figure 5-5 shows the shift of the carbonyl peak to lower wavenumbers for the investigated wood species. The exact difference in cm^{-1} is displayed numerically. Softwoods display a larger shift than hardwoods except for tulipwood. Interestingly, the tulipwood, which was grouped in cluster B together with Radiata pine in the hierarchical cluster analysis in Chapter 3.4.1., again shows a similar behaviour to the softwoods. Moreover, hardwood species that were

assigned to cluster A (i.e., lime, beech, birch) tend to have a smaller shift in Figure 5-5 than those hardwoods assigned to cluster D (i.e., sycamore, willow). In the same line, lime wood which was shown to have a distinct chemical composition in Chapter 3.4.2, shows the smallest shift in Figure 5-5. In the following, an attempt is made to explain the carbonyl shift in all observed wood species.

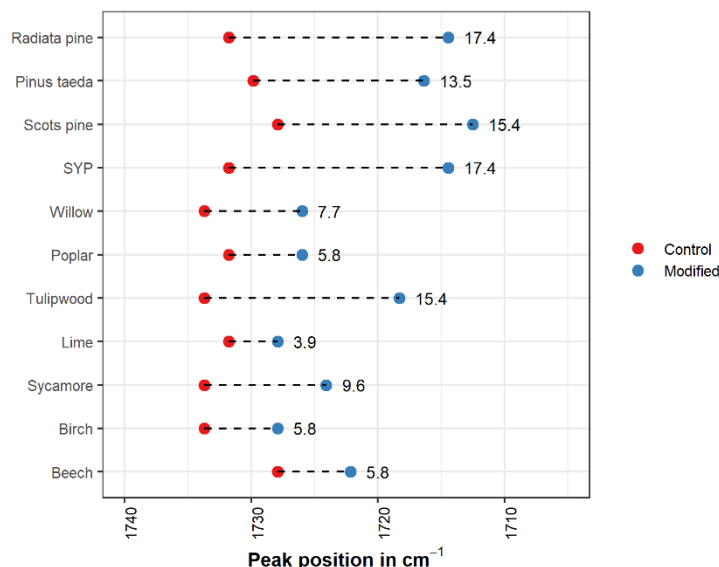


Figure 5-5 The carbonyl peak shifts to lower wavenumbers after PUF modification indicating changes in the hemicelluloses fraction. The difference in wavenumbers is displayed numerically.

In the presence of hot water, acetyl groups are converted to acetic acid via auto-hydrolysis²²⁶, which was already observed in alkaline buffer capacity measurements (see Chapter 3.4.3). Auto-hydrolysis occurs in an acidic environment. However, deacetylation of hemicelluloses may also occur via an alkaline mechanism in which an acetate salt is formed⁵⁰. Both pathways are illustrated in Appendix 8. The active mechanism during the modification treatment depends on the alkalinity of the resin.

This kind of deacetylation explains the observed carbonyl shift. Since O-acetyl groups are removed, but carboxylic acid groups remain in the modified wood, the carbonyl peak shifts to lower wavenumbers and decreases in intensity. Deacetylation of hemicelluloses introduces a smaller and more polar hydroxyl group in place of an acetyl group, possibly leading to a reduction in cell wall volume. The nature of this degradation could counterbalance the cell wall bulking effect of the resin and would have detrimental effects on the dimensional stability of the modified wood. Therefore, the degree of deacetylation during the modification process may influence the ASE and will be discussed later.

5.4.2. The ASE of various Wood Species after the same Resin Treatment

5.4.2.1. Density, Liquid Resin Uptake, Bulking Coefficient and Microscopic Observations

The overarching goal of the studied wood modification is to enhance the dimensional stability and biological durability of typically low-quality timbers. The dimensional stability of a timber is reflected by its swelling coefficient, and the enhancement of this dimensional stability resulting from modification is quantified through the ASE. While the ASE value stands out as the primary outcome of this test, the procedure yields a substantial amount of other data, and it is worth exploring these results in the following. The analysis of ASE results is complemented by microscopy images of the examined specimens. Therefore, this ASE testing section includes the analysis of the resin impregnation and curing stages, the cyclic swelling and drying of treated samples, and the characterisation of the soaking solution in which samples were submerged for five days.

Table 5-2 Average values for modified test groups. $\rho_{control}$ – oven dry density before modification, ρ_{mod} – oven dry density after modification, LU – liquid resin uptake before curing, WPG – weigh percentage gain after curing, BU – bulking coefficient, $S_{control}$ – swelling coefficient of unmodified wood, S_{mod} – swelling coefficient post-modification. Both $S_{control}$ and $S_{modified}$ refer to the first swelling cycle. ASE 1 – anti-swelling efficiency during the first soaking cycle, ASE 2 – anti-swelling efficiency during the second soaking cycle. Standard deviations are in parenthesis.

Species	$\rho_{control}$ in g/cm ³	ρ_{mod} in g/cm ³	LU in %	WPG in %	BU in %	$S_{control}$ in %	S_{mod} in %	ASE 1 in %	ASE 2 in %
Beech	0.73 (0.01)	0.74 (0.01)	50.9 (0.21)	25.9 (1.47)	18.5 (0.81)	26.8 (1.82)	9.4 (0.87)	64.8	58.5
Birch	0.64 (0.03)	0.65 (0.02)	48.9 (2.48)	24.0 (2.67)	13.9 (2.50)	20.1 (1.07)	8.2 (1.64)	59.3	45.2
Sycamore	0.60 (0.02)	0.66 (0.01)	49.1 (2.18)	24.3 (2.15)	9.4 (0.89)	13.3 (0.47)	5.7 (0.18)	56.8	46.3
Lime	0.55 (0.01)	0.61 (0.02)	56.4 (1.17)	33.7 (1.41)	15.0 (0.44)	21.5 (0.64)	6.7 (0.59)	68.7	59.5
Tulipwood	0.44 (0.01)	0.55 (0.01)	64.9 (0.48)	47.8 (1.04)	10.2 (0.34)	13.7 (0.59)	6.1 (0.40)	56.5	45.2
Poplar	0.44 (0.02)	0.50 (0.03)	57.4 (3.25)	36.6 (10.12)	8.6 (1.27)	13.1 (1.24)	7.3 (0.74)	44.2	34.6
Willow	0.36 (0.02)	0.47 (0.02)	66.2 (1.76)	51.4 (3.59)	6.5 (0.93)	8.7 (0.84)	4.5 (0.30)	48.8	35.1
SYP	0.64 (0.01)	0.71 (0.01)	55.4 (0.72)	31.1 (0.96)	10.5 (0.38)	16.5 (0.27)	8.1 (0.52)	50.9	44.8
Scots Pine	0.53 (0.01)	0.66 (0.01)	60.3 (0.71)	45.8 (1.33)	12.0 (0.31)	17.7 (0.12)	7.5 (0.32)	57.9	53.4
Pinus taeda	0.46 (0.03)	0.62 (0.02)	64.0 (2.41)	54.1 (5.45)	8.7 (0.39)	12.9 (0.64)	6.0 (0.39)	53.4	43.9
Radiata Pine	0.45 (0.01)	0.61 (0.01)	66.8 (0.37)	53.8 (1.19)	8.9 (0.43)	12.2 (0.53)	5.6 (0.17)	52.8	44.2

Table 5-2 displays the average results of modification related properties for each timber. The oven dry density of the unmodified wood species varies between 0.356 – 0.734 g/cm³ in hardwoods and between 0.448 – 0.635 g/cm³ in softwoods. Differences in density among wood species are attributed to variations in wood anatomy. In their microscopic structure, high-density species have a lower void volume compared to low-density species. On the other hand, high-density species often have thicker cell walls compared to low-density species.

This is illustrated Figure 5-6 by SEM images of unmodified willow ($\rho = 0.356$ g/cm³) and beech ($\rho = 0.734$ g/cm³). Figure 5-6 shows the transverse section of both timbers at the same magnification. The transverse section of willow displays larger vessels and fibre diameters compared to beech wood. Both species are diffuse porous hardwoods, meaning that the vessel diameter remains consistent in both the earlywood and latewood. Rays, which appear as horizontal or diagonal lines in the micrograph, are larger in beech. For reference, Appendix 9 shows a full comparison of all eleven wood species in SEM images at the same magnification.

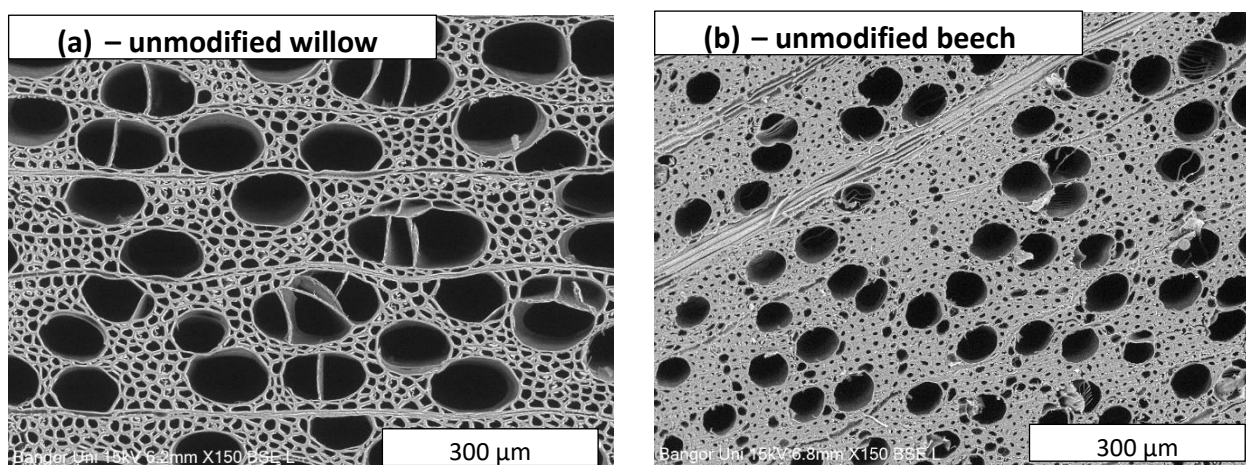


Figure 5-6 Anatomical difference between low-density and high-density wood species. Low-density species contain a greater void volume and have thinner cell walls compared to high-density species. Example micrographs of (a) willow and (b) beech wood in the transverse section at 150x magnification. Detector for Back Scattered Electrons (BSE) was used.

Considering the density of a wood species in the modification process is crucial, as it governs the available void volume. The macroscopic void volume, in turn, determines the liquid resin uptake (LU) during impregnation, particularly in small specimens where factors like pit aspiration and tyloses do not disrupt the impregnation process. However, in larger samples, these factors become highly relevant.

Figure 5-7 illustrates the relationship between the LU and the density of unmodified wood (ρ_{control}) in the small specimens used for this study. Clearly, there is an inverse linear relationship between the two factors. As depicted in Figure 5-6, this relationship is influenced by the available void volume, which decreases with increasing density.

Figure 5-7 suggests that hardwoods ($R^2 = 0.75$) exhibit more variability in this relation compared to softwoods ($R^2 = 0.93$). Nevertheless, both correlations are relatively high. Within the softwoods, the gradient is more distinctly defined for the entire group of species studied, and LU is almost exclusively dependent on density. Among the hardwoods, certain species like tulipwood and beech lie above the apparent trendline connecting the majority of hardwood samples, indicating that they take up more resin than their density alone suggests. Conversely, hardwood species such as poplar, birch, and sycamore lie below the trendline, indicating that they take up less resin than their density suggests.

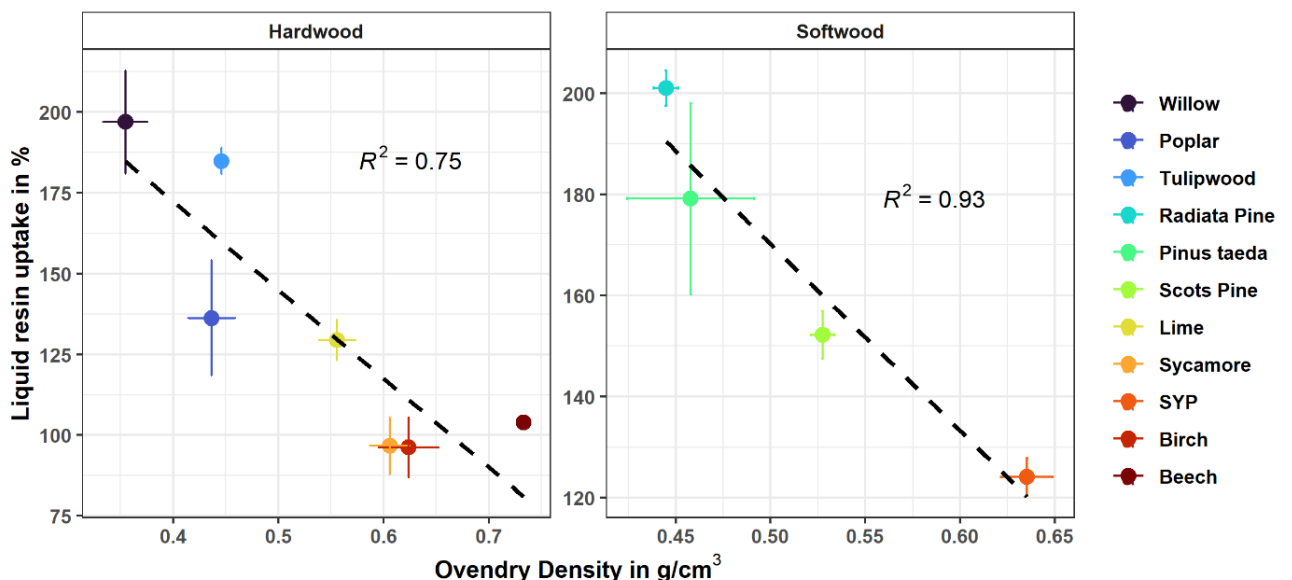


Figure 5-7 Relationship between liquid resin uptake (LU) and the oven dry unmodified density of different wood species that were impregnated with PUF resin in an identical treatment. A greater void volume in low-density species allows a higher liquid uptake compared to high-density species.

This could indicate that LU in the hardwoods is not solely determined by the available void volume. Certain species, like beech wood, are known for their tendency to rapidly swell in water. Likewise, these species might experience faster swelling during resin impregnation, resulting in a disproportionate deposition of resin in both the expanding cell walls and the cell lumen. This implies that the composition of the cell wall may also play a role in determining whether a wood species falls above or below the trendline in Figure 5-7.

Resin modification results in both an increased dry volume and an increased dry weight. Depending on the extent of these changes, the dry density may also vary during the treatment. Table 5-2 shows that the dry density after modification (ρ_{mod}) ranges between 0.47 – 0.74 g/cm³ in hardwoods and between 0.61 – 0.71 g/cm³ in softwoods. Thus, the modification generally leads to an increase in density across most species, with a more pronounced effect observed in low-density species such as willow or poplar.

Conversely, certain high-density species, such as beech and birch, show almost no change in density after modification, suggesting that their volume gain aligns with their weight gain. The varied increase in density during modification could be associated with the distribution of resin deposits. Resin impregnated into the wood structure may diffuse into the cell walls and polymerise *in situ*, or it may remain in the cell lumen, forming resin deposits (i.e., lumen filling) upon heat curing. Presumably, resin in the cell wall causes both a mass and a volume gain, whereas resin deposits in the lumen cause a weight gain without volume gain.

This indicates that low-density species have a higher proportion of filled lumens compared to high-density species, leading to a more pronounced increase in density among the former. In fact, a strong correlation was observed between the oven dry unmodified density and the oven dry modified density in hardwoods ($R^2 = 0.96$) and softwoods ($R^2 = 0.78$), as shown in Appendix 11.

Resin deposits in the cell lumen have been studied by light microscopy and SEM, as shown in Figure 5-8 (a-h). Evidently, these filled lumens could be observed in all modified wood species. In the reflected light images, resin deposits appear as silverish-grey structures (Figure 5-8 a-b). In transmitted light images, they are shown reddish-brown (Figure 5-8 c-f), and in SEM images as smooth surfaces (Figure 5-8 g-h). Additional micrographs are presented in 5-9 (a-h).

The frequency of filled lumens is consistent throughout all three imaging techniques but was best visible in transmitted light microscopy. Some low-density species such as Radiata pine, tulipwood, poplar, or willow display a surprisingly high number of resin-filled tracheids or vessels. In high-density species, most prominently beech, resin deposits are present, but to a much lower extent than in the low-density species. Resin deposits seem to be equally distributed between early and latewood in the hardwood species. This is probably because all studied hardwoods are diffuse porous, meaning that anatomical differences between earlywood and latewood (e.g., vessel diameter) are small. Resin deposits in the hardwoods often appear as clusters within a patch of empty cells (Figure 5-8 a). In the softwoods, resin deposits are more frequent in the latewood and clusters of filled lumens often extend in the radial direction (Figure 5-8 b, d).

In some cases, the cured resin seems to coat the SW3-layer evenly on its surface. This coating effect is poorly visible in the transverse section, but the tangential longitudinal (TL) plane in Figure 5-8 (g-h) and Figure 5-9 (e-f) clearly shows crossfield pits under a layer of resin. Both the resin deposits and the cell wall coating effects constitute a physical barrier against moisture and wood destroying organisms, which may partially contribute to the property improvement of modified wood, but eventually, moisture and fungi will penetrate these physical barriers.

The resin-fraction responsible for the permanent property improvement is crosslinked inside the cell wall and is therefore not visible in light or electron microscopy. Cell walls of modified and unmodified wood appear similar under the microscope. The only difference is that modified cells often show a rougher surface, because of their brittle mode of failure during microtome cutting. Theoretically, the dimensional change of single cell walls upon resin impregnation can be determined by light microscopy, but that was found impractical for the current study and was therefore not further investigated²⁶⁸.

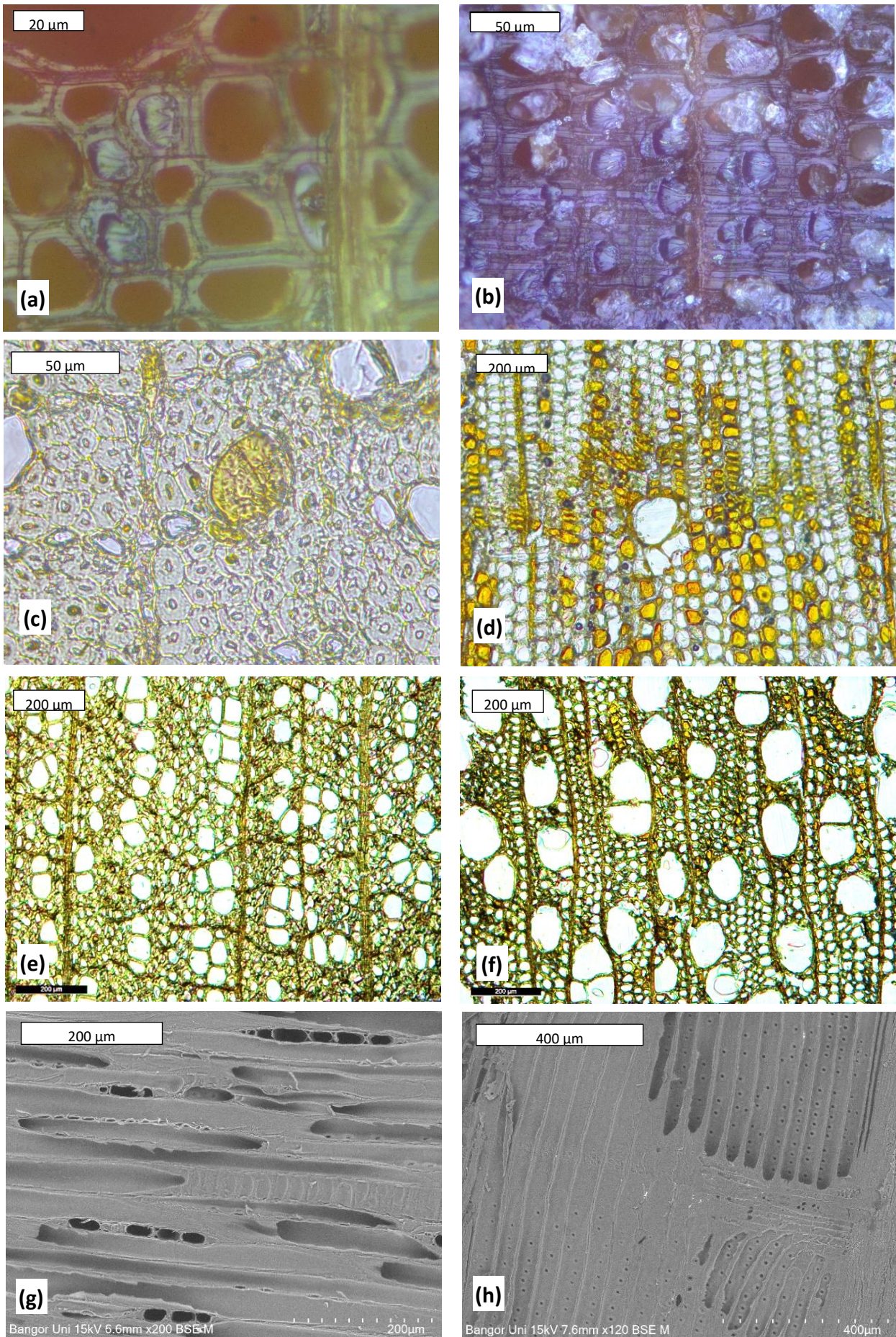


Figure 5-8 Resin deposits in the cell lumen can be observed in light and electron microscopy. (a-b) Show reflected light microscopy directly on the surface of small blocks. (c-f) Show transmitted light microscopy of sections prepared with a microtome. Prior to sectioning, these samples were embedded in methacrylate resin. (g-h) Show the longitudinal-tangential plane in SEM images. A detector for Back Scattered Electrons (BSE) was used. (a) poplar, (b) Radiata pine latewood, (c) beech, (d) Radiata pine, (e) lime, (f) poplar, (g) Radiata pine, (h) SYP. All samples are modified.

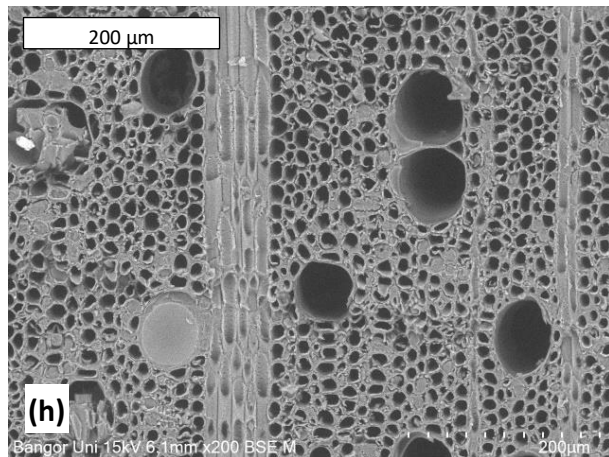
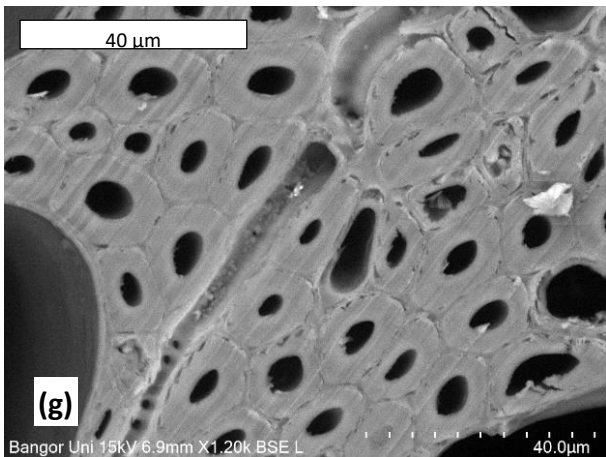
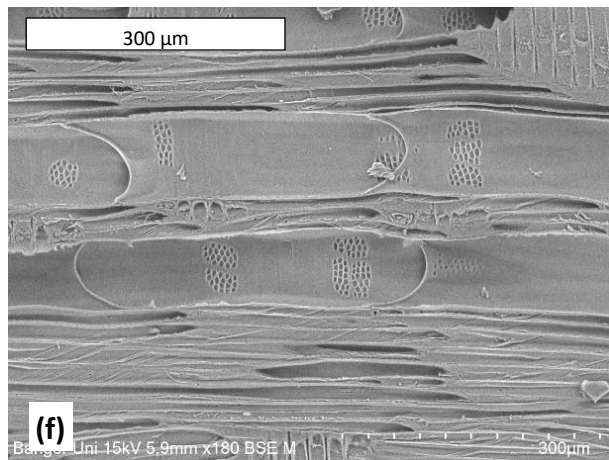
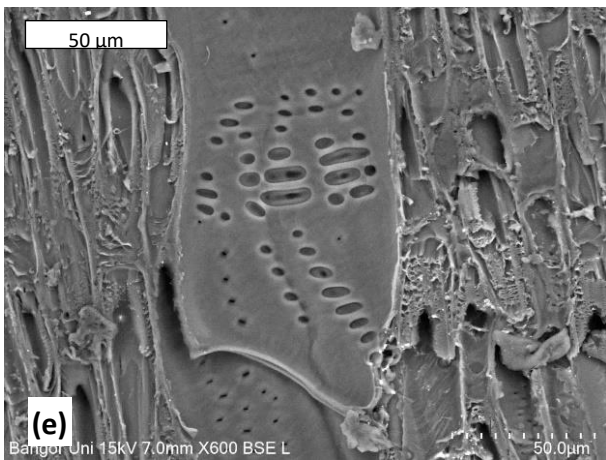
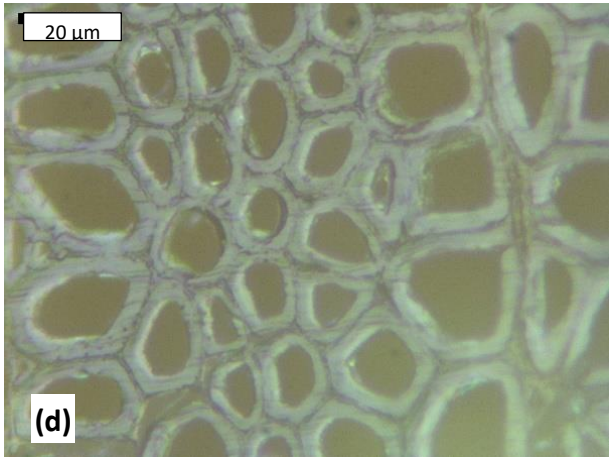
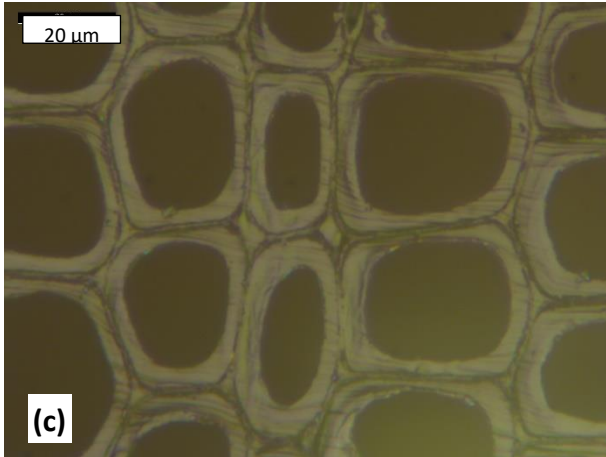
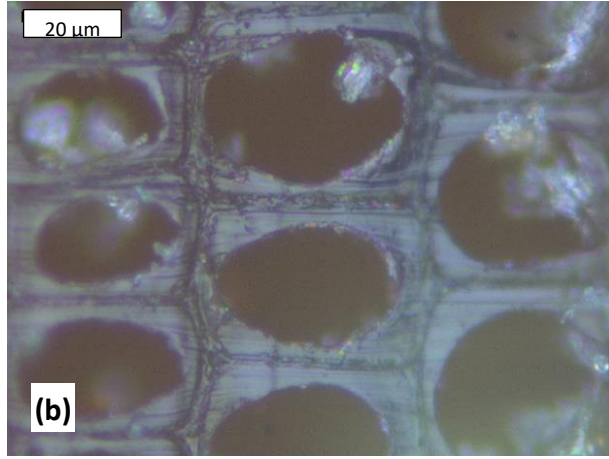
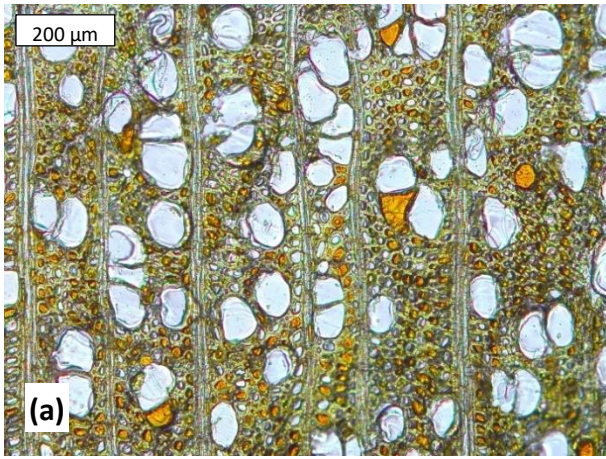


Figure 5-9 Additional micrographs of modified and unmodified wood. (a) Shows transmitted light microscopy image of modified tulipwood in the transverse section. (b-d) Show reflected light microscopy directly on the surface of small blocks. (b) modified Radiata pine, (c) unmodified Radiata pine, (d) unmodified poplar. (e-h) Show SEM images with BSE detector. (e) modified beech in transverse section, (f) modified willow in TL plane, (g) modified beech in transverse section, (h) modified sycamore in transverse section.

The bulking coefficient (BU) serves as a more practical measure to quantify the amount of resin located within the cell wall, where it contributes most effectively to the property improvement of modified wood. BU describes the permanent volume gain resulting from resin modification. According to Table 5-2, BU ranges from 6.52 – 18.50% in hardwoods and 8.60 – 12.03% in softwoods. Generally, high-density species tend to exhibit a higher BU compared to low-density species. The correlation between BU and oven-dry density is strong in hardwoods ($R^2 = 0.73$) and weak in softwoods ($R^2 = 0.33$). Thus, BU is partly influenced by density, probably because thicker cell walls in high-density species can accommodate more resin, leading to a more pronounced cell wall bulking effect.

In the context of this thesis, it is practical to differentiate the BU trends within a single species and across different species. Across multiple species, BU is influenced by density, along with other factors, and is less indicative of treatment quality. Within a single species, BU can be an indicator for effective modification because it is linked to the effective cell wall penetration of resin. In this case, BU can be employed as a measure of quality control, proving useful when evaluating the same species under different conditions. This could include comparisons of resin properties such as molecular weight and solids content, as well as comparisons of process conditions^{86,269}.

A more illustrative way of studying resin cell wall penetration involves light microscopy in combination with safranin staining^{97,120,121}. As mentioned earlier, directly measuring the amount of resin inside the cell wall is not feasible through light or electron microscopy. However, this becomes indirectly possible through safranin staining of thin wood sections. In unmodified wood, safranin typically produces an intense magenta stain that facilitates microscopic observation of wood tissue, which otherwise appear colourless. This staining effect is observable because the safranin molecules bind to the cell wall polymers. In resin-modified wood, where the resin has diffused into the cell wall, the binding of safranin to wood polymers is restricted. As a result, modified wood appears less intensely stained compared to unmodified wood.

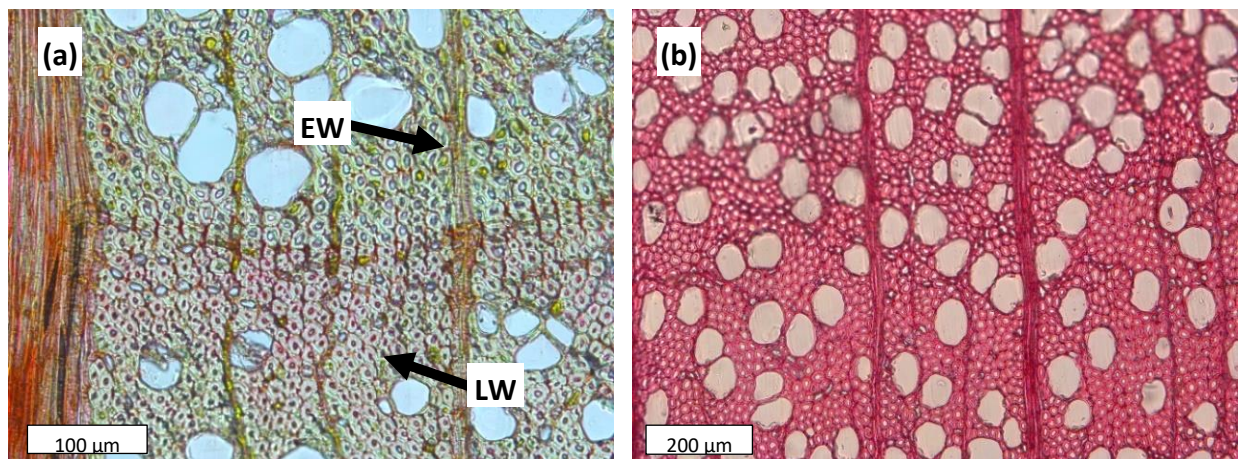


Figure 5-10 Safranin staining of thin wood sections can be used to measure the cell wall penetration of resin indirectly. Modified wood appears less intensely stained compared to unmodified wood. (a) Modified beech wood in the transverse section displays nearly no stain uptake in the earlywood (EW) and minimal uptake in the latewood (LW). (b) Unmodified beech in the transverse section displays a homogeneous magenta stain.

Safranin-stained sections of both modified and unmodified beech wood are illustrated in Figure 5-10. Following staining, the unmodified control section exhibits a homogeneous deep magenta colour. In contrast, the modified beech wood takes up minimal amounts of safranin in the earlywood and only small amounts in the latewood. This observation is in good agreement with previous studies suggesting that resin molecules in the cell wall prevent the safranin stain from binding to the cell wall polymers^{97,120,121}.

In the latewood cells, staining intensity is most pronounced in the SW3-layer near the lumen. Possibly, the less efficient resin penetration in the latewood, compared to the earlywood, is due to thicker and less porous cell walls that are more difficult to penetrate for resin molecules.

Figure 5-11 displays safranin-stained sections of modified and unmodified tulipwood. The staining intensity in both tulipwood sections seems comparable, although some variations are noticeable. Modified tulipwood contains cells with a relatively low staining intensity, and the earlywood exhibits a lower staining intensity compared to the latewood, as previously observed in beech. However, the overall trend differs from beech, as both the modified and unmodified sections appear intensely magenta. This raises the question why the method succeeded in beech but failed in tulipwood.

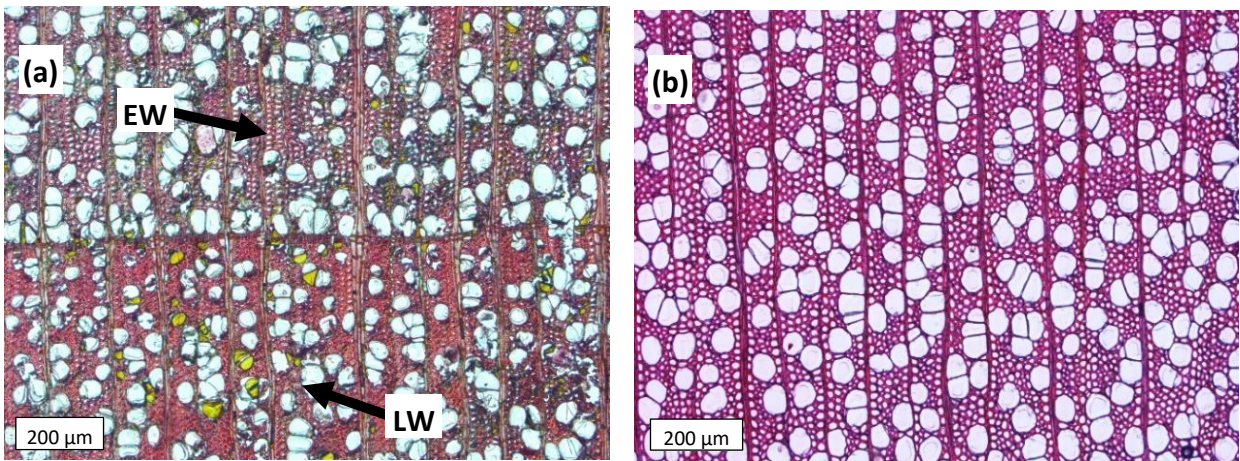


Figure 5-11 (a) Modified tulipwood in the transverse section. (b) Unmodified tulipwood in the transverse section.

Possibly resin cell wall penetration is more effective in beech than in tulipwood. This would align with higher BU and ASE values for beech compared to tulipwood (see Table 5-2). In this scenario, the safranin staining has not failed. Instead, it has revealed the effective resin cell wall penetration in beech and the comparatively poor resin cell wall penetration in tulipwood. However, although tulipwood displays BU and ASE values lower than beech, these values are relatively high with regards to its density. Therefore, is it unlikely that resin cell wall penetration has completely failed in tulipwood.

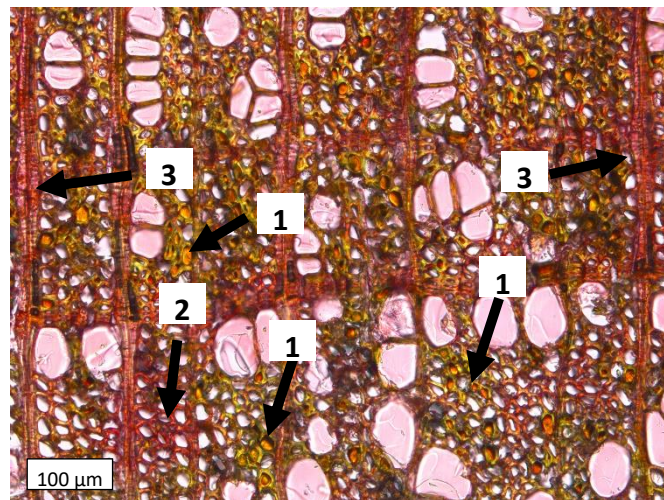


Figure 5-12 Modified tulipwood in the transverse section. Magenta colour in the lumen indicates leaching of stain from the wood. Thus, cleaning the section in methylated spirit did not sufficiently remove excess safranin stain. (1) Area where cell walls are not stained. (2) Area where cell walls appear stained. (3) Ray cells that appear stained.

More likely, the issue lies in the sample preparation or the microscopy observation itself. Concerning microscopic observation, the magnification in Figure 5-11 is relatively low, and the overall colour might result from an averaging effect. This becomes more apparent at higher magnification in Figure 5-12. Notably, the cell lumens in Figure 5-12 appear magenta, indicating that safranin has leached out of the wood into the glycerol mount. Thus, the washing step did not sufficiently clean the safranin from sample, leading to an image that appears reddish at lower magnification. Despite errors in sample preparation that constrain interpretation possibilities, Figure 5-12 reveals additional trends that are worth considering. Certain regions seem to feature unstained cell walls (1), while others display higher staining intensity (2). Ray cells, in general, exhibit higher staining intensity (3). To validate these observations, further investigation would be necessary with adequately prepared samples.

In conclusion, resin migrates into the cell wall and polymerises *in situ*. This fraction of the resin is more crucial for the property improvement of modified wood compared with the resin deposits in the cell lumen⁸⁶. The liquid resin uptake during impregnation (LU) depends primarily on the available void volume, i.e., density. Resin deposits in the lumen contribute to an increased density, while the density of unmodified wood can be maintained if the number of resin-filled lumens is low.

The BU serves as an indicator of resin cell wall penetration, although it is influenced by density and potentially other factors. Therefore, using the BU as an indicator for resin cell wall penetration within a single species is more meaningful than using it between species. Resin cell wall penetration can be indirectly examined through light microscopy in combination with safranin staining, although sample preparation can pose challenges.

It is worth noting that the safranin staining technique effectively differentiates between modified and unmodified wood tissue. However, making nuanced statements about the resin cell wall penetration is difficult, as previous attempts failed to distinguish wet curing from dry curing with safranin staining⁹⁷. Thus, it remains questionable whether this technique can differentiate an 'effective' modification from an 'ineffective' one. Other methods, such as thermoporosimetry and solid-state NMR, are more suitable for this task and will be discussed later in this thesis.

5.4.2.2. Swelling Coefficient

The swelling coefficient of unmodified wood is a crucial property during its service life, varying in the three principal directions. Typically, the highest swelling is observed in the tangential direction (T), followed by the radial (R) and the longitudinal (L) directions, with a ratio of swelling coefficients generally around 20 (T) : 10 (R) : 1 (L) for most timbers. In the following analysis, an area-based swelling coefficient is employed, considering (R) and (T) while neglecting (L).

Table 5-2 shows that the swelling coefficient of unmodified wood (S_{control}) varies between 8.71 – 26.76% in hardwoods and between 12.20 – 17.71% in softwoods. Hence, S_{control} differs significantly between wood species. Part of this variation can be attributed to different densities, where high-density species have thicker cell walls that expand more than thinner cell walls. The correlation between the oven dry unmodified density and S_{control} is relatively high in unmodified hardwoods ($R^2 = 0.74$) and moderate softwoods ($R^2 = 0.55$), suggesting that other factors play a role (Appendix 12).

The fact that other factors play a role is evident in lime and sycamore, which have a comparable density of 0.55 g/cm³ and 0.60 g/cm³, respectively. Despite the slightly lower density, lime displays a significantly higher S_{control} of 21.46% compared to sycamore with a S_{control} of 13.28%. This difference is probably due to variations in the chemical composition

of both timbers, as lime has a much higher hemicellulose content (44.2%) compared to sycamore (33.9%), as shown in Table 3-2. Additional factors that affect S_{control} might include anatomical factors, such as the width of annual growth rings.

The swelling coefficient post-modification (S_{mod}) is an indicator for the performance of modified wood. It is an important parameter for the application of modified wood in a commercial context, possibly more than the ASE value. A customer will be primarily interested in the properties of the modified material (i.e., S_{mod}), rather than in the comparison of the modified wood to an unmodified reference (i.e., ASE).

Table 5-2 illustrates that S_{mod} varies between 4.46 – 9.42% in hardwoods and between 5.75 – 8.08% in softwoods. Notably, the range of S_{mod} is much narrower than the range of S_{control} both for softwoods and hardwoods. As before, interesting trends emerge in relation to density. In unmodified hardwoods, S_{control} could be explained reasonably well by variations in the unmodified density ($R^2 = 0.74$). However, in modified hardwoods, the modified density ceases to be an influential factor as the correlation coefficient decreases to a R^2 value of 0.49 (Appendix 13). This is probably due to the effect of resin deposits in the cell lumen, which affect the density but not the swelling coefficient, and have been shown to be more frequent in low-density species.

In unmodified softwoods, the correlation between density and S_{control} was relatively low ($R^2 = 0.55$), suggesting that its effect is comparatively small. After modification, this trend notably changed. The correlation coefficient between the oven dry modified density and S_{mod} is very high ($R^2 = 0.94$). The opposite behaviour of hardwoods and softwoods in this relation is an interesting trend that cannot be fully explained. One possible explanation could be that the density of softwoods governs the liquid resin uptake ($R^2 = 0.93$), which, in turn, governs the swelling coefficient post-modification (S_{mod}). In the hardwoods, the matter seems to be more complicated.

5.4.2.3. Anti-Swelling Efficiency

The anti-swelling efficiency (ASE) is a comparative measure that considers the swelling of a wood species in the unmodified and modified state. It is especially relevant for research purposes because it allows one to make statements about the modification mechanism. The ASE is a value between 0 – 100%, where a higher number represents a greater reduction in the swelling coefficient. Table 5-2 shows that the ASE during the first soaking cycle (ASE 1) of the treatment ranges between 44.2 – 68.7% in hardwoods and between 50.9 – 57.9% in softwoods. In comparison to other studies, these ASE values are relatively high indicating an effective treatment (see Table 5-1).

However, the ASE after the second soaking cycle (ASE 2) is notably lower, ranging between 34.6 – 59.5% in hardwoods and between 43.9 – 53.4% in softwoods. The decreasing dimensional stability upon water storage could be explained by the loss of bulking agent or thermally instable degradation products¹¹. Hence, it is possible that small quantities of resin are not well-fixed in the cell wall and leach upon water soaking. Alternatively, the treatment might cause some degree of cell wall degradation and the degradation products, which may also bulk the cell wall initially, leach upon water soaking. This question is addressed in the analysis of the soaking solution in Chapter 5.4.3.

Particular interest is drawn by the question why some timbers with similar swelling coefficient post-modification (S_{mod}) have such different ASE values. Therefore, this discussion focuses on specific case studies involving wood species with similar characteristics.

One such case study compares sycamore and lime, which share similar values for unmodified density and S_{mod} , but lime demonstrates a much higher ASE. Micrographs in Appendix 9 show some anatomical differences (e.g., in ray width, vessel, and fibre diameter) but it is difficult to derive the swelling behaviour from that alone. Differences in the hemicellulose content of both timbers have been discussed earlier in this chapter, where a much higher hemicellulose content was noted for lime. Thus, the hemicellulose content could play a role in the explanation of different ASE values.

Another example involves SYP and Scots pine, where Scots pine has the higher ASE. Both species have a similar density and chemical composition. In this case, the annual growth ring width could be critical (Appendix 14). Scots pine has narrower growth rings and a higher proportion of latewood than SYP. Possibly, there are differences in the efficiency with which the latewood and earlywood are modified.

A third case compares birch and SYP, which have a similar value for the unmodified density and S_{mod} , but birch displays higher ASE. The treatment is more efficient in birch ($ASE\ 1 = 59.3\%$) than in SYP ($ASE\ 1 = 50.9\%$). This trend is consistent with the observations in lime ($ASE\ 1 = 68.2\%$) and Scots pine ($ASE\ 1 = 57.9\%$), suggesting that hardwoods tend to exhibit a higher ASE than softwoods with similar density.

5.4.2.4. Swelling Coefficient in Water and Liquid Resin

Figure 5-13 compares the swelling coefficient of wood blocks in different fluids. The water-induced swelling was measured in the unmodified control groups after the first soak cycle and is therefore equal to $S_{control}$. The resin-induced swelling was recorded directly after the impregnation step when the samples were wet, but before heat curing, and is equal to S_{resin} . The boxplots in Figure 5-13 represent $S_{control}$ and S_{resin} for each species, allowing for a direct comparison. The aim of this comparison is to investigate whether the resin-induced swelling differs from the water-induced swelling coefficient. Therefore, a two-way ANOVA was used to test whether $S_{control}$ and S_{resin} exhibit statistically significant differences.

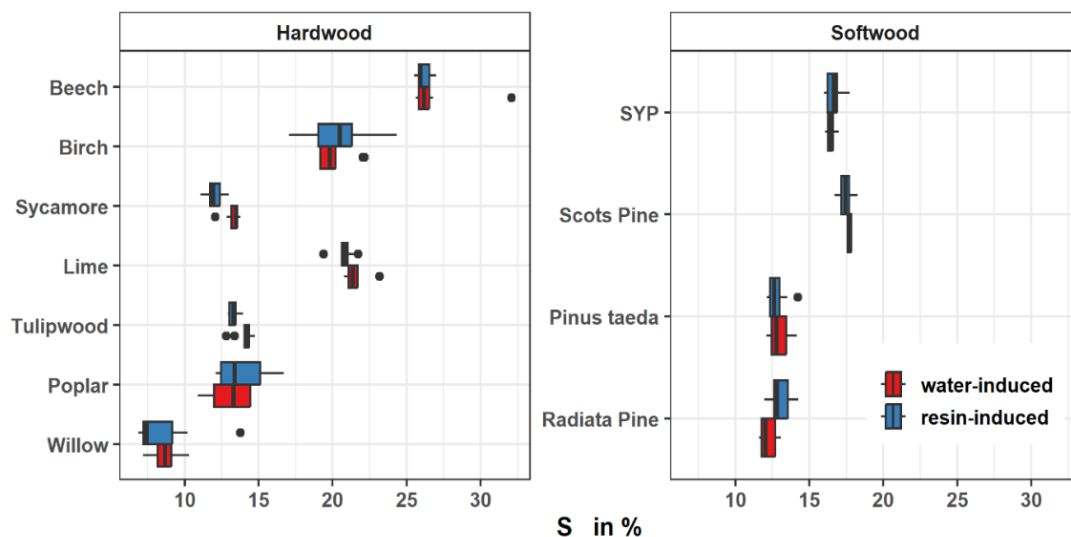


Figure 5-13 Comparison of water-induced swelling ($S_{control}$) and resin-induced swelling (S_{resin}) of modified groups. Species on the y-axis are arranged by decreasing density. S_{resin} is approximately equal to $S_{control}$ for most species.

This analysis has shown that there is no significant correlation ($p > 0.05$) between the fluid in which the wood is soaked and the swelling coefficient overall (Appendix 15). However, the pairwise Tukey test, which compared the difference within every species, revealed a statistically significant difference in the wood species sycamore, tulipwood, and Radiata pine (Appendix 16). Sycamore and tulipwood swell more in water than in resin, whereas Radiata pine swells more in

resin than in water. It is currently not known why these three species exhibit different swelling coefficients in liquid resin and water. In the eight remaining wood species, this difference is not statically significant, as indicated by the overlapping boxplots in Figure 5-13.

For various reasons, it was surprising to observe that S_{resin} is approximately equal to $S_{control}$. The former was measured after a 20-minute impregnation time, while the latter was measured after soaking for five days. Additionally, resin and water exhibit distinct chemical properties concerning polarity, molecular weight, and pH value which were expected to cause a different swelling behaviour.

5.4.2.5. Total Swelling of Modified and Unmodified Wood.

Figure 5-14 illustrates the total water-induced swelling (TS) for both modified and unmodified control groups. TS represents the swelling from the unmodified dry state (OD 0) to the first water-soaked state (WS 1) in the cyclic swelling experiment. Therefore, in unmodified wood, TS is equal $S_{control}$. In modified wood, TS encompasses both the swelling coefficient post-modification (S_{mod}) and the permanent volume gain introduced by cell wall bulking (BU). While TS holds minor significance for the application of modified wood, it may provide insights into the modification mechanism. Wood modifications employing a bulking agent are typically expected to exhibit a TS value that is the sum of BU and S_{mod} . Consequently, the swelling of unmodified timber could be anticipated to be reduced by the value of BU if BU has no effect on TS^{270} . In other words, if the assumption is correct, TS should be comparable for modified and unmodified wood.

Figure 5-14, however, shows that TS in modified wood consistently exceeds that in unmodified wood, and this difference is statistically significant for all species (see Appendix 17 & 18). In hardwoods, TS varies between 11.26 – 29.65%, and in softwoods, it ranges from 15.17 – 20.41%, approximately 1 – 3.5% higher than $S_{control}$ (Appendix 19). Remarkably, the smallest difference between TS and $S_{control}$ is observed in lime wood, with only 1.25%, while the largest difference is observed in poplar, with 3.49%. The contrasting behaviour of lime and poplar wood has been noted multiple times and can often be attributed to differences in chemical composition, particularly the hemicellulose content.

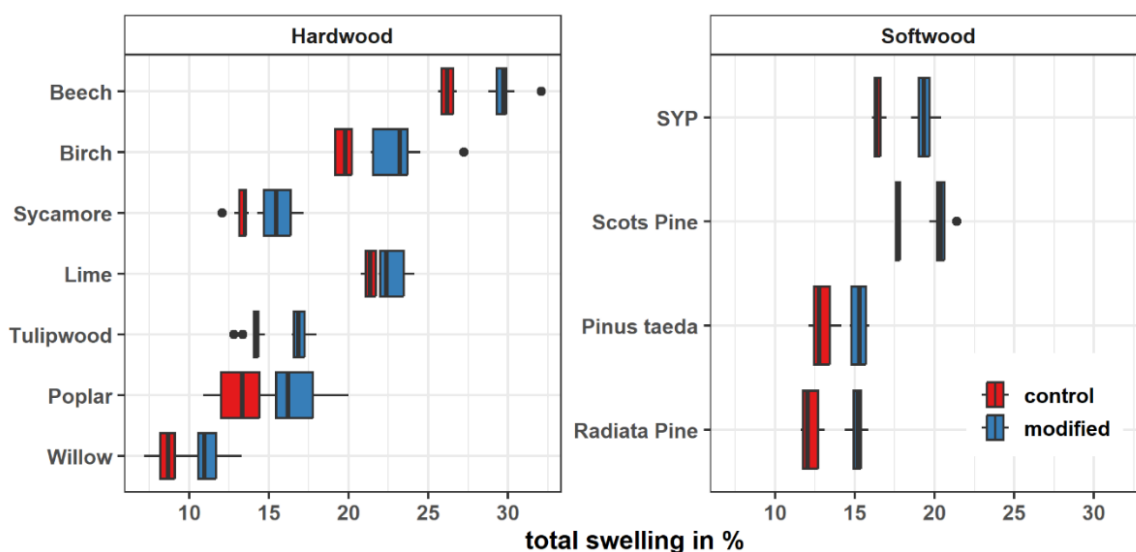


Figure 5-14 Comparison of total water-induced swelling (TS) between unmodified controls and modified wood during the first soak cycle. TS encompasses the swelling through water and cell wall bulking in modified wood. Species on the y-axis are arranged by decreasing density.

Once the modified wood is cured, it swells beyond the point that is reached in the control groups just by soaking in water. In other words, cured resin plus water swells the cell wall more than water alone. Various effects could play a role in explaining this phenomenon. E.g., resin that is not completely cured in the modified wood may provide additional sorption sites that lead to contribute to the increased swelling coefficient.

DVS studies in Chapter 4.4.4. have shown that resin with a relative low degree of cure absorbs up to 20% of its weight in water, hence the resin itself could provide additional sorption sites, leading to increases TS values. Alternatively, new sorption sites could be introduced through cell wall degradation, where an acetyl group is replaced by a hydroxyl group, which is more hydrophilic in comparison (see 5.4.1).

5.4.2.6. Water Uptake during ASE Tests

During ASE tests, wood samples are immersed in deionised water for a duration of five days, resulting in water absorption. This procedure is repeated three times on the specimens. The water uptake quantified in these tests could be relevant for exterior applications, such as the cladding of buildings, where both unmodified and modified wood absorb water during rainy periods.

Figure 5-15 (a) shows the water uptake in modified and unmodified wood during the second soak cycle (WS_2). Notably, the values for WU_2 decrease with the increasing dry density of a timber, both in modified and unmodified specimens. Since the water uptake in Figure 5-15 (a) includes the weight of the resin in modified samples, the values for WU_2 are much lower in modified wood compared to unmodified wood. WS_2 ranges between 100.6 – 235.1% in all unmodified wood species and between 67.9 – 132.5% in all modified timbers (Appendix 20).

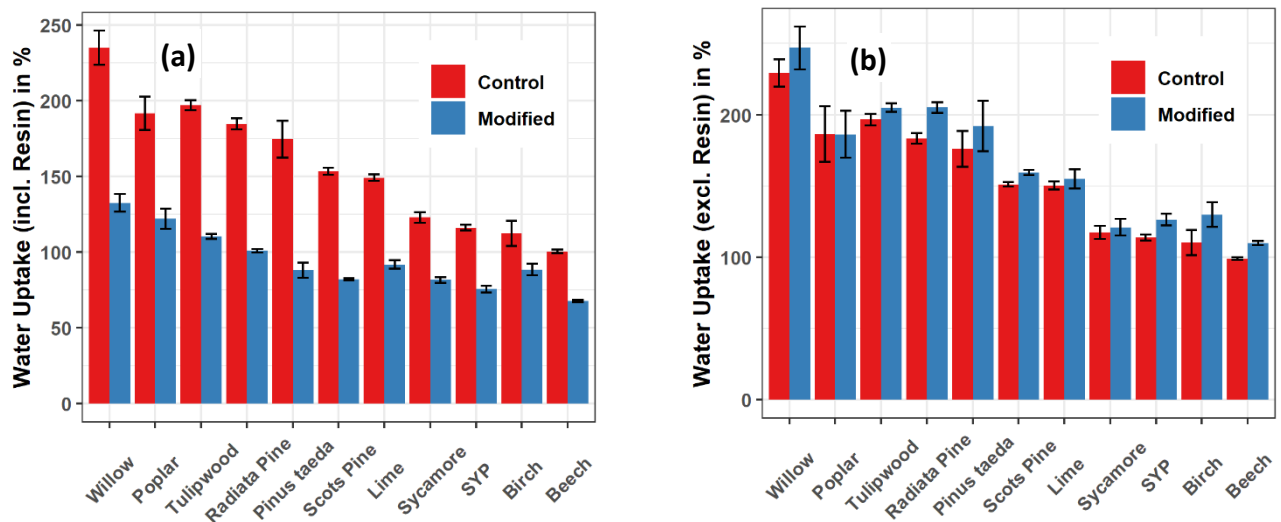


Figure 5-15 (a) Water Uptake in modified and unmodified control groups during the second soak cycle. If the weight of resin is included in the calculation, modified wood has a lower water uptake than unmodified wood. (b) Water uptake excluding the weight of resin in the calculation. If the resin weight is excluded, modified wood has a higher water uptake than unmodified wood. Species on the x-axis are arranged by increasing density.

This observation is exclusively due to the effect of resin weight within the calculated value for the modified wood. When resin weight is excluded, the water uptake in modified groups is higher as shown in Figure 5-15 (b). In the first soak cycle of modified wood, the resin weight can simply be excluded by using WU_0 instead of WU_1 (see 5.3.9). WU_0 varies between 99.0 – 229.1% in unmodified wood and between 110.0 – 246.8% in modified timbers (Appendix 21).

The water uptake including resin weight in Figure 5-15 (a) is lower in the modified wood, because of resin deposits in the cell lumen and cell wall bulking. Both lumen filling and cell wall bulking reduce the void volume of wood that can be

filled by water upon soaking. After excluding the resin weight in Figure 5-15 (b), the water uptake is higher in modified wood, possibly indicating the formation of new sorption sites.

Figure 5-16 illustrates how the water uptake changes over multiple cycles of water soaking in modified (a) and unmodified wood (b). From Figure 5-16 (a), it is evident that the water uptake in modified wood increases with each cycle for most species, except willow and Radiata pine. As previously mentioned, this increase could be linked to the creation of new sorption sites, resulting from the leaching of not fully crosslinked resin or degradation products. Conversely, Figure 5-16 (b) shows that the water uptake of unmodified wood is relatively constant for most species, except lime, birch, and beech, which display a small increase over cycles.

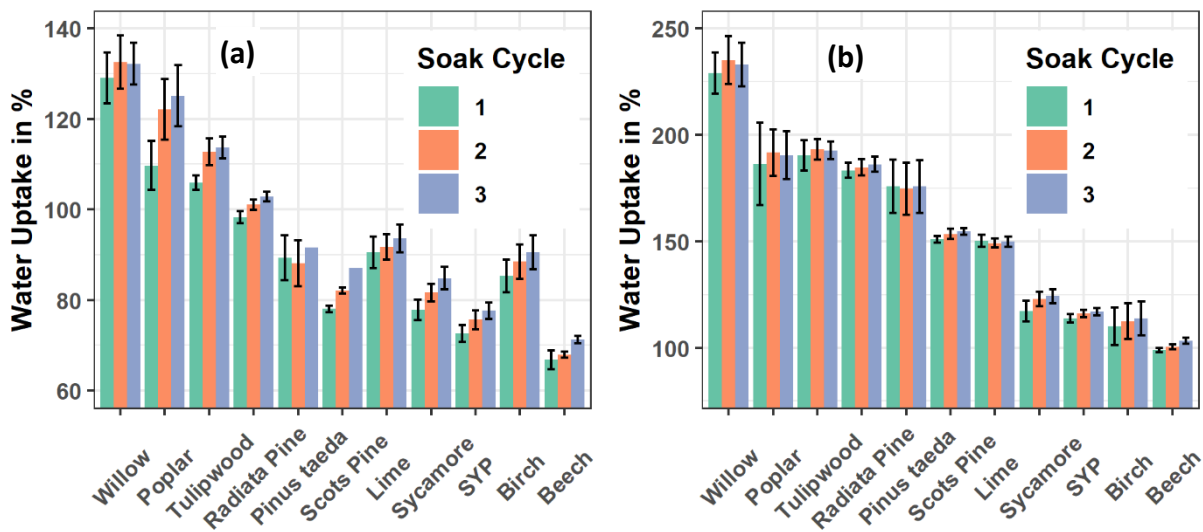


Figure 5-16 (a) Water uptake over the course of three soak cycles in modified wood. Most species display an increasing water uptake. (b) Water uptake over course of three soak cycles in unmodified wood. Most species display a constant water uptake.

5.4.2.7. Mass Loss during ASE Tests

During ASE tests, modified and unmodified specimens undergo three cycles of soaking and oven drying. Water soaking dissolves hydrophilic substances, resulting in a loss of dry wood mass after each soak cycle. Generally, the greatest mass loss occurs after the first soak cycle. However, it appears that not all hydrophilic substances dissolve in a single cycle, as a measurable loss of dry mass is observed in the second and third cycles too. The total mass loss (ML_{total}) is the sum of the mass loss from each cycle.

Table 5-3 displays ML_{total} for all modified and unmodified wood species. In unmodified hardwoods, ML_{total} ranges between 1.01 – 2.51%, while in unmodified softwoods, it ranges between 0.61 – 1.83%. These values account for water-soluble extractives and could be expected to fall within a similar range as the water-soluble extractives fraction (ExtrW) determined in Chapter 3.4.2 through hot water extractions and freeze-drying. However, with values ranging from 0.15 – 0.62%, the ExtrW values were significantly lower compared to those of ML_{total} in Table 5-3. This difference could possibly be attributed to the use of different methods.

The average total mass loss of modified groups varies between 1.07 – 2.47% in hardwoods and 1.44 – 2.47% in softwoods. Notably, there is no clear difference in ML_{total} between modified and unmodified hardwoods. In some cases, the mass loss of the modified wood is significantly higher (e.g., in poplar, tulipwood, birch) compared to unmodified wood, whereas in other cases, ML_{total} displays no significant difference between modified and unmodified wood (e.g., in willow, poplar, lime, sycamore). Appendix 22 shows the pairwise comparison in each species using the Tukey test.

Table 5-3 Total mass loss (ML_{total}) in % over the course of the ASE experiment. Average values of ten. Standard deviation in parenthesis.

	ML_{total} in %										
	Willow	Poplar	Tulipwood	Lime	Sycamore	Birch	Beech	Radiata pine	Pinus taeda	Scots pine	SYP
control	2.08 (0.22)	1.5 (8.33)	1.01 (0.07)	1.49 (0.11)	2.51 (1.94)	1.03 (0.09)	1.06 (0.14)	0.93 (0.37)	0.61 (0.07)	1.83 (0.09)	1.13 (0.07)
modified	1.99 (0.07)	2.34 (0.12)	2.47 (0.17)	1.43 (0.09)	2.07 (0.12)	1.79 (0.09)	1.07 (1.08)	2.08 (0.33)	2.14 (0.1)	2.47 (0.04)	1.44 (0.07)

Conversely, the trend in softwoods is clear. The modified softwoods all display a significantly higher mass loss than the unmodified softwoods. As the mass loss results from substances leaching from the wood, there appears to be a difference between hardwoods and softwoods in this regard. In unmodified wood, these substances are water-soluble extractives (e.g., pectins). In modified wood, such substances could also include uncured resin that is not fixed in the wood, or degradation products (e.g., from deacetylation) that have been deposited in the wood structure. The next section explores the nature of leached substances by analysing the soaking solution.

5.4.3. The Soaking Solution from ASE Tests

5.4.3.1. pH value, Solid Residue, and UV Absorbance at 272 nm

Results from the previous section have shown that a small mass fraction, in the range of 0.61 – 2.51% (w/w) of both unmodified and modified wood, dissolves in cold water during repeated cycles of soaking. In modified wood, this fraction could include uncured resin or degradation products. Analysis of this soaking solution helps to understand which processes cause the mass loss by considering the leached products. To obtain meaningful readings of the UV absorbance, all tests were conducted after diluting the soaking solution to a constant volume of 1 litre.

Table 5-4 presents the pH values of the soaking solution over three cycles. In unmodified controls, the pH during the first cycle is mildly acidic or neutral, ranging between 4.45 – 6.94 in unmodified hardwoods and 4.51 – 6.62 in unmodified softwoods. In most unmodified timbers, the pH increases in subsequent cycles. The pH values in Table 5-4 align well with hot-water extract measurements in Chapter 3.4.3.3, despite the cold-water used for soaking solution in this chapter. The slightly higher pH values measured in this chapter result from dilution to a constant volume of 1 litre.

In the first cycle, the pH of modified timbers is neutral or mildly alkaline, ranging between 6.37 – 8.12 in modified hardwoods and 6.31 – 7.94 in modified softwoods. This can be attributed to the presence of the alkaline catalyst (potassium hydroxide) in the resin, which is highly soluble in water and leaches from the modified wood into the soaking solution. In subsequent cycles, the pH generally decreases, indicating that the alkaline catalyst is successively washed out with each soaking cycle.

Table 5-4 pH value of the ASE soaking solution in modified and unmodified control groups over the course of three soak cycles. Missing values are indicated by a hyphen.

Cycle No.	pH value											
	Willow	Poplar	Tulipwood	Lime	Sycamore	Birch	Beech	Radiata Pine	Pinus taeda	Scots Pine	SYP	
control	1	5.35	6.62	6.94	5.16	4.45	6.74	4.75	6.14	6.62	4.51	5.91
	2	5.82	6.40	7.48	5.13	7.40	7.48	6.35	7.55	6.19	7.35	6.44
	3	6.28	6.06	6.78	6.31	6.19	6.35	7.88	7.52	-	5.75	7.42
modified	1	6.67	8.12	7.22	6.63	6.37	6.68	6.91	7.52	7.94	6.31	7.25
	2	6.53	6.58	6.74	6.33	6.75	6.70	6.80	7.14	7.45	6.90	6.71
	3	6.47	6.65	6.28	5.40	6.31	6.42	6.87	6.67	-	6.20	6.38

Table 5-5 shows the solid residue of the soaking solution over the course of three soak cycles. Missing values indicated by a hyphen in the Table, are the result of errors during the measurement. In the first cycle, the solid residue of the unmodified controls varies between 0.066 – 0.151 g/l in hardwoods and between 0.067 – 0.144 g/l in softwoods. The solid residue decreases in all cases in subsequent cycles.

The soaking solution of modified wood often exhibits a higher solid residue than the corresponding control group, except for willow and sycamore. In the first cycle, it ranges between 0.092 – 0.213 g/l in hardwoods and 0.141 – 0.330 g/l in softwoods. Consequently, the soaking solution of modified wood contains additional substances compared to unmodified wood. Softwoods display a greater disparity between modified and control groups than most hardwoods, consistent with the trend observed in the total mass loss in Table 5-3.

Table 5-5 Solid residue of the ASE soaking solution in modified and unmodified control groups over the course of three soak cycles. Missing values are indicated by a hyphen.

		solid residue in g/l										
	Cycle No.	Willow	Poplar	Tulipwood	Lime	Sycamore	Birch	Beech	Radiata Pine	Pinus taeda	Scots Pine	SYP
control	1	0.123	0.066	-	0.077	0.137	0.151	0.112	0.067	0.092	0.144	-
	2	-	0.019	-	0.044	0.013	0.048	0.029	0.006	0.075	0.079	-
	3	0.090	-	0.012	0.006	-	0.011	0.023	0.027	0.069	0.087	-
modified	1	0.092	0.134	-	0.213	0.129	0.209	0.152	0.141	0.293	0.330	-
	2	0.045	0.031	-	0.078	0.073	0.029	0.100	0.033	0.137	0.107	-
	3	0.023	0.062	0.018	0.012	0.052	0.006	0.018	0.052	0.149	0.121	-

Aromatic compounds in solution absorb UV light at a wavelength of 272 nm. The analysis of UV absorbance is therefore intended to evaluate the resin leaching from the modified samples. Table 5-6 shows that the UV absorbance of the soaking solution in the first cycle varies between 0.08 – 0.35 for unmodified hardwoods and between 0.21 – 0.40 in unmodified softwoods. In the following two soak cycles, these values decrease in all cases. These values measured in the control groups indicate that aromatic substances other than PUF resin absorb UV light at a wavelength of 272 nm.

The UV absorbance in the modified groups is usually slightly higher than in the control groups, but as with previous data, this was not a consistent trend throughout all species. In modified hardwoods, the UV absorbance in the first cycle ranges between 0.08 – 0.42. In modified softwoods, it varies between 0.23 – 0.51. Hence, the concentration of aromatic compounds is often higher in the soaking solution of modified wood compared to the controls. However, it remains unclear whether this is due to leaching resin or other leaching substances that absorb UV light at a given wavelength. Therefore, while the results of UV absorption should be interpreted with caution, it appears that the leaching of resin from modified wood is kept to a minimum.

Table 5-6 UV absorbance at 272 nm of the ASE soaking solution in modified and unmodified control groups over the course of three soak cycles. Missing values are indicated by a hyphen.

		UV absorbance at 272 nm										
	Cycle No.	Willow	Poplar	Tulipwood	Lime	Sycamore	Birch	Beech	Radiata Pine	Pinus taeda	Scots Pine	SYP
control	1	0.17	0.08	0.23	0.15	0.32	0.27	0.35	0.21	0.21	0.40	0.25
	2	0.05	0.06	0.19	0.10	0.12	0.17	0.24	0.15	0.15	0.24	0.22
	3	0.01	0.01	0.11	0.07	-	0.13	0.15	0.11	0.13	0.18	0.14
modified	1	0.08	0.13	0.22	0.21	0.38	0.42	0.34	0.23	0.46	0.51	0.25
	2	0.12	0.15	0.22	0.21	0.26	0.31	0.29	0.26	0.30	0.34	0.26
	3	-	0.01	0.12	0.17	0.16	0.22	0.21	0.18	0.27	0.30	0.20

5.4.3.2. Solution-State NMR

The soaking solution of modified wood contains additional substances compared to the soaking solution of the controls. The previous section has shown that these substances include the alkaline catalyst from the resin as well as other aromatic compounds that absorb UV light at 272 nm. However, it remains unclear whether these compounds originate from the resin fraction or whether they are degradation products from the wood. When considering outdoor applications of modified wood, minimising the leaching of resin is essential for environmental reasons and to maintain high dimensional stability and durability. Therefore, to clarify the nature of the leached compounds, the soaking solution was analysed by solution-state ^{13}C NMR and ^1H - ^{13}C HSQC NMR spectroscopy. This was done to confirm whether or not resin leaches into the water.

Figure 5-17 compares the partly cured PUF resin (see Chapter 4.4.3.), the hot water extract of unmodified beech wood (see Chapter 3.4.4.), and the soaking solution of modified beech wood (this Chapter). The Figure shows the ^1H - ^{13}C HSQC NMR spectrum of those three samples. Evidently, the spectrum of the soaking solution shows some similarities with the hot water extract in the region between 80 – 50 ppm, indicating the presence of alcohol groups. The soaking solution, however, contains no sugars since the anomeric signal between 105 – 90 ppm is absent in the spectrum.

The hot water extract displays a peak at 1.9/21.5 ppm, which corresponds to the methyl group of acetic acid. Acetic acid is the product of auto-hydrolysis generated in an acidic environment during hot water extraction²²⁶. The soaking solution displays a similar signal at 1.8/22.9 ppm, that is assigned to the methyl group in and acetate salt, which is the degradation product of the alkaline deacetylation of hemicelluloses²⁴⁷. The acetate salt constitutes the main component of the soaking solution, with the most intense peak.

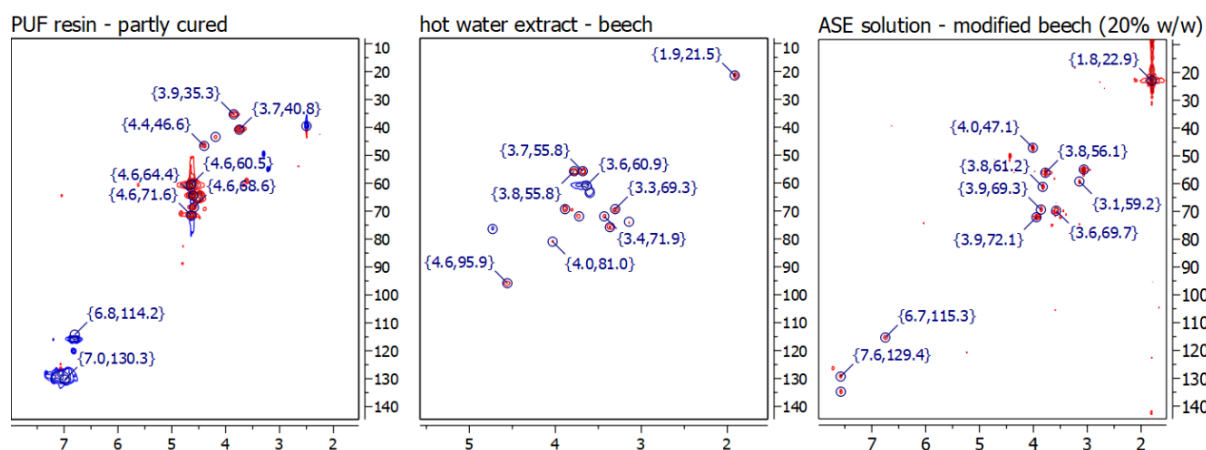


Figure 5-17 ^1H - ^{13}C -HSQC NMR spectra showing the partly cured PUF resin in $\text{DMSO}-d_6$ (left), the hot-water extract of beech wood in D_2O (centre), and the ASE soaking solution of modified beech wood in D_2O (right)

Furthermore, the soaking solution exhibits signals in the aromatic regions that are absent in the hot water extract. Presumably, these aromatic signals represent the same substances that caused the higher UV absorbance in the soaking solution of modified wood in the previous section. The aromatic signal at 6.7/115 ppm is also present in the PUF resin, where it is assigned to the unsubstituted ortho-position of the phenolic ring. Aside from that, the spectra of the soaking solution and resin have little in common. Typical resin signals corresponding to methylene bridges (between 3.7/30 ppm – 4.4/47 ppm) and hydroxymethyl groups (between 4.4/60 ppm – 4.8/72 ppm) are not reflected in the spectrum of the soaking solution. Hence, the soaking solution contains aromatic substances, as indicated by UV measurements, but these substances are not related to PUF resin.

Figure 5-18 compares the soaking solutions from different samples. The ^{13}C NMR spectra of modified beech with 20% and 40% (w/w) resin concentration and Radiata pine with 20% resin concentration 20% (w/w) are presented. Spectra are normalised to the acetate peak at 22.9 ppm. The two major peaks at 22.9 ppm and 181.5 ppm originate from an acetate salt, as previously discussed. To a smaller extent, the beech soaking solution shows peaks at 10 ppm and 31 ppm, which could indicate propanoic acid salts²⁴⁷.

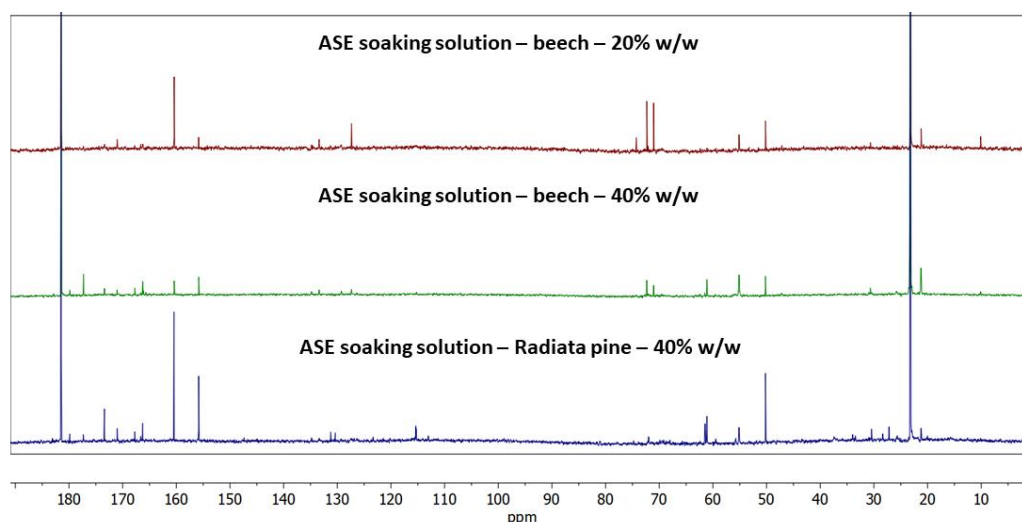


Figure 5-18 ^{13}C DEPTQ NMR spectra of ASE soaking solution beech and Radiata pine treated with different concentration of PUF resin in D_2O .

Apart from the acetate salt, the three samples show identical signals but different intensities at 160 ppm, 155 ppm, 55 ppm, and 50 ppm. As these signals are found in all three samples, they might indicate a common degradation product rather than a water-soluble extractive. The extractive fractions of different timbers were shown to differ in Chapter 3.4.4.

Signals between 180 – 160 ppm may correspond to various compounds, such as aldehydes, carboxylic acids, or esters. When combined with the aromatic signals between 160 – 100 ppm and the alcohol signals between 80 – 50 ppm, these compounds could originate from lignin-carbohydrate-complexes (LCCs). All softwood lignin moieties are incorporated in LCCs, while only 47 – 66% of hardwood lignin moieties⁵¹ are involved. Thus, if LCCs are another main degradation product, this could explain some of the trends observed before, such as the high disparity between the mass loss of modified and unmodified softwoods.

To conclude, the soaking solution is in the near neutral range and the primary degradation product is potassium acetate. This proves that the degradation of wood during modification occurs via an alkaline pathway. Deacetylation of hemicelluloses is the main degradation reaction. The soaking solution probably contains no PUF resin, but other

aromatic and non-aromatic substances that absorb UV light at 272 nm. Possibly, these substances are LCCs that are partially degraded during the resin treatment.

5.4.4. Discussion of Factors that Influence the ASE of a Wood Species

This section systematically examines the results obtained from different methods and their implications for the ASE of various wood species. Figure 5-19 plots the correlation between selected wood properties and the ASE values for each species, as recorded in Table 5-2. Two trendlines are shown in each plot, one for softwoods and the other for hardwoods. In one case, SYP was identified as an outlier and excluded from the trendline, a consideration that will be discussed later.

Previously in Chapter 5, wood density was shown to govern important properties in the modification process, such as the liquid resin uptake during impregnation, water uptake, and to lesser extent the swelling coefficients S_{mod} and S_{unmod} . And while it is widely recognised that density is an important factor in the modification process, there are no publications available to validate the connection between density and ASE. In fact, this correlation as shown in Figure 5-19 is relatively weak in hardwoods ($r^2 = 0.5$) and very weak in softwoods ($r^2 = 0.07$). Therefore, the oven dry density of a wood species is a factor that contributes relatively little to the ASE of a wood species.

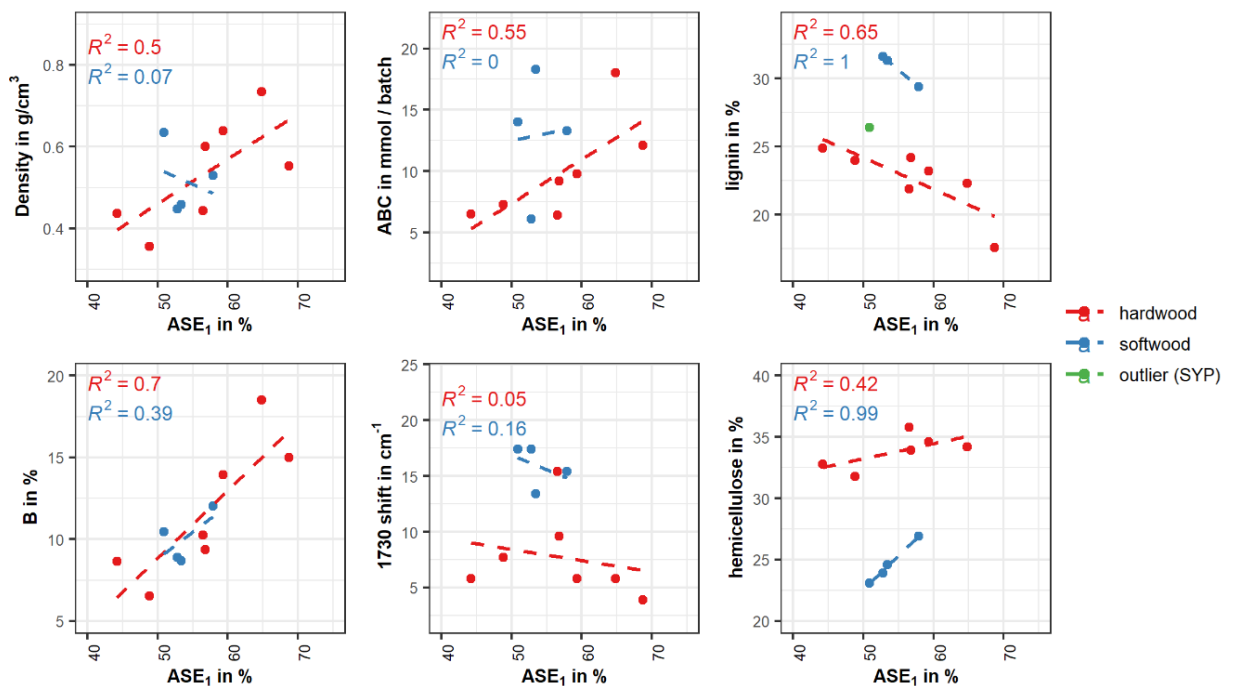


Figure 5-19 Correlation between selected wood properties and the anti-swelling efficiency achieved after the treatment with PUF resin. Trends are displayed for softwoods and hardwoods. Top R^2 -value represents hardwoods and bottom R^2 -value represents softwoods. SYP is classified as an outlier in the sub-plot showing lignin content against ASE.

Another factor that was obtained for each species in Table 5-2 is the BU. The correlation between BU and ASE is moderate in hardwoods ($r^2 = 0.7$) and weak in softwoods ($r^2 = 0.39$). This relatively good correlation is attributed to the effectiveness of BU as an indicator for the amount of resin located in the cell walls, where it is most effective, as opposed to resin deposits in cell lumens⁸⁶. However, despite the relatively good correlation, it is essential to note that cell wall bulking is typically the result of effective cell wall penetration rather than an inherent property of the wood. Consequently, BU does not explain why the modification was more effective in some species than in others.

Chemical effects between wood and resin must be considered to explain the observed trends in the ASE. One effect that was mentioned in previous chapters is based on the neutralisation that occurs when alkaline resin interacts with the acidic wood substrate. In this context, the differential scanning calorimetry (DSC) results in Chapter 4.4.1. have demonstrated that a neutralised PUF resin has a significantly slower curing rate compared to the alkaline default resin. At the same time, the results of the alkaline buffer capacity (ABC) measurements in Chapter 3.4.3.3. have shown that different wood species possess a varying neutralisation potential. Such differences could impact on the ASE of a wood species. However, Figure 5-19 shows no correlation between ABC of a wood species and ASE for softwoods ($r^2 = 0$) and a moderate positive correlation for hardwoods ($r^2 = 0.55$). Thus, while neutralisation effects probably occur during the modification process, they have no notable effect on the ASE of a wood species.

Another effect that could be related to the alkalinity of the resin in combination with the elevated temperatures during heat cure, is the degradation of the cell wall. Evidence for cell wall degradation was supplied by FTIR and NMR spectroscopy in this chapter. The adverse effect of cell wall degradation on the ASE is acknowledged in the literature⁹⁶, but lacks a comprehensive explanation. One plausible interpretation would be that the removal of acetyl groups, as the main degradation product, diminishes the cell wall volume and counterbalances the cell wall bulking effect.

The degree of cell wall degradation in Figure 5-19 is represented by the shift in the FTIR carbonyl band (1730 cm^{-1}) to lower wavenumbers, mainly accounting for the deacetylation of hemicelluloses. Figure 5-19 shows a weak negative correlation between the carbonyl shift and the ASE for both softwoods ($r^2 = 0.16$) and hardwoods ($r^2 = 0.05$). The negative sign of this correlation indicates that cell wall degradation has a detrimental impact on the ASE, as expected. However, the low r^2 values suggest either this effect is small or the selected method is unsuitable. A more accurate method might achieve better correlations.

The correlations with the highest r^2 values in Figure 5-19 were achieved with the lignin and hemicellulose content. The ASE of wood species increases with the former and decreases with the latter. In the sub-plot showing lignin content against ASE, SYP was classified as an outlier. This can be justified because the three other correlations in the right-hand column of Figure 5-19 are either weak ($r^2 = 0.42$), moderate ($r^2 = 0.62$) or high ($r^2 = 0.99$), and the hemicellulose content is complementary to the lignin content.

A correlation between wood chemistry and ASE has not been reported in the literature previously and opens new avenues for further research. Possibly, the hemicellulose fraction in the cell wall is more accessible to resin molecules, leading to a better penetration on a nanometre scale. More research is needed to clarify this relationship.

5.5. Conclusions from Chapter 5

Chemical changes during the modification of softwoods and hardwoods were monitored by FTIR-ATR spectroscopy in combination with PCA analysis in this chapter showing that:

- The PCA distinguishes reliably between modified and unmodified timbers, and between softwoods and hardwoods. This analysis worked better with FTIR spectra in reflectance mode compared to spectra in absorbance mode.
- Chemically, the modified wood differs from the unmodified control samples by the presence of resin as shown by the wavenumbers 1639 cm^{-1} , 1548 cm^{-1} , and 1482 cm^{-1} , but also by changes in the carbonyl region, represented by a shift of the 1730 cm^{-1} peak to lower wavenumbers.
- The shift of the carbonyl peak to lower wavenumbers was observed for all timbers, but softwoods (and tulipwood) displayed a greater shift than most hardwoods.
- The shift of the carbonyl peak is linked to the deacetylation of hemicelluloses via an alkaline mechanism during the modification process.

The liquid resin uptake during modification, the density before and after modification, and the bulking coefficient were studied in this Chapter, showing that:

- The liquid resin uptake depends on the oven dry unmodified density, particularly in softwoods rather than in hardwoods.
- The density of low-density species (e.g., willow, poplar) increases after the modification, whereas it remains nearly unchanged in high-density species (e.g., beech, birch). This relates to a larger number of resin deposits in the lumen of low-density species.
- Resin deposits in the lumen are observed in light microscopy and SEM observations throughout all species.
- The modification leads to a cell wall bulking effect, which is the result of resin cell wall penetration.
- The bulking coefficient correlates well with the unmodified density in hardwoods, but poorly in softwoods.
- Resin cell wall penetration was studied by light microscopy observations in combination with safranin staining.

The swelling coefficient is a crucial characteristic for both unmodified and modified wood in service. Measurements of the swelling coefficient before modification (S_{control}) and after modification (S_{mod}) reveal the following insights:

- S_{control} varies considerably between species and depends partly on the density, however, other factors such as the hemicellulose content or the growth ring width seems to play a role.
- S_{control} displays a broad range between of 8.71 – 26.76% for all timbers. After modification, S_{mod} decreases significantly to 4.46 – 9.42% and the ranges narrows down as well.

The reduction in the swelling coefficient was quantified by the ASE, showing high values ranging between 44.2 – 68.7% during the first soak cycle. After the second cycle, these values decreased to 34.6 – 59.5%. Furthermore, variations in the ASE of the observed wood species were evident based on factors such as hemicellulose content, growth ring width, and the differentiation between hardwoods and softwoods.

A comparison of water-induced and resin-induced swelling coefficients has shown that there is no significant difference between the two values, except for sycamore, tulipwood, Radiata pine.

The total swelling was defined as the volume gain from the unmodified dry state to the first water-soaked state for both modified and unmodified wood. In modified wood, it includes the permanent volume gain through cell wall bulking. It could be shown that:

- The total swelling was significantly higher in all modified timbers, compared to the unmodified controls.
- The difference between the total swelling of modified and unmodified wood was highest in lime and lowest in poplar, indicating that the chemical composition of a timber plays a role in this regard.
- The higher total swelling of modified wood suggest that new sorption sites are created during the treatment.

The water uptake of modified and unmodified wood was measured after five days of soaking in deionised water. The results have shown that:

- The water uptake is lowered from 100.6 – 235.5% in unmodified wood to 67.9 – 132.5% in modified wood.
- This effect is exclusively due to the addition weight of resin in modified wood.
- Over the course of three soak cycles, the water uptake increases in most modified timbers and remains constant in most unmodified timbers.

During repeated cycles of water soaking, a mass loss of 0.61 – 2.51% was observed in modified and unmodified samples. The results have shown that:

- Among the hardwoods, the mass loss is sometimes higher in modified samples than in unmodified samples. In other hardwoods, there is no significant difference.
- All modified softwoods display a significantly higher mass loss than the corresponding control groups.

Analysis of the soaking solution, using various methods such as pH, UV, and solid residue measurements as well as solution-state NMR spectroscopy, was used to determine the nature of the leached substances. The results show that:

- The soaking solution of the unmodified wood controls contains water-soluble extractives.
- The soaking solution of the modified wood contains additional substances since the solid residue in most modified timber is higher than in most unmodified controls.
- The pH value of the soaking solution is higher in soaking solution of modified wood, indicating that the alkaline catalyst potassium hydroxide leaches from the modified wood into the water.
- The UV absorbance at 272 nm is often higher in the soaking solution of modified wood, suggesting that the addition substances are aromatic.
- Solution-state NMR analysis shows that the main constituent in the soaking solution of modified wood is an acetate salt, which corresponds well to the previously observed deacetylation of hemicelluloses.
- Most NMR signals that are indicative of PUF resin are absent in the soaking solution of modified wood, indicating that resin does not leach into the water.
- Possibly, Lignin-Carbohydrate-Complexes (LCCs) in the wood are degraded during the modification process which could explain the higher UV absorbance and aromatic NMR signals in the soaking solution of modified wood.

Finally, the ASE of all timbers was correlated with the results from various methods in order to number of hypotheses about which factors contribute to the ASE of wood species. This discussion has shown that:

- The oven dry unmodified density is a relatively poor indicator for the ASE of wood species.
- The bulking coefficient exhibits a relatively good correlation with the ASE, however, it is more a consequence of the modification process than an intrinsic property of wood capable of explaining the origin of the ASE.
- Neutralisation effects between alkaline resin and acidic wood substrate that reduce the curing rate of the resin have probably no effect on the ASE of a timber.
- Cell wall degradation, arising from alkaline conditions and elevated temperature during heat cure, could potentially have a detrimental effect on the ASE. However, the method employed to monitor cell wall degradation, specifically the change in the carbonyl peak in the FTIR spectrum, is probably a poor indicator for this task.
- The best correlations were achieved between the ASE and the chemical composition, i.e., hemicellulose and lignin content, of a wood species. Timber with a high hemicellulose and low lignin content achieved the best ASE values.

6. Wood Modification with Phenol Urea Formaldehyde Resin: The Influence of Processing Conditions

6.1. Introduction to Chapter 6

Wood modification with low molecular weight thermosetting resin is a complex process that is influenced by various factors, including the impregnated material, the impregnation solution, and the atmospheric conditions in the drying and curing stages. The impregnated material was addressed in Chapter 5, showing that the wood species selection has a significant influence on all aspects of the modification.

In order to evaluate this influence, various wood species in Chapter 5 were treated under identical process conditions. These conditions included a resin concentration of 30% (w/w), a resin pH of 9.2, an impregnation time of 20 minutes, a 16-hour drying step at 50°C, an 8-hour curing time, and a curing temperature of 150°C. In principle, each of these process conditions individually affects the properties of the modified wood, and interactions between different factors are possible. For example, the ASE of modified wood is influenced by the resin concentration during impregnation⁸⁷, but the relationship between ASE and resin concentration may vary between species, possibly leading to different wood species favouring distinct resin concentrations.

This chapter delves into the impact of specific process conditions, particularly those related to the impregnation solution and atmospheric conditions. ASE tests serve as a means to assess the influence of various process conditions, such as curing time, resin concentration, resin alkalinity, and drying conditions, each explored in a separate experiment. The comparison of different resin concentrations in this chapter is also used to evaluate a FTIR-based partial least square (PLS) model. This model is tested as a potential tool for predicting the weight percentage gain (WPG) in modified wood, showcasing an approach that could serve as a quality control measure for commercial wood modification.

Furthermore, this chapter establishes the concept of resin cell wall diffusion to explain the impact of different atmospheric conditions in the process. Given the significance of this concept in interpreting the results in sections 6.4.5 and Chapter 8, it is described here in more detail.

Cell wall diffusion is defined in the following as the migration process of resin molecules into the cell wall, which can be promoted in the drying stage between impregnation and heat curing. The mechanism is illustrated in Figure 6-1. Resin already migrates into the cell walls during the impregnation step, but cell wall diffusion in the drying stage may further promote this transport process. In Chapter 5.4.2.1, it was shown that one fraction of the resin cures inside the cell wall and another fraction cures inside the lumens. In the same section, it was concluded that cell wall bulking is the result of resin deposits inside the cell wall. Thus, the bulking coefficient (BU) can be used to quantify the degree of cell wall diffusion that has occurred within one wood species under the specific conditions used.

Cell wall diffusion is detached from the impregnation of the macroscopic voids (i.e., lumens) in the bulk structure of a wood species. Therefore, a timber might display a high gravimetric resin uptake, but a low cell wall resin content, resulting in poor performance. This scenario could occur if the molecular weight of the resin is too high⁸⁶ or the affinity of the resin towards the cell wall is low¹⁰¹. Although the concept of a separate diffusion and drying phase between impregnation and curing dates back to the early days of wood modification in the 1950s¹²⁶, the recent literature is divided about the practicality of this process step.

Zheng et al.⁹² (2018) visualised cell wall diffusion and its positive effect on the BU using a technique called Time-Of-Flight Secondary Ion Mass Spectrometry (cryo-TOF-SIMS). The study showed that the RH in the drying step of Melamine Formaldehyde (MF) impregnated wood influences the location or resin deposits inside the wood structure. If the MF impregnated wood was dried in a high-RH environment (RH 75%), resin diffused increasingly into the cell walls, leading to a higher BU. Conversely, MF impregnated wood that was dried in a low-RH environment (RH 11%) displayed more resin filled lumens.

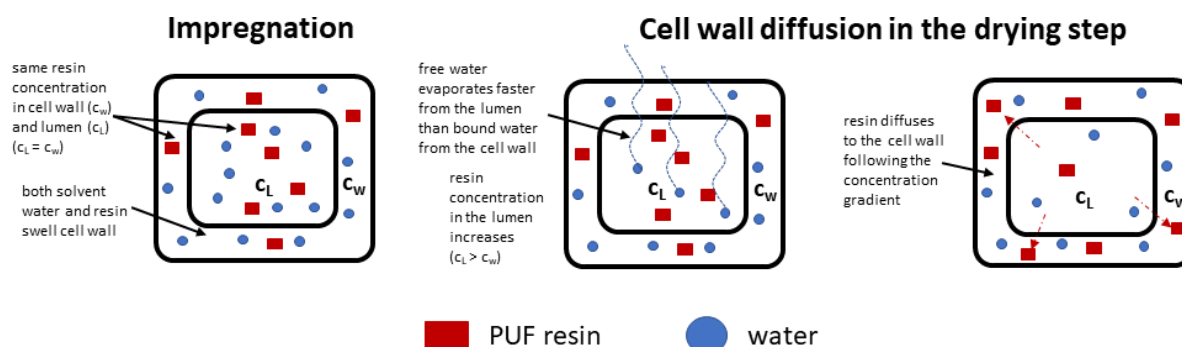


Figure 6-1 Cell wall diffusion mechanism of resin molecules as described by Tanaka et al.⁸⁸⁻⁹¹. PUF resin and water are equally distributed between cell wall and cell lumen after impregnation. Free water in lumen evaporates faster than bound water in the cell wall introducing a concentration gradient. PUF resin starts diffusion along this concentration gradient from the lumen to the cell wall.

Contrary to the results of Zheng et al.⁹², it was reported by Klüppel & Mai⁹³ (2013) that a separate diffusion phase between impregnation and curing led to a lower BU in both PF and MF modified wood. In their study, the samples were stored in closed boxes over water at a RH near 100% to promote cell wall diffusion, whereas the control group was dried directly after impregnation.

The main difference between the two studies is the RH employed during the diffusion phase (see Figure 6-1 left). A high RH seems to be beneficial, whereas too high can be problematic. To gain a better understanding of these results, it is worth considering the theoretical framework of cell wall diffusion, especially the effect of the RH in the diffusion phase. This framework dates back to the work of Stamm²⁷¹ (1956) and was refined more recently by Tanaka et al.⁸⁸⁻⁹¹, who studied the impregnation of wood with polyethylene glycol (PEG). In this process, cell wall diffusion in the drying stage depends primarily on two mechanisms, namely:

- i. a concentration gradient between the cell wall and the cell lumen and
- ii. the mobility of the resin molecule.

It is assumed that during impregnation, the resin penetrates the cell wall and the cell lumen equally. Therefore, the impregnated wood initially exhibits the same concentration of resin in both the cell wall and the cell lumen, without a concentration gradient at this starting point. Tanaka et al.⁹¹ used this and other assumptions to mathematically model of the material transport in the diffusion phase, but the mathematical details are not elaborated here.

As the wood starts to dry, it is further assumed that free water evaporates more rapidly from the lumen than bound water from the cell wall. Consequently, a concentration gradient is introduced (see Figure 6-1 right). The concentration of the resin fraction in the lumens starts to surpass that within the cell wall, causing resin molecules to diffuse from areas of high concentration (i.e., cell lumen) to regions of low concentration (i.e., cell wall). During the diffusion stage, a lower RH accelerates water evaporation from the lumen, resulting in a more significant concentration gradient.

The mobility of the resin molecule relates to its kinetic energy and the physical state of the wood polymers, which depends on whether they are in a glassy or rubbery state and whether they are dry or hydrated. Tanaka et al.⁹¹ assumed that the mobility of the resin molecules increases with the moisture content of the samples. Given that moisture content increases with RH during the diffusion phase, it is assumed that resin mobility also increases with RH.

Evidently, the RH applied in the diffusion stage affects the concentration gradient and the resin mobility in opposite ways. A low-RH environment favours the concentration gradient, while a high-RH environment increases the resin mobility. However, the material transport model of Tanaka et al.⁹¹, coupled with their experimental results, suggest that the resin mobility has a more substantial effect on the cell wall diffusion than the concentration gradient.

Therefore, it could be proposed that the degree of cell wall diffusion reaches an optimum value in a high-RH environment (Appendix 23). Nevertheless, if the RH exceeds this optimum, the concentration gradient diminishes, and the cell wall diffusion process is not promoted. This explains the conflicting results of Zheng et al.⁹² and Klüppel & Mai⁹³, as the 100% RH used by Klüppel & Mai was too high to promote cell wall diffusion.

In several other studies, the effect of further processes conditions on the degree of cell wall diffusion was explored by Tanaka et al.⁸⁸⁻⁹⁰. To summarise briefly, it was shown that the drying temperature increases the mobility of the resin and therefore improves cell wall diffusion⁹⁰. However, the curing temperature of the resin must not be exceeded at this stage, because crosslinking would increase the molecular weight of the resin and lower its mobility. Regarding resin concentration, there exists an optimum concentration for the most efficient cell wall diffusion process⁸⁸. This optimum depends on the amount of water required to open enough micropore spaces and on the amount of molecules required to occupy those spaces. Additionally, when drying the timber, the RH schedule should exhibit a gradual decrease to retain the resin in the cell wall⁸⁹. The experiments used to study cell wall diffusion in this chapter explore the principles established by Tanaka et al.⁸⁸⁻⁹¹ in the context PUF resin modification.

6.2. Materials

6.2.1. Wood Samples and Resin

The wood species used in this chapter were European beech (*Fagus sylvatica*), tulipwood (*Liriodendron tulipifera*), SYP, and Radiata pine (*Pinus radiata*). Small blocks with the dimensions 20 (r) x 20 (t) x 5 (l) mm are used for all analyses in this chapter. Samples treated with a resin concentration of 30% (w/w) are not the same as those used in Chapter 5. Therefore, different ASE results may be reported. New specimens were prepared for this chapter. Every test group is made up of 10 small blocks.

6.3. Methods

6.3.1. ASE Analysis – Resin Treatment of Small Blocks

The methods used in the resin treatments of small blocks are the same as in the Chapter 5.3.6. Variations in the curing time, resin pH value, resin concentration, and drying schedule are outlined in the following.

6.3.2. ASE Analysis – Design of Experiments

6.3.2.1. Curing Time

The role of the curing time was investigated in small blocks of beech, Radiata pine, and tulipwood treated with a resin concentration of 20% (w/w). Following the standard procedure from Chapter 5.3.6, each test group was placed in an

oven set to 150°C for 8 h. Then the samples were removed from the oven and allowed to cool down in a desiccator, before taking the dry weight and dimensions of each sample. This was used to calculate the weight percentage gain (WPG) and bulking coefficient (BU).

Subsequently, the same test groups were put back in the oven at 150°C for additional 16 h, and then again for additional 28 h, after which weight and dimensions were reported again. Hence, the same test group was always measured after 8 h, 24 h, and 52 h.

Unmodified wood and neat PUF were used as controls along with the modified wood to investigate whether thermal degradation occurs primarily in the resin or in the wood fraction. Unmodified small blocks of beech, Radiata pine, and tulipwood were dried at 105°C to determine their dry mass. Three replicates were used per species. Then, the unmodified samples were placed in an oven set to 150°C for 8 h, 24 h, 96 h, 120 h, 148 h, and 172 h. After each step, the weight and dimensions were reported.

For the PUF control, three replicates, each containing approx. 10 g of liquid resin (pH 9.5 and 50% w/w), were poured into silicon cases, and put in an oven set to 150°C. The weight of each replicate was measured after 3 h, 16 h, 25 h, 43 h, 48 h, 64 h, 88 h, and 160 h. This was done to show thermal degradation effects of the cured resin over time. In order to calculate relative mass, it was assumed that the resin is fully cured after 16 h, so that the mass loss before this point indicates heat curing, and the mass loss after this point indicates thermal degradation or over curing.

6.3.2.2. Resin Concentration

The role of the resin concentration was investigated in small blocks of beech, Radiata pine, and tulipwood. Test groups of each species were treated with a resin concentration of 20%, 30%, and 40% (w/w) using the standard procedure described in Chapter 5.3.6.

There is an overlap between test groups that are used to study the effect of curing time and those intended for the investigation of resin concentration, i.e., test groups treated with a concentration of 20% (w/w). To ensure uniform conditions, the groups treated with 30% and 40% (w/w) resin were also cured for 52 h, although deviating from the standard procedure.

The soaking solution of some of these test groups was freeze dried and sent to Cardiff University of solution-state NMR analysis. Results of this analysis were shown in Chapter 5.4.3.

6.3.2.3. Resin Alkalinity

The role of the resin pH value was investigated in small blocks of beech, Radiata pine, SYP, and tulipwood. Therefore, the default resin was diluted to 30% (w/w) in line with the standard procedure described in Chapter 5.3.6. The initial pH value of this diluted stock solution was pH 9.16. By adding potassium hydroxide pellets (85% w/w) to two aliquots of the stock solution, the resin pH value was raised to either pH 9.45 or pH 9.87. Small blocks of each species were treated with all three stock solutions according to the standard procedure.

6.3.2.4. Resin Cell Wall Diffusion

In this experiment, nine test groups each consisting of 10 small blocks of tulipwood, were impregnated according to the standard procedure. Subsequently, the role of cell wall diffusion was studied in a separate diffusion phase, which took place directly after the impregnation step and before heat curing. The investigated factors in the diffusion phase were:

- diffusion relative humidity (RH_{diff}),
- diffusion temperature (T_{diff}),
- diffusion time ($time_{diff}$),
- drying relative humidity (RH_{dry}).

These factors were chosen on the basis of the work of Tanaka et al.^{88–91}. Each of the four factors was tested on a low level and on a high level. For the diffusion relative humidity (RH_{diff}), these levels were 7% and 75% RH, for the diffusion temperature (T_{diff}) it was 4°C and 30°C, for the diffusion time ($time_{diff}$) it was 1 day and 7 days, and for the drying relative humidity (RH_{dry}), it was 7% and 33% RH. These four factors, each on two levels, were combined using a half-factorial design of experiments, which is summarised in Table 6-1. The control group in Table 6-1 was treated according to standard procedure without a separate diffusion phase.

Table 6-1 Half-factorial experiment plan used to investigate the effect of cell wall diffusion in ASE test. The control group was modified according to the standard procedure in Chapter 5.3.6 without a separate diffusion step.

Test Group	RH_{diff} in %	RH_{dry} in %	$time_{diff}$ in days	T_{diff} in °C
control	-	-	-	-
A	7	7	1	30
B	75	7	1	4
C	7	33	1	4
D	7	33	7	30
E	7	7	7	4
F	75	33	1	30
G	75	7	7	30
H	75	33	7	8

Saturated salt solutions were used to adjust RH_{diff} and RH_{dry} to the required level, namely NaCl for 75% RH, $MgCl_2$ for 33% RH, and KOH for 7% RH. These values are stable between 0 – 60°C provided that the solutions remain saturated. Hence, when the solutions were prepared at room temperature, it was ensured that it remained saturated at 50°C by adding a generous surplus of salt. Each solution was poured into a 2-litre plastic container, to a depth of 2 – 3 cm from the bottom (Figure 6-2). A plastic sample holder was used to contain one test group of ten samples keeping them above the level of the solution. This way, test groups could easily be moved between containers with different RH. The boxes were covered with the lid and the RH was monitored with a hygrometer that was placed on the sample holder next to

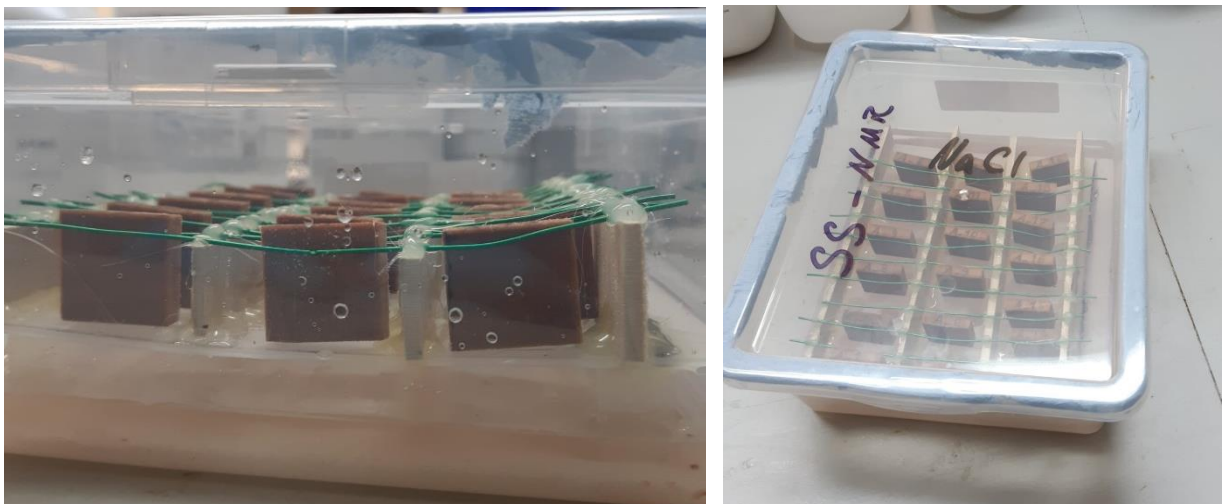


Figure 6-2 Set up of cell wall diffusion experiments. Specimens were placed in a sample holder over saturated salt solution to adjust the RH in the sealed plastic container. Containers were moved between different temperatures.

the small blocks. The RH measured in the containers was 5 – 10% higher than the theoretical values. The mass and volume of each specimen was monitored daily. Samples that came into contact with the salt solution at any point of the experiment were rejected.

6.3.3. ASE Analysis – Statistics

Statistical analysis using ANOVA and Tukey tests were performed as previously described in Chapter 5.3.10. Moreover, the half-factorial design used to study the cell wall diffusion allows one to calculate the statistical effect that each factor has on a certain result (e.g., BU, S_{mod} , WPG). The theory behind this effect calculation is described in detail by Siebertz²⁷². In this method, the average results (e.g., BU, S_{mod} , WPG) of each test groups are used. To calculate the statistical effect of a factor, one compares the average results obtained on the high level are compared with those obtained on the low level. This is illustrated for an example in the following equation:

$$E_{Diffusion\ RH} = \frac{BU_B + BU_F + BU_G + BU_H}{4} - \frac{BU_A + BU_C + BU_D + BU_E}{4}$$

test groups set to high level test groups set to low level

In this example, the effect (E) of the factor RH_{diff} on the result BU is calculated. The average BU of all groups tested at a low RH_{diff} (i.e., groups A, C, D, E) is subtracted from the average BU of all groups tested at a high RH_{diff} (i.e., groups B, F, G, H). Hence, the effect shows whether a certain factor can be used to manipulate BU (or any other result) in the desired way. An effect of zero means that factor has no impact on the result.

6.3.4. Multivariate Analysis of FTIR spectra – Predicting the WPG with a PLS model

The resin treatment with different resin concentrations produced modified wood samples with a range of different WPGs. In conjunction with FTIR-ATR spectroscopy, this offered the opportunity to develop a multivariate model, which can predict the WPG of a sample spectroscopically. Therefore, a partial least square (PLS) model was used.

The PLS model was developed by using a training set and a validation set. For the training set, additional small blocks were treated with PUF resin at the concentrations 10%, 15%, 20%, 25%, 30%, 35%, 40%, and 50% (w/w) with one replicate per resin concentration. Subsequently, the WPG of each specimen was noted, and each sample was milled in a cutting mill to obtain a homogeneous powder. This was done to prevent measuring inaccuracies as a results of varying resin uptake in different regions of the wood (see Figures 5-8 & 5-9). FTIR-ATR spectra were acquired in dry conditions for each concentration. The spectra were converted to absorbance mode, baseline corrected, and normalised between 0 and 1. The training set was then used to calibrate a PLS model by using the R function *plsrf()*. The optimum number of components for the PLS model was calculated by applying the R function *RMSE()* to the model, and the number of components which was shown to result in the lowest Root Mean Square Error (RMSE) was selected for the model.

The small blocks described in Chapter 6.3.2.2. treated at 20%, 30%, and 40% (w/w) resin concentration were used as a validation set for the PLS model. Therefore, the FTIR-ATR spectra of one representative per concentration were collected and converted to absorbance mode, baseline corrected, and normalised between 0 and 1. Subsequently, the PLS model was used to predict the WPG from each sample in the validation set. The predicted value of the WPG was then compared against the gravimetrically measured value of the WPG. The whole procedure was done for beech and Radiata pine samples.

6.4. Results and Discussion

6.4.1. The Effect of Curing Time

The curing time and temperature directly influence the degree of cure of the resin and the type of bonds that are formed^{175,273}. A high degree of cure leads to the build-up of a more rigid resin network in the cell wall. Therefore, the impact bending strength and fatigue strength decrease with longer curing times and higher curing temperatures, as the material loses the ability to accumulate plastic deformations^{123,251}. On the other hand, longer curing times and higher temperatures help decreasing the strictly regulated formaldehyde emissions of the modified wood²⁵¹. In this section, the focus is on the BU and WPG.

Table 6-2 shows the BU and WPG of beech, Radiata pine, and tulipwood treated with 20% (w/w) PUF resin. After 8 h, the three timbers display a BU between 9.13 – 12.58% and a WPG between 18.4 – 45.1%. As the curing time proceeds to 52 h, those values decrease consistently to 7.40 – 10.15% for BU and to 15.7 – 39.7% for the WPG. Comparing the results after 8 h and 52 h, the WPG decreases more in Radiata pine (5.4%) than in beech (2.7%) and tulipwood (3.9%). However, the BU decreases more notably in beech (2.43%) and is on a similar level for Radiata pine (1.76%) and tulipwood (1.73%). Thus, while thermal degradation is evident, the dry mass loss is not equivalent to the dry volume loss. The question arises whether the wood or the resin fraction is more susceptible to thermal degradation.

Table 6-2 Average values for test groups treated with 20% resin concentration and cured for 8 h, 24 WPG – weigh percentage gain after curing, BU – bulking coefficient. Standard deviations are in parenthesis.

Species	WPG in %			BU in %		
	8 h	24 h	52 h	8 h	24 h	52 h
Beech	18.4 (0.41)	16.5 (0.33)	15.7 (0.35)	12.58 (1.56)	11.00 (0.62)	10.15 (0.77)
Radiata pine	45.1 (0.38)	41.8 (0.23)	39.7 (0.25)	9.13 (0.50)	8.20 (0.49)	7.40 (0.46)
Tulipwood	26.4 (3.16)	24.1 (2.82)	22.9 (2.83)	10.29 (1.28)	9.23 (1.29)	8.53 (1.25)

The curing temperature of 150°C used here is lower than the temperatures used for thermal modification, where hemicellulose degradation is intentional⁴⁰. But even at a temperature lower than 150°C, minor changes do occur in the wood²⁷⁴, and the alkali present in the resin might accelerate wood degradation, as previously discussed in Chapter 5. After heat curing, phenolic resins are usually temperature-stable between 100 – 400°C, but the addition of methylated urea lowers this stability and might cause a higher mass loss at lower temperature²¹¹.

Figure 6-3 (a) shows the relative mass loss in the modified wood samples treated with 20% (w/w) resin concentration. As mentioned earlier, the relative mass loss is most pronounced in Radiata pine, followed by tulipwood and beech. This order aligns with the relative resin content in the timbers, suggesting that the mass loss is higher in the resin fraction than in the wood fraction.

To assess the impact of thermal degradation on the resin and wood fractions, a comparison is made between unmodified timbers and pure PUF resin in Figure 6-3(b). The relative mass curve for the pure resin starts at 16 hours with a relative mass value of 1.00, reflecting its initial uncured liquid state. To establish a reference for fully cured resin, one requires a reference at which the resin is assumed to be fully cured. This was estimated to be the case after 16 h at 150°C.

The mass loss of unmodified wood in Figure 6-3 (b) during the first 24 h of the experiment is negligible (< 0.5%). However, after extended periods longer than 96 h, the mass loss becomes notable, and even accelerates after 148 h. The mass loss in unmodified beech is higher than in other species, which could be related to a higher proportion of acetyl groups in the hemicelluloses that are converted to acetic acid and promote degradation¹⁵³.

However, the neat PUF control shows a higher mass loss than all the unmodified timbers, especially during the first 100 h of the experiment. The reference point after 16 h is a generous estimate in so far that the pure resin can probably be assumed to fully cured even earlier and this would result in an even higher relative mass loss in Figure 6-3. Nevertheless, after 150 h the shape of the PUF curve approaches an equilibrium, suggesting that the thermal degradation of the resin slows down.

To conclude, both the wood and the PUF resin are thermally degraded if the modified wood is overcured. But especially during the first 52 h, the resin fraction is responsible for most of the mass loss in modified wood, where the urea fraction displays a weakness for thermal degradation. The equilibrium state which is approached after 150 h, could suggest the depletion of the urea fraction in the resin²⁷³.

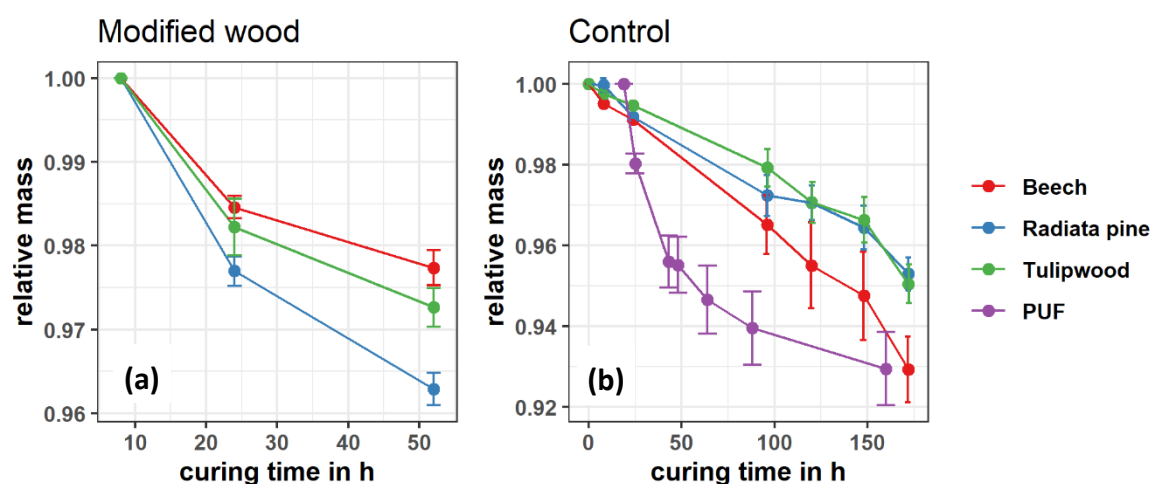


Figure 6-3 The mass relative to oven dry state decreases with curing time at 150°C. The modified wood samples (left) show different rates depending on the wood species. (right) Pure PUF resin shows a higher loss in relative mass compared to unmodified wood.

6.4.2. The Effect of Resin Concentration

The characteristics of modified wood, including WPG, BU, ASE, and biological durability, are markedly impacted by the resin concentration applied during impregnation. Grinins et al.¹¹² (2018) obtained a 30% ASE (WPG 6.6%) in birch wood using a 5% (w/w) PF resin concentration. In contrast, Franke et al.⁸⁷. (2017) achieved a substantially higher ASE of 77% (WPG 53%) in beech wood by using a much higher resin concentration of 45% (w/w)

It is worth noting that as the resin content increases, the performance of the modified wood improves, however, the product also becomes denser (see Table 6-3) and more expensive. Therefore, the resin concentration can be optimised based on performance or economic considerations, depending on the intended application. Additionally, it is important to highlight that the molecular weight and microscopic location of resin often have a more significant impact than resin concentration^{86,131}.

This section looks into the effects of resin concentration on liquid resin uptake (LU), bulking coefficient (BU), weight percentage gain (WPG), and the swelling coefficient post-modification in the first (S_{mod1}) and second soak cycle (S_{mod2}).

Table 6-3 Average values for test groups modified at the resin concentrations 20%, 30%, 40%. $\rho_{control}$ – oven dry density before modification, ρ_{mod} – oven dry density after modification, LU – liquid resin uptake before curing, WPG – weigh percentage gain after curing, BU – bulking coefficient, S_{mod1} – swelling coefficient post-modification after first soak cycle, S_{mod2} – swelling coefficient post-modification after second soak cycle. Standard deviations are in parenthesis.

Species	conc. in %	$\rho_{control}$ in g/cm ³	ρ_{mod} in g/cm ³	LU in %	WPG in %	BU in %	S_{mod1} in %	S_{mod2} in %
Beech	20%	0.73 (0.01)	0.77 (0.02)	95.9 (1.28)	15.7 (0.34)	10.15 (0.77)	12.88 (0.51)	14.02 (0.29)
	30%	0.73 (0.01)	0.82 (0.01)	96.9 (1.07)	25.2 (0.45)	11.96 (0.58)	11.56 (0.51)	13.86 (0.33)
	40%	0.74 (0.01)	0.84 (0.02)	98.4 (2.18)	29.2 (1.07)	12.71 (0.65)	11.20 (0.40)	12.91 (0.47)
	0%	0.73 (0.01)	-	-	-	-	23.65 (0.53)	24.32 (0.67)
Radiata pine	20%	0.41 (0.00)	0.53 (0.00)	223.5 (1.66)	39.7 (0.27)	7.38 (0.45)	6.07 (0.16)	6.48 (0.30)
	30%	0.41 (0.01)	0.61 (0.01)	227.8 (1.76)	62.8 (0.29)	8.97 (1.97)	5.24 (0.27)	6.91 (0.36)
	40%	0.41 (0.01)	0.68 (0.01)	230.7 (2.81)	78.7 (1.15)	7.01 (0.47)	6.08 (0.55)	7.91 (0.48)
	0%	0.41 (0.01)	-	-	-	-	11.62 (0.56)	10.11 (0.72)
Tulip wood	20%	0.53 (0.02)	0.61 (0.02)	133.6 (15.90)	24.1 (2.81)	9.23 (1.29)	8.73 (0.73)	10.41 (0.69)
	30%	0.52 (0.02)	0.66 (0.01)	152.2 (10.81)	40.0 (2.36)	10.09 (0.78)	8.14 (0.48)	10.05 (0.53)
	40%	0.52 (0.01)	0.71 (0.01)	152.2 (8.97)	51.9 (3.22)	10.10 (0.85)	8.28 (0.35)	9.89 (0.27)
	0%	0.52 (0.02)	-	-	-	-	18.09 (1.01)	16.33 (1.23)

Table 6-3 presents the key modification results for beech, Radiata pine, and tulipwood when treated with PUF resin at concentrations of 20%, 30%, and 40% (w/w). All specimens involved in this experiment underwent a curing time of 52 h. The average LU ranged from 95.9% to 98.4% in beech, 223.5% to 230.7% in Radiata pine, and 133.6% to 152.2% in tulipwood. The respective differences between the groups treated with 20% and 40% concentration were 2.5%, 7.2%, and 18.6%.

The differences in WPG are even more pronounced in all three timbers. Between 20% and 40% resin concentration, the WPG increased from 15.7% to 29.2% in beech, from 39.7% to 78.7% in Radiata pine, and from 24.1% to 51.9% in tulipwood. Thus, the WPG approximately doubled in all three species. Since the WPG increased drastically and the BU changed only slightly in comparison, the modified wood becomes notably denser with increasing resin concentration.

Interesting trends between the three species were observed for BU, S_{mod1} , and S_{mod2} . Evidently, these trends are more species dependent. The BU of beech increases gradually with each step in the resin solids content. The differences are statistically significant for each level as shown by Tukey tests in Appendix 24. For Radiata pine, the BU increases from 20% to 30%, but declines significantly from 30% to 40%. For tulipwood, the BU increases significantly from 20% to 30% but remains unaffected by the step from 30% to 40%.

Trends observed for the swelling coefficients S_{mod1} and S_{mod2} are similarly inconsistent across different timbers. For beech, S_{mod2} decreases significantly with each resin concentration. For Radiata pine, S_{mod2} increases with each increment of resin concentration. For tulipwood, S_{mod2} significantly decreased from 20% to 30%, but shows no difference from 30% to 40%. Results of the according Tukey test are provided in Appendix 25.

One possible explanation for these observations is that every wood species has an optimum resin concentration at which the cell wall is saturated, and no further improvement can be made with a higher concentration (see Figure 6-4). Micrographs in Chapter 5.4.2.1. have shown extensive resin deposits in the lumen of Radiata pine and tulipwood, treated with a 30% (w/w) concentration. Beech treated at the same concentration showed notably fewer deposits in the lumens. Hence, the optimum resin concentration in Chapter 5 might have already been surpassed for Radiata pine and tulipwood, but not for beech.

Radiata pine, on the other hand, not only exhibits minimal improvement at higher resin concentrations but, in fact, its properties deteriorate at elevated concentrations. Similar trends have been documented in the literature for low-density wood species. Tanaka et al.⁸⁸ (2016) observed that hinoki wood with a oven dry density of 0.289 g/cm³, treated with polyethylene glycol (PEG), reached a concentration optimum at 20% (w/w), resulting in the maximum BU. At higher concentrations, polymer mobility decreased, and there was less solvent water available to swell the micropore network. Consequently, the excess amount of PEG polymer could not be accommodated in the cell wall.

The observed trends in S_{mod2} among different species suggest that the optimum resin concentration for a species is influenced by its density. Given that Radiata pine, with the lowest density, experiences deteriorating properties at higher resin concentrations, it probably has a lower optimum resin concentration. In contrast, beech, with the highest density, shows improved properties at higher concentrations, suggesting its saturation point may lay at even higher resin concentrations. If this explanation holds true, a more universal relationship between performance and resin concentration may exist. The varying trends in the three timbers could represent different segments of this relationship, illustrated in Figure 6-4.

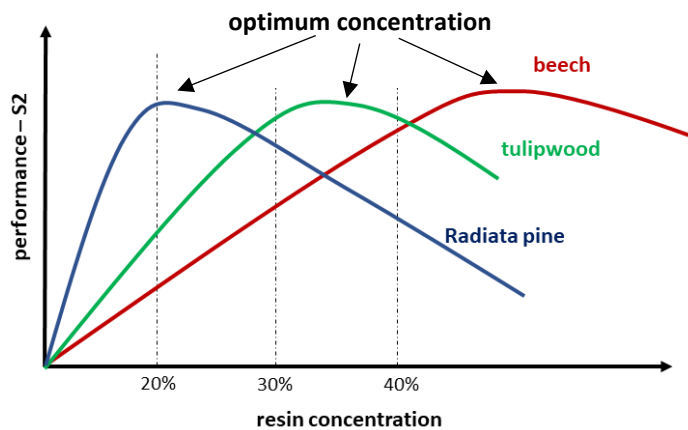


Figure 6-4 A potential general relationship may exist between the performance of timber (e.g., BU, S_{mod1} , S_{mod2}) and resin concentration. The findings in this chapter indicate that various wood species exhibit distinct optimum concentrations, beyond which properties do not further improve and instead deteriorate. This optimum concentration might be linked to the density of a wood species and the saturation point of the cell wall.

Figure 6-5 shows the water uptake for all resin concentrations and species during the second soak cycle. Evidently, the water uptake decreases with the resin concentration in all species, hence, less water can be accommodated in the macroscopic wood structure. Presumably, this occurs mainly due to resin deposits in the lumens rather than in the cell walls.

The decreasing water uptake is especially interesting in relation to the different species trends observed for BU, S_{mod1} , and S_{mod2} . In beech wood, the swelling coefficient S_{mod2} decreases along with the water uptake, as would normally be expected. In the case of Radiata pine, where the water uptake decreases even though S_{mod2} increases with the concentration, it is evident that less water is present, but it swells the cell wall to a greater extent. This example shows once again that it is important to differentiate between bulk structure and microstructure of modified wood.

In Radiata pine samples treated with a 40% resin concentration, it seems that resin deposits block many macropores (lumens), reducing the capacity for gravimetric water uptake compared to samples treated with lower resin concentrations.

Conversely, the micropores within the cell wall, expanding upon water swelling, absorb more water in Radiata pine samples treated with 40% resin than in samples treated at lower concentrations, resulting in a higher swelling coefficient at higher concentrations.

Possibly this was the case for Radiata pine because resin cell wall diffusion was promoted more at lower resin concentrations than at higher concentrations. At 20% solids content, there are fewer resin deposits in the lumen, which could explain the higher water uptake in Figure 6-5. However, resin deposits in the cell wall are increased, explaining the higher BU and lower S_{mod2} compared to 40% resin solids content. To validate this assumption, porosity measurements would be required.

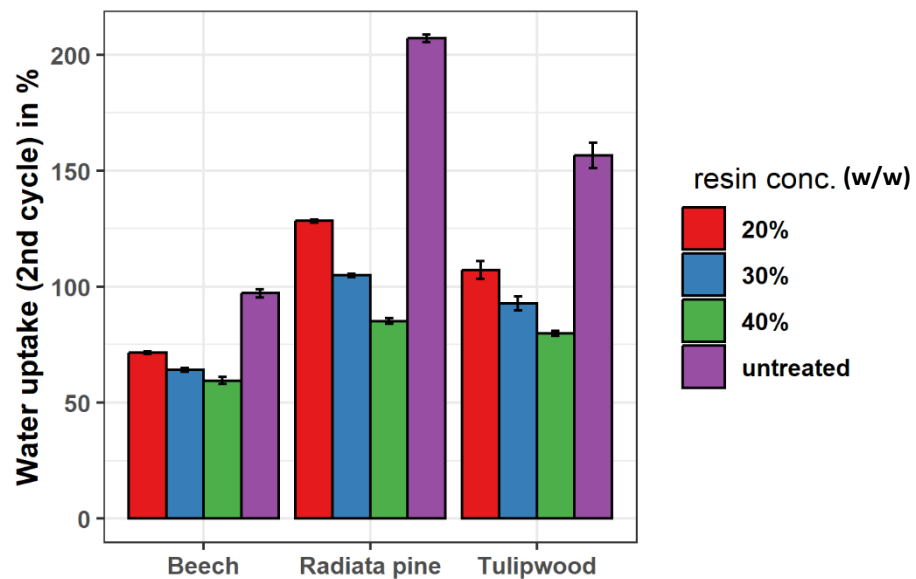


Figure 6-5 The gravimetric water uptake in the second soak cycle of ASE tests. The water uptake decreases with a higher resin concentration in all samples.

6.4.3. Multivariate Analysis of FTIR Spectra – Predicting the WPG with a PLS Model

The WPG is an important measure of quality control in wood modification. It describes the resin uptake from a dry unmodified to a dry modified state. While the dry unmodified weight can easily be measured in small laboratory specimens, it is often a unknown variable in the scaled-up process⁹⁴. Hence, it is desirable to find other forms of quality control alongside the gravimetric method.

FTIR-ATR spectroscopy in combination with a partial least square (PLS) model could be used to predict the WPG of modified wood with minimal sample preparation and is therefore a suitable candidate technique¹³². To clarify, this is after the PLS models has been established. It can be relatively effortful the to train and validate such a model with sufficient accuracy. But once this step was successful, the WPG of sample can be estimated instantly.

Using hyperspectral imaging, the WPG of resin modified wood was even estimated with a spatial dimension, showing the resin distribution in planks of wet cured and dry cured timbers⁹⁹. In Chapter 5.4.1, the FTIR spectra in reflectance mode were analysed by a principal component analysis (PCA) to show qualitative differences between modified and unmodified wood with reasonable accuracy. The quantitative analysis in the PLS model requires FTIR spectra in absorbance mode.

The results of the PLS analysis for modified beech and Radiata pine are illustrated in Figure 6-6 (a-d). Figure 6-6 (b, d) show the FTIR spectra of the training sets, hence, Radiata pine and beech samples treated with resin concentrations

between 10 – 50%. Figure 6 (a, c) shows how the predicted WPG compares against the gravimetrically measured WPG. The correlations in both Radiata pine ($R^2 = 0.99$) and beech ($R^2 = 1$) are very high, which means that the model predicts the WPG with good accuracy.

It is noted here that the offset and incline of the linear regression line in Figure 6-6 (a, c) were initially different and had to be adjusted to obtain a regression line in the approximate form of $y = x$. The R^2 value was not affected by this conversion. In conclusion, FTIR-ATR spectroscopy in combination with a PLS model can be used to predict the WPG in PUF modified wood with high accuracy.

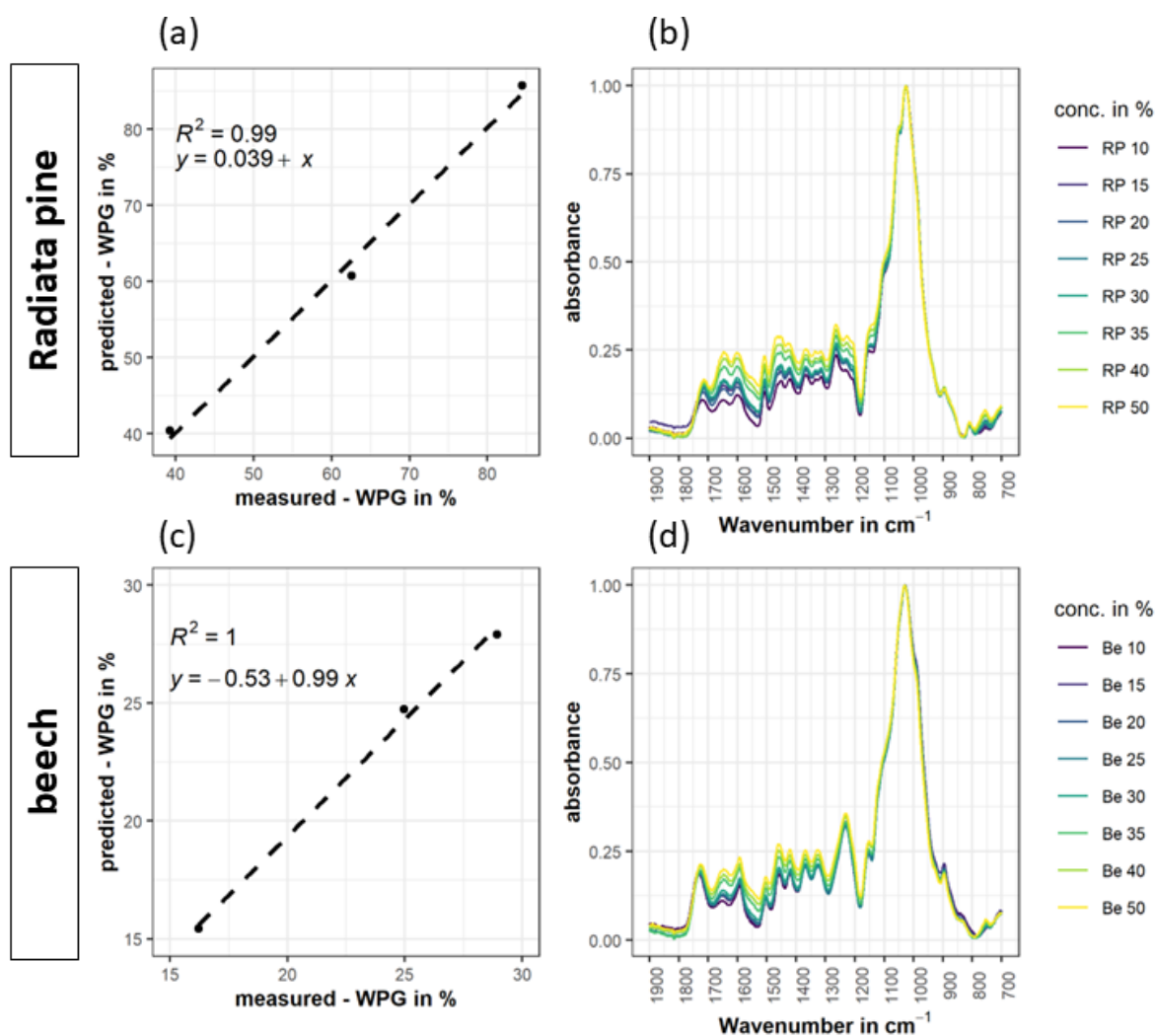


Figure 6-6 Partial least square (PLS) model that predicts the WPG from the FTIR-ATR spectra of Radiata pine and beech wood with high accuracy. (a) and (c) show the comparison of predicted and gravimetrically measured WPG values. (b) and (d) show the spectra of corresponding training sets at different resin concentrations.

6.4.4. The Effect of Resin Alkalinity

The alkalinity of the resin is another factor that probably influences the properties of modified wood during and after the treatment. Furuno et al.⁸⁶ (2004) compared the performance of neutral and alkaline PF resins in pure culture fungal decay tests. At low resin uptake, the neutral resin provided less protection against decay than the alkaline one. At higher resin uptake, the difference between neutral and alkaline resin ceased to be an issue. Additionally, the effects of different resin pH values have been demonstrated several times in this thesis.

Differential scanning calorimetry (DSC) results in Chapter 4.4.1. have shown that the curing rate of the resin depends on its pH value. Moreover, the impacts of neutralisation between alkaline resin and acidic wood substrate, along with

effects related to cell wall degradation on the ASE, have been discussed in Chapter 5.4.4. This experiment investigates the role of resin alkalinity on the liquid resin uptake (LU), weight percentage gain (WPG), bulking coefficient (BU), swelling coefficient post-modification S_{mod1} , and the total mass loss after three cycles of soaking (ML_{total}).

Table 6-4 shows the main modification results for tulipwood, beech, Radiata pine, and SYP treated with PUF resin at pH 9.17, pH 9.45, and pH 9.87. Comparing the density before modification ($\rho_{control}$) with the density post-modification (ρ_{mod}) shows species related trends. In tulipwood the density increases from 0.45 g/cm³ in the unmodified state to 0.55 g/cm³ after modification. In beech, the density increases slightly from 0.73 g/cm³ to 0.74 – 0.75 g/cm³. As previously shown in Chapter 5.4.2.1, the density changes less in the high-density species like beech. In Radiata pine, the density increases from 0.44 – 0.45 g/cm³ to 0.61 g/cm³. For SYP, the increase from the unmodified state at 0.63 – 0.64 g/cm³ to the modified state varies according to the resin pH between 0.71 – 0.74 g/cm³.

Table 6-4 Average values for test groups modified at the resin pH 9.16, pH 9.45, pH 9.87. $\rho_{control}$ – oven dry density before modification, ρ_{mod} – oven dry density after modification, LU – liquid resin uptake before curing, WPG – weigh percentage gain after curing, BU – bulking coefficient, S_{mod1} – swelling coefficient post-modification after first soak cycle, S_{mod2} – swelling coefficient post-modification after second soak cycle. ML_{total} – total mass loss over three cycles of water soaking. Standard deviations are in parenthesis.

Species	pH	$\rho_{control}$ in g/cm ³	ρ_{mod} in g/cm ³	LU in %	WPG in %	BU in %	S_{mod1} in %	S_{mod2} in %	ML_{total} in %
Tulip wood	9.16	0.45 (0.01)	0.55 (0.01)	184.8 (3.89)	47.8 (1.04)	10.24 (0.34)	6.11 (0.40)	7.35 (0.24)	2.40 (0.16)
	9.45	0.45 (0.01)	0.55 (0.01)	190.9 (3.26)	49.4 (2.74)	10.47 (0.64)	6.28 (0.53)	7.39 (0.26)	2.85 (1.22)
	9.87	0.45 (0.01)	0.55 (0.01)	190.6 (3.63)	47.2 (1.35)	10.18 (0.36)	6.96 (0.23)	8.05 (0.32)	3.99 (0.10)
Beech	9.16	0.73 (0.01)	0.74 (0.01)	103.9 (0.85)	25.9 (1.47)	18.50 (0.81)	9.42 (0.87)	10.21 (0.52)	1.07 (1.08)
	9.45	0.73 (0.01)	0.74 (0.01)	99.5 (1.64)	24.5 (0.41)	17.70 (0.69)	10.42 (0.44)	11.10 (0.30)	1.83 (0.10)
	9.87	0.73 (0.00)	0.75 (0.01)	98.9 (2.28)	24.0 (0.60)	16.46 (0.55)	11.39 (0.35)	12.16 (0.40)	2.76 (0.07)
Radiata pine	9.16	0.44 (0.01)	0.61 (0.01)	201.0 (3.32)	53.8 (1.19)	8.90 (0.43)	5.75 (0.17)	6.86 (0.18)	2.08 (0.33)
	9.45	0.45 (0.01)	0.61 (0.01)	199.2 (3.35)	51.8 (0.86)	8.29 (0.32)	6.19 (0.68)	7.01 (0.24)	2.47 (0.14)
	9.87	0.45 (0.01)	0.61 (0.01)	196.4 (4.89)	50.5 (2.03)	8.21 (0.33)	6.27 (0.21)	8.18 (0.25)	4.13 (0.80)
SYP	9.16	0.64 (0.01)	0.71 (0.01)	124.1 (3.59)	31.1 (0.96)	10.46 (0.38)	8.08 (0.52)	8.89 (0.60)	1.44 (0.07)
	9.45	0.63 (0.02)	0.72 (0.01)	127.8 (4.11)	31.8 (1.10)	10.07 (0.43)	8.30 (0.53)	9.38 (0.50)	1.62 (0.06)
	9.87	0.63 (0.02)	0.74 (0.01)	129.6 (5.89)	32.0 (2.93)	9.45 (0.49)	8.81 (0.39)	10.40 (0.47)	2.46 (0.16)

The trends within LU and WPG also vary between different species. Tulipwood shows a LU of 184.8% and WPG of 47.8% at pH 9.16. At pH 9.45, the LU and WPG show their highest values with 190.9% and 49.4%, respectively, followed by a slight decrease at pH 9.87. Beech and Radiata pine show decreasing values for both LU and WPG as the pH increases from 9.16 to 9.87. In contrast, Radiata pine displays slightly increasing values for LU and WPG.

While there could be a connection between these trends and the chemical properties of the timbers, it should be noted that the observed differences are relatively small in relation to the standard deviations shown in Table 6-4. Therefore, it is assumed that variations in LU and WPG are caused by data variability rather than by pH-related effects.

Regardless of the variable WPG, all timbers in Table 6-4 show a common trend for the BU, S_{mod1} , S_{mod2} , and ML_{total} . That is, the BU decreases in most cases significantly with an increasing resin pH value (Appendix 26), and most values of S_{mod1} and S_{mod2} increase significantly with higher resin alkalinity (Appendix 27). Additionally, ML_{total} increases significantly with each increment of the resin pH value (Appendix 28) and is higher in timbers tulipwood and Radiata pine, which also have a high WPG, compared to beech and SYP. The deteriorating properties at higher resin pH could be a result of increasingly severe cell wall degradation, which counterbalances the cell wall bulking effect.

6.4.5. The Effect of Cell Wall Diffusion

In section 6.1, the concept of cell wall diffusion was delineated, and it was described how process conditions in the diffusion and drying stage between impregnation and curing, such as the relative humidity (RH), and the temperature, have impacted on the BU in polyethylene glycol (PEG) modified wood in the studies of Tanaka et al.⁸⁸⁻⁹¹. The experiment in this section explores similar process conditions, aiming to verify their effect on cell wall diffusion in the slightly different modification process using PUF resin. The main difference between the two processes is the presence of heat curing step in PUF resin modification as well as chemical differences between both bulking agents, i.e., PUF and PEG.

Table 6-5 presents the primary outcomes of the modifications observed in tulipwood treated with PUF resin. The wood underwent drying through nine distinct schedules, as detailed in the Table. The control group in Table 6-5 was treated following the standard procedure outlined in Chapter 5.3.6, without a distinct diffusion step. In other words, after impregnation, the controls were directly dried in an oven at 50°C with close to 0% RH.

Table 6-5 Process conditions used and average values for test groups modified with different drying schedules in a half-factorial design to study cell wall diffusion. RH_{diff} – relative humidity in the separate diffusion step, RH_{dry} – relative humidity in the drying step at 50°C, t – time of the separate diffusion step, T_{diff} – Temperature in the separate diffusion step, $\rho_{control}$ – oven dry density before modification, ρ_{mod} – oven dry density after modification, LU – liquid resin uptake before curing, WPG – weigh percentage gain after curing, BU – bulking coefficient, S_{mod1} – swelling coefficient post-modification after first soak cycle, S_{mod2} – swelling coefficient post-modification after second soak cycle. Standard deviations are in parenthesis.

Test Group	RH_{diff} in %	RH_{dry} in %	t in days	T_{diff} in °C	$\rho_{control}$ in g/cm ³	ρ_{mod} in g/cm ³	LU in %	WPG in %	BU in %	S_{mod1} in %	S_{mod2} in %
Control	-	-	-	-	0.46 (0.02)	0.59 (0.01)	163.5 (13.1)	49.4 (4.13)	10.43 (0.37)	6.20 (0.41)	7.70 (0.31)
A	7	7	1	30	0.46 (0.01)	0.59 (0.01)	169.9 (5.6)	50.7 (2.08)	11.28 (0.37)	5.79 (0.24)	7.43 (0.28)
B	75	7	1	4	0.45 (0.02)	0.59 (0.01)	169.9 (9.4)	50.2 (4.06)	10.45 (0.37)	5.72 (0.32)	7.60 (0.86)
C	7	33	1	4	0.45 (0.01)	0.58 (0.01)	165.9 (4.7)	49.4 (4.87)	11.81 (1.46)	5.45 (0.31)	7.12 (0.60)
D	7	33	7	30	0.45 (0.01)	0.59 (0.01)	172.0 (5.3)	51.5 (1.99)	11.18 (0.53)	5.58 (0.31)	7.34 (0.27)
E	7	7	7	4	0.46 (0.01)	0.59 (0.01)	165.1 (9.9)	49.3 (3.29)	9.80 (0.35)	6.55 (0.31)	8.20 (0.18)
F	75	33	1	30	0.46 (0.00)	0.59 (0.01)	174.4 (4.4)	52.2 (1.58)	11.93 (0.78)	4.99 (0.87)	7.15 (0.35)
G	75	7	7	30	0.46 (0.01)	0.60 (0.01)	165.3 (5.1)	53.5 (3.09)	11.47 (0.46)	5.65 (0.23)	7.94 (0.74)
H	75	33	7	8	0.45 (0.01)	0.60 (0.01)	173.6 (3.9)	53.0 (1.37)	11.45 (0.59)	5.52 (0.25)	7.10 (0.36)

The density in Table 6-5 exhibits a relatively homogeneous change from 0.45 – 0.46 g/cm³ before treatment increasing to 0.58 – 0.60 g/cm³ after the process. All other properties vary between the nine test groups. The LU ranges between 163.5 – 174.4%, the WPG between 49.3 – 53.5%, the BU between 9.80 – 11.93%, S_{mod1} between 4.99 – 6.55%, and S_{mod2} between 7.12 – 8.20%. The observed range in the parameters LU and WPG results from data variation, possibly caused by the anisotropy of wood, leading to different resin uptakes during impregnation and unintentional variations across different batches. The drying conditions should not affect the two parameters LU and WPG because there was no difference in the impregnation procedure.

The variations in BU, S_{mod1} , and S_{mod2} arise from differences in both resin uptake and in cell wall diffusion, which was either promoted for restricted by the applied process conditions in the different drying schedules of each test group. In a typical half-factorial design of experiments, one can calculate the individual effects of each process condition. However, this is ideally done when the experimental framework conditions remain constant. Given the observed range in LU and WPG, this ideal scenario does not hold true. Consequently, the parameters must be factored into the effect calculation, considering the broader experimental context.

Generally, the results obtained for BU and $S_{\text{mod}2}$ exhibit greater variability between test groups than within each test group, as indicated by the one-way ANOVA tests in Appendices 29 and 30. Tukey tests in Appendices 31 and 32 reveal which test groups significantly differ from each other. The more interesting questions revolve around the origins of these differences, specifically whether they stem from cell wall diffusion, and if so, identifying the responsible factors. Therefore, one should compare test groups A to H with the control in Table 6-5.

The control group exhibits a BU of 10.43%, $S_{\text{mod}1}$ of 6.20%, and $S_{\text{mod}2}$ of 7.70%. In most test groups that included a separate diffusion phase, performance surpasses that of the control, except for group E. Their values (excluding group E) ranged between 10.45 – 11.93% for BU, 4.99 – 5.79% for $S_{\text{mod}1}$, and 7.10 – 7.94% for $S_{\text{mod}2}$. The least favourable were observed in test group E, recording a BU of 9.80%, $S_{\text{mod}1}$ of 6.55%, and $S_{\text{mod}2}$ of 8.20%. This comparison implies that, overall, the diffusion phase has a beneficial effect (excluding test group E) when compared to the control group.

Among test groups A – H, the most favourable results were observed in group F, showing a BU of 11.93%, $S_{\text{mod}1}$ of 4.55%, and $S_{\text{mod}2}$ of 7.15%. This represents a considerable difference compared to the outcomes in test group E and the control. Notably, test group F was subjected to process conditions that were expected to promote cell wall diffusion, including high RH_{diff} , RH_{dry} , and T_{diff} . Conversely, the process conditions applied in test group E were expected to restrict cell wall diffusion, including a low high RH_{diff} , RH_{dry} , and T_{diff} . Hence, it is evident that the investigated process conditions in this experiment can influence cell wall diffusion and, consequently, the properties of the modified wood.

However, drawing definitive conclusions is difficult as both the control and test group E exhibit a relatively low resin uptake, with 49.3% and 49.4% WPG, respectively, in contrast to the 52.2% WPG in test group F. This introduces uncertainty regarding the impact of different WPGs. Although it should be noted that test group C, subjected to a high RH_{dry} in the drying step, demonstrates superior results compared to the control and test group E, despite having a similarly low WPG of 49.4%. Nevertheless, a comprehensive assessment of individual test groups is hindered by the half-factorial experiment design.

The problem with this conclusion is that both the control and test group E display also a relatively low resin uptake with 49.3% and 49.4% WPG compared to 52.2% WPG in test group F. Hence, an uncertainty about the influence of different WPGs remains. Although it should be noted that test group C, where cell wall diffusion is promoted through a high RH_{dry} in the drying step, displays superior results compared to the control and test group E, despite having a similarly low WPG of 49.4%. Nevertheless, the comparison of individual test groups may be insufficient due to the limitations of the half-factorial experiment design.

Therefore, all test groups were simultaneously considered in calculating the statistical effect of each factor (RH_{diff} , RH_{dry} , $\text{time}_{\text{diff}}$, and T_{diff}). Figure 6-7 illustrates the statistical effect of these factors on WPG, BU, $S_{\text{mod}1}$, and $S_{\text{mod}2}$. As mentioned before, the WPG shows some variability between test groups, although it cannot be influenced by cell wall diffusion. Nevertheless, the WPG is included in Figure 6-7 to demonstrate the apparent effect that the four factors have on it. In other words, the WPG is included to show which of the factors in the diffusion stage are most likely to have been distorted by differences in the WPG.

Evidently, the RH in the diffusion stage (RH_{diff}) has the highest apparent effect (2.03%) on the WPG and the RH during the drying step (RH_{dry}) has the lowest (0.62%). This means that the effect of RH_{diff} on BU, $S_{\text{mod}1}$, and $S_{\text{mod}2}$ is overestimated, because test groups with a high RH_{diff} also have a 2.03% higher WPG on average. The effect of the RH_{dry}

is also slightly overestimated, because groups with a high RH_{dry} have a 0.62% higher WPG. Hence, both factors are unintentionally influenced by differences in WPG, but in RH_{dry} this contribution is reasonably small.

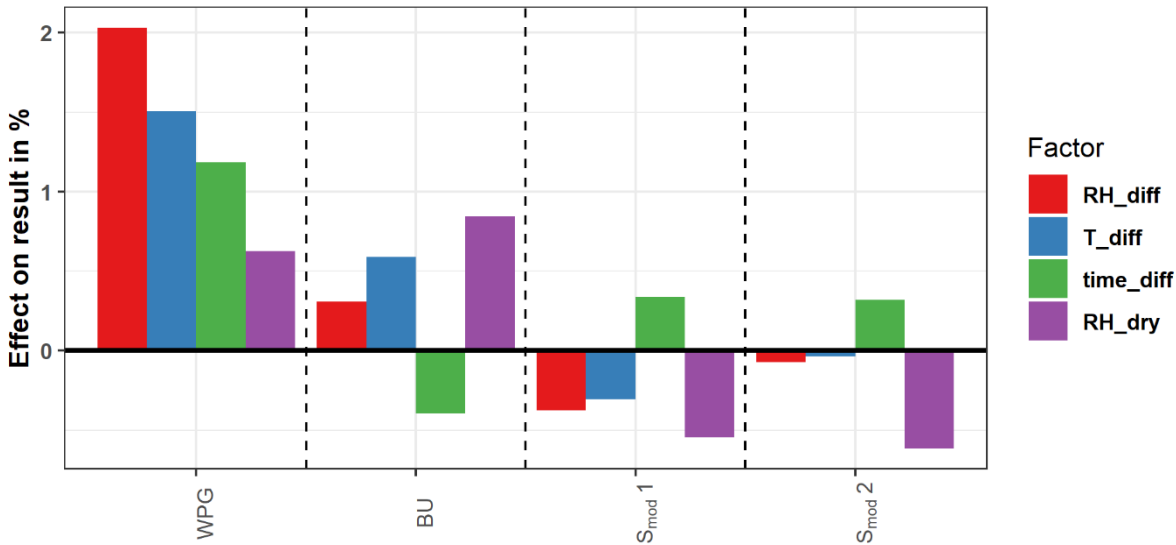


Figure 6-7 The statistical effect of four investigated factors (RH_{diff} , RH_{dry} , $time_{diff}$, and T_{diff}) on the results from ASE tests (BU , S_{mod1} , and S_{mod2}). The apparent effect on the WPG is included to show how much each factor might be influenced by differences in the WPG between test groups.

While RH_{dry} is not as significantly influenced by variations in WPG compared to the other three factors, it exhibits the most pronounced effect on BU , S_{mod1} , and S_{mod2} in Figure 6-7. Specifically, test groups with a RH_{dry} of 33% show, on average, a 0.84% higher BU , a 0.55% lower S_{mod1} , and a 0.61% lower S_{mod2} compared to test groups with RH_{dry} set to 7%. The factors RH_{diff} and T_{diff} also exert a beneficial effect on the results of BU , S_{mod1} , and S_{mod2} when set to the high level. Test groups where RH_{diff} was set to 75% display a 0.31% higher BU , a 0.37% lower S_{mod1} , and a 0.07% lower S_{mod2} , compared to test groups where RH_{diff} was set to 33%. Test groups where the temperature during diffusion was set to 30°C display a 0.59% higher BU , a 0.31% lower S_{mod1} , and a 0.04% lower S_{mod2} compared to test groups where T_{diff} was set to 4°C. However, it is important to note that both factors may be influenced by differences in the WPG and their effect on S_{mod2} is close to zero. Consequently, the role of RH_{diff} and T_{diff} remains inconclusive.

A longer diffusion time ($time_{diff}$) appears to have adverse effects on BU , S_{mod1} , and S_{mod2} in the observed small specimens. Test groups subjected to 7-day diffusion time exhibit a 0.40% lower BU , 0.34% higher S_{mod1} , and 0.32% higher S_{mod2} compared to test groups with a diffusion time of 1 day. Additionally, this is observed despite the fact that test groups with longer diffusion time also display a 1.50% higher WPG. Hence, the adverse effect of a long diffusion time can be confirmed for this experiment, although the small sample size should be emphasised. Larger specimens might benefit from longer diffusion periods.

In conclusion, implementing a separate diffusion phase appears to yield beneficial effects compared to the standard procedure described in Chapter 5.3.6, where samples were directly dried after impregnation. Among the investigated factors, the RH_{dry} used in the in the drying step at 50°C seems the key variable. Drying the samples with a high RH_{dry} at this temperature produced the most favourable results for BU , S_{mod1} , and S_{mod2} . On the other hand, RH_{diff} and T_{diff} used during the separate diffusion step, preceding the temperature increase to 50°C, seem to have minor effects. A longer diffusion time showed adverse effects on BU , S_{mod1} , and S_{mod2} . Unintentional variations in the WPG of test groups posed a challenge in the analysis of the half-factorial experiment but were adequately considered.

6.5. Conclusions from Chapter 6

This Chapter investigated the influence of various process conditions in the modification process, using ASE tests as the primary means of quality control. Additionally, the concept of resin cell wall diffusion in a separate process step was introduced. The results in this chapter have shown that:

- The BU and WPG of modified wood decrease due to overcuring between 8 – 52 h. This is caused by the thermal degradation of the resin, and potentially by the hydrolysis of urea entities in the PUF resin.
- Increasing the resin concentration between 20% and 40% (w/w) had a notably positive effect in beech, minimal impact on tulipwood, and partially negative effects in Radiata pine. This implies the presence of distinct optima for resin concentration in different types of timber.
- FTIR-ATR spectroscopy in combination with PLS modelling was demonstrated as a technique to predict the WPG of resin modified wood – suitable for commercial situations where the initial dry weight data are unavailable.
- Increasing the alkalinity of resin from pH 9.16 to pH 9.87 led to adverse effects in all observed timbers, indicating that cell wall degradation is the responsible mechanism in this context.
- A separate diffusion phase after the impregnation step promotes cell wall diffusion and has overall positive effects on BU, $S_{\text{mod}1}$, and $S_{\text{mod}2}$. The most favourable results, characterised by the highest bulking and lowest swelling, were achieved when the relative humidity (RH) remained high as the temperature increased during the wood drying process.

7. Chemical Interactions between Wood and Phenol Urea Formaldehyde resin

7.1. Introduction to Chapter 7

So far, this thesis has focussed on the anti-swelling efficiency (ASE) of resin modified wood, both to compare different treatments and as a tool to interpret the underlying modification mechanisms. The extent to which this method can be used to study the modification mechanisms, however, is limited and further ways of studying these phenomena are required.

The analysis of ASE and complimentary techniques used in the Chapters 5 and 6 strongly suggested that chemical interactions between the resin fraction and the wood play an integral role in the dimensional stabilisation of modified wood. This became evident in Chapter 5.4.2 when the ASE of 11 wood species varied considerably between 44% in poplar and 69% in lime wood and non-chemical parameters such as wood density or gravimetric resin uptake could not fully explain the results. FTIR and NMR analysis of the soaking solution subsequently revealed that hemicelluloses undergo deacetylation during modification and leach in the form of potassium acetate salts after the samples are soaked in water (see sections 5.4.1 and 5.4.3.1). This suggests that cell wall degradation could be a relevant chemical interaction.

Chapter 5.4.4 further demonstrated a positive correlation between the hemicellulose content and the ASE of a wood species, implying some form of covalent or non-covalent interaction with the resin. Yet another form of chemical interaction was suggested by the differential scanning calorimetry (DSC) scans of neat resin in Chapter 4.4.1, where it was shown that neutralisation of the alkaline resin catalyst retards the curing reaction substantially. Given that wood is a mildly acidic material, it is likely that a neutralisation reaction with the resin takes place during the modification.

Those chemical interactions, i.e., cell wall degradation, neutralisation, covalent bonding, are summarised in Table 7-1. In the context of this discussion, neutralisation refers to the consumption of the resin's alkaline catalyst by acidic extractives, the degradation of hemicelluloses through deacetylation and peeling, or interactions with other wood constituents. As the pH value of the curing system decreases, the crosslinking reactions proceed at a lower rate, ultimately resulting in a lower crosslinking density^{190, 212, 214}. A well-known consequence of this neutralisation is the poor bond performance of acidic timbers (e.g., oak, chestnut, birch) bonded with alkaline adhesive^{173, 215, 275}. In the previously cited studies, the neutralisation effect was ascribed to high contents of water-soluble extractives, especially if heartwood was present.

The alkaline buffer capacity (ABC) results from Chapter 3.4.3.1 can be used to compare the effect of different extractives on the curing reaction. It is noted, however, that non-polar extractives such as fatty acids and resin acids as well as neutralisation via hemicellulose degradation are not fully considered in a water extract^{225, 229}. Therefore, solvent extractives and isolated wood polymers are assessed separately.

To establish the effect of both solid wood and individual wood constituents (e.g., extractives, hemicellulose, lignin) on the resin curing reaction, those constituents were mixed with the resin and analysed in DSC scans. Similar to the approach in Chapter 4.4.1, this allows for a comparison of the reactivity of different mixtures. The results from Chapter 4.4.1 serve as a baseline for the neat resin.

In the past, DSC has been used frequently to investigate the effect of extractives^{214,276}, solid wood^{190,212,213}, and wood constituents²¹⁶ on the resin curing kinetics. However, it is often difficult to isolate the individual contributions of different constituents.

Table 7-1 Review of possible chemical interactions between phenol urea formaldehyde resin and wood.

Chemical Interaction	Concept and Description
Neutralisation of the resin	<p>General effect of wood on the resin curing kinetics.</p> <ul style="list-style-type: none"> the consumption of alkali lowers the reactivity of the resin leading to a lower resin curing rate and a lower degree of crosslinking^{190,213} interactions with wood that may consume alkali include those with acidic wood extractives (both water-soluble and solvent extractives), deacetylation of hemicelluloses, and peeling of hemicelluloses, cleavage of lignin^{214,275}
Cell wall degradation	<p>A destructive effect on the cell wall ultrastructure.</p> <ul style="list-style-type: none"> can be caused by the combination of resin, alkali, and elevated temperatures²⁷⁷ cell wall degradation is prominent in the hemicellulose fraction and occurs to a lesser extent in the lignin fraction^{96,198}.
Covalent bonding	<p>The formation of covalent bonds between resin and wood, specifically exploring the possibilities of methylene bridge formation with lignin and ester link formation with hemicellulose.</p> <ul style="list-style-type: none"> PF resin and guaiacyl (G) lignin can condense via methylene bridges¹⁹⁸. hydroxymethylated resorcinol resin and hemicelluloses can form ester linkages²⁷⁸.

**Note: While there is overlap and interplay between neutralisation of resin and cell-wall degradation, it is helpful to consider them separately on the basis of the effect they have on the component, i.e., the resin and the cell wall.*

Covalent bonds between PUF resin and wood might form at low abundance. One likely reaction site in wood is the unsubstituted G₅-position in guaiacyl (G) lignin where methylene bridges could be formed with the resin¹⁹⁸. Another possibility for covalent bonding is an esterification reaction between wood carboxylic acids and resin hydroxymethyl group²⁷⁸.

Since these covalent bonds are rare and structurally similar to linkages that occur in native wood, a high-resolution method is required to accurately observe new covalent bonds. Two dimensional ¹H-¹³C heteronuclear single quantum coherence (HSQC) solution-state NMR in combination with cell wall solubilisation is a suitable method and has been used in the past to detect even rare covalent bonds in wood. In this method, a ball-milled wood powder is dissolved in DMSO-*d*₆, which yields a viscous gel that can be handled like a liquid in solution-state NMR^{197,279}. Since this method is semi-quantitative, it can also be used to investigate changes in the cell wall composition, which could be the results of cell wall degradation. The aim of this chapter is to investigate the previously outlined chemical interactions using DSC and solution-state NMR.

7.2. Materials

7.2.1. Wood Samples, Extractives, isolated Cell Wall Polymers, and Resin

The selected wood species and the default PUF resin used in this chapter are the same as in Chapters 3.2.1 and 4.2.1, respectively. Extractives used in this Chapter are the freeze-dried hot water extractives (ExtrW) and rotary evaporated solvent extractives (ExtrS), previously described in Chapters 3.3.3.1 and 3.3.4. Cell wall polymers (i.e., α -cellulose, holocellulose, Klason-lignin) are the samples previously described in Chapter 3.3.3. All samples were dried (either freeze drying or oven drying) before they were mixed with the resin.

7.3. Methods

7.3.1. DSC – Sample Preparation

This Chapter describes three separate DSC experiments which investigate the curing reaction in PUF resin impregnated in solid wood blocks, in PUF resin combined with ExtrW and ExtrS, and PUF resin combined with isolated cell wall polymers.

Resin in combination with wood was prepared as follows: solid wood cubes with an approximate edge length 3 mm were cut with a razor and subsequently vacuum impregnated with the PUF resin (pH 9.5, 50% w/w). Before the scan, sections were wiped with tissue to remove excess resin. The mass of the sections was noted before impregnation, before the scan, and after the scan to calculate the resin uptake.

Resin combined with extractives was tested by mixing the resin (pH 9.5, 50% w/w) with ExtrW or ExtrS in separate vials until the extractives dissolved completely. The mass of each component was noted to calculate the extractives concentration in the resin sample.



Figure 7-1 High-pressure crucible next to a one penny coin and wood section inside the pressurised crucible before it is sealed.

Resin in combination with cell wall polymers was prepared as follows: cell wall polymers were weighed in a glass vial and subsequently mixed with deionised water to measure the pH value of each component. The pH value of α -cellulose and holocellulose was in the near neutral range (pH 6.5 and pH 6.1), hence, both vials were placed in an oven set to 105°C overnight to evaporate the water. The pH value of Klason-lignin was 4.5, hence, potassium hydroxide solution (0.1 N) was added dropwise to neutralise the solution. This was done to exclude pH effects as much as possible. When the pH value reached 6.4, the lignin was decanted over Whatman filter paper and washed thoroughly with deionised water. The neutralised lignin was transferred back into the vial and dried at 105°C overnight. On the next day, the dry mass was noted, and each cell wall polymer was mixed with resin in the corresponding vial. Each sample was tested at three heating rates. The three samples were taken from the same stock.

7.3.2. DSC – Sample Collection and Analysis

The sample collection and analysis using the Kissinger method were conducted analogously to the procedures outlined in the Chapters 4.3.2 and 4.3.3.

7.3.3. Solution-State NMR – General Notes about the Sample Preparation

Solution-state NMR experiments were performed on modified and unmodified small blocks of lime and poplar wood after three cycles of water soaking. The whole cell wall dissolution of wood requires the preparation of very small particles, hence, ball milling. However, conventional stainless steel ball mills introduce paramagnetic iron particles, which interfere with the strong magnetic fields used in the NMR analysis.

A simple way to bypass this problem is to use a ball mill with a ceramic jar and ceramic balls. This step in the sample preparation was kindly done by Dr Daniel Yelle from the US Forrest Products Laboratory. Subsequently, the powder is quasi-dissolved in a solvent to yield a viscous gel that can be analysed like a liquid in solution-state NMR experiments. The details of the sample preparation are described in the following.

7.3.4. Solution-State NMR – Ball Milling

Each sample with the dimensions 20 (r) × 20 (t) × 5 (l) mm was weighed to the nearest 0.1 mg and sliced in the radial direction to give approximately 1 mm thick sections using a knife. Six 50 ml milling jars, along with several 20 mm and 10 mm balls, made from ZrO₂ were cleaned using hot water and mild detergent and finally rinsed with reverse-osmosis water. The jars and balls were dried at 50°C for approximately 2 h prior to milling. Once dry, a clean and dry rubber gasket was placed into the groove of each jar cover. Each sliced sample was placed into each 50 ml jar (with a label as to which sample is inside) followed by three 20 mm balls and secured in a *Retsch PM-400* planetary ball-mill (Newtown, PA) and milled at 300 rpm for 24 h (20 min milling, 10 min pause). Afterward, the three 20 mm balls were removed, shaken briefly in a copper sieve to recover material coating the balls, and replaced by ten 10 mm balls. Ball-milling was then continued at 300 rpm for a total of 24 h (20 min milling, 10 min pause). Following milling, the 10 mm balls were removed, shaken briefly in a copper sieve, and the milled sample scraped from the jar and weighed to the nearest 0.1 mg.

7.3.5. Solution-State NMR – Solubilisation of Wood in DMSO-d₆ and Pyridine-d₅

Approximately 30 mg of each ball milled sample was dissolved directly in 500 µl of a DMSO-d₆ and Pyridine-d₅ mixture with a ratio of 4:1 (v/v) within a 5 mm NMR tube. Pyridine-d₅ was added to disrupt hydrogen bonds and facilitate the dissolution process. Each sample was sonicated at 35°C for 1 h in an ultrasonic bath until a homogeneous gel evolved. The sample preparation is shown in Figure 7-2.

7.3.6. Solution-State NMR – Spectra Acquisition Parameters

The solution-state NMR analysis in this chapter is analogous with the method described in Chapter 3.3.6, except for the following variations. In the ¹H–¹³C HSQC NMR method, the recycle delay time D1 was reduced to 0.5 s as relaxation times are faster in the gel-state. The number of scans was increased to 150, requiring a total run time of 17 h for each specimen.

The pulse program used for ^{13}C DEPTQ NMR experiments was deptqgsp.2. The number of scans was adjusted to 20,000 with a recycle delay time D1 of 0.5 s and a scanning a range between 0 – 250 ppm. Each ^{13}C DEPTQ NMR scan required a total scanning time of 5 h. Spectra were post-processed in MestreNova, where the gaussian broadening (GB) in F2 dimension was set to 0.001 and line broadening (LB) to -0.3. The chemical shift of DMSO- d_6 was set to 2.50/39.52 ppm. For a semi-quantitative analysis of the wood polymer structures present in the spectra, specific chemical shifts were integrated and referenced to the lignin methoxy signal at 56 ppm using MestreNova software.

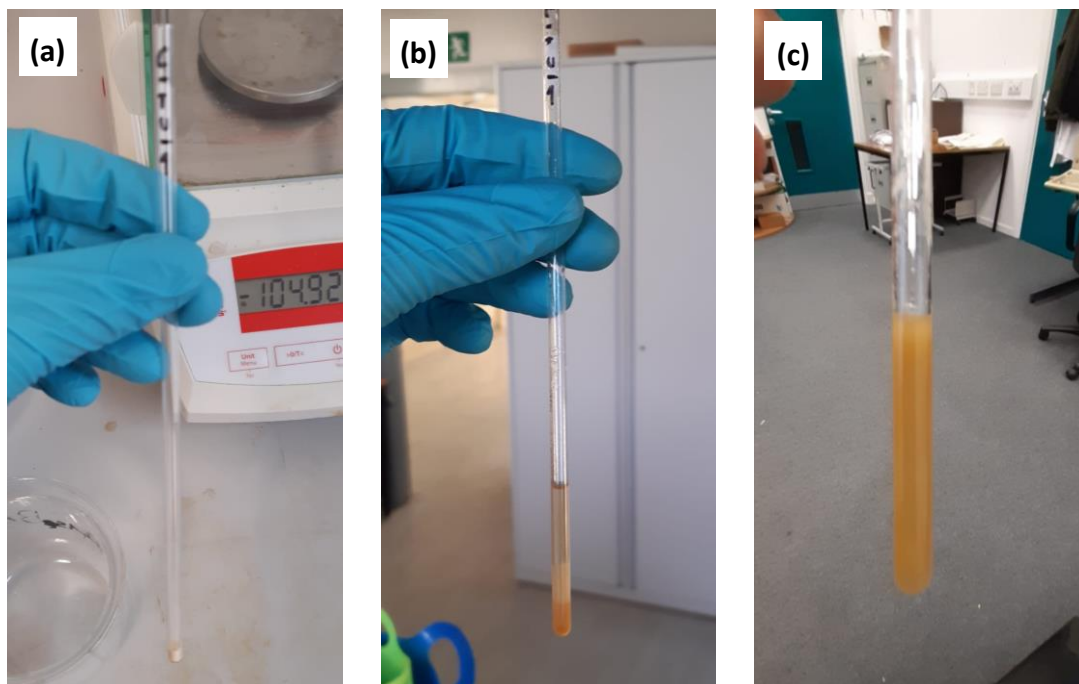


Figure 7-2 Sample preparation for solution-state NMR. (a) Ball-milled wood powder (approximately 30 mg) is filled in 5 mm NMR tube. (b) Solvent is added to the tube resulting in an inhomogeneous gel. (c) Gel is homogeneous after mechanical mixing and sonication.

7.4. Results and Discussion

7.4.1. The Curing Reaction of Resin in the Presence of Wood and Wood Constituents studied by DSC

The PUF resin achieves its maximum reaction rate within a mild alkaline range, specifically between pH 8 and 9²⁵⁸. When the PUF resin is combined with an acid or introduced into an acidic substrate, such as wood, neutralisation occurs. The impact of neutralisation on the resin curing kinetics was detailed in Chapter 4.4.1. Acidifying the resin with acetic acid to pH 6.3 significantly reduced the resin curing rate (k) from 0.56 s^{-1} to 0.21 s^{-1} – a retardation of 62%. This confirmed the assumption that neutralisation retards the curing reaction by consuming the alkali catalyst. The aim of this section is to investigate the curing reaction in the presence of wood and wood constituents, with a focus on the reaction rate (k).

Table 7-2 shows the DSC results of the resin curing reaction in the presence of solid wood of different wood species. Evidently, the curing rate (k) is significantly reduced by the presence of solid wood. Depending on the wood species and whether earlywood or latewood is considered, k ranges between $0.24 - 0.32\text{ s}^{-1}$ and is therefore 43 – 57% slower than in the neat resin. Previous studies have linked this retardation with the neutralisation of alkaline catalyst by the extractives fraction, especially in the heartwood portions of the tree^{173, 215,275,276}. However, the question remains whether the presence of extractives, which in sapwood occur in relatively low concentrations, can fully account for the retardation observed in Table 7-2.

Table 7-2 Kinetic parameters determined in differential scanning calorimetry showing the effect of the presence of solid wood on the curing reaction. The WPG varied across species due differences in the liquid uptake during impregnation.

Sample	WPG in %	T _p in °C			R ²	E _A in kJ/mol	Z in s ⁻¹	k at 150°C in s ⁻¹
		5	10	20				
Resin + tulipwood	43.68 (11.03)	146.71	159.23	171.45	0.9997	79.73	2.24E+09	0.32
Resin + RP (EW)	72.48 (12.85)	146.62	154.81	174.55	0.9706	66.65	5.05E+07	0.3
Resin + RP (LW)	28.03 (5.16)	145.67	160.66	179.08	0.9991	58.01	3.48E+06	0.24
Resin + lime	51.02 (15.04)	152.18	161.93	175.85	0.9956	85.03	8.15E+09	0.26
Resin + beech	30.60 (2.50)	150.55	161.1	177.14	0.9937	74.57	4.10E+08	0.26
Resin + poplar	56.60 (3.60)	146.26	159.92	174.73	0.9999	68.84	8.84E+07	0.28

To explore whether the presence of the water-soluble extractives, which in solid wood occur in relatively low concentrations, induces a similar retardation in the resin curing reaction, the resin was blended with freeze-dried hot-water extractives (ExtrW) of tulipwood lime, as well as with solvent extractives (ExtrS) of poplar and lime as shown in Table 7-3. Lime extractives were selected as examples for highly acidic extractives, whereas poplar and tulipwood extractives were considered less acidic (see Chapter 3.4.3.3). The combination of ExtrW from tulipwood and ExtrS from poplar was necessitated by a shortage of material, and additionally, the extractives of both species exhibit a relatively similar composition.

Table 7-3 Kinetic parameters determined in differential scanning calorimetry showing the effect of water extractives (ExtrW) and solvent extractives (ExtrS) on the curing reaction. Results for pure resin are included for better comparison (see chapter 4).

Sample	ABC in mmol* batch ⁻¹	Ex. conc. in liquid resin in %	T _p in °C			R ²	E _A in kJ/mol	Z in s ⁻¹	k at 150°C in s ⁻¹
			5	10	20				
Pure resin (pH 9.5)	-	-	136.52	148.94	160.96	0.9996	76.80	2E+09	0.56
Pure resin (pH 6.3)	-	-	149.32	168.08	180.53	0.9888	62.22	1E+07	0.21
Resin + ExtrW (lime)	12.1	11.1	143.81	156.73	171.45	0.9998	70.11	1E+08	0.33
Resin + ExtrW (tulipwood)	6.1	12.1	136.66	149.97	164.71	0.9999	66.68	8E+07	0.44
Resin + ExtrS (lime)	-	10.0	143.39	156.71	169.28	0.9993	74.81	6E+08	0.36
Resin + ExtrS (poplar)	-	9.6	134.20	148.01	160.56	0.9988	70.10	2E+08	0.54

The ExtrW fraction of tulipwood and lime displayed an ABC of 6.1 mmol/batch and 12.1 mmol/batch, respectively (see Chapter 3.4.3.3). Table 7-3 shows that the resin curing rate (k) was reduced relative to the neat resin by 21% to 0.44 s⁻¹ after adding tulipwood extractives and by 41% to 0.33 s⁻¹ after adding the higher ABC lime extractives. Thus, the ABC of an extract corresponds well with the reduction of the resin curing rate. A higher ABC extract neutralises more alkali, which causes more retardation.

In both timbers, the ExtrW fraction makes up around 0.15% (w/w) of the dry wood mass (Table 3-2). For the DSC measurements the concentration used was notably higher with 11% and 12% (w/w). Consequently, if the retardation effect caused by freeze-dried hot-water extractives is adjusted to the actual concentration present in solid wood (i.e., divided by roughly 100), the remaining neutralisation effect would be rather small in both cases. Hence, during the wood modification process, neutralisation via water-soluble compounds is small for the investigated timbers, which were all sapwood. In the heartwood of some timbers, the neutralisation via water-soluble extractives may be more pronounced²⁷⁵.

Table 7-3 further presents the DSC results of resin mixed with the ExtrS fraction of lime and poplar wood. At a concentration of approximately 10% (w/w), the ExtrS fraction of lime had a significantly more pronounced effect on the resin curing rate compared to the ExtrS fraction of poplar. Lime extractives reduced the curing rate to 0.36 s^{-1} , while poplar extractives had minimal impact on the reaction rate (0.54 s^{-1}). Notably, in lime wood both ExtrW and ExtrS have a strong effect on the resin curing rate, although NMR scans have shown that the two fractions have a substantially different chemical composition (see Chapter 3.3.6). In lime wood, ExtrW contained mainly carbohydrates and acetic acid, while ExtrS contained mainly fatty acids. Additionally, the ExtrS content in lime wood was relatively high at 3.95% (w/w). Hence, the elevated ExtrS content in lime wood might contribute more significantly to the retardation of the resin curing reaction compared to other timbers with lower extractives content.

Generally, in the context of wood modification, it is essential to consider both ExtrW and ExtrS, however, their impact on the resin curing rate is highly dependent on the chemical composition and content of the extractives fraction. In certain timbers, the effect of this fraction may be substantial (e.g., lime wood), while in others, it may be small (e.g., poplar, tulipwood).

Table 7-4 shows the effect that different cell wall polymers have on the resin curing kinetics in DSC scans. If one of the cell wall polymers was interacting with the resin via neutralisation, degradation, or covalent bonding, significant changes in the resin curing rate (k) would be expected. Cellulose was tested at two different cellulose-to-resin ratios. At low cellulose-resin ratio, the resin curing rate was reduced from 0.56 s^{-1} in neat resin to 0.51 s^{-1} . At high cellulose-resin ratio, the resin curing rate decreased slightly more to 0.46 s^{-1} . Hence, the presence of cellulose has relatively little impact on the resin curing rate, which is in good agreement with previous literature²¹². The moderate reduction of the resin curing rate could be caused by steric hindrances associated with the dispersion of resin on the cellulose surface. It is also possible that the amorphous cellulose fraction is subject to a peeling reaction, which consumes the alkaline catalyst. The effect of lignin on the resin curing rate is similar to cellulose, where the resin curing rate (k) remains relatively high, hence relatively little interaction between lignin and resin was evident.

Table 7-4 Kinetic parameter determined in differential scanning calorimetry for isolated cell wall polymers mixed with PUF resin. The pH value in the table refers to a suspension of the cell wall polymer in water.

Sample	cell wall polymer: resin in g/g	pH value	T_p in °C			R^2	E_A in kJ/mol	Z in s^{-1}	k at 150°C in s^{-1}
			5	10	20				
Resin + α -cellulose (low)	0.23	6.5	135.14	144.97	162.44	0.9874	66.54	$8.39\text{E}+07$	0.51
Resin + α -cellulose (high)	0.44	6.5	138.01	148.85	164.76	0.9948	69.87	$1.95\text{E}+08$	0.46
Resin + lignin	0.14	6.4	136.81	148.85	162.80	0.9996	72.18	$4.11\text{E}+08$	0.51
Resin + holocellulose	0.30	6.1	147.18	159.70	173.40	0.9999	75.30	$5.86\text{E}+08$	0.30

Holocellulose, however, has a significant effect on the curing kinetics since an intermediate holocellulose-to-resin ratio leads to a drastic reduction in the rate (0.30 s^{-1}). This suggests that the hemicellulose fraction interacts with the resin either via neutralisation, degradation, or possibly via covalent bonding. The hemicellulose fraction is completely amorphous and frequently substituted with O-acetyl groups. Therefore, neutralisation via hemicelluloses degradation probably occurs in the form of peeling and deacetylation⁵⁰. Another explanation for the altered resin curing rate in Table 7-4 could be the formation of covalent bonds between the resin and the hemicellulose fraction. The most likely reaction would be an esterification involving glucuronic acids and resin hydroxymethyl groups²⁷⁸, as investigated by ^{13}C DEPTQ NMR, see later.

To further investigate potential interactions between resin and isolated cell wall polymers, the corresponding thermograms are presented in Figure 7-3 (a-b). The thermograms of resin mixed with each cell wall polymer in Figure 7-3 (a) exhibit no additional peaks. However, upon deconvolution of the scan in Figure 7-3 (b), two distinct signals emerge in the resin mixed with holocellulose. The first exotherm in the deconvoluted scan is associated with the resin curing reaction, displaying peaks at 138°C, 152°C, and 161°C for heating rates of 5°C/min, 10°C/min, and 20°C/min, respectively (refer to Appendix 33). The second, much smaller signal peaks at 181°C, 189°C, and 208°C, respectively.

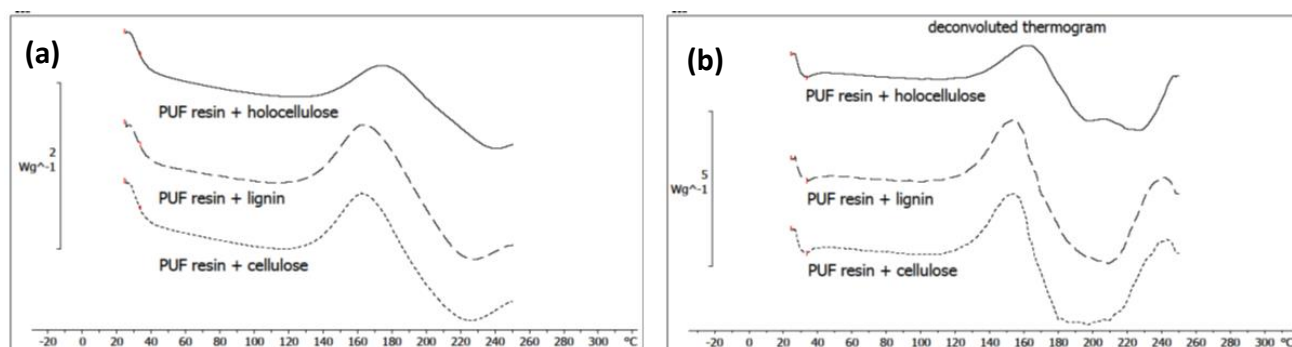


Figure 7-3 (a) Thermogram of PUF resin mixed with either cellulose, lignin, or holocellulose showing heat flow against sample temperature. (b) Deconvoluted thermogram shows a new signal in resin mixed with holocellulose at 208°C. The cell wall polymers were isolated from tulipwood. The heating rate was 20°C/min.

The presence of an additional peak during deconvolution further suggests reactivity between the resin and the hemicellulose fraction in the holocellulose sample. Thermal decomposition was ruled out through additional experiments using a similar setup with pressurised crucibles and a heating rate of 10°C/min. Pure holocellulose exhibited decomposition at significantly higher temperatures, displaying exothermic peaks at 231°C and 276°C (Appendix 34). Furthermore, the deconvolution approach was applied to all other scans in Figure 7-3 (b), confirming the absence of a second signal for resin mixed with cellulose and lignin. This implies that the hemicellulose fraction of the holocellulose is the likely contributor to this effect.

The second peak likely represents either deacetylation and peeling, accelerated at elevated temperatures, or the formation of covalent bonds with the resin. In conclusion, when the resin reacts directly with the wood polymers, the hemicellulose fraction is the most likely contributor to this effect.

Regarding Table 7-3, it must be noted that the WPG varies among wood species due to different liquid resin uptake during vacuum impregnation (see Chapter 5.4.2.1). This variable resin content in solid wood samples has not been considered so far, although it might explain the difference between Radiata pine earlywood and latewood observed in Table 7-3.

To elaborate, He & Riedl²¹² (2004) identified steric hindrances in the cell wall as a crucial mechanism limiting resin cure in wood. If a resin molecule infiltrates the cell wall, where it is spatially confined, it will require significantly more time to reach a reaction site. This is not the case in neat resin. Therefore, it is reasonable to distinguish resin located in the cell wall (cell wall resin) from resin deposits in the lumen (neat resin).

Thus, one plausible explanation for the disparity between Radiata pine earlywood and latewood is that the latewood contains a higher relative proportion of cell wall resin and a lower relative proportion of neat resin compared to the earlywood. Consequently, the elevated cell wall resin content in Radiata pine latewood contributes to the slower curing rate compared to the earlywood.

7.4.2. Chemical Interactions between Wood and Resin studied by whole Cell Wall Dissolution in Combination with Solution-State NMR.

7.4.2.1. Modified and Unmodified Wood

To investigate the chemical interactions between wood and resin *in situ*, a whole cell wall dissolution technique was used to prepare samples for solution-state NMR spectroscopy²⁷⁹. Chemical bonds in resin and wood polymers are semi-quantifiable with this method.

Figure 7-4 (a-b) show the whole ^1H - ^{13}C -HSQC NMR spectra of modified poplar and modified lime wood, and Figure 7-4 (c-b) display the assignment of selected peaks in the wood and resin fraction. The spectra of unmodified wood are provided in Appendix 35 for reference. Figure 7-4 (a-b) illustrate certain qualitative chemical differences in the lignin fraction of treated poplar and treated lime. Poplar lignin contains *p*-hydroxybenzoates (PB) and resinol (C) structures, which were not detected in the lime sample. Lime contains a cinnamyl alcohol (X_1) signal which was faint in poplar. These qualitative differences apply both to modified and unmodified samples of lime and poplar.

Other differences concern the abundance of certain functional groups as shown in Table 7-5. Both treated and untreated lime wood has a higher acetyl and glucuronic acid content, and significantly lower G/S-lignin ratio than treated and untreated poplar. In Chapter 3.4.1, these quantitative differences were already indicated by the principal component analysis of FTIR spectra, leading to the separation of eleven wood species into four clusters. The present NMR results confirm the assignment from previous chapter.

The integrated peak areas in Table 7-5 also show some signs of cell wall degradation from the resin treatment. After modification, the methyl acetyl peak at 21 ppm decreases by 9% in lime and 13% in poplar. Acetylated xylan ring carbons in the C2 and C3 positions (approx. 73 ppm) decrease by 32% and 28% in lime and by 28% and 8% in poplar. The discrepancy between the methyl acetyl and the acetylated xylan ring signals could mean that acetyl groups are cleaved from the xylan ring but remain partly in the wood, probably in the form of an acetate salt. Hence, the decrease in the acetylated xylan ring signal is higher than the decrease of the methyl acetyl signal because the methyl is also present in the acetate salt.

β -O-4 linkages in lignin decrease by 12% in lime but show no notable difference in poplar. The G/S ratio in modified wood is reported Table 7-5, but the $G_{5/6}$ position overlaps considerably with the $PF_{2/4/6}$ positions. Hence, a corrected G/S ratio is used, including only the G_2 signal. The corrected ratio G/S_{cor} decreases by 25% in lime and by just 12.4% in poplar. To conclude, evidence of the deacetylation of hemicelluloses is directly shown in the NMR spectra for both species, while changes in lignin were more species specific.

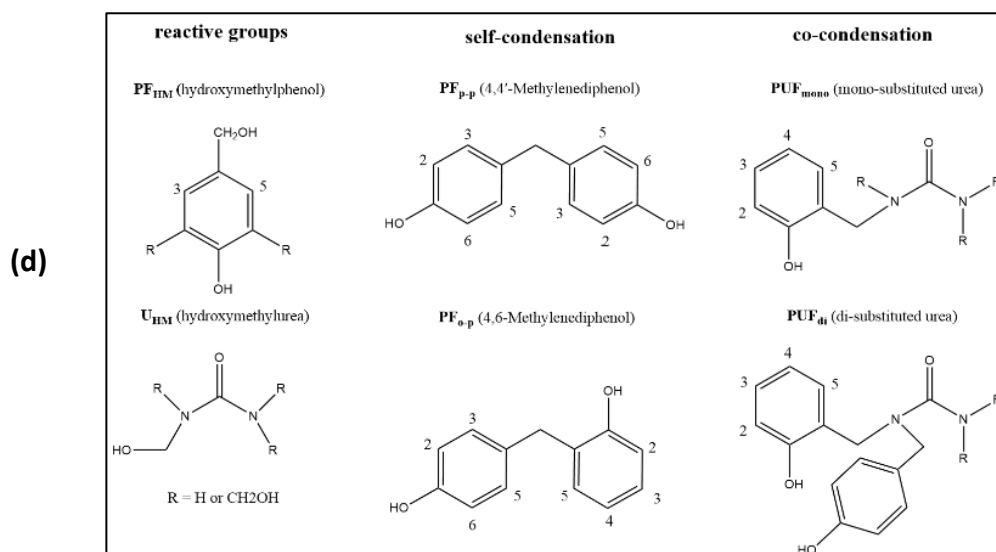
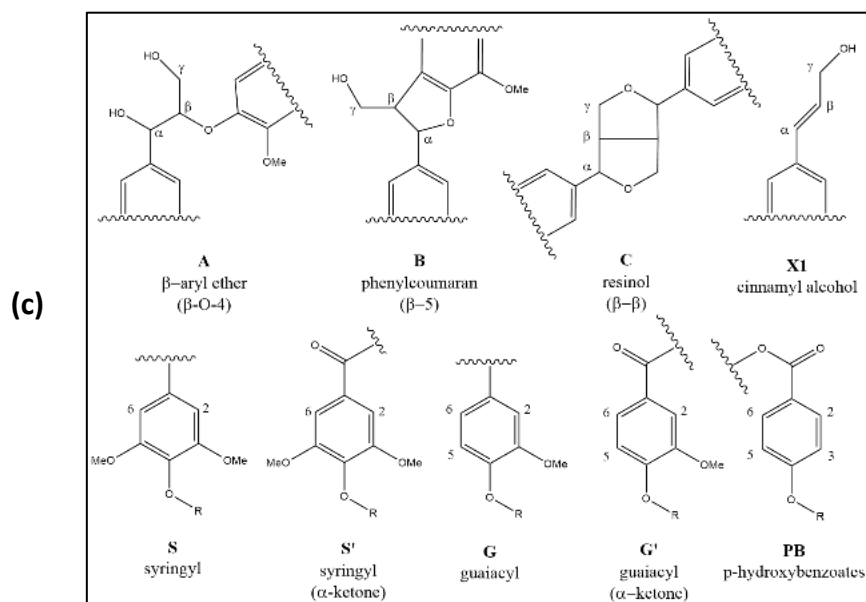
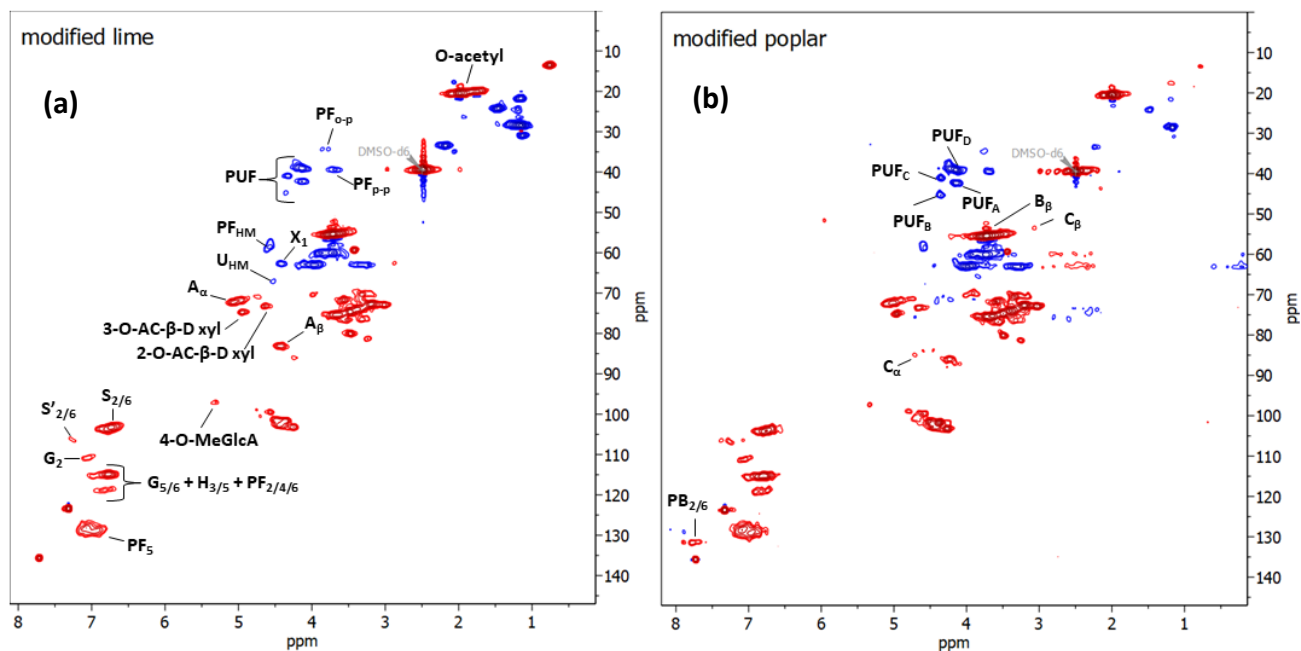


Figure 7-4 ^1H - ^{13}C -HSQC NMR spectrum of (a) modified lime and (b) poplar wood with the assignments of chemical structures. (c) Common structures in lignin. (d) Common structures in PUF resin.

Table 7-5 Integrated peak areas measured in 1H-13C HSQC NMR spectrum. Values refer to average of two replicates. Values are normalised to lignin methoxy signal at 56 ppm.

Signal	Lime		Poplar	
	Control	Modified	Control	Modified
PF _{O-p}	-	0.018	-	0.017
PF _{p-p}	-	0.035	-	0.037
PUF _A	-	0.020	-	0.022
PUF _B	-	0.042	-	0.110
PUF _C	-	0.030	-	0.024
PUF _D	-	0.106	-	0.102
PF _{HM}	-	0.049	-	0.034
p-p/o-p	-	1.917	-	2.212
PUF _{all} /PF _{all}	-	3.743	-	4.849
PUF _{C-D} / PUF _{A-B}		2.195		0.954
O-acetyl	0.853	0.780	0.566	0.488
2-O-Ac-β-D-xylyp	0.059	0.040	0.047	0.033
3-O-Ac-β-D-xylyp	0.057	0.041	0.050	0.046
4-O-MeGlcA	0.027	0.024	0.017	0.021
α-D-GlcpR	0.010	0.011	0.008	0.009
A _α (G/H)	0.134	0.119	0.103	0.101
A _α (S)	0.026	0.022	0.028	0.023
A _β (G/H)	0.065	0.068	0.019	0.027
A _β (S)	0.030	0.023	0.074	0.066
B _β	0.012	0.014	0.010	0.009
C _α	0.005	0.006	0.016	0.015
C _β	0.003	0.002	0.009	0.011
G:S	0.651	1.146	1.187	1.903
G:S _{corrected}	0.196	0.147	0.217	0.190

7.4.2.2. The Resin Fraction in Modified Wood

Table 7-5 also shows that the individual methylene bridge constellations formed by self-condensation (PF_{O-p} and PF_{p-p}) or co-condensation¹⁸² (PUF_{A-D}) have slightly different integration values in lime and poplar wood, which could be the result of different chemical interactions with both timbers. Hence, it is evident that the resin cures differently in lime and poplar. This phenomenon is further explored in the following.

Figure 7-5 shows a close up of the methylene bridge region in the ¹H-¹³C-HSQC NMR spectra of partly cured pure PUF resin, cured modified poplar, and cured modified lime wood. Self-condensation and co-condensation occur in the neat PUF resin as well as in the modified timbers. But interestingly, the peaks corresponding to PUF_C at 4.34/41.1 ppm and PUF_D at 4.15/39.2 ppm were not detected in the neat resin, but only in the modified wood.

The chemical shift prediction tool in the Chemdraw 21.0.0 software was used to assign the peaks PUF_{A-D} as follows (Appendix 36 – 38). PUF_A was assigned to 1,3-bis(4-hydroxyphenyl) urea, hence, crosslinking in the PF₄ position. PUF_B was assigned to 1,1-bis(2-hydroxyphenyl) urea, hence, crosslinking in the PF_{2/6} position. The most likely assignment of PUF_D according to predictions is 1,3-bis(2-hydroxyphenyl) urea. The PUF_C signal at 4.34/41.1 ppm is currently not assigned, but probably represents a similar form of co-condensation via methylene bridges. PUF_{A, B} are the sterically favoured constellations in the neat resin. The methylene bridge constellations PUF_C and PUF_D occur only when the resin cures inside the cell wall. This shows how steric effects in the cell wall influence the reaction pathway of the resin.

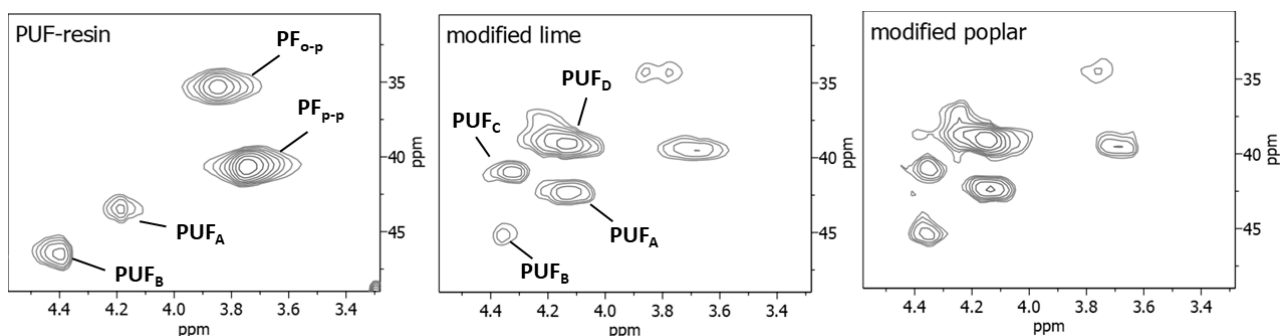


Figure 7-5 Partial ^1H - ^{13}C HSQC NMR spectrum of partly cured PUF resin, modified lime, and modified poplar in the methylene bridge region. Structures PUF_A and PUF_B indicate novel methylene bridges that were not previously observed in the pure PUF resin. PUF_A and PUF_B might correspond to methylene bridges of resin interacting closely with the wood polymer surface.

Moreover, Table 7-6 shows that methylene bridge signals in modified wood displayed an upfield shift of approximately 1 – 1.5 ppm compared to the neat resin signals. It is possible that different conformations of the methylene bridges exist, meaning that sometimes the bonds will move and rotate, making neighbouring atoms either come closer or move farther away from each other. These conformational effects can lead to 1 – 1.5 ppm differences in chemical shifts of ^{13}C compared to the neat resin²⁸⁰.

Another difference in the resin chemistry of both modified timbers is the abundance of unreacted hydroxymethyl groups (PF_{HM}), which is 44% higher in lime than in poplar (Table 7-3). This could be related neutralisation effects, that have been discussed previously. As lime wood has a higher alkaline buffer capacity (ABC) than poplar, it neutralises more alkaline catalyst in the resin, possibly resulting in more unreacted hydroxymethyl groups.

Table 7-6 The peak locations of resin specific signals in pure resin and modified wood. Conformational effects in modified wood might change the chemical shift by 1 – 1.5 ppm.

Signal	Pure PUF Resin		Modified Lime		Modified Poplar	
	$\delta(^1\text{H})/\text{ppm}$	$\delta(^{13}\text{C})/\text{ppm}$	$\delta(^1\text{H})/\text{ppm}$	$\delta(^{13}\text{C})/\text{ppm}$	$\delta(^1\text{H})/\text{ppm}$	$\delta(^{13}\text{C})/\text{ppm}$
$\text{PF}_{\text{O-P}}$	3.85	35.31	3.86	34.34	3.76	34.34
$\text{PF}_{\text{P-P}}$	3.75	40.81	3.68	39.52	3.69	39.52
PUF_A	4.19	43.4	4.13	42.43	4.14	42.43
PUF_B	4.4	46.64	4.36	45.34	4.35	45.34
PUF_C	-	-	4.32	40.81	4.36	41.14
PUF_D	-	-	4.13	39.21	4.15	39.21
PF_{HM}	4.64	60.55	4.56	58.61	4.57	58.61

7.4.2.3. Study of Covalent Bonds between Resin and Wood

Section 7.4.1 has indicated a certain connectivity between PUF resin and the hemicellulose fraction. This section investigated the possibility of covalent bonds between resin and hemicelluloses, as well as between resin and lignin.

Figure 7-6 shows the region in the ^{13}C DEPTQ NMR spectrum of poplar and lime, where ester bonds between wood hemicelluloses and hydroxymethylated resorcinol resin have previously been detected²⁷⁸. The ^{13}C DEPTQ NMR spectrum is used instead of the HSQC spectrum because quaternary carbons in an ester bond are not visible in the latter.

However, the DEPTQ spectrum in Figure 7-6 shows no novel peaks in the modified poplar and lime wood, despite a reasonable signal-to-noise ratio, so ester linkage formation could not be confirmed. Similarly, the aromatic region where covalent bonds between resin and G-lignin have been observed previously, did not show any new signals in Appendix 39. Therefore, the formation of covalent bonds between resin and cell wall polymers is generally unlikely under the current conditions.

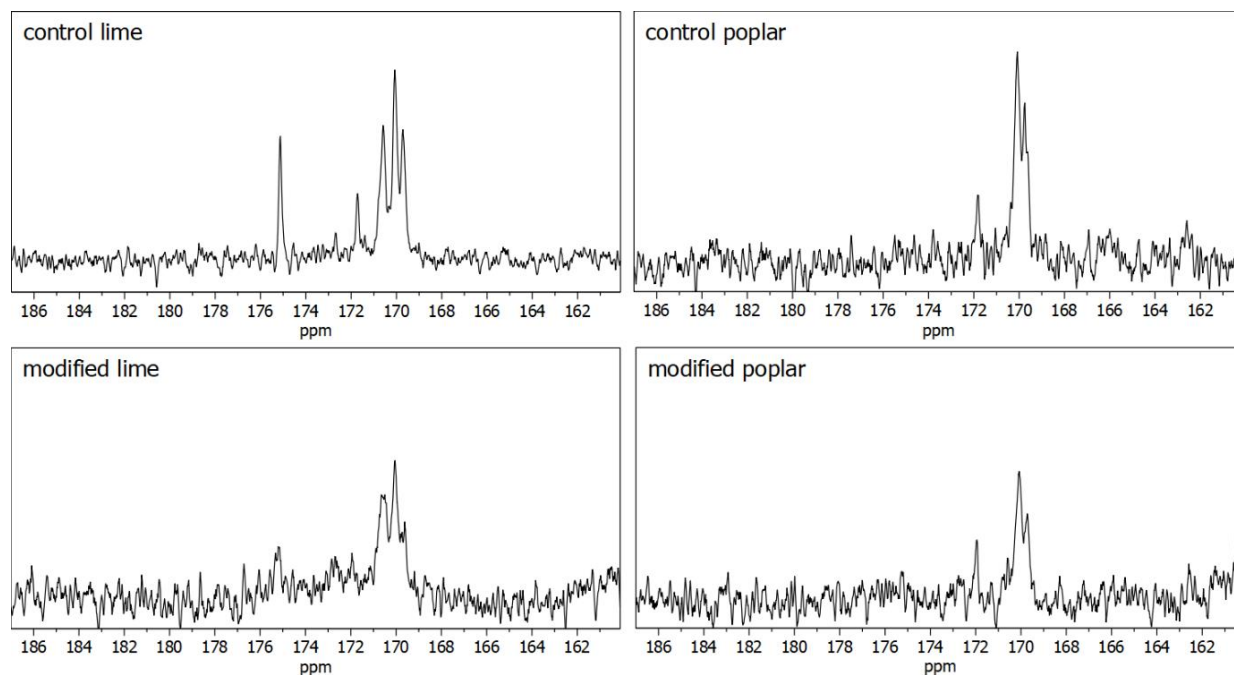


Figure 7-6 Partial ^{13}C DEPTQ NMR spectrum of modified and unmodified lime and poplar wood in the ester bond region of the spectrum. No novel ester bonds could be detected.

There are several possible explanations why previously observed covalent bonds have not been detected in this experiment. For one, previous studies investigated coniferous wood species, which are rich in G-lignin. Hardwoods, which were used in the current experiment contain an approximately equal share of G-lignin and S-lignin. The S-lignin generally shows a higher degree of substitution in the aromatic ring and is therefore less likely to react with the resin via methylene bridge formation.

Another possibility is that different process conditions enabled the formation of covalent bonds in the previous studies, whereas the conditions used in this experiment restricted covalent bonds. E.g., the ratio of resin solids to wood was 2:1 in Yelle & Ralph's¹⁹⁸ study compared to a ratio of approximately 1:3 in this experiment. The pH value, solids content, type of catalyst, and molecular weight of the resin were also different. Similar explanation can be found for the absence of ester bonds in Figure 7-6.

7.5. Conclusions from Chapter 7

The chemical interactions between resin and wood, which were defined as neutralisation of catalyst, cell wall degradation, and covalent bonding, were further investigated in the current chapter using DSC and solution-state NMR spectroscopy. DSC scan of resin impregnated solid wood samples have shown that:

- Compared to neat resin, the curing rate in the presence of solid wood is 43 – 57% slower.
- Resin reacts significantly slower in the latewood than in the earlywood of Radiata pine, which is explained by steric hinderance effects in the cell wall.

To investigate the retardation effect in solid wood further, the resin was mixed with various wood constituents in DSC experiments. Blending the resin with water extractives (ExtrW) and solvent extractives (ExtrS) showed that:

- The effect of ExtrW on the curing rate correlates with the ABC measurements, where a higher ABC extract causes a more pronounced retardation effect.
- The ExtrW concentration in solid wood is too small to explain the retardation effect alone.
- The ExtrS fraction might be significant in some timbers (e.g., lime).
- Generally, the effect of extractives on the resin curing rate depends on the chemical composition of the extractives and on the extractives content in solid wood.
- In lime wood, both ExtrW and ExtrS are likely to neutralise considerable amounts of the alkaline catalyst, whereas in poplar and tulipwood, the extractives fraction seems to be of minor importance.

Blending the resin with isolated wood polymers in DSC experiments has shown that:

- Isolated holocellulose had the highest impact on the resin curing rate, causing a major retardation.
- The corresponding thermogram displayed a side reaction, which was assigned to the deacetylation and/or peeling reaction of the hemicellulose fraction in the presence of resin.
- Isolated cellulose and lignin had relatively little impact on the curing reaction.

Modified and unmodified specimens of lime and poplar wood, which were previously used in Chapter 5 were subjected to a whole cell wall dissolution technique to enable solutions-state NMR investigations of these specimens. Solution-state NMR spectroscopy has shown that:

- Previously observed covalent bonds between resin and wood polymers did not form in the current investigation.
- Compared to the neat resin, different bonds are formed when resin is cured inside the wood.
- Resin cured slightly differently in lime and poplar wood, as shown by differences in the integrated peak areas of methylene bridges.
- The signals from methylene bridges exhibit an upfield shift of 1 – 1.5 ppm in modified wood in comparison to pure resin. This shift may be attributed to conformational effects occurring within the cell wall.
- The deacetylation of the hemicellulose fraction is confirmed, and acetate salts remain in the wood.

8. Cell Wall Diffusion in Phenol Urea Formaldehyde Resin Modified Wood

8.1. Introduction to Chapter 8

In Chapter 6.1 the concept of resin cell wall diffusion was established, which was described as the process during which resin molecules migrate from the cell lumen into the cell wall as the resin impregnated wood is dried. In Chapter 6.4.5 it was shown that certain process conditions in the drying stage facilitate the resin monomer diffusion to micropores in the cell wall, whereas other conditions impede this process. The best results in ASE tests were achieved when the specimens were dried with an initially high relative humidity of 75% and a relatively high temperature of 30°C. An initially low relative humidity and low temperature of 4°C resulted in comparably poor performance.

The current chapter aims to understand the migration process during resin cell wall diffusion in more detail and investigates the sub-microscopic location of resin in the cell wall. This is done in a case study, where the conditions under which resin impregnated wood was dried were adjusted to either facilitate (Wood A) or restrict (Wood B) cell wall diffusion, using the knowledge gained from Chapter 6. Both test groups were compared in anti-swelling efficiency (ASE) tests to investigate the macroscopic performance of the modified wood. DSC was used to investigate the micropore size distribution and micropore blocking effects via thermoporosimetry, and to probe the wood-water interactions before and after modification. Solid-state NMR in combination with relaxation time analysis was used to show how molecular motions of wood polymers are affected in both test groups.

Thermoporosimetry is a well-established method used to study the pore size distribution in porous materials including wood, as well as certain aspects of the wood-water relationship^{61, 63,64,71,72}. The fundamentals of this method were outlined in section 2.1.3.5. of this thesis. Generally, thermoporosimetry distinguishes bulk water (BW), freezing bound water (FBW), and non-freezing bound water (NFBW). The measurement is performed with a water-soaked wood sample, i.e., in which the micropore spaces between microfibrils and macrofibrils are fully swollen by water. Resin molecules partially fill these micropores during the modification, leading to permanent macroscopic volume gain (i.e., cell wall bulking) after heat curing. Consequently, the resin renders a certain volume of micropores inaccessible for water. This mode of action is called micropore blocking. Due to micropore blocking, one can measure a difference in the FBW content of wood before and after modification. The NFBW fraction constitutes the tightly bound water in the cell wall, although the exact nature of this fraction is still debated²⁷⁰. How this fraction will be affected by the modification is less clear from the literature.

In previous chapters, solution-state NMR was used to investigate the chemical composition of wood extractives, PUF resin, and even the whole cell wall after solubilisation (see Chapters 3, 4, 5, 7). Solution-state NMR provides a high resolution and enables the identification of rare and structurally similar chemical bonds. This is because in a solution, the molecular tumbling of nuclei averages the anisotropic interactions between the external magnetic field and the nucleus. In solid state NMR, these anisotropic interactions (i.e., magnetic interactions of non-zero spin and anisotropic shielding with respect to the external magnetic field) are present and lead to considerable line broadening, although the combination of cross polarization (CP) and magic angle spinning (MAS) help to minimise these effects.

Nevertheless, the spectral resolution of solid-state NMR at natural abundance is still lower than in solution-state NMR. The advantage of solid-state NMR, however, is that relaxation times of different nuclei can be used to study the molecular motions of different polymers as well as their morphology on a nanometre level. This becomes relevant since

previous chapters have shown that the interactions between wood and resin polymers are not determined by covalent bonding. It is more likely that the molecular arrangement and the sub-microscopic location of resin in the cell wall affects the performance of a resin treatment.

Resin deposits in micropores are in close contact with the interfaces of micro- and macrofibrils. Interactions at this length scale can be studied by solid-state NMR spectroscopy and relaxation time analysis, where different relaxation times, such as T_1 (^1H), $T_{1\rho}$, T_1 (^{13}C) correspond to distinct timescales of motions, and therefore, to different ranges of distance^{281,282}. The method is suitable to study morphological phase differences of polymers in the cell wall. Laborie²²⁰ (2002) argued that the spin-lattice time in the rotating frame $T_{1\rho}$ and spin-lattice time T_1 correspond to a morphological phase distance of 2 – 30 nm and >30 nm.

The morphological phase size in the cell wall is such that spin-diffusion is ineffective under certain conditions (e.g., in wet state), which results in distinct relaxation times for different cell wall polymers^{283,284}. Spin-diffusion is a phenomenon wherein separate nuclear spins undergo continuous exchange of energy, leading to a common relaxation time for different nuclei. Spin-diffusion depends on various factors including the distance of interaction nuclei (see above). Therefore, one can use the presence or absence of spin-diffusion to study the morphological phase at different levels of scale. Spin-coupled carbons show identical $T_{1\rho}$ values even if they are in a different chemical environment. The signals of cellulose domains 1 and 2 are typically spin-coupled showing similar $T_{1\rho}$ relaxation times^{220,284}. In 1D solid-state NMR, both domains are distinguished by different chemical shifts of their C4 and C6 signals.

Laborie (2002) showed that neither heat treatments, mild alkali treatments, nor modification with high molecular weight resin disturbed the spin coupling of the two cellulose domains. However, the treatment with a low molecular weight resin caused significantly different $T_{1\rho}$ values for domains 1 and 2, suggesting that resin monomers diffused close to the microfibril interacting with its surface. Similar studies have been published more recently^{221,222}, but many aspects of the nanoscale interaction between wood and resin remain elusive.

In this chapter, the resin-wood interactions at the nanoscale are explored, with the cell wall diffusion mechanism employed as a tool to unravel these dynamics. In turn, a deeper understanding of cell wall diffusion is achieved by examining the underlying mechanisms at the polymer level.

8.2. Materials

8.2.1. Wood Samples and Resin

The sapwood of tulipwood was cut into specimens with the dimensions 20 (r) × 20 (t) × 5 (l) mm. All specimens were cut from a single strip of wood to minimise the variability. For each of the three test groups (Wood A, Wood B, Control), 20 specimens were randomly selected from within this strip.

The default resin described in Chapter 4.2.1 was used at a concentration of 20% (w/w). A lower concentration than in previous chapters was chosen to increase the relative amount of cell wall resin by reducing the number of resin deposits in the lumens.

8.3. Methods

8.3.1. Resin Treatment and ASE Tests

Batches of 20 specimens were vacuum impregnated with the PUF resin for 20 min. The subsequent drying procedure was performed in two different ways to either promote or restrict cell wall diffusion. One set (Wood A) was placed in a sealed container over saturated NaCl solution to maintain a relative humidity of 75%. In the diffusion step, this container was placed in an oven set to 30°C for 7 days. The weight and dimensions of each sample were monitored daily. In the drying step, the sample holder was transferred to another container with saturated MgCl₂ solution to maintain a relative humidity of 33%. This container was placed in an oven set to 50°C for 1 day. Another set (Wood B) was placed in a container over saturated KOH solution to maintain a relative humidity of 7%. In the diffusion step, this container was placed in a fridge set to 4°C for 7 days. In the drying step, the whole container was transferred to an oven set to 50°C for 1 day. After each diffusion and drying step, some specimens were put aside for later analysis.

The remaining specimens were heat cured at 150°C for 8 h. The moisture content (determined gravimetrically) before heat curing was 9.66% (±0.34) in Wood A and 5.67% (±0.10) in Wood B. Temperature measurements, performed using a thermocouple in the core of one sample from each set, were very similar, despite the different moisture contents prior to cure indicating no major differences in the heat curing step (Appendix 40).

Some cured samples were put aside for later analysis. The other cured samples were subjected to three cycles of oven drying and water soaking to determine swelling coefficients (S_{mod1} , S_{mod2} , S_{mod3}), mass loss due to leaching (ML_{total}), and gravimetric water uptake (WU). Details about their calculations are described in Chapter 5.3.9.

8.3.2. SEM – Imaging

SEM micrographs of the tangential-longitudinal faces were acquired as described in Chapter 5.3.5.

8.3.3. Thermoporosimetry – Isothermal Method

The bound and bulk water content was measured using a Differential Scanning Calorimeter (*TA Instruments, Q20*) equipped with a cooling unit (*RCS 90, Refrigerated Cooling Unit*). The DSC calibration was performed using an Indium standard (8 mg), which was heated through its melting transition at 156.60°C at a heating rate of 10 °C/min. The ratio of the theoretical melting transition to the real value was used to calibrate the cell constant and temperature. Before the scan, water-soaked samples were briefly wiped with tissue to remove excess water. Subsequently, the solid wood sections were placed in an aluminium crucible and sealed with a sealing press (see Figure 8-1). During the scan, each sample was stabilised at –30°C to guarantee complete freezing of FBW and BW. Subsequently, the temperature was raised with a heating rate of 1 °C/min between discrete isothermal steps. These temperature steps were performed at –20, –15, –10, –6, –4, –2, –1.5, –1.1, –0.8, –0.5, –0.2, –0.1, and 5°C. Pore diameters calculated by this method assume a cylindrical pore shape and can be calculated with the Gibbs-Thomson equation (1) as follows:

$$D = \frac{4 T_m \gamma \cos \theta}{(T_m - T_m(D)) \rho H_f} \quad (1)$$

where D is the micropore diameter, T_m is the melting point of water (273.15K), γ is the surface tension of the ice-water interface (12.1 J/m²), θ is the contact angle (180°), $T_m(D)$ is the melting point of water at a given pore size, ρ is the water density (10⁶ g/m³), and H_f is the latent heat of fusion of water which is 333.7 J/g.

The isothermal steps between -15°C and -0.1°C correspond to pore size diameters of 2.6 nm, 4.0 nm, 6.6 nm, 9.9 nm, 19.8 nm, 26.4 nm, 36.0 nm, 49.5 nm, 79.2 nm, 198 nm, and 396 nm. The first segment (-30 to -20°C) was used to determine sensible heat H_s according to equation (2) and assuming no melting occurred in this range. The last segment (-0.1 to 5°C) showed two endotherms (Appendix 41).

These were assigned to FBW in pores larger than 396 nm and to BW. Each isothermal step was maintained until the heat flow returned to the baseline value. The total endothermic heat H_t during each isothermal step consists of the sensible heat H_s and the heat of melting water H_m .

$$H_s = c_p \Delta T \quad (2) \quad \text{and} \quad c_p = \frac{H_{t(-30 \text{ to } -20^{\circ}\text{C})}}{\Delta T} \quad (3)$$

Where c_p is the specific heat capacity of the sample. To calculate the heat of melting in each step, the sensible heat was subtracted from the total heat (4).

$$H_m = H_t - H_s \quad (4)$$

The mass of FBW residing at each pore size was calculated from the melting enthalpy at each isothermal step, using equation (5). The mass of BW was calculated in a similar manner using the last signal of the scan (6). The mass of NFBW was calculated by subtraction of FBW and BW from the total amount of water in the sample (7).

$$FBW \left[\frac{g}{g} \right] = \frac{H_{m,FBW}}{H_f} \quad (5) \quad BW \left[\frac{g}{g} \right] = \frac{H_{m,BW}}{H_f} \quad (6)$$

$$NFBW \left[\frac{g}{g} \right] = \frac{m_{WS} - m_{OD} - m_{FBW} - m_{BW}}{m_{WS}} \quad (7)$$

H_f is the latent heat of fusion of water (333.7 J/g), m_{WS} is the water-soaked mass of the sample, and m_{OD} is the oven dry mass of the sample. The total amount of bound water in the cell wall (TCW) is calculated using equation (8). By comparing TCW of the unmodified and modified wood, one can estimate the efficiency of micropore blocking during a treatment. The micropore blocking efficiency (MBE) is calculated with equation (9).

$$TCW \left[\frac{g}{g} \right] = FBW + NFBW \quad (8)$$

$$MBE [\%] = \frac{TCW_{control} - TCW_{modified}}{TCW_{control}} * 100\% \quad (9)$$



Figure 8-1 DSC crucibles used for thermoporosimetry next to a one penny coin. Water-soaked solid wood samples were sealed in the crucible using sealing tool.

8.3.4. Thermoporosimetry – Dynamic Method

An alternative to the isothermal DSC method is the dynamic method. In this method, the water-soaked specimen is subjected to a constant heating rate instead of the isothermal step scan. The scan time with this method is faster than with the isothermal method, however, it provides no information about the pore size distribution. The dynamic DSC method is included as another triangulation point for this investigation.

Similar to the isothermal methods, each specimen was stabilised at -30°C to guarantee complete freezing of FBW and BW. Subsequently, the temperature was raised at a constant heating rate until the melting transition was completed and the heat flow is back at baseline level. Each specimen was run consecutively at the heating rates $1^{\circ}\text{C}/\text{min}$, $5^{\circ}\text{C}/\text{min}$, and $10^{\circ}\text{C}/\text{min}$. In the dynamic method, the melting transition of water-soaked wood displays two overlapping endothermic peaks, one for FBW and one for BW (Appendix 42). The whole melting transition was integrated between -15°C and 25°C , using a sigmoidal baseline to account for height difference between baselines. The sub-peaks were split at the local maximum, using a perpendicular drop separation. This provides the melting enthalpy of FBW and BW. The values for NFBW, FBW, BW, TCW and MBE were calculated with the equations (1) – (9).

8.3.5. Solid-state NMR Spectroscopy and Relaxation Time Analysis

All solid-state NMR analysis were performed by Mohammed Rahman from the Warwick Analytical Science Centre. The cooperation between the BioComposites Centre and Warwick University was enabled by the Seedcorn access scheme of the Warwick Analytical Science Centre using EPSRC funding.

For relaxation time analysis, we selected samples of the unmodified control groups with a dry and ambient moisture content, a resin impregnated but uncured sample with an ambient moisture content, and dry heat cured specimens of Wood A and B which were not soaked in water. All samples were crushed to a fine powder using a laboratory dismembrator.

Experiments were performed using a 4 mm triple-resonance *Bruker* HXY probe that operated at a magic angle spinning (MAS) frequency of 12.5 kHz in double-resonance mode. The Larmor frequency of the ^1H and ^{13}C nuclei were 500 and 125 MHz, respectively. Spectra of ^1H and ^{13}C were referenced indirectly to TMS using the ^1H and ^{13}C peaks of the external reference alanine. These peaks were at 1.1 ppm and 20.5 ppm for ^1H and ^{13}C , respectively. A ^1H 90° pulse with a length of $2.5\ \mu\text{s}$ was used corresponding to a nutation frequency of 100 kHz. All experiments were performed at varying contact time of 2 ms or 5 ms using a recycle delay of 3 to 4 seconds (apart from ^{13}C one pulse experiments). The number of co-added transients for each experiment ranged from 812 to 1024. Heteronuclear decoupling was performed in all CP experiments²⁸⁵.

The spin-lattice relaxation $T_{1\rho}$ was measured in a CP experiment. In this case, a second 90° ramp ^1H pulse spin-locks the magnetisation and a ^{13}C pulse is simultaneously applied on the ^{13}C channel. The time applied for both of these pulses is known as the contact time (2 ms and 5 ms). On the ^1H channel, a ramp of 70 – 100% was used to meet the Hartman-Hahn condition, hence, magnetisation is transferred from ^1H to ^{13}C via ^1H - ^{13}C dipolar couplings²⁸⁶. Thus, magnetisation will build up on the ^{13}C channel. The ramp 90° pulse applies a range of frequencies to try and obey the Hartmann Hahn condition. The only difference for the $T_{1\rho}$ experiment pulse sequence is that there is a variable delay between the two 90° pulses on the ^1H channel. This variable delay is also known as the recovery time τ . The recycle delay is the time between consecutive repetitions in the NMR experiment. Spin-lattice relaxation time T_1 (^1H) was measured using

inversion recovery. A 180° inversion pulse was applied followed by a variable delay (τ) to allow for the sample to reach equilibrium. Subsequently a ^1H 90° pulse was applied, and the signal intensity was measured. The relaxation time was calculated according to Frye (1989)²⁸⁷.

Finally, the T_1 (^{13}C) relaxation time was measured using the Torchia method²⁸⁸. The experiment starts off as a normal CP experiment. After the CP, a 90° pulse on the ^{13}C channel rotates the magnetisation from the transverse to the longitudinal plane. The nuclei then relax during the recovery time, τ . A final 90° pulse on the ^{13}C channel then rotates the magnetisation back into the transverse plane. This method measured T_1 (^{13}C) relaxation times up to 25 s directly, whereas higher values were interpolated based on plots of signal intensity against contact time. Long relaxation times were more prone to error, therefore, all T_1 (^{13}C) relaxation times of resin and most values for C1 (105ppm) and C4 (89 ppm) were excluded. Similar issues have been reported previously in the literature^{220,221}.

8.4. Results and Discussion

8.4.1. Resin Treatment and ASE Tests

Table 8-1 summarises the properties of Wood A and Wood B after heat curing. Liquid resin uptake (LU) and weight percentage gain (WPG) show that both groups contain the same amount of resin. Differences in the bulking coefficient (BU) and swelling coefficient ($S_{\text{mod}1}$, $S_{\text{mod}2}$, $S_{\text{mod}3}$) are thus the result of different resin cell wall diffusion.

The BU values suggest that cell wall diffusion took place in both groups, although, it was intentionally minimised in Wood B. As expected, Wood A has a significantly higher BU and lower $S_{\text{mod}1}$, $S_{\text{mod}2}$, $S_{\text{mod}3}$ than Wood B. The mass loss during the first soaking cycle (ML_1) was also lower in Wood A, indicating better resin fixation. The mass loss in the successive cycles and the water uptake during each soak cycle shows no difference (Appendix 43).

Table 8-1 The effect of different diffusion and drying conditions on the performance of Wood A and Wood B in ASE tests during the 1st cycle water soaking. Standard deviation in parenthesis.

	LU in %	WPG in %	BU in %	$S_{\text{mod}1}$ in %	$S_{\text{mod}2}$ in %	$S_{\text{mod}3}$ in %	ML_1 in %	WU_1 in %
Wood A	1.52 (0.03)	31.53 (1.28)	9.70 (0.35)	9.67 (0.45)	11.92 (0.43)	12.37 (0.34)	2.65 (0.08)	98.32 (3.08)
Wood B	1.51 (0.03)	32.63 (0.69)	7.06 (0.26)	11.47 (0.21)	13.91 (0.44)	14.07 (0.73)	3.10 (0.17)	97.28 (2.01)

Figure 8-2 shows the mass relative to the cured state and the volume relative to the dry unmodified state throughout the diffusion and drying stages. The initial volume increase (IVI) after impregnation is higher in Wood A than in Wood B. This difference is observed, despite the fact that both groups have a similar moisture content at this stage of the drying process (*Diff_1*).

Moreover, the moisture content at this point is approximately 60% and therefore well above fibre saturation point. The difference in the relative volume early in the drying process is therefore more likely connected to the resin fraction than to the differences in the moisture content. However, this changes later in the drying stage from *Diff_2* onwards. The relative volume in Wood B displays a prominent drop from *Diff_3* to *Diff_6*, which coincides with decrease in the moisture content from 20% to 8%. A similar drop is observed in Wood A from *Diff_7* to the dried state. In both cases, the drop in the relative volume is probably connected to the partial collapse of the micropore network upon drying.

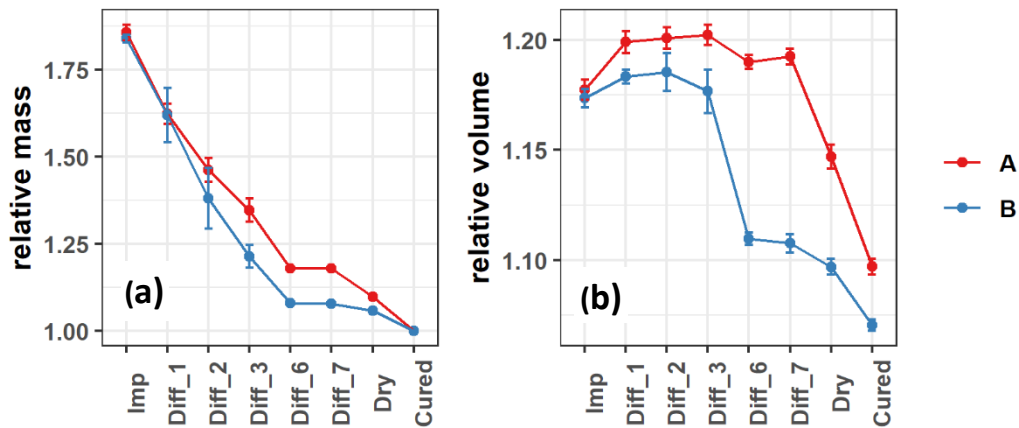


Figure 8-2 Relative mass (a) and volume (b) throughout the diffusion and drying stages. The relative mass refers to the cured state and can easily be converted to the moisture content. The relative volume refers to the oven dry unmodified state to better illustrate the initial similarity after impregnation and how both groups separate over the course of the process. The x-axis indicates the day (1 – 7) on which volume and mass were measured.

8.4.2. Scanning Electron Microscopy

Scanning electron micrographs (SEM) of Wood A and B are shown in Figure 8-3. More images are provided in Appendix 44 and 45. As shown in previous studies, we observed resin coated lumens and resin filled lumens^{86,289}. There was no notable difference in the share of resin filled lumens between Wood A and B. However, Figure 8-3 shows slightly different features in Wood A and B.

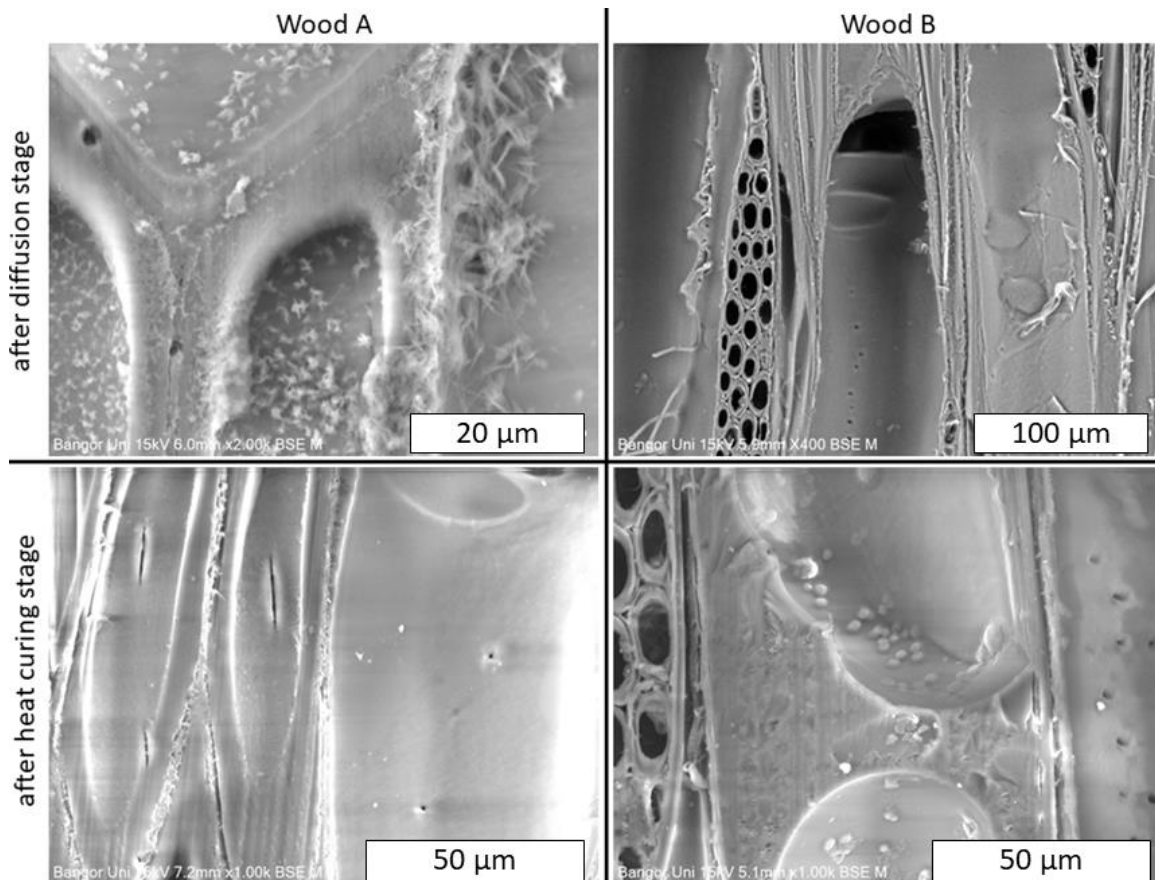


Figure 8-3 Scanning electron microscopy images of Wood A and B in different stages of the modification process. Views are on the tangential-longitudinal plane. Sections were prepared using a dry cut to avoid leaching of resin which might have occurred if samples were softened in water in a wet cut.

After diffusion, the resin in Wood A forms needle-like structures that merge to larger cobweb-like structures in the cell lumens. These resin “needles” or “cobwebs” disappeared after heat curing. The resin in Wood B agglomerates to a hemispheric shape after diffusion. After curing, these hemispheres detach and shrink to a diameter of 1 – 5 μm . The number of these resin spheres in the lumen is much lower than in previous studies, where similar structures have been observed⁹⁷.

The morphology of these resin deposits might hint toward the resin mobility. The higher humidity and temperature in treatment A improve the mobility of resin monomers during the diffusion stage, hence resin is dispersed across the macroscopic internal wood surface and delicate resin structures form in the lumens. Also, the moisture content in the diffusion stage remained high for longer in Wood A, hence the micropore network remained open for longer (Figure 8-2). Given enough time, cell wall diffusion might achieve an equilibrium state where resin monomers are dispersed uniformly throughout the cell wall micropores. The hemispherical structures in Wood B, on the other hand, indicate that resin monomers might fail to overcome cohesive forces and tend to agglomerate. The moisture content in Wood B drops below 10% early in the diffusion process, resulting in the partial collapse of the micropore network (Figure 8-2).

8.4.3. Thermoporosimetry

8.4.3.1. Isothermal Method

Table 8-2 shows the non-freezing bound water (NFBW), freezing bound water (FBW), total cell wall water (TCW), and bulk water (BW) content for the unmodified control and heat cured samples of Wood A and Wood B. Uncured samples were not included in these tests, because the sample preparation involved water soaking, which would have removed uncured resin from the micropores.

The water ratio (WR) ranged between 0.82 – 1.20 $\mu\text{l}/\text{mg}$ which is the result of different capillary void volume available in modified and unmodified tulipwood²⁹⁰. When the cell wall and the micropore network are fully saturated with water, any additional water ceases to affect the values of FBW and NFBW, hence, any variation between samples is caused by the modification itself and not by differences in the WR. Park et al.⁶⁴ (2006) have shown this for kraft pulp fibres, where NFBW and FBW ceased to change above a WR of 0.8 $\mu\text{l}/\text{mg}$ and the same is assumed for this experiment

The TCW content, which is the sum of FBW and NFBW, was 0.243 g/g in the control group and is therefore at the lower end of literature values. Thybring & Fredriksson²⁷⁰ (2023) report values between 0.25 – 0.44 g/g for the TCW in various unmodified wood species measured by DSC. One possible explanation for the relatively low TCW content in this experiment could be the rearrangement of hemicelluloses, which have gone through three cycles of water soaking and oven drying before the DSC analysis.

Both resin treatments decrease the TCW content to 17.1 – 17.4 g/g, thus to a similar extent. However, there are small differences in the NFBW and FBW contents of Wood A and B. NFBW decreased from 0.170 g/g in the control to 0.116 g/g in Wood A and to 0.122 g/g in Wood B. FBW decreased from 0.073 g/g in the control to 0.058 g/g in Wood A and to 0.049 g/g in Wood B. Thus, the NFBW content decreased slightly more in Wood A than in Wood B, however, FBW decreased more in Wood B. The blocking of micropores by the cured resin is effective in both treatments, reducing the amount of cell wall water to a similar extent. It remains unclear what is causing the differences in BU, $S_{\text{mod}1}$, $S_{\text{mod}2}$, $S_{\text{mod}3}$ at this point (see Table 8-1).

Table 8-2 Average values of water ratio (WR), non-freezing bound water (NFBW), freezing bound water (FBW), total cell wall water (TCW), bulk water (BW), and micropore blocking efficiency (MBE) determined by the isothermal DSC method. Standard deviation in parenthesis.

	HR in °C/min	WR in µl/mg	NFBW in g/g	FBW in g/g	TCW in g/g	BW in g/g	MBE in [%]
Control	1	1.20 (0.23)	0.170 (0.03)	0.073 (0.00)	0.243	0.27 (0.05)	
A	1	0.90 (0.05)	0.116 (0.01)	0.058 (0.01)	0.174	0.30 (0.03)	28.50
B	1	0.82 (0.15)	0.122 (0.01)	0.049 (0.00)	0.171	0.28 (0.04)	29.61

Figure 8-4 shows the pore size distribution between 2 – 400 nm in the water-swollen cell wall for the control and cured Wood A and B. The FBW in pores larger than 400 nm is shown on a separate y-axis as the values are one order of magnitude higher and the corresponding pores might include water in intercellular spaces such as pits⁶⁹.

In unmodified wood, FBW resides primarily in pores smaller than 30 nm. Both treatments (A & B) decrease the pore water content in micropores with a diameter between 6 – 30 nm notably, demonstrating the role of micropore blocking. In micropores between 30 – 100 nm, this effect is less pronounced, and between 100 – 400 nm one can even observe an increased pore volume for Wood A. This increase could indicate microscopic cracks in the wood structure, although it is unclear why such cracks would only occur in Wood A and not in Wood B.

Water in pores larger than 400 nm decreases in both treatments, but interestingly, treatment B shows lower values than A. Resin in Wood B resides in larger micropores, whereas in Wood A, the resin reduces NFBW more efficiently. Hence, cell wall diffusion took place in both treatments, but resin monomers migrated to different areas within the cell wall.

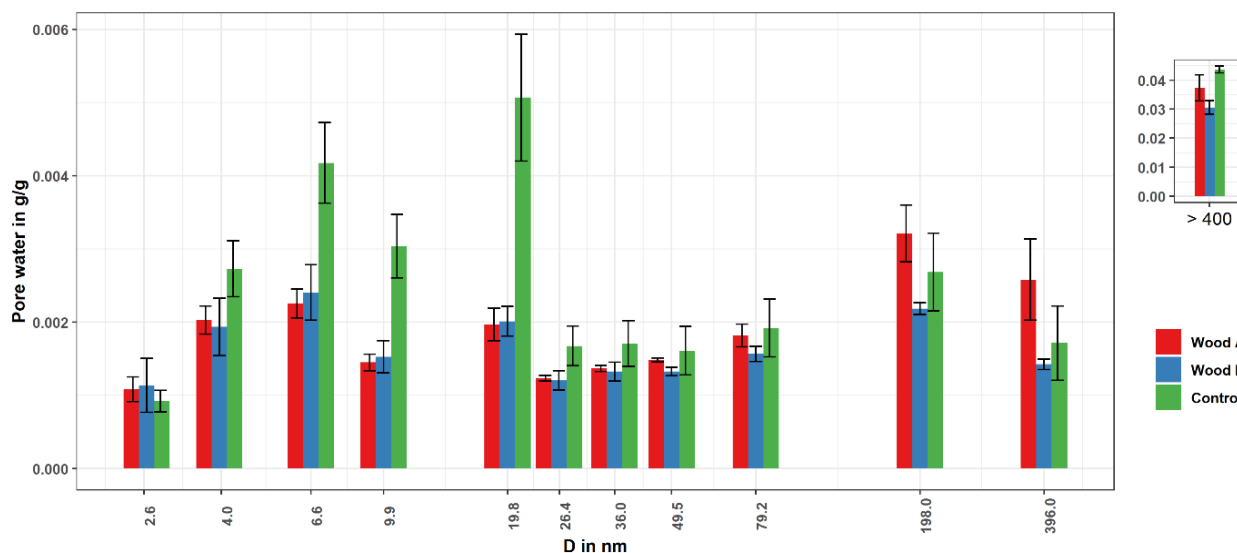


Figure 8-4 Micropore size distribution determined in DSC scans for unmodified controls, cured wood A, and cured wood B. Error bars indicate standard deviation of three replicates. D is the diameter of micropores assuming a cylindrical shape. Micropores with a diameter larger than 400 nm are shown on a separate axis.

8.4.3.2. Dynamic Method

Table 8-3 shows the main results obtained by the dynamic DSC method. WR ranges between 0.81 – 0.96 $\mu\text{l}/\text{mg}$ which is the result of different capillary void volume available (see 8.4.3.1). The values of WR are different to the isothermal method because different samples were used.

The results of NFBW and FBW in Table 8-2 differ slightly between heating rates. This is because at a faster heating rate, the melting onsets of FBW and BW are more convoluted, and the BW starts melting while FBW is not completely melted yet. Therefore, the results obtained at slow heating rates should be closer to the real value. Nevertheless, is interesting to note that MBE_{dyno} is similar for Wood A and B at $1^\circ\text{C}/\text{min}$, but different at $5^\circ\text{C}/\text{min}$ and $10^\circ\text{C}/\text{min}$.

Regardless of the heating rate, the amount of NFBW is reduced by roughly 50% in Wood A and by just 36% in Wood B in comparison to the control. This trend is similar to, but more pronounced compared to the isothermal method. The reduction of FBW depends on the heating rate and varies between 0% at $1^\circ\text{C}/\text{min}$ to 40% at $10^\circ\text{C}/\text{min}$ in Wood A. Regardless of the heating rate, the reduction of FBW remains constant around 30% in Wood B. TCW values are similar to the isothermal method, but also depend on heating rate.

To conclude the thermoporosimetry section, the measured values for TCW correspond to the lower end of literature values. A reduction in the TCW, ranging from 28.50% to 46.23% depending on the method used and whether Wood A or Wood B is considered, is achieved by the resin treatment. The NFBW content is reduced more in Wood A than in Wood B. Conversely, the FBW content is reduced more in Wood B than in Wood A. Micropore blocking was most effective in pores smaller than 30 nm in both treated timbers. The dynamic method confirmed most trends observed in the isothermal method, while testing a different set of replicates. However, the heating rate should be considered – a lower heating rate generates more reliable results.

Table 8-3 Average values of water ratio (WR), non-freezing bound water (NFBW), freezing bound water (FBW), total cell wall water (TCW), bulk water (BW), and micropore blocking efficiency (MBE) determined by the dynamic DSC method using the heating rates $1^\circ\text{C}/\text{min}$, $5^\circ\text{C}/\text{min}$, $10^\circ\text{C}/\text{min}$. Standard deviation in parenthesis.

	HR in $^\circ\text{C}/\text{min}$	WR in $\mu\text{l}/\text{mg}$	NFBW in g/g	FBW in g/g	TCW in g/g	BW in g/g	MBE_{dyno} in %
Control	1	0.96 (0.11)	0.198 (0.03)	0.072 (0.00)	0.269	0.22 (0.05)	
A	1	0.81 (0.16)	0.103 (0.03)	0.071 (0.02)	0.174	0.27 (0.02)	35.51
B	1	0.89 (0.17)	0.126 (0.02)	0.051 (0.00)	0.177	0.29 (0.03)	34.36
Control	5	0.96 (0.11)	0.192 (0.03)	0.060 (0.01)	0.251	0.24 (0.05)	
A	5	0.81 (0.16)	0.094 (0.02)	0.041 (0.01)	0.135	0.31 (0.03)	46.23
B	5	0.89 (0.17)	0.115 (0.03)	0.042 (0.01)	0.157	0.31 (0.02)	37.49
Control	10	0.96 (0.11)	0.186 (0.03)	0.049 (0.01)	0.235	0.25 (0.04)	
A	10	0.81 (0.16)	0.093 (0.02)	0.035 (0.01)	0.128	0.32 (0.02)	45.43
B	10	0.89 (0.17)	0.113 (0.03)	0.037 (0.00)	0.149	0.32 (0.02)	36.31

8.4.4. Solid-State NMR

Figure 8-5 shows ^{13}C CP MAS NMR spectra of unmodified wood (i.e., control) and heat cured PUF resin. Note that the concept used in this section, with cellulose domain 1 (D1) mainly constituting the core of the microfibril and cellulose domain 2 (D2) primarily at the surface of the microfibril, was outlined in Chapter 2.1.3.4. Peaks in the unmodified control are assigned as follows: The anomeric carbon bearing the glycosidic bond (C1) is shown at 105 ppm. The other glycosidic carbon (C4) is observed further upfield and can be separated into a C4^{D1} (89 ppm) and C4^{D2} (84 ppm) signal corresponding to cellulose domain 1 and 2. Similarly, the exocyclic carbon (C6) in cellulose shows a C6^{D1} (66 ppm) and a C6^{D2} (62 ppm) signal. The large peak at 74 ppm corresponds to the overlapping of three different ring positions (C2, C3, C5) in cellulose as well as the majority of hemicellulose shifts. The lignin methoxy group shows a distinct peak at 57 ppm. Lignin aromatic signals are observed at 136 ppm with low intensity. Quaternary lignin carbons bearing the phenoxy group are shown at 153 ppm. Xylan, which is the only acetylated hemicellulose in hardwoods, is represented by the methyl acetate signal at 21 ppm and the carbonyl acetate at 172 ppm.^{221,222}

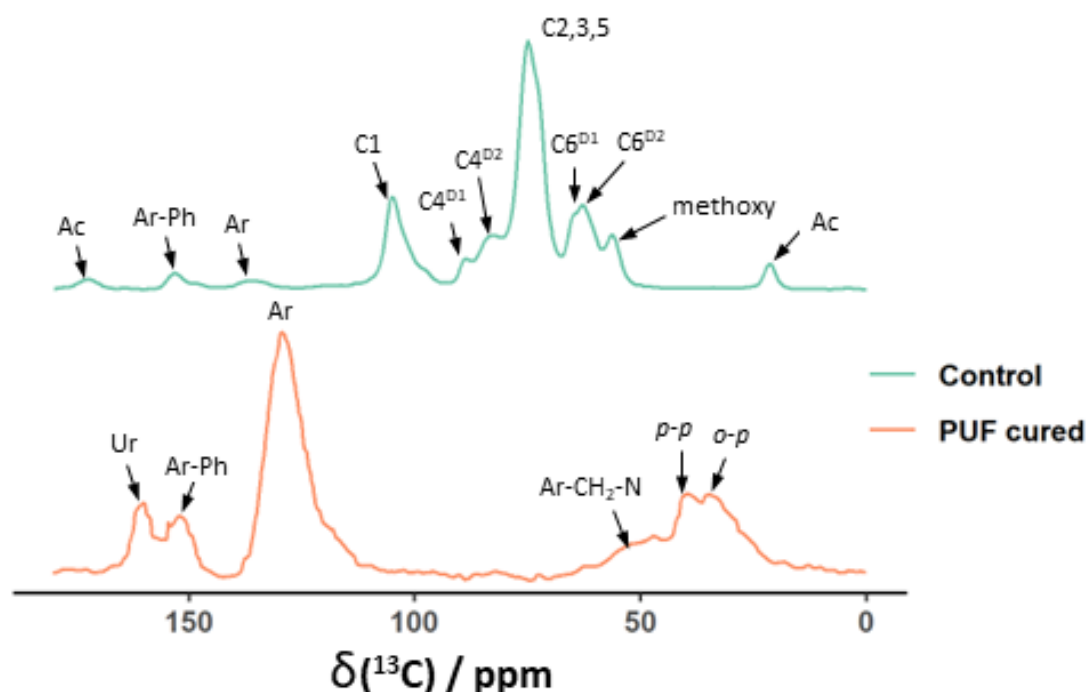


Figure 8-5 ^1H (500 MHz) ^{13}C CP MAS (12.5kHz) NMR spectra of unmodified tulipwood and pure heat cured PUF resin with peak assignments. AC indicates O – acetyl group in hemicellulose, C1 to C6 indicate cellulose ring positions in domain 1 (D1) or 2 (D2), Ar indicates aromatic ring carbons, Ar-Ph indicates phenoxy carbons, o-p and p-p indicate methylene bridges in ortho-para and para-para constellation, Ar-CH₂-N indicates methylene bridges of co-condensed urea and phenol, Ur indicates the urea carbonyl signal. The number of co-added transients for each experiment ranged from 812 to 1024.

The cured PUF resin shows a major peak at 130 ppm which is assigned to all phenolic ring positions. Phenoxy carbons are shown at 152 ppm and urea carbonyls at 161 ppm^{179,182}. Methylene bridges (o-p, p-p) of self-condensed phenolic cores display an intense double peak between 40 – 34 ppm. Methylene bridges of co-condensed phenolic and urea structures show up as a shoulder between 55 – 45 ppm¹⁸². Hydroxymethyl groups, which crosslink during heat curing, are depleted in the cured resin, and show only a small shoulder at 61 ppm.

The spectra of unmodified wood, modified wood before heat cure, and modified wood after heat cure are presented in Figure 8-6 (a-d). It is important to note that the spectra of unmodified wood and resin barely overlap, which is crucial for the analysis of relaxation times in the following section. Hence, it is reasonable to assume that in modified wood the

region between 105 – 65 ppm corresponds exclusively to wood carbohydrates, the region between 160 – 120 ppm and the peak at 40 ppm to PUF resin, and the peaks at 21 and 172 ppm to xylan. There is some degree of overlapping in the region of 65 – 50 ppm which may affect the analysis of C6 and methoxy carbons. Figure 8-6 (a) shows that there are no new peaks present in the modified wood, suggesting the absence of new covalent bonds between resin and wood²²¹.

The effect of resin impregnation and heat curing can be observed in Figure 8-6 (a). The presence of uncured resin causes an increase in the resin specific peaks at 161, 152, 130, and 40 – 30 ppm. Figure 8-6 (b) and (d) show close ups of peaks corresponding to the C4 and C6 regions. Resin impregnation (without curing) reduces the C4^{D2} and C6^{D2} signals compared to their domain 1 counterpart and leads to peak narrowing, which indicates an increase in mobility or a more organised structure. The peak at 74 ppm is shown in Figure 5 (c). The single peak present in unmodified wood splits into a double peak in the presence of uncured resin.

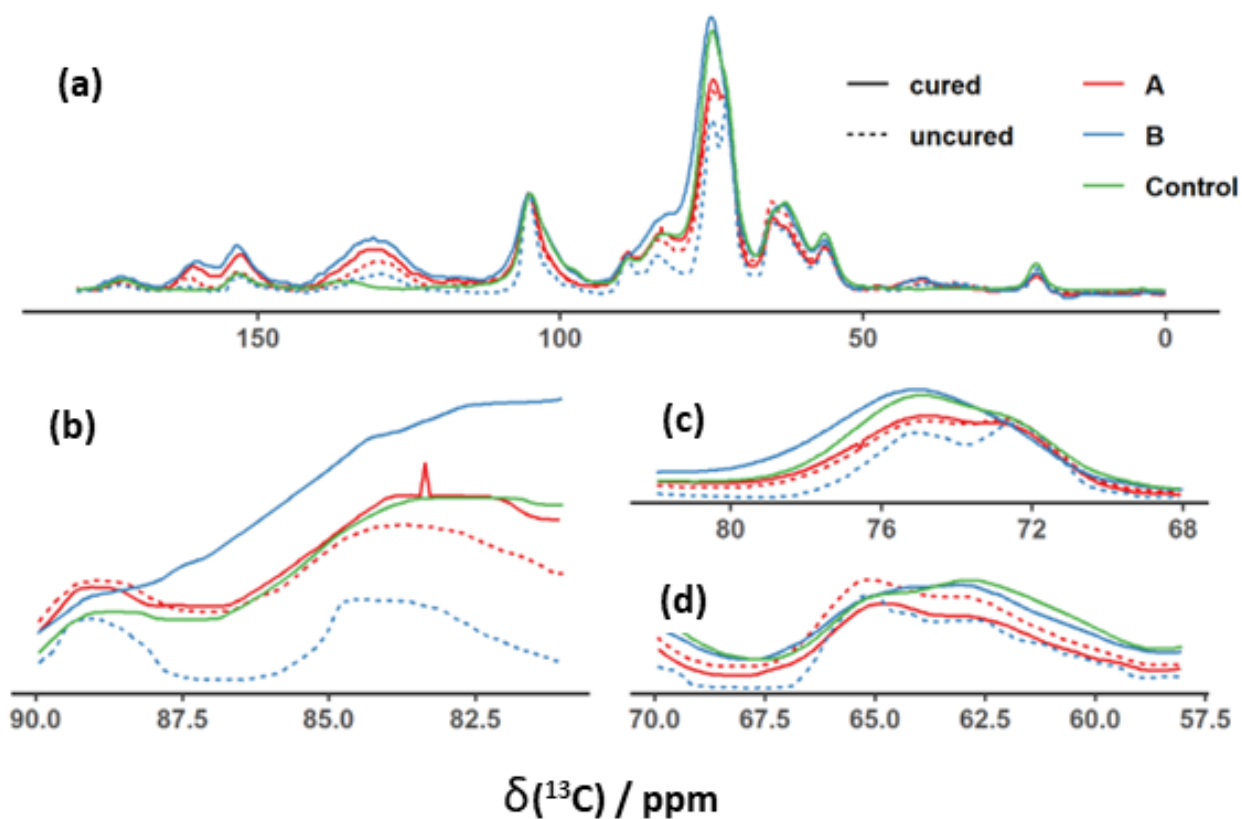


Figure 8-6 ¹H (500 MHz) ¹³C CP MAS (12.5kHz) (a) NMR spectra untreated control and modified Wood A and B before and after heat cure. (a) comparison of uncured and cured Wood A and Wood B. Dashed lines indicate spectra of resin impregnated but uncured samples. Plain lines represent spectra of heat cured wood samples. (b) close-up of the C4 signal which is divided in a C4^{D1} (89 ppm) and C4^{D2} signal (84 ppm), (c) close-up of the C2, C3, C5 signal, (d) close-up of the C6 signal which is divided in a C6^{D1} (66 ppm) and C6^{D2} (62 ppm) signal. The number of co-added transients for each experiment ranged from 812 to 1024.

After curing, resin signals at 161, 152, and 130 ppm intensify further in comparison to carbohydrate region. This likely indicates a change in the molecular mobility of the resin when its monomers polymerise on curing. The partial degradation of carbohydrates during curing might also have an effect on peak height ratios. Figure 8-6 (a - d) show the distinct behaviour of Wood A after heat curing. The cellulose domain 2 signals maintain a reduced intensity compared to their domain 1 equivalents in unmodified wood. Also, the C2, C3, C5 peak remains split in Wood A. On the other hand, cured Wood B resembles the unmodified control in the carbohydrate region of the spectrum. Significant peak broadening of the C4 and C6 signals can be observed in cured Wood B to an extent that domain 1 and 2 signals can no longer be distinguished. This indicates a decrease in mobility or a less organised structure.

The relative ratio of peak areas in the C4 region is frequently used to study the morphology of carbohydrates in wood²⁹¹⁻²⁹³. Usually, this is done after separating the sub-spectrum of cellulose from those of lignin and hemicellulose based on different $T_{1\rho}$ time constants of these components²⁹¹. In this study, no sub-spectra were obtained, therefore, we acknowledge some degree of overlapping between hemicellulose and cellulose in the region of 84 – 80 ppm²⁹². Furthermore, the ratio in this study is based on CP experiments, where the peak intensity is not fully quantitative but also depends on the molecular mobility of the components. Thus, the ratio of cellulose domains D1:D2 must be interpreted cautiously in this study. Nevertheless, we choose to include the ratio D1:D2 in Table 8-4 because it illustrates interesting differences between Wood A and B.

Table 8-4 The effect of different diffusion and drying conditions in Wood A and Wood B on their performance in ASE tests.

Sample	State	Moisture Content in %	Ratio (D1:D2)
Control	unmodified	0.00	0.34
Control	unmodified	7.48	0.50
PUF	cured	0.00	-
A	cured	0.00	0.41
A	uncured	7.93	0.70
B	cured	0.00	0.26
B	uncured	10.31	0.51

Previous studies observed an increasing ratio after resin impregnation but did not elaborate further²²². This increase corresponds to the current study where the presence of uncured resin increases the ratio significantly in Wood A and only slightly in Wood B. After cure, Wood A maintains a higher ratio than the dry control. In Wood B, the D1:D2 ratio decreases below the value of the dry control. Although it is difficult to extract clear information from this ratio, the opposite behaviour of Wood A and B indicates differences in the interaction of resin with the microfibril. The unmodified control groups show that the ratio increases upon water absorption in ambient conditions, which is in contrast to previous studies that investigated a softwood⁴⁰.

8.4.5. Solid-State Nuclear Magnetic Relaxation Time Analysis

8.4.5.1. T_1 (^1H) Relaxation Times

Table 8-5 shows T_1 (^1H) relaxation times measured by inversion recovery, which correspond to slow molecular motions of protons in the kHz range. The relaxation times in Table 8-5 are derived from the broad peak at 3.2 ppm in the ^1H MAS NMR spectrum (Appendix 46). Consequently, T_1 (^1H) provides an average for all protons in a sample and is not specific to any functional group. The plots of signal intensity against contact time generally showed very close fit to a T_1 build-up curve, as shown in Appendix 47.

Previous studies have shown that T_1 (^1H) of cellulose and lignin in wood decreases from approx. 1 s in dry conditions to less than 0.2 s at fibre saturation point²⁸⁴. This is because water molecules that are absorbed to the polymer surface transfer magnetisation between water and the polymer through “spin-spin flip flop exchange”^{281,284}. In dry conditions, however, the T_1 (^1H) relaxation occurs preferentially via the lignin methoxy group²²². This corresponds well with our

results for T_1 (^1H) in unmodified wood, where the presence of just 7.48% water lowers the relaxation time considerably from 2.1 s to 0.8 s (see Table 8-5).

Table 8-5 Proton spin-lattice relaxation times T_1 (^1H) and ratio of integrated areas under the peaks representing the cellulose domain 1 (89 ppm) and domain 2 (84ppm) signals in wood. MC is the gravimetric moisture content before the measurement.

Sample	State	Moisture Content in %	T_1 (^1H) in s
Control	unmodified	0.00	2.1 (0.06)
Control	unmodified	7.48	0.8 (0.02)
PUF	cured	0.00	1.2 (0.02)
A	cured	0.00	3.1 (0.16)
A	uncured	7.93	2.7 (0.11)
B	cured	0.00	1.3 (0.04)
B	uncured	10.31	2.6 (0.14)

Cured PUF resin has a lower T_1 (^1H) time than dry unmodified wood, with 1.2 s and 2.1 s respectively, indicating that protons in the resin are more mobile on average. Since this is not necessarily expected, the faster relaxation in the resin may be driven by a single mobile functional group, that is lowering the average. In the presence of uncured resin, T_1 (^1H) values increase to 2.7 s in Wood A and to 2.6 s in Wood B, which is an increase beyond the level of dry wood (2.1 s) and pure resin (1.2 s).

The T_1 (^1H) relaxation times of uncured Wood A (2.7 s) and Wood B (2.6 s) are similar at this stage of the process (i.e., uncured state). This increase is evident despite an ambient moisture content suggesting that the relaxation mechanism via water is hindered in both treatments. A similar trend was observed in previous studies where the T_1 (^1H) relaxation time of Japanese cypress wood increased from 1.2 s to 2.1 s after PF resin impregnation²²¹. Variations to literature values are likely caused by different resin formulations and different chemical wood composition of hardwoods and softwoods. To restrict the relaxation via water, the resin must be in close contact to the microfibril and disturb the formation of hydrogen-bonds with the tightly bound water. Previous work has shown that the T_1 (^1H) relaxation time of isolated cellulose increases with its potential to form hydrogen-bonds as a function of the pH value²⁹⁴. In other words, the presence of hydrogen-bonding restricts molecular motions in the bonding polymers which leads to a longer T_1 (^1H) relaxation time. Therefore, hydrogen-bonding between uncured resin and carbohydrates could also play a role in the increased T_1 (^1H) relaxation time of uncured Wood A and Wood B.

After heat curing, Wood A and B act in diametrically opposite ways. The T_1 (^1H) time of Wood A increases from 2.7 s before curing to 3.1 s after curing. An increase of T_1 (^1H) time upon curing has not been previously observed and suggests that *in situ* resin cure restricts proton mobility in Wood A. Whilst the T_1 (^1H) time of Wood B decreases from 2.6 s before curing to 1.3 s after curing, which is faster than the T_1 (^1H) time for our control of dry unmodified wood. The decrease in the T_1 (^1H) time of Wood B upon curing is known in the literature²²² and is a result of the averaging of the T_1 (^1H) relaxation times of dry unmodified wood and pure resin. Therefore, in Wood A, the interaction between wood and resin leads to an increased relaxation time, beyond the level of both individual components. This suggests that the resin and wood create a nanoscale composite at a scale of > 30 nm, which has different properties to the individual components. Whereas, in Wood B, the resultant average of wood and resin T_1 (^1H) relaxation times indicates that the resin and wood might co-exist at a nanoscale but do not interact substantially as in Wood A.

8.4.5.2. $T_{1\rho}$ Relaxation Times

Figure 8-7 shows $T_{1\rho}$ relaxation times measured in the ^{13}C CP MAS NMR experiment. Each value in the Figure corresponds to a peak in the ^{13}C spectrum and is specific to a certain functional group. $T_{1\rho}$ corresponds to fast molecular motions of protons in the MHz range. The numerical values corresponding to the Figure below are shown in Appendix 48 and an example of the data fit is shown in Appendix 49.

Previous studies on unmodified wood with a moisture content of 35% show that the $T_{1\rho}$ relaxation times of hemicellulose and lignin are highly correlated suggesting compatibility on a nanoscale, while the $T_{1\rho}$ relaxation of cellulose is typically longer, both in dry and wet conditions^{281,284}. Newman (1992) measured a $T_{1\rho}$ relaxation time of 7.2 ms at 89 ppm for C4^{D1} and 3.9 ms at 56 ppm for the lignin methoxy group in wet Radiata pine samples²⁸⁴. The same study noted that $T_{1\rho}$ relaxation mechanism via water is more significant in lignin and hemicelluloses than in cellulose. Most of these observations about unmodified wood correspond well with our results in Figure 8-7.

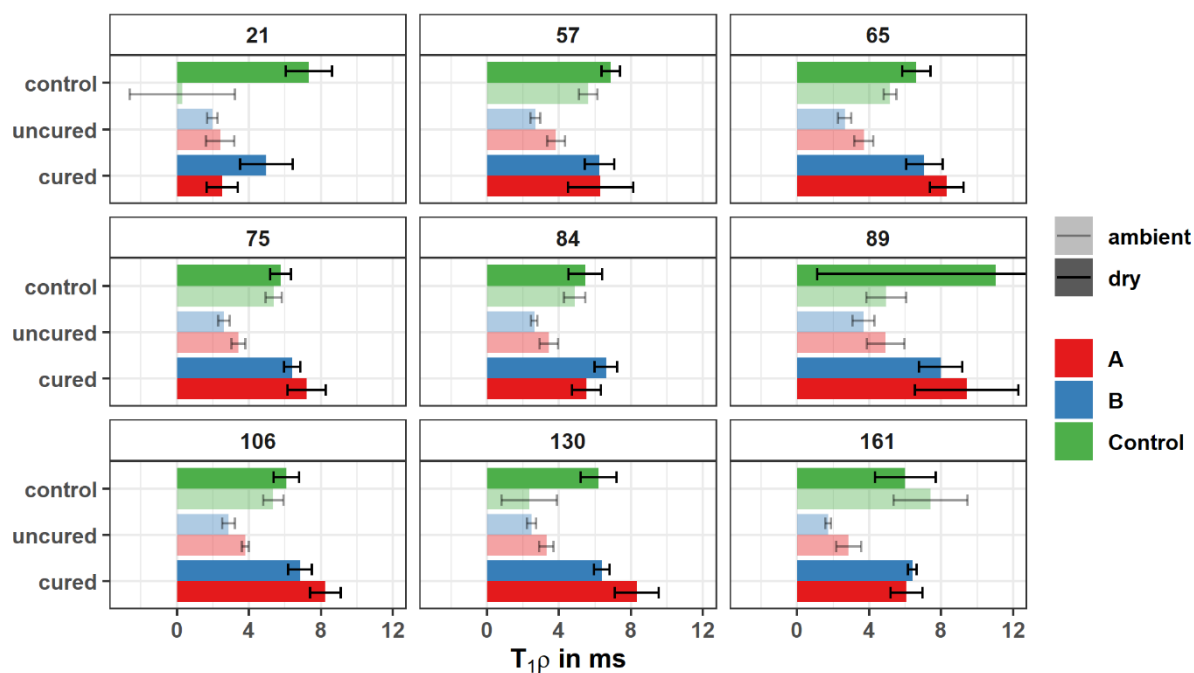


Figure 8-7 ^1H (500 MHz) $T_{1\rho}$ of unmodified control, uncured, and cured samples of Wood A and B. Each sub-plot shows $T_{1\rho}$ for the resolved ^{13}C peaks in the ^{13}C CP MAS NMR spectrum (see Figure 8-5). The unmodified control was tested at two moisture contents to account for the effect of water in the cell wall. All uncured samples were tested at ambient condition and all cured samples were tested at dry conditions. The chemical shift at 21 ppm represents the hemicellulose methyl acetate group, 57 ppm represents the lignin methoxy group, shifts between 106 – 65 ppm represents holocellulose, and chemical shifts between 161 – 130 ppm represent PUF resin relaxations. Note that for illustration reasons, the lignin signals of unmodified wood at 136 ppm and 153 ppm are included in the panels 130 ppm and 161 ppm, which are the prominent signal in modified wood.

The $T_{1\rho}$ relaxation times in the dry control are consistently between 6 – 7 ms indicating that cellulose, lignin, and hemicellulose are spin-coupled in dry conditions. Changing the moisture content from dry to ambient conditions has two effects on the unmodified control. For one, $T_{1\rho}$ decreases in all parts of the spectrum (except 161 ppm) suggesting faster molecular motions of protons²²¹. The second feature is a phase separation between slower cellulose signals (105 – 60 ppm) and faster lignin and xylan signals (136 ppm and 21 ppm), which display a more pronounced decrease in the presence of water^{281,284}. This phase separation in the ambient moisture state corresponds well with a more recent model of the hydrated cell wall, where the absorption of water disturbs the interface between the lignin-hemicelluloses phase

and the cellulose phase⁴⁰. An illustration by Cresswell⁴⁰ et al. (2021) is included in Figure 8-8 to demonstrate how water and drying affect wood at the level of the microfibril.

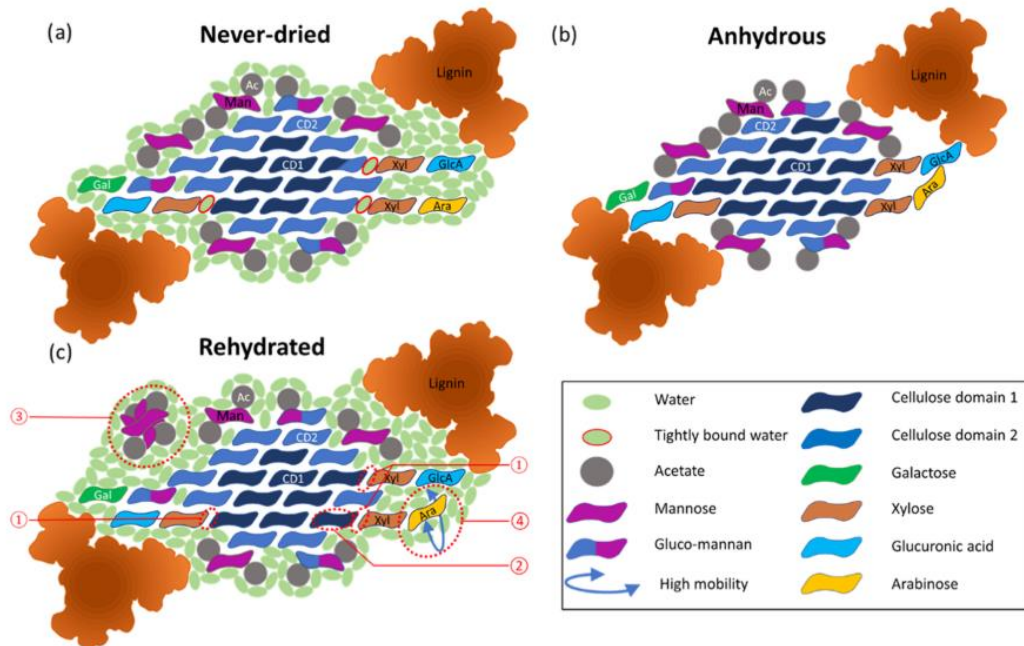


Figure 8-8 In the hydrated state, the microfibril consists of cellulose surrounded by a matrix of hemicellulose and lignin, with water molecules tightly bound at the cellulose-xylan interface. Dehydration causes matrix collapse, leading to size shrinkage and closer proximity of lignin to cellulose. Upon rehydration, the microfibril expands, but certain changes persist: the xylan-cellulose interface remains unrehydrated, some cellulose retains a non-domain 2 conformation, a fraction of galactoglucomannan (GGM) molecules becomes more mobile, and arabinose side chains show increased order. Image from Cresswell⁴⁰ et al. (2021).

In the presence of uncured resin, $T_{1\rho}$ values in the carbohydrate region (105 – 60 ppm) decrease slightly compared to the ambient untreated control, hence, uncured resin enhances the fast molecular motions in this region, in contrast to the slow molecular motions, represented by T_1 (^1H), which are restricted (see Table 8-5). The same trend was observed by Nishida et al. (2017), although in their study the $T_{1\rho}$ relaxation time of the 75 ppm signal, for both modified and unmodified wood, was generally longer than in the present study with 10 – 17 ms²²¹.

In uncured Wood A, the $T_{1\rho}$ relaxation times of lignin (57 ppm), cellulose C1, C2, C3, C4^{D2}, and resin (130 ppm) are all in the range of 3 – 4 ms, which could be caused by spin-diffusion though close spatial proximity. The hemicellulose methyl acetate (21 ppm) in uncured Wood A has a faster $T_{1\rho}$ relaxation time (2.5 ms) than the other cell wall constituents as it is a side chain, which will always be more mobile than the polymer backbone. The relaxation pathway via water might still be effective in the hemicelluloses of uncured Wood A. The $T_{1\rho}$ relaxation time of cellulose C4^{D1} is notably slower than the rest of the sample with 4.9 ms. Hence, with a difference of 1.5 ms between 84 ppm and 89 ppm, it is likely that the two cellulose domains are not spin-coupled, which would align with the observations from Laborie²²⁰ (2002). This implies that core of the microfibril displays distinct molecular motions compared to the surface of the microfibril, most likely because the surface interacts with the resin fraction. The trends in uncured Wood B are similar to those of Wood A, with the only difference being that the $T_{1\rho}$ relaxation times are typically 0.5 – 1 ms shorter than in uncured Wood A (see Appendix 48).

After heat curing, the $T_{1\rho}$ relaxation time increases to a level similar to or slightly beyond that of unmodified dry wood in most parts of the spectrum. The literature shows that $T_{1\rho}$ of pure resin increases with the degree of crosslinking as the molecular mobility decreases, which is consistent with our study²⁹⁵. In cured Wood A, cellulose C1, C2, C3, C5 and

resin (130 ppm) have a similar $T_{1\rho}$ relaxation time between 7.2 – 8.3 ms. Lignin (57 ppm), cellulose C4^{D2}, and the resin carbonyl (161 ppm) might constitute a slightly more mobile phase with $T_{1\rho}$ between 5.5 – 6.3 ms. Cellulose C4^{D1} has a notably longer $T_{1\rho}$ relaxation time of 9.2 ms, which indicates that the phase separation between domain 1 and 2 persists after cure, however, the error in Wood A is relatively high. Surprisingly, after curing Wood A, the $T_{1\rho}$ relaxation time of hemicellulose is still as low as in the uncured state - only 2.5 ms. This suggests that the molecular mobility of the hemicellulose fraction is less affected by heat curing in Wood A. Despite the increased mobility of the methyl acetate group, due to being a sidechain on the xylan, it is clear that the $T_{1\rho}$ is affected differently in Wood A and Wood B.

The trends upon curing in Wood B are slightly different, mainly because the $T_{1\rho}$ relaxation time of all components are in a much closer range. Except for hemicellulose and C4^{D1}, all $T_{1\rho}$ relaxation times are between 6.2 – 7.1 ms. The hemicellulose fraction has a $T_{1\rho}$ relaxation time of 5 ms and is therefore slightly less mobile than in Wood A. The $T_{1\rho}$ relaxation time of C4^{D1} is 8 ms, which indicates a more mobile cellulose domain 1 in cured Wood B compared to cured Wood A.

8.4.5.3. T_1 (¹³C) Relaxation Times

The T_1 (¹³C) relaxation times were measured by the Torchia method in the ¹³C CP MAS NMR experiment. These values are specific to certain functional groups and represent the slow molecular motions of carbon (kHz range). Figure 8-9 shows the T_1 (¹³C) relaxation times at different chemical shifts, Appendix 50 shows the numerical values, and Appendix 51 shows an example of the data fit.

Previous studies on unmodified wood have shown that T_1 (¹³C) relaxation times of cellulose and hemicellulose decrease with a growing moisture content^{221,281}. In the case of hemicelluloses, where T_1 (¹³C) is more sensitive to the presence of water, that can be explained by a moisture induced glass transition around 15% moisture content²⁹⁶. The trend from the literature is partly confirmed in our study as the T_1 (¹³C) relaxation times for the lignin methoxy group (57 ppm), and the cellulose positions C2, C3, C5, and C6 decrease slightly in ambient conditions. The T_1 (¹³C) relaxation times of the other signals in the spectrum displayed a high error, which is similar to other studies^{220–222}.

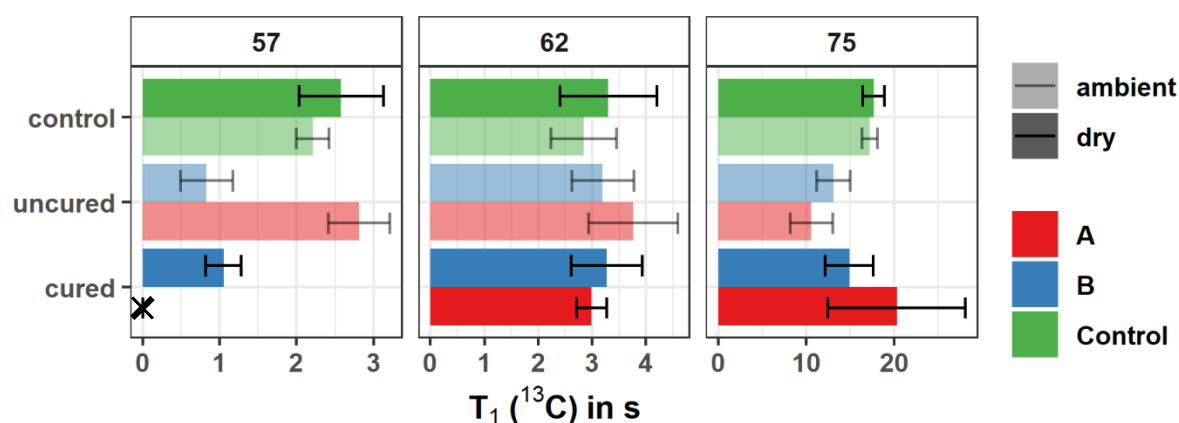


Figure 8-9 ¹³C (125 MHz) T_1 (¹³C) of unmodified control, uncured, and cured samples of Wood A and B. Each sub-plot shows T_1 (¹³C) for the resolved ¹³C peak in the ¹³C CP MAS NMR spectrum (see Fig. 3). The unmodified control was tested at two moisture contents to account for the effect of water in the cell wall. All uncured samples were tested at ambient condition and all cured samples were tested at dry conditions. The chemical shift at 57 ppm represents the lignin methoxy group, chemical shifts between 62 ppm and 75 ppm represent holocellulose. Chemical shifts between 160 – 105 ppm did not give credible results and are therefore not included. Missing values are indicated by a X-symbol.

Previous literature suggests that the presence of uncured resin prolongs T_1 (^{13}C) at 74 ppm, whereas absorbed water shortens T_1 (^{13}C) at 74 ppm²²¹. Nishida et al. (2017) measured a T_1 (^{13}C) relaxation time of 28 – 35 s at 74 ppm for unmodified wood at different moisture contents. In their study, the presence of uncured resin (20% w/w) caused an increase to 53 s when measured in dry conditions, however, in the ambient uncured state, T_1 (^{13}C) was 34 s. Hence, the effects of water and uncured resin on the T_1 (^{13}C) relaxation time at 74 ppm counterbalance each other.

Figure 8-9 shows that in this experiment, the T_1 (^{13}C) relaxation time at 74 ppm is generally shorter in uncured wood than in the unmodified wood. The effect of moisture on 74 ppm seems to be minor as the T_1 (^{13}C) relaxation time is the same value for the ambient and dry control group. In contrast to previous work, uncured resin seems to reduce T_1 (^{13}C) of C2, C3, C5. Concerning, the T_1 (^{13}C) relaxation time of C6, the literature suggest that this value should be in a similar range to the lignin methoxy group and that both C6 and methoxy are one order of magnitude faster than C2, C3, C5. This is confirmed for the present study, but the high deviation in the C6 signal allows no further discussion of trends.

An interesting trend is observed in the lignin methoxy group at 57 ppm. In uncured Wood B, the T_1 (^{13}C) relaxation time at 57 ppm decreases from 2.2 – 2.6 s in the controls to 0.8 s in the presence of uncured resin. This decrease is not observed in Wood A and indicates that resin in Wood B is more associated with the lignin fraction at a scale of > 30 nm. This could be either within the secondary cell wall or in the middle lamella. After heat curing the T_1 (^{13}C) relaxation time of lignin in Wood B remains lower than in the control groups (1.1 s). Further statements about the effect of heat curing on T_1 (^{13}C) cannot be made due to the high experimental uncertainty.

8.4.6. Discussion of Solid-State NMR Results

Based on observations from this chapter, a model regarding wood-resin interactions is proposed, which is illustrated in Figure 8-10 and Figure 8-11. The microfibril is presented as previously described by Terrett³⁸ et al. (2019) containing several microfibrils with a 2-3-4-4-3-2 arrangement of cellulose chains. Parts of the hemicelluloses are directly absorbed to the microfibril surface via hydrogen-bonding, while other parts exist more independently, forming a matrix between microfibrils. Lignin encrusts the microfibril and is in direct contact of with some of the bound hemicelluloses. This model is extended by Cresswell⁴⁰ et al. (2021) for the hydrated cell wall, where adsorbed water acts as a structural element in the microfibril. Water absorption disturbs the lignin-hemicellulose and cellulose interface. Hydrogen-bonding between water and the surface of the microfibril changes the C4^{D2} conformation to C4^{D1} in some cellulose chains. Resin penetrates the interface region between cellulose and hemicellulose, where it breaks existing hydrogen-bonds and deacetylates parts of the hemicelluloses as described by Nishia²²¹ et al. (2017). It is known from the literature that an disproportionately high concentration of bound water in the cell wall is found at the interface of cellulose and hemicellulose, and that this interface plays an important role in the absorption of water as well as in the swelling and shrinking of the cell wall^{297,298}.

In our model, we distinguish two fractions of resin in the cell wall. It is proposed that one resin fraction is located directly in the interface region between cellulose and hemicellulose. The second resin fraction is also located inside the cell wall and probably inside the microfibril, but it is not in direct contact with the microfibril surface. It is assumed that the atmospheric conditions applied to Wood A have favoured the diffusion of resin to the interface region. In Wood B, however, diffusion conditions have probably disfavoured the resin diffusion to the interface region, leading to a higher proportion of the second resin fraction.

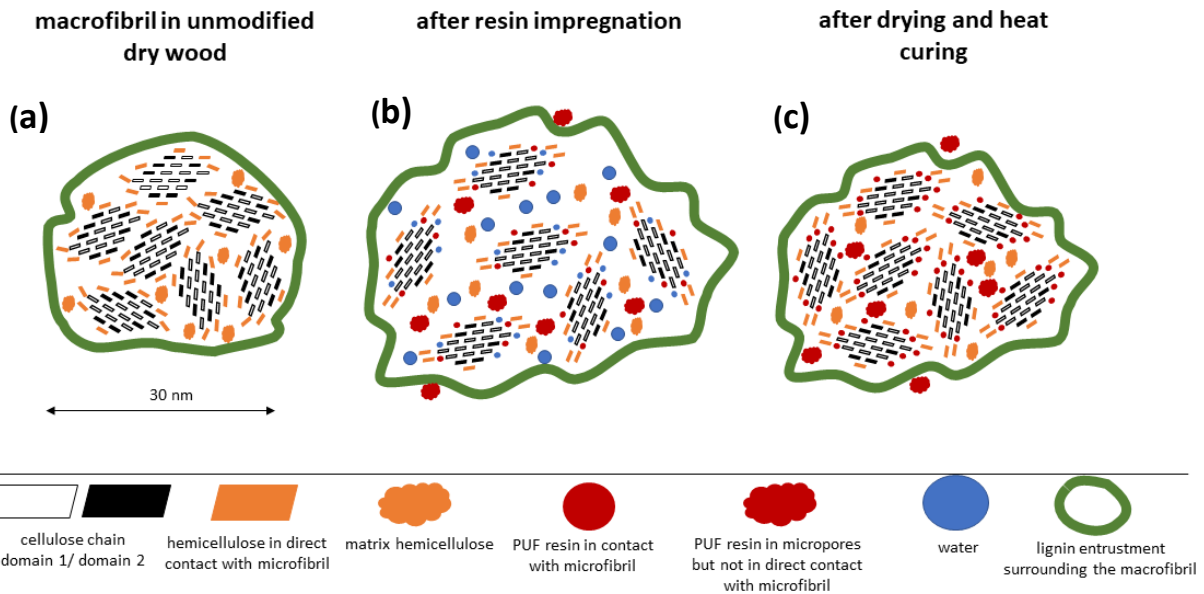


Figure 8-10 (a) The macrofibril in different stages of the resin treatment. In the dry unmodified state, the macrofibril and microfibrils are illustrated according to recent literature^{38,40}. (b) Upon resin impregnation, both water and resin molecules create micropore spaces between the microfibrils. One fraction of the water is close contact with the microfibril surface, while another fraction is not closely associated with it. These water populations have been called NFBW and FBW in Chapter 8.4.3. Similarly, it is proposed that resin occurs in at least two distinct populations. Resin in direct contact with the microfibril disturbs hydrogen-bonding between water and cellulose causing T_1 (^1H) to increase and the NFBW content to decrease. The disruption of hydrogen-bonding at the microfibril interface might cause some cellulose chains to change from domain 1 to domain 2. The other fraction of resin located in the micropores is responsible for micropore blocking. Resin in micropores is more closely associated with matrix hemicellulose and lignin. (c) After heat curing, the resin induces a cell wall bulking effect.

Previous studies have specialised on the softwood cell wall, which has a different chemistry than the hardwood cell wall in terms of hemicelluloses and lignin composition²⁷. This is mentioned here because it might influence the current study, where tulipwood – a hardwood was used. Nevertheless, our results for unmodified wood confirm many aspects of these models. In the dry control group, all cell wall polymers are in the same morphological phase of 2 – 30 nm as suggested by a common T_{1p} relaxation time between 6 – 7 ms. Water absorption in the control leads to a phase separation as the mobile lignin-hemicellulose phase is pushed away from the more rigid cellulose phase. The cellulose domains 1 and 2 have a common T_{1p} relaxation time in ambient conditions and are therefore in the same morphological phase. In ambient conditions, water adsorbed to the microfibril transfers magnetisation via spin-spin relaxation and thereby decreases the T_1 (^1H) significantly compared to the dry state. The decrease of T_1 (^{13}C) at 21 ppm indicates a softening of hemicelluloses in ambient conditions (Appendix 50).

Both modified timbers display a very different behaviour to the control groups indicating various changes in the molecular architecture of the cell wall. In uncured Wood A, we observed peak narrowing of both C4 signals indicating an increase in mobility or a more ordered structure. The ratio D1:D2 shifts towards domain 1 and T_1 (^1H) becomes higher than in the controls, indicating that relaxation via water is restricted. The three observations can be interpreted so, that the uncured resin breaks hydrogen-bonds between hemicellulose and cellulose and penetrates the region of the microfibril. There it restricts the formation of strong hydrogen-bonds between water and cellulose, so that T_1 (^1H) is much higher than in the unmodified control. In Terrett³⁸ et al.'s (2019) model, hydrogen bonds between glucomannan and the microfibril surface induce a conformational change in certain cellulose chains on the surface, adopting a domain 1 conformation, while most cellulose chains on the microfibril surface are domain 2. Since previous work has shown that hydrogen-bonds at the hemicellulose-cellulose interface are broken down in the resin treatment²²¹, it is possible that some domain 1 cellulose chain on the surface of the microfibril convert to a domain 2 conformation, similar to the

effect of drying in Cresswells⁴⁰ model. The likely change from cellulose domain 1 to domain 2 could also mean that microfibrils collapse upon each other, which would increase the ratio D1:D2 of microfibril core to surface (Table 8-4).

At the microfibril interface, the uncured resin has a plasticising effect on the cell wall, decreasing both $T_{1\rho}$ and T_1 (¹³C) of cellulose C2, C3, C5, hemicellulose methyl acetyl, and lignin methoxy. This plasticising effect explains the pliable character of uncured wood. The stark difference between $T_{1\rho}$ of C4^{D1} and C4^{D2} indicates a phase separation of the two cellulose domains, although it is unlikely that the distance between domain 1 and 2 has increased by more than 30 nm. A more reasonable explanation is that domain 2 interacts more intensely with the uncured resin than domain 1, e.g., by hydrogen-bonding, non-polar interactions, or steric hinderances. The separate hemicellulose phase with a much lower $T_{1\rho}$ relaxation time seems to be less affected by interactions with the resin. Even after heat curing of Wood A, the $T_{1\rho}$ relaxation time of hemicellulose remains on a very low level, indicating high mobility. The microfibril interface region, however, has gone from plastic to rigid after heat curing. T_1 (¹H) of cured Wood A increases beyond the level of both individual components (i.e., resin and dry wood) indicating the formation of a rigid nanoscale composite at a level of > 30 nm. This is currently interpreted as a macrofibril that is uniformly penetrated by a crosslinked resin matrix. The heterogenous $T_{1\rho}$ indicates phase differences within the macrofibril (2 – 30 nm).

Whilst Wood B shows many similar trends to Wood A there are also some significant differences (Figure 8-11). The ratio D1:D2 is less affected by the presence of uncured wood and becomes even lower than in the control groups after curing of Wood B. The T_1 (¹H) relaxation time, which has a similar value to Wood A in the uncured state, decreases after cure and reflects a weighted average of T_1 (¹H) relaxation times of dry wood and cured resin. This is interpreted as coexistence rather than interaction of both components on a level of > 30 nm. Thus, at the level of the macrofibril and above, there might exist resin phases and wood phases that are largely separated. On a level of 2 – 30 nm, cured Wood B might be more homogeneous than Wood A, since the $T_{1\rho}$ relaxation times are in a closer range.

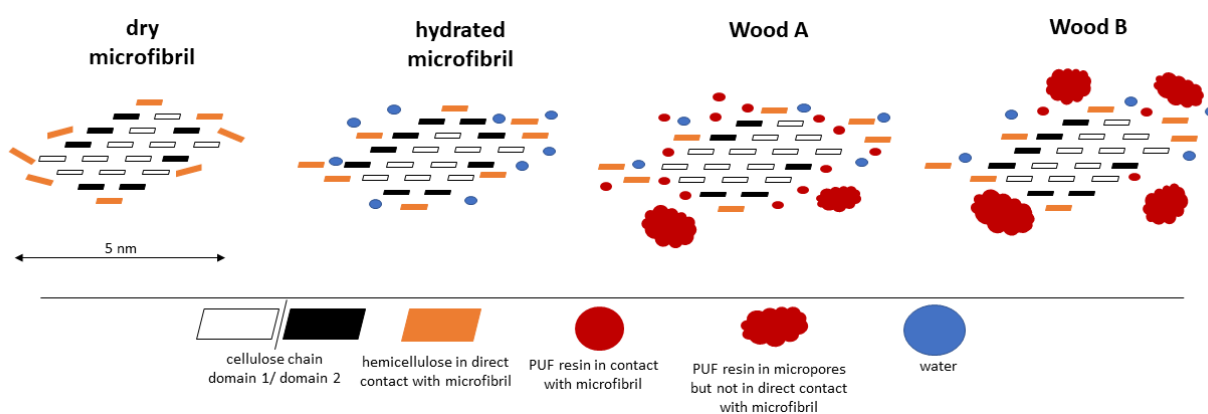


Figure 8-11 The main difference between Wood A and Wood B could be the relative content of both resin populations, where Wood A contain more resin that is in direct contact with the microfibril, and Wood B contains more resin in micropores that is more associated with matrix hemicelluloses and lignin. Atmospheric conditions applied to Wood A have promoted the diffusion to the microfibril surface and subsequent curing in this location. Conditions applied to Wood B have potentially favoured resin agglomerations in the micropores.

The hemicellulose fraction in cured Wood B is not as mobile as in Wood A, since the $T_{1\rho}$ is twice as long in Wood B. This might indicate that the matrix hemicellulose is more closely incorporated in the resin network in cured Wood B, whereas it is virtually unaffected in Wood A. The T_1 (¹³C) relaxation time of lignin constitutes a major difference between Wood A and Wood B. Uncured resin in Wood B shortens T_1 (¹³C) beyond the level that is achieved by water. In Wood A, the lignin fraction is much less affected by uncured resin. This might indicate that the resin in Wood B is located closer to lignin-rich areas in the cell wall, such as the entrustment of the macrofibril or the middle lamella.

The different behaviour of Wood A and B is caused by the different atmospheric conditions in the drying stage, which changes the way of cell wall diffusion for both timbers. In Wood A, the high diffusion temperature increases the mobility of resin molecules, and the high relative humidity readily swells the micropore spaces in the cell wall. The resin in Wood A penetrates the interface of the microfibril to a greater extent and is therefore in closer contact with the cellulose, compared to resin in Wood B. The penetration of this interface can be related to both the greater reduction in swelling²⁹⁷ and to the more effective decrease of NFBW in Wood A. The resin diffused into the cell wall of both Wood A and Wood B, as shown by the positive BU and the similar MBE. However, within the cell wall, the resin migrates to different locations. In Wood A there seems to be a preference for the microfibril interface and in Wood B for the lignin-rich areas and matrix hemicelluloses.

Differences between Wood A and Wood B are evident, but the data presented in this study leaves room for interpretation. More evidence would be needed to clarify the exact locations of resin after cell wall diffusion. Further work with ¹³C enriched PUF resin could provide a much greater deal of information by enabling the use of quantifiable (e.g., DP-MAS NMR) and 2-dimensional NMR techniques (e.g., CP INDADEQUATE NMR).

8.5. Conclusions from Chapter 8

Two identical sets of resin impregnated wood were dried under different temperature and humidity conditions. This was shown to promote (Wood A) or restrict (Wood B) the cell wall diffusion of resin monomers. The resin-wood interactions were monitored on a macro scale (using ASE tests), on a micro scale (using SEM), and on a sub-micro scale (using DSC and NMR).

ASE tests in this chapter have shown that:

- Wood A and B contain the same gravimetric amount of resin which implies that differences between groups are due to differences in resin cell wall diffusion.
- The BU of Wood A is 37% higher than in Wood B.
- S_{mod1} is 16% lower in Wood A than in Wood B.
- The initial volume increase during diffusion and drying is higher in Wood A than in Wood B.
- Wood A dries slower than Wood B due to the higher relative humidity schedule.

SEM observations have shown that the resin agglomerates to form distinct shapes in Wood A and B, which might hint towards differences in resin mobility. Isothermal and dynamic DSC scans have shown on a microscopic level that:

- Micropore blocking occurs to a similar extent in both Wood A and Wood B.
- Micropore blocking occurs mainly in pores with diameter smaller than 30 nm.
- The amount of tightly bound water (NFBW) is reduced significantly in both test groups compared to the unmodified control.
- but the NFBW content is reduced slightly more in Wood A than in Wood B.

Generally, in Wood A the resin seems to interact more intimately with the cell wall polymers than in Wood B. While a similar amount of resin was present in the cell walls of both sets, the resin seems to be differently arranged on a sub-microscopic level. NMR observations and relaxation time analysis indicate that:

- Inside the cell wall, there are at least two resin populations, which interact differently with the wood polymers.

- One resin population is in direct contact with the microfibril surface (this fraction reduces the amount of NFBW more notably).
- The other resin population occupies micropores in the cell wall but is not in direct contact with the microfibril surface.
- Both resin populations are present in Wood A and B, however, it can be assumed that relative share of each population differs between Wood A and B.
- The resin in Wood A diffused preferentially to the microfibril interface, where existing hydrogen-bonds are broken down and replaced by a resin matrix.
- In Wood B, the resin diffused preferentially to the lignin-rich and matrix hemicellulose areas within the macrofibril.
- In Wood B, a smaller amount of resin is in direct contact with the microfibril interface.

This explanation would be consistent with the ASE and thermoporosimetry data, but further research is needed to understand the resin arrangement at the lowest level of scale. An improved understanding of the resin cell wall diffusion process could help to optimise the drying process of resin modified wood on a commercial level.

9. Discussion

This discussion chapter is separated into three parts. The first part provides a recapitulation of the state-of-technology in wood modification with thermosetting resins, illustrating how this thesis contributes to the current scientific consensus in the field. The second part conducts a critical review of the methods employed in this thesis, presenting alternative techniques that could be explored in future investigations. Lastly, the third section delves into potential future developments around wood modification with thermosetting resins.

The following hypotheses have been tested throughout various chapters of this thesis. This discussion chapter details how exactly each of these hypotheses could be answered.

- The efficiency of the resin modification process depends on the choice of wood species.
- Chemical and non-chemical interactions between wood and resin influence the efficiency of the resin modification process.
- Process conditions in the impregnation, drying, and heat curing stages of the resin modification process impact on the properties of the resin modified wood.

9.1. Significance of this Thesis

The focus of this thesis is the modification of solid wood using a low molecular weight phenol urea formaldehyde (PUF) resin. This process, along with related techniques using alternative resins such as furfural alcohol (FA), melamine formaldehyde (MF), or 1,3-dimethylol-4,5-dihydroxyethyleneurea (DMDHEU), belongs to the broader category of recently developed wood treatments known as resin wood modification. While thermal wood modification and acetylation are more established in the commercial realm, resin modifications remain relatively limited in production volume. This limitation can be attributed to the complex multistep production process, contributing to elevated investment and production costs.

Despite these challenges, resin modified wood exhibits notable features that justify continued exploration in research endeavours. The material demonstrates high biological durability in above-ground, ground-contact, and marine applications, coupled with high dimensional stability and an aesthetically pleasing appearance. Notably, PUF resin modified wood, previously produced by *Lignia Wood Company Ltd.*, has secured a Class A certification in fire retardancy testing following ASTM-E 84 standards²⁹⁹. Given these promising features, resin modified wood has the potential to find a specialised place in the market. Yet, to fully leverage this potential, it is crucial to gain a more nuanced understanding of specific aspects of the modification process.

The chapters within this thesis contribute distinct insights to the current state-of-technology. Chapters 3 and 4 were designed to establish the groundwork for subsequent chapters by comprehensively characterising both wood and resin.

Notably, certain findings in Chapter 4 represent novel contributions not previously documented in the literature. The investigation of resin curing reactions in both open and closed systems is novel. The results from differential scanning calorimetry (DSC) and Fourier-transform infrared spectroscopy (FTIR) in this chapter revealed variations in the resin curing rate, degree of cure, and the morphology of the cured resin between both systems. Consequently, these results could bear significance for commercial processes operating in both open and closed pressurised systems, as discussed in Chapter 2. Additionally, Chapter 4 revealed the influence of the resin pH value on the curing rates and the nature of the formed bonds.

In Chapter 5, the role of different wood species in the modification was investigated. The comparison of eleven wood species in an identical treatment is a novel contribution to the state-of-technology and has not been published before. A noteworthy discovery from Chapter 5 is the correlation between the anti-swelling efficiency (ASE) and the hemicellulose and lignin content of different wood species. Another highlight is the observation that the total swelling of resin-modified wood, encompassing both cured resin and water, surpasses that of unmodified wood subjected to water alone. Both findings bear significance in the theoretical framework of this modification, presenting novel insights absent in existing literature and challenging previous assumptions.

However, when considering only the swelling coefficient post-modification (S_{mod}), the majority of wood species in Chapter 5 showed relatively constant values, typically ranging between 6 – 8%. Exceptions were limited to beech with an S_{mod} value of 9.4% and willow with 4.5%. While these findings suggest general suitability at the laboratory scale, it is crucial to recognise the distinct challenges posed by industrial application.

On an industrial scale, where plank-sized specimens undergo modification, it is widely recognized that limited treatability of the timber during impregnation and frequent failures during kiln drying and heat curing stages are significant limiting factors. Additionally, heat transfer into plank-sized specimens creates a notable gradient in temperature and moisture content between the core and surface regions of the plank. Moreover, controlling temperature and relative humidity (RH) in an industrial kiln or reactor, filled with several cubic meters of impregnated (wet) timber, is more difficult than in a small laboratory oven. Consequently, precision in managing temperature and RH, as well as ensuring a uniform distribution of both conditions across the reactor, becomes a challenge in the industrial process.

As a result, it was difficult to identify parameters that might entirely restrict the use of certain wood species within the confines of laboratory-scale testing in this thesis. The small specimen size throughout the experimental chapters allows for an assumption of complete resin penetration, the absence of a temperature and moisture content gradient during drying and heat curing, and precise measurements of process conditions. None of these assumptions can be made for the resin modification on the industrial scale.

Provided that these problems associated with the treatability and drying can be solved, the results from Chapter 5 suggest that S_{mod} values between 6 – 8% could be reached for most species, despite differences in their chemical composition or anatomy.

Nevertheless, in the upscaling process, it is advisable to tailor process conditions for each new wood species, considering variations in density, alkaline buffer capacity (ABC), chemical wood composition, or wood anatomy. Chapter 6 provides a demonstration of this approach using small specimens with the dimensions 20 (r) x 20 (t) x 5 (l) mm. In this Chapter various wood species underwent treatment with different curing times, resin concentrations, and resin pH values. It was shown that prolonged curing periods at 150°C negatively impacts BU and S_{mod} in all specimens, with varying sensitivity among species. The influence of resin concentration is species dependent. Chapter 6 results also indicated the existence of an optimum resin concentration between 20 – 40% for each of the three wood species, resulting in minimal values for S_{mod} and maximum BU. Consequently, a screening test with different resin concentrations is recommended for the upscaling of each new wood species considered for commercial production.

Another process variable that could be of interest is the pH value of the resin. Throughout various chapters in this thesis, it has been demonstrated that the alkaline catalyst in the resin undergoes neutralisation by wood or wood constituents, resulting in a substantially slower resin curing rate. To address this neutralisation effect, one consideration was to increase the resin's alkalinity by adding potassium hydroxide before the impregnation. However, the findings in Chapter 6 demonstrated that an increased resin pH consistently diminished BU values and increased S_{mod} across four different timbers. Consequently, neutralisation of the resin by the wood may not necessitate intervention. This aligns with the observations in Chapter 5, where the ASE of a wood species was compared with its ABC. Even in wood species with the most acidic extracts (e.g., lime, Scots pine), the treatment yielded high ASE values, and the resin exhibited effective fixation, as shown by the low mass loss after water soaking. Thus, the resin achieved a sufficiently high degree of cure despite neutralisation effects.

However, the question still remains: why do BU and S_{mod} worsen with the use of a more alkaline resin in Chapter 6? This may be connected to the degradation of the cell wall during the treatment. FTIR and solution-state NMR scans in Chapter 5 have shown that the hemicellulose fraction undergoes deacetylation during the treatment. Such chemical interactions between wood and resin were explored in the next chapter. In Chapter 7, the occurrence of cell wall degradation during treatment was confirmed. Observations also indicated the degradation of certain lignin bonds. However, it was not possible to reconnect the extent of cell wall degradation in a wood species to its ASE (see Chapter 5).

Moreover, Chapter 7 revealed variations in the curing rates of resin impregnated into different wood species, highlighting the presence of a retardation effect induced by specific wood constituents. While the retarding influence of acidic wood extractives was previously noted, the impact of wood hemicelluloses on the curing reaction has not been previously addressed in the literature. Our current working hypothesis is that the degradation of hemicelluloses through deacetylation and peeling processes consumes the resin's alkaline catalyst, leading to a reduction in the pH value of the system and subsequently resulting in a slower curing rate.

This hypothesis introduces an unresolved dilemma in this thesis. The DSC results in Chapter 7 show unambiguously that certain wood constituents, particularly extractives and hemicelluloses, exhibit a retardation effect. Logically, one would anticipate that wood species with elevated extractives content, high ABC, or increased hemicellulose content would achieve a lower degree of cure and demonstrate inferior performance in ASE tests compared to wood species, where the curing reaction is not as much retarded by extractives or hemicelluloses. However, the findings in Chapter 5.4.4 contradict this expectation. Wood species characterised by both high ABC and high hemicellulose content achieve the highest ASE values, with a positive correlation between hemicelluloses content and ASE.

There is evidently a nuanced interplay between hemicelluloses (and other cell wall polymers) and the resin within the cell wall. The specific nature of this interaction remains unclear. Initial considerations revolved around the potential for covalent bonding between the resin and cell wall constituents. However, solution-state NMR scans in Chapter 7 effectively ruled out this possibility with a high level of confidence. Additionally, previously identified linkages between resin and G-lignin, as noted in earlier studies¹⁹⁸, could not be confirmed in this thesis. Consequently, it is suggested that the properties of resin modified wood are influenced on a micro scale by non-covalent interactions between resin and wood polymers, especially hemicelluloses, within the cell wall.

The blocking of micropores is a well-known non-covalent mechanism extensively discussed in the literature. What has not been considered in these discussions is the recent model of the molecular architecture of the cell wall, recently

studied by Terrett et al.³⁸ (2019), Cresswell⁴⁰ et al. (2021) and others, using solid-state NMR. The micropore blocking and related effects at this length scale were investigated in Chapter 8 in the light of these recent advances, and the phenomenon of resin cell wall diffusion, established in Chapter 6, was chosen as the subject of study.

Resin cell wall diffusion was shown to influence BU and S_{mod} in Chapter 6, depending only on the atmospheric conditions during the drying stage. Therefore, it was suspected that resin cell wall diffusion also affects micropore blocking or other non-covalent interactions at this length scale. Hence, a case study with three test groups was devised for Chapter 8. In one group, resin cell wall diffusion was promoted by atmospheric conditions, and in another, resin wall diffusion was restricted. A third group served as the unmodified control.

In Chapter 8, the thermoporosimetry section confirmed the occurrence of micropore blocking in both treatments of the case study. Notably, the micropores with a diameter between 2 – 100 nm are blocked to the same extent by both treatments, failing to explain the significant differences observed in BU and S_{mod} between the test groups. Conversely, a more efficient reduction in non-freezing bound water (NFBW) content was achieved when cell wall diffusion was facilitated, suggesting the existence of two resin populations in the modified cell wall—one involved in micropore blocking and the reduction of freezing bound water (FBW), and the other preventing the absorption of tightly bound water (NFBW).

The solid-state NMR section in Chapter 8 further demonstrated that the molecular motions of wood polymers differ in both treatments, strengthening the hypothesis of distinct resin populations.

Collectively, these findings contributed to a new model for the interaction between resin and wood at the nanometre length scale. In this, the existence of at least two resin populations that interact differently with wood polymers is proposed, where both resin fractions have distinct effects on the dimensional stabilisation of wood and on the wood-water interaction.

Therefore, non-covalent interactions at the microfibril surface, specifically at the cellulose-hemicellulose interface, emerge as an important factor, which contributes to the modified wood performance. The optimisation of these interactions becomes feasible through adjustments in process conditions. Additionally, these effects at the cellulose-hemicellulose interface may be involved in the previously discussed dilemma, wherein the ASE of a wood species correlates with hemicellulose content. However, further research is needed to elucidate this relationship, and potential roadmaps for future studies will be discussed in the following section of this discussion.

9.2. Critical Review of Methodology

This section provides a critical review of the methods employed and the results obtained in the previous chapters. It also explores alternative methods for future work.

In Chapter 3.4.2, the chemical composition of the wood species in this thesis was determined using classical wood chemistry techniques (see Table 3-2). Some trends are evident from Table 3-2, such as differences in the lignin and hemicellulose content of hardwoods and softwoods. However, within hardwoods and softwoods, differences are more subtle. In later chapters, it is sometimes unclear whether the chemical composition adequately explains certain trends (e.g., in the FTIR cluster analysis in Chapter 3.4.1, or in the ASE tests of Chapter 5, or in the DSC scans in Chapter 7.4.1). Future studies should measure the chemical composition with several replicates to account for measuring inaccuracies.

In Chapter 3.4.3, the ABC method employed a hot water extract for comparing the acidity of different timbers. Despite its frequent mention in literature, hot water extraction introduces degradation products, primarily acetic acid, into the extract, and their contribution to the ABC measurement remains unclear. This degradation of hemicelluloses through deacetylation may explain the elevated ABC in wood species with high hemicellulose content, such as lime and beech, due to acetic acid release. Consequently, extractions with cold water might yield differing ABC results.

Although the thesis often refers to the acetyl content in the context of cell wall degradation, and both FTIR and NMR spectroscopy validate the deacetylation of hemicelluloses in all timbers, more precise data for the acetyl content would have been desirable. Future studies could employ saponification in combination with HPLC³⁰⁰ or GC¹⁵⁴ to measure acetyl content before and after modification, possibly providing a more detailed understanding of cell wall degradation.

The extractives fraction in Chapter 3.4.4 was analysed by solution-state NMR, revealing significant differences between water extractives (ExtrW) and solvent extractives (ExtrS) within individual species, as well as variations of ExtrS and ExtrW between different species. However, this method alone does not allow for the determination of specific molecules present in the extract. The incorporation of GC-MS could have offered a more comprehensive understanding³⁰¹. This additional insight would have been particularly valuable in Chapter 7.4.1, where distinct types of extractives demonstrated varying impacts on the curing rate.

Generally, the DSC analysis in this thesis has indicated clear differences in the reaction rate among certain samples, e.g., between pure resin and resin impregnated into solid wood in Chapter 7.4.1. However, in other cases, the distinctions were more subtle and might not be captured by the curing rate (k) as a single variable. All DSC sections in this thesis rely on the Kissinger method, which makes assumptions about curing kinetics that might be oversimplified³⁰². The main issue is that the Kissinger method yields only one value for the activation energy, although it has been shown that multiple reactions occur during heat curing. A prospect for future work could be to apply a different analysis to the DSC data, for example, the model-free kinetics approach described by Vyazovskii^{303,304}. In this method, the activation energy is illustrated as a function of the degree of conversion, hence, a more detailed picture can be obtained.

The sub-microscopic localisation of resin within the modified wood cell wall presents challenges in determination. In Chapter 5, safranin staining effectively demonstrated the penetration of resin into the cell walls of beech and tulipwood. However, this method was not applied to other samples in the context of this thesis due to the complicated sample preparation and limited output, particularly in terms of the spatial resolution. More suitable techniques for future investigations in this context could involve UV-microscopy¹⁰⁸, Raman-microscopy³⁰⁵, or atomic force microscopy (AFM).

Although AFM was attempted in some samples (see Appendix 52) in this thesis, the results were constrained by sample surface roughness and the instrument's sampling mode (i.e., tapping mode). In future studies utilising AFM, meticulous sample preparation will be crucial. Successful AFM studies in the past embedded wood samples in a matrix polymer and utilised ultramicrotome sectioning to achieve a sufficiently even surface in the cross-section³⁰⁶. Promising AFM sampling modes include peak-force quantitative nano-mechanics³⁰⁶ (PF-QNM), infrared radiation¹⁰² (IR), or scanning thermal microscopy³⁰⁷ (SThM).

The ASE analysis in Chapter 5 includes eleven wood species and yields robust results. In hindsight, it would have been interesting to include additional wood species, not necessarily suitable for upscaling, but potentially beneficial in testing certain hypotheses developed during the production of this thesis. For instance, inclusion of a highly acidic timber like

oak could have provided insights into the neutralisation mechanism. Additionally, expanding the density range by including timbers like balsa (160 g/cm³) or ebony (1160 g/cm³) could have been beneficial. The value of such outlier species in understanding the active modification mechanisms is exemplified by lime wood on multiple occasions in this thesis.

The solution-state NMR analysis of the ASE soaking solution in Chapter 5.4.3 strongly suggests that resin is not leaching from the modified wood. However, a chromatography technique such as LC-MS or GC-MS could have offered more insight into the leached substances³⁰⁸, particularly in the context of wood degradation products.

An aspect that was not pursued further is the varying chemical resistance of different carbohydrates in softwoods and hardwoods towards alkaline degradation³⁰⁹. To explore the degradation of different carbohydrates in various timbers, future studies could employ high performance anion exchange chromatography^{226,310}. Using this technique, one could analyse the sugar profile of the soaking solution, enabling more accurate conclusions about leached substances and degraded carbohydrates.

In Chapter 6.4.2, the impact of the resin concentration on S_{mod} and BU is investigated after 52 hours of heat curing at 150°C. This setup enabled the simultaneous examination of curing time and resin concentration within a single experiment. However, such an extended curing time is untypical. Conducting two separate experiments, one for resin concentration and another for curing time, would have potentially yielded more precise results.

The partial least square (PLS) linear regression model in Chapter 6.4.3 serves as a proof of concept, which can be used for predicting the resin content of an unknown modified sample. In this model, eight samples were designated for the training set, and three samples were allocated for the validation set. For future studies or companies that apply this approach, it is advisable to incorporate a higher number of replicates. Expanding the dataset and employing a greater number of replicates enhances the accuracy of the model. Additionally, separating the data into calibration, validation, and test sets can contribute to improving model precision, while k-fold cross-validation could be used to further enhance its robustness. Moreover, it is worth noting that the PLS model in Chapter 6.4.3 was developed using powdered samples. If the intention is to apply the model to measure solid wood, e.g., in an industrial process, solid samples should also be considered for the calibration, validation, and test sets.

In Chapter 6.4.5, the diffusion of resin within the cell wall is investigated through a half-factorial design of experiments, encompassing four factors simultaneously, with each factor tested at only two levels. For future work, a more in-depth exploration could involve studying individual factors, such as drying temperature, across multiple levels. This approach would provide a more comprehensive understanding of the influence of each factor at varying intensities, allowing for a more detailed analysis of their impact on resin cell wall diffusion.

In Chapter 7.4.2, the chemical interactions between resin and wood were investigated after cell wall solubilisation, utilising solution-state NMR. No covalent bonds between wood and resin were detected in these NMR studies. This observation aligns with findings from other techniques, such as DSC and FTIR, and is considered reliable. An alternative high-sensitivity method that could have been used for this investigation is pyrolysis-GC-MS. In this method, a solid sample is pyrolyzed for a few seconds at 550°C, and the pyrolysis products are analysed by GC-MS^{152,308}. This method was attempted in some samples from this thesis, and the analysis was conducted by David Hentges at the University of Lorraine. Appendix 53 displays the chromatograms of unmodified lime, modified lime, and pure PUF resin. The absence

of new peaks in the chromatogram of modified wood aligns with the conclusions drawn from the solution-state NMR results. Therefore, it is assumed that no covalent bonds between wood and resin were established. While the pyrolysis-GC-MS work was not continued, it is mentioned here because it could prove useful in future investigations.

In Chapter 8.4.3, the thermoporosimetry measurements, using DSC, revealed significant differences in the freeing bound water (FBW) and non-freezing bound water (NFBW) contents, as well as in the pore size distributions of modified and unmodified wood. However, between Wood A and Wood B, the differences are more subtle. The discrepancy in the NFBW content between Wood A and Wood B is particularly interesting but small. To establish statistical significance, especially in cases where differences are expected to be subtle, it would be desirable to increase the number of replicates in future studies. This would enhance the robustness of the analysis and provide more confidence in the observed differences.

Furthermore, the determination of the pore size distribution in Chapter 8.4.3 relies on the application of the Gibbs-Thomson equation. This equation necessitates specific material constants, such as the surface tension at the ice-water interface (γ) and the contact angle of water within the cell wall (θ). However, these constants have not yet been established for water in wood. Many thermoporosimetry studies rely on assumptions about these constants, derived from the behaviour of bulk water, which differs from bound water within the cell wall. Consequently, the pore size diameters determined using the Gibbs-Thomson equation in Chapter 8 may not be exact values. While the comparative analysis of Wood A, Wood B, and the control using this method remains valid, it is important to acknowledge that the true pore size may not be accurately represented.

The relaxation time analysis in Chapter 8.4.5 revealed clear differences between the unmodified control, Wood A, and Wood B, indicating distinct molecular motions of wood polymers in all three samples. While relaxation times are relatively straightforward to measure, their interpretation can be challenging. The model proposed in Chapter 8.4.6 aligns with the experimental data and makes sense in explaining the differences between Wood A and Wood B. However, it is important to note that this model is largely based on interpretation, and there is a certain margin for error with these measurements. Further study is recommended to elucidate the wood-resin interactions at the nanometre length scale. Solid-state NMR stands out as the most suitable method for such investigations, although the spectral resolution at natural abundance of ^{13}C is relatively low. Future work could involve using ^{13}C enriched PF resin, synthesised in a laboratory, to increase signal intensity by approximately 100 times. This enhancement would enable additional solid-state NMR experiments such as CP INADEQUATE, CP HETCOR, or DD-MAS, providing more detailed insights into the molecular arrangement of resin in the cell wall³⁸. These experiments could be coupled with molecular dynamics simulations⁴⁰, which holds the potential to significantly enhance our understanding of modification mechanisms in modified wood (not only resin modified wood). While the study of wood modification with solid-state NMR under ^{13}C enriched conditions is not currently a subject of research, it represents a promising avenue for future work.

9.3. Outlook and Possible Future Developments

Wood modification is poised to play an important role in the future of the wood products industry¹⁶. Whether the utilisation of low molecular thermosetting resin will emerge as a commercially relevant technique in this picture remains uncertain, despite numerous advantages of the material.

While this thesis has concentrated on the dimensional stability and fundamental aspects of resin modified wood, the following outlook section explores the broader context of resin modification. It highlights subjects worth investigating in future research endeavours and those crucial for the successful commercialisation of products. These subjects include treatability issues, the use of bio-based resins, drying conditions facilitating cell wall diffusion, fire retardancy properties, weathering resistance, volatile organic compounds (VOC) emissions, and mechanical properties, some of which are elaborated in the following.

The treatability of wood species is a significant concern in wood modification as it requires a uniform treatment of the entire specimen. Unlike conventional preservative treatments, an envelope treatment of outer regions is unsuitable for resin modification. Various techniques, such as laser incision, enzymatic or fungal treatments, or the use of supercritical fluid as an impregnation medium, can enhance treatability¹³. However, many of these techniques are not yet commercially viable. Future research could explore the compatibility of treatability-enhancing techniques with resin modification, potentially allowing for the utilisation of wood species studied in this thesis on a larger scale.

An alternative approach involves resin impregnation of veneers to create laminated veneer-type products. This eliminates treatability issues, and product dimensions can be adjusted by gluing layers together post-modification. This approach is currently under investigation in research projects focusing on resin treated and acetylated beech wood veneers. Hence, while solid beech wood is unsuitable for an impregnation process, beech veneers are a promising alternative^{311,312}.

Among treatments that improve the biological durability, wood modification is often distinguished from conventional wood protection by a non-fungicidal mode of action. While this implies a certain environmental benefit over conventional preservatives, it should be noted that phenolic resins are non-renewable and toxic, especially during the manufacturing process. A highly desirable alternative is bio-based resin, with potential substitutes like lignin³¹³ or alkaline bark extractives³¹⁴.

Prefere GmbH produces phenolic foams from lignin³¹⁵ and *Stora Enso* is working on a fully lignin-based resin for plywood³¹⁶. Hence, there are possibilities to produce lignin-based resins. Challenges with lignin-based resin include the low purity of lignin from pulp mills, low reactivity, and variable properties of the raw material. Additionally, wood modification requires a relatively low molecular weight resin, whereas lignin has a relatively high molecular weight. Hence, an additional processing step would be necessary to decrease the molecular weight. This has been investigated using a vacuum pyrolysis process in the laboratory, allowing 45% substitution in the resin modification treatments³¹⁷. However, industrial solutions for vacuum pyrolysis are currently not available, limiting the potential for commercialisation.

Chapter 8 has demonstrated the beneficial effect of cell wall diffusion on the dimensional stability, and a theoretical framework for the underlying mechanism was proposed, however, the experiments were conducted on small specimens and in a controlled environment. Future work could investigate whether a commercial resin modification process, where

plank-sized specimens are treated and typically kiln-dried after impregnation, could benefit from the principles that govern cell wall diffusion.

A first step in this direction was already taken during this PhD project, although the results have not been presented in this thesis so far. The preliminary study investigated intermediate-sized tulipwood specimens with dimensions of 200 (l) x 60 (t) x 25 (r) mm and found that the dimensional stability of these specimens differed significantly according to the selected drying schedule. A research poster presented on this topic is shown in Appendix 54. The dimensional stability was highest after air drying, followed by vacuum drying, oven drying, and kiln drying. The observed differences between drying schedules are currently explained by differences in the cell wall diffusion process, however, more work needs to be done to verify the trends and scale the testing up to plank-sized specimens. Moreover, one could investigate how cell wall diffusion affects other properties of the resin modified wood, such as durability.

Generally, the scientific foundation of wood modification with thermosetting resins is extensive, but the challenge lies in translating this knowledge into industrial applications. The transition from the laboratory to an industrial process introduces practical issues related to treatment scale. Addressing these issues requires a solid understanding of scientific principles, attention to non-scientific aspects like funding during the pilot-scale phase, and effective marketing in a mature market³¹⁸.

Commercially produced resin modified wood by *Lignia Wood Company Ltd.* displayed interesting characteristics, including promising fire retardancy properties, mechanical properties, weathering resistance, and durability against various agents. These findings warrant further research on the modification process, as well as additional efforts towards commercialisation and market introduction¹²⁹.

List of References

1. Dominguez-Rodrigo M, Serrallonga J, Juan-Tresserras J, Alcalá L & Luque L. (2001) Woodworking activities by early humans: A plant residue analysis on Acheulian stone tools from Peninj (Tanzania). *J. Hum. Evol.* **40**, 289–299.
2. Wimmers G. (2017) Wood: a construction material for tall buildings. *Nat. Rev. Mater.* **2**, No. 17051.
3. Forest Europe. (2015) State of Europe's Forests 2015. in *Ministerial Conference on the Protection of Forests in Europe 2015*.
4. Hill CAS & Dibdiakova J. (2016) The environmental impact of wood compared to other building materials. *Int. Wood Prod. J.* **7**, 215–219.
5. Churkina G, Organschi A, Reyer CPO, Ruff A, Vinke K, Liu Z, Reck BK, Graedel TE & Schellnhuber HJ. (2020) Buildings as a global carbon sink. *Nat. Sustain.* **3**, 269–276.
6. Becker J & Wittmann C. (2019) A field of dreams: Lignin valorization into chemicals, materials, fuels, and health-care products. *Biotechnol. Adv.* **37**, 107360.
7. Schmitz N, Krause A & Ludtke J. (2023) Critical review on a sustainable circular bio-economy for the forestry sector. in *Thünen Report 109*.
8. Seidl R, Thom D, Kautz M, Martin-Benito D, Peltoniemi M, Vacchiano G, Wild J, Ascoli D, Petr M, *et al.* (2017) Forest disturbances under climate change. *Nat. Clim. Chang.* **7**, 395–402.
9. Hlásny T, Barka I, Roessiger J, Kulla L, Trombik J, Sarvašová Z, Bucha T, Kovalčík M & Čihák T. (2017) Conversion of Norway spruce forests in the face of climate change: a case study in Central Europe. *Eur. J. For. Res.* **136**, 1013–1028.
10. Dyderski MK, Paž S, Frelich LE & Jagodziński AM. (2018) How much does climate change threaten European forest tree species distributions? *Glob. Chang. Biol.* **24**, 1150–1163.
11. Hill CAS. (2006) *Wood Modification: Chemical, Thermal and Other Processes*. Wiley, West Sussex.
12. Evans P. (2003) Emerging technologies in wood protection. *For. Prod. J.* **53**, 14–21.
13. Tarmian A, Tajrishi ZI, Oladi R & Efhamisis D. (2020) Treatability of wood for pressure treatment processes: a literature review. *Eur. J. Wood Wood Prod.* **78**, 635–660.
14. EU Regulation No 524/2013 of the European Parliament and of the Council (2012). *Official Journal of the European Union* 123.
15. Zelinka SL, Altgen M, Emmerich L, Guigo N, Keplinger T, Kymäläinen M, Thybring EE & Thygesen LG. (2022) Review of Wood Modification and Wood Functionalization Technologies. *Forests* **13**, 1004.
16. Sandberg D, Kutnar A & Mantanis G. (2017) Wood modification technologies - A review. *IForest* **10**, 895–908.
17. Spear MJ. (2018) Natural Materials – Composition and Combinations. in *Designing with Natural Materials* (eds. Ormondroyd GA & Morris AF), CRC Press, London.
18. Ni J & Frazier CE. (1996) Molecular Correlations to Macroscopic Wood Performance Using CP/MAS NMR. *Mater. Sci.*, **50**, 327–334
19. Chen C, Kuang Y, Zhu S, Burgert I, Keplinger T, Gong A, Li T, Berglund L, Eichhorn SJ, *et al.* (2020) Structure–property–function relationships of natural and engineered wood. *Nat. Rev. Mater.* **5**, 642–666.
20. Wagenführ R. (1999) *Anatomie des Holzes*. DRW-Verlag, Leinfelden-Echterdingen.
21. IAWA. (1964) Multilingual Glossary of Terms used in Wood Anatomy. *Comm. Nomencl. Int. Assoc. Wood Anat.* **23**.
22. Taylor AM, Gartner BL & Morrel JI. (2002) Heartwood formation and natural Durability - A review. *Wood Fiber Sci.* **34**, 587–611.
23. Carrodus BB. (1971) Carbon dioxide and the formation of heartwood. *New Phytol.* **70**, 939–943.
24. Hillis WE. (1986) *Heartwood and Tree Exudates*. Springer, Berlin, Heidelberg.
25. Hillis WE. (1968) Heartwood Formation and its Influence on Utilization. *Wood Sci. Technol.* **2**, 260–267.

26. Bossard HH. (1967) Über die fakultative Farbkernbildung. *Holz als Roh- und Werkst* **11**, 409-416.
27. Sjöström E. (1994) *Wood Chemistry: Fundamentals and Applications*. Academic Press.
28. Siau JF. (1984) *Transport Processes in Wood*. Springer, Berlin Heidelberg.
29. Olaniran SO, Löning S, Buschalsky A & Militz H. (2022) Impregnation Properties of Nigerian-Grown *Gmelina arborea* Roxb. *Wood. Forests* **13**,.
30. Oltean L, Teischinger A & Hansmann C. (2007) Influence of temperature on cracking and mechanical properties of wood during wood drying - A review. *BioResources* **2**, 789–811.
31. Harris JM. (1954) Heartwood formation in *Pinus Radiata* D Don. *New Phytol.* **53**, 517–24.
32. Spear M, Holmberg J, Nath S, Pitman A, Waugh D, Curling S, Mason P & Ormondroyd G. (2018) Fluid flow in wood: investigation of the influence of laser incision parameters on uptake and flow paths in four wood species. *in Timber 2018*, London.
33. Côté WA. (1981) Ultrastructure - Critical Domain for Wood Behavior. *Wood Sci. Technol* **9**, 1–2.
34. Hon DNS. (1996) Chemical modification of cellulose. *in Chemical Modification of Lignocellulosic Materials (eds. Hon DNS)*, Marcel Dekker Inc, New York.
35. O’Sullivan AC. (1997) Cellulose: the structure slowly unravels. *Cellulose* **4**, 173–207.
36. Jarvis MC. (2018) Structure of native cellulose microfibrils, the starting point for nanocellulose manufacture. *Philos. Trans. R. Soc. A Math. Phys. Eng. Sci.* **376**,.
37. Ciolacu D, Ciolacu F & Popa VI. (2011) Amorphous cellulose - Structure and characterization. *Cellul. Chem. Technol.* **45**, 13–21.
38. Terrett OM, Lyczakowski JJ, Yu L, Iuga D, Franks WT, Brown SP, Dupree R & Dupree P. (2019) Molecular architecture of softwood revealed by solid-state NMR. *Nat. Commun.* **10**, No. 4978.
39. Simmons TJ, Mortimer JC, Bernardinelli OD, Pöppler AC, Brown SP, DeAzevedo ER, Dupree R & Dupree P. (2016) Folding of xylan onto cellulose fibrils in plant cell walls revealed by solid-state NMR. *Nat. Commun.* **7**, 1–9.
40. Cresswell R, Dupree R, Brown SP, Pereira CS, Skaf MS, Sorieul M, Dupree P & Hill S. (2021) Importance of Water in Maintaining Softwood Secondary Cell Wall Nanostructure. *Biomacromolecules* **22**, 4669–4680.
41. Park S, Baker JO, Himmel ME, Parilla PA & Johnson DK. (2010) Cellulose crystallinity index: Measurement techniques and their impact on interpreting cellulase performance. *Biotechnol. Biofuels* **3**,.
42. Åkerholm M & Salmén L. (2001) Interactions between wood polymers studied by dynamic FT-IR spectroscopy. *Polymer (Guildf)*. **42**, 963–969.
43. Matthews JF, Skopec CE, Mason PE, Zuccato P, Torget RW, Sugiyama J, Himmel ME & Brady JW. (2006) Computer simulation studies of microcrystalline cellulose I β . *Carbohydr. Res.* **341**, 138–152.
44. Lehtiö J, Sugiyama J, Gustavsson M, Fransson L, Linder M & Teeri TT. (2003) The binding specificity and affinity determinants of family 1 and family 3 cellulose binding modules. *Proc. Natl. Acad. Sci. USA.* **100**, 484–489.
45. Hofstetter K, Hinterstoisser B & Salmén L. (2006) Moisture uptake in native cellulose - The roles of different hydrogen bonds: A dynamic FT-IR study using Deuterium exchange. *Cellulose* **13**, 131–145.
46. Paajanen A, Zitting A, Rautkari L, Ketoja JA & Penttilä PA. (2022) Nanoscale Mechanism of Moisture-Induced Swelling in Wood Microfibril Bundles. *Nano Lett.* **22**, 5143–5150.
47. Sjöström E & Alén RJ. (1999) *Analytical Methods in Wood Chemistry, Pulping, and Papermaking*. Springer, Berlin Heidelberg.
48. Andersson SI, Samuelson O, Ishihara M & Shimizu K. (1983) Structure of the reducing end-groups in spruce xylan. *Carbohydr. Res.* **111**, 283–288.
49. Dammström S, Salmén L & Gatenholm P. (2009) On the interactions between cellulose and xylan, a biomimetic simulation of the hardwood cell wall. *BioResources* **4**, 3–14.
50. Patil RA. (2012) Cleavage of acetyl groups for acetic acid production in Kraft pulp mills. *MSc thesis* at The University of Maine.

51. Tarasov D, Leitch M & Fatehi P. (2018) Lignin-carbohydrate complexes: Properties, applications, analyses, and methods of extraction: A review. *Biotechnol. Biofuels* **11**, 1–28.
52. Kerr AJ & Goring DAI. (1975) The ultrastructural arrangement of the wood cell wall. *Cellul. Chem. Technol.* **9**, 563–573.
53. Åkerholm M & Salmén L. (2003) The oriented structure of lignin and its viscoelastic properties studied by static and dynamic FT-IR spectroscopy. *Holzforschung* **57**, 459–465
54. Åkerholm M & Salmén L. (2004) Softening of wood polymers induced by moisture studied by dynamic FTIR spectroscopy. *J. Appl. Polym. Sci.* **94**, 2032–2040.
55. Cosgrove DJ & Jarvis MC. (2012) Comparative structure and biomechanics of plant primary and secondary cell walls. *Front. Plant Sci.* **3**, 1–6.
56. Stevanic JS & Salmén L. (2009) Orientation of the wood polymers in the cell wall of spruce wood fibres. *Holzforschung* **63**, 497–503.
57. Jakes JE, Hunt CG, Zelinka SL, Ciesielski PN & Plaza NZ. (2019) Effects of moisture on diffusion in unmodified wood cell walls: A phenomenological polymer science approach. *Forests* **10**,.
58. Salmén L & Burgert I. (2009) Cell wall features with regard to mechanical performance - A review. *Holzforschung* **63**, 121–129.
59. Fengel D. (1971) Ideas on the ultrastructural organization of the cell wall components. *J. Polym. Sci. Part C* **36**, 383–392.
60. Wang T & Hong M. (2016) Solid-state NMR investigations of cellulose structure and interactions with matrix polysaccharides in plant primary cell walls. *J. Exp. Bot.* **67**, 503–514.
61. Maloney TC. (2015) Thermoporosimetry of hard (silica) and soft (cellulosic) materials by isothermal step melting. *J. Therm. Anal. Calorim.* **121**, 7–17.
62. Thommes M, Kaneko K, Neimark A V., Olivier JP, Rodriguez-Reinoso F, Rouquerol J & Sing KSW. (2015) Physisorption of gases, with special reference to the evaluation of surface area and pore size distribution (IUPAC Technical Report). *Pure Appl. Chem.* **87**, 1051–1069.
63. Wardrop AB & Davies GW. (1962) Morphological Factors Relating to the Penetration of Liquids into Wood. *Holzforschung* **15**, 129–141.
64. Hill CAS, Forster SC, Farahani MRM, Hale MDC, Ormondroyd GA & Williams GR. (2005) An investigation of cell wall micropore blocking as a possible mechanism for the decay resistance of anhydride modified wood. *Int. Biodeterior. Biodegrad.* **55**, 69–76.
65. Park S, Venditti RA, Jameel H & Pawlak JJ. (2006) Changes in pore size distribution during the drying of cellulose fibers as measured by differential scanning calorimetry. *Carbohydr. Polym.* **66**, 97–103.
66. Hill CAS, Forster SC, Farahani MRM, Hale MDC, Ormondroyd GA & Williams GR. (2005) An investigation of cell wall micropore blocking as a possible mechanism for the decay resistance of anhydride modified wood. *Int. Biodeterior. Biodegrad.* **55**, 69–76.
67. Thybring EE, Digaitis R, Nord-Larsen T, Beck G & Fredriksson M. (2020) How much water can wood cell walls hold? A triangulation approach to determine the maximum cell wall moisture content. *PLoS One* **15**,.
68. Nopens M, Sazama U, König S, Kaschuro S, Krause A & Fröba M. (2020) Determination of mesopores in the wood cell wall at dry and wet state. *Sci. Rep.* **10**, 1–12.
69. Zhang X, Song S, Li X, Zhu Y, Li X, Xu K, Lyu J & Wu Y. (2022) Effect of low molecular weight melamine-urea-formaldehyde resin impregnation on poplar wood pore size distribution and water sorption. *Ind. Crops Prod.* 115700.
70. Park BD, Riedl B, Bae HJ & Kim YS. (1999) Differential scanning calorimetry of phenol-formaldehyde (PF) adhesives. *J. Wood Chem. Technol.* **19**, 265–286.
71. Dieste A, Krause A, Mai C, Sèbe G, Grelier S & Militz H. (2009) Modification of *Fagus sylvatica* L. with 1,3-dimethylol-4,5-dihydroxy ethylene urea (DMDHEU). Part 2: Pore size distribution determined by differential scanning calorimetry. *Holzforschung* **63**, 89–93.

72. Donaldson LA, Cairns M & Hill SJ. (2018) Comparison of micropore distribution in cell walls of softwood and hardwood xylem. *Plant Physiol.* **178**, 1142–1153.
73. Grigsby WJ, Kroese H & Dunningham EA. (2013) Characterisation of pore size distributions in variously dried *Pinus radiata*: Analysis by thermoporosimetry. *Wood Sci. Technol.* **47**, 737–747.
74. Thybring EE, Piqueras S, Tarmian A & Burgert I. (2020) Water accessibility to hydroxyls confined in solid wood cell walls. *Cellulose* **27**, 5617–5627.
75. Hill CAS, Hughes M & Gudsell D. (2021) Environmental impact of wood modification. *Coatings* **11**, 1–15.
76. Roberts G, Skinner C & Ormondroyd GA. (2022) The environmental and social impacts of modified wood production: effect of timber sourcing. *Int. Wood Prod. J.* **13**, 236–254.
77. Mania P, Wróblewski M, Wójciak A, Roszyk E & Moliński W. (2020) Hardness of densified wood in relation to changed chemical composition. *Forests* **11**, 1–12.
78. Schwarzkopf M. (2020) Densified wood impregnated with phenol resin for reduced set-recovery. *Wood Mater. Sci. Eng.* **16**, 35–41.
79. Hackenberg H, Zauer M, Dietrich T, Hackenberg KAM & Wagenführ A. (2021) Alteration of bending properties of wood due to ammonia treatment and additional densification. *Forests* **12**, 1–7.
80. Sun J, Tu K, Büchele S, Koch SM, Ding Y, Ramakrishna SN, Stucki S, Guo H, Wu C, *et al.* (2021) Functionalized wood with tunable tribopolarity for efficient triboelectric nanogenerators. *Matter* **4**, 3049–3066.
81. Koch SM, Pillon M, Keplinger T, Dreimol CH, Weinkötz S & Burgert I. (2022) InterCellular Matrix Infiltration Improves the Wet Strength of Delignified Wood Composites. *ACS Appl. Mater. Interfaces* **14**, 31216–31224.
82. Bardet M, Gerbaud G, Trân QK & Hediger S. (2007) Study of interactions between polyethylene glycol and archaeological wood components by ¹³C high-resolution solid-state CP-MAS NMR. *J. Archaeol. Sci.*
83. EN 350 (2016) Durability of wood and wood-based products-Testing and classification of the durability to biological agents of wood and wood-based materials.
84. Bliem P, Konnerth J, Frömel-Frybort S, Gartner C, Mauritz R & van Herwijnen HWG. (2020) Influence of drying and curing parameters on phenol-formaldehyde impregnated wood veneers. *J. Adhes.* **96**, 253–271.
85. Wascher R, Bittner F, Avramidis G, Bellmann M, Endres HJ, Militz H & Viöl W. (2020) Use of computed tomography to determine penetration paths and the distribution of melamine resin in thermally-modified beech veneers after plasma treatment. *Compos. Part A Appl. Sci. Manuf.* **132**, 105821.
86. Furuno T, Imamura Y & Kajita H. (2004) The modification of wood by treatment with low molecular weight phenol-formaldehyde resin: A properties enhancement with neutralized phenolic-resin and resin penetration into wood cell walls. *Wood Sci. Technol.* **37**, 349–361.
87. Franke T, Axel M, Lenz C, Nadine H & Pfrieder A. (2017) Microscopic and macroscopic swelling and dimensional stability of beech wood impregnated with phenol-formaldehyde. *Pro Ligno* **13**, 373–378.
88. Tanaka S, Seki M, Miki T, Shigematsu I & Kanayama K. (2016) Solute diffusion into cell walls in solution-impregnated wood under conditioning process II: effect of solution concentration on solute diffusion. *J. Wood Sci.* **62**, 146–155.
89. Tanaka S, Seki M, Miki T, Umemura K & Kanayama K. (2017) Solute diffusion into cell walls in solution-impregnated wood under conditioning process III: effect of relative humidity schedule on solute diffusion into shrinking cell walls. *J. Wood Sci.* **63**, 263–270.
90. Tanaka S, Seki M, Miki T, Umemura K & Kanayama K. (2017) Solute diffusion into cell walls in solution-impregnated wood under conditioning process IV: effect of temperature on solute diffusivity. *J. Wood Sci.* **63**, 644–651.
91. Tanaka S, Seki M, Miki T, Shigematsu I & Kanayama K. (2015) Solute diffusion into cell walls in solution-impregnated wood under conditioning process I: effect of relative humidity on solute diffusivity. *J. Wood Sci.* **61**, 543–551.
92. Zheng P, Aoki D, Seki M, Miki T, Tanaka S & Kanayama K. (2018) Visualization of solute diffusion into cell walls in solution-impregnated wood under varying relative humidity using time-of-flight secondary ion mass spectrometry. *Sci. Rep.* **8**, No. 9819.

93. Klüppel A & Mai C. (2013) The influence of curing conditions on the chemical distribution in wood modified with thermosetting resins. *Wood Sci. Technol.* **47**, 643–658.
94. Pitman AJ. (2020) Personal Communication.
95. Schaffert S, Krause A & Militz H. (2005) Upscaling and Process Development for Wood Modification with N-methylol Compounds using Overheated Steam Crosslinking reaction. in *2nd European Conference on Wood Modification*.
96. Altgen M, Awais M, Altgen D, Klüppel A, Mäkelä M & Rautkari L. (2020) Distribution and curing reactions of melamine formaldehyde resin in cells of impregnation-modified wood. *Sci. Rep.* **10**, No. 3366.
97. Behr G, Bollmus S, Gellerich A, Militz H, Behr G, Bollmus S, Gellerich A & Militz H. (2018) The influence of curing conditions on the properties of European beech (*Fagus sylvatica*) modified with melamine resin assessed by light microscopy and SEM-EDX. *Int. Wood Prod. J.* **9**, 22–27.
98. Krause A & Militz H. (2009) Process for Improving the Durability, Dimensional Stability and Surface Hardness of a Wood Body. US Patent No. 7,595,116 B2
99. Altgen M, Awais M, Altgen D, Klüppel A, Koch G, Mäkelä M, Olbrich A & Rautkari L. (2023) Chemical imaging to reveal the resin distribution in impregnation- treated wood at different spatial scales. *Mater. Des.* **225**,.
100. Hill CAS & Ormondroyd GA. (2004) Dimensional changes in Corsican pine (*Pinus nigra* Arnold) modified with acetic anhydride measured using a helium pycnometer. *Holzforschung* **58**, 544–547.
101. Emmerich L, Ehrmann A, Brischke C & Militz H. (2021) Comparative studies on the durability and moisture performance of wood modified with cyclic N-methylol and N-methyl compounds. *Wood Sci. Technol.* **55**, 1531–1554.
102. Wang X, Zhao L, Deng Y, Li Y & Wang S. (2018) Effect of the penetration of isocyanates (pMDI) on the nanomechanics of wood cell wall evaluated by AFM-IR and nanoindentation (NI). *Holzforschung* **72**, 301–309.
103. Kielmann BC, Adamopoulos S, Militz H, Koch G & Mai C. (2014) Modification of three hardwoods with an N-methylol melamine compound and a metal-complex dye. *Wood Sci. Technol.* **48**, 123–136.
104. Jakes JE, Frihart CR, Hunt CG, Yelle DJ, Plaza NZ, Lorenz L, Grigsby W, Ching DJ, Kamke F, *et al.* (2019) X-ray methods to observe and quantify adhesive penetration into wood. *J. Mater. Sci.* **54**, 705–718.
105. McKinley P, Kamke FA, Sinha A, De Andrade V & Jakes JE. (2018) Analysis of adhesive penetration into wood using nano-x-ray computed tomography. *Wood Fiber Sci.* **50**, 66–76.
106. Rapp AO, Bestgen H, Adam W & Peek RD. (1999) Electron energy loss spectroscopy (EELS) for quantification of cell-wall penetration of a melamine resin. *Holzforschung* **53**, 111–117.
107. Singh AP, Nuryawan A, Park BD & Lee KH. (2015) Urea-formaldehyde resin penetration into *Pinus radiata* tracheid walls assessed by TEM-EDXS. *Holzforschung* **69**, 303–306.
108. Huang Y, Fei B & Zhao R. (2014) Investigation of low-molecular weight phenol formaldehyde distribution in tracheid cell walls of Chinese fir wood. *BioResources* **9**, 4150–4158.
109. Mahnert KC, Adamopoulos S, Koch G & Militz H. (2013) Topochemistry of heat-treated and N-methylol melamine-modified wood of koto (*Pterygota macrocarpa* K. Schum.) and limba (*Terminalia superba* Engl. et. Diels). *Holzforschung* **67**, 137–146.
110. Jeremic D, Cooper P & Brodersen P. (2007) Penetration of poly (ethylene glycol) into wood cell walls of red pine. *Holzforschung* **61**, 272–278.
111. Ormondroyd GA. (2007) An Investigation of Novel Wood Protection Methods. *PhD thesis* at University of Wales, Bangor.
112. Grinins J, Irbe I, Biziks V, Rizikovs J, Bicke S & Militz H. (2018) Investigation of Birch Wood Impregnation with Phenol-Formaldehyde (PF) Resins. in *European Conference on Wood Modification 2018*.
113. Deka M, Saikia CN & Baruah KK. (2002) Studies on thermal degradation and termite resistant properties of chemically modified wood. *Bioresour. Technol.* **84**, 151–157.
114. Westin M, Rapp A & Nilsson T. (2006) Field test of resistance of modified wood to marine borers. *Wood Mater. Sci. Eng.* **1**, 34–38.

115. Beck G, Thybring EE & Thygesen LG. (2018) Brown-rot fungal degradation and de-acetylation of acetylated wood. *Int. Biodeterior. Biodegrad.* **135**, 62–70.
116. Ringman R, Pilgard A, Brischke C & Richter K. (2014) Mode of action of brown rot decay resistance in modified wood: A review. *Holzforschung* **68**, 239–246.
117. Alfredsen G, Pilgard A & Fossdal CG. (2016) Characterisation of *Postia placenta* colonisation during 36 weeks in acetylated southern yellow pine sapwood at three acetylation levels including genomic DNA and gene expression quantification of the fungus. *Holzforschung* **70**, 1055–1065.
118. Jakes JE, Zelinka SL, Hunt CG, Ciesielski P, Frihart CR, Yelle D, Passarini L, Gleber SC, Vine D, *et al.* (2020) Measurement of moisture-dependent ion diffusion constants in wood cell wall layers using time-lapse micro X-ray fluorescence microscopy. *Sci. Rep.* **10**, No. 9919.
119. Biziks V, Bicke S, Koch G & Militz H. (2021) Effect of phenol-formaldehyde (PF) resin oligomer size on the decay resistance of beech wood. *Holzforschung* **75**, 574–583.
120. Grinins J, Biziks V, Irbe I & Rizikovs J. (2019) Water related properties of birch wood modified with phenol-formaldehyde (PF) resins. *Key Eng. Mater.* **800**, 246–250.
121. Biziks V, Bicke S & Holger Militz. (2019) Penetration depth of phenol-formaldehyde (PF) resin into beech wood studied by light microscopy. *Wood Sci. Technol.* **53**, 165–176.
122. Wang X, Chen X, Xie X, Cai S, Yuan Z & Li Y. (2019) Multi-scale evaluation of the effect of phenol formaldehyde resin impregnation on the dimensional stability and mechanical properties of *Pinus massoniana* Lamb. *Forests* **10**, 646.
123. Pečnik JG, Kutnar A, Militz H, Schwarzkopf M & Schwager H. (2020) Fatigue behavior of beech and pine wood modified with low molecular weight phenol-formaldehyde resin. *Holzforschung* **75**, 37–47.
124. Behr G, Bollmus S, Gellerich A & Militz H. (2017) Improvement of mechanical properties of thermally modified hardwood through melamine treatment. *Wood Mater. Sci. Eng.* **13**, 262–270.
125. Epmeier H, Westin M & Rapp A. (2004) Differently modified wood: Comparison of some selected properties. *Scand. J. For. Res.* **19**, 31–37.
126. Millett MA & Stamm AJ. (1954) *Wood Treatment with Resin forming Systems. Part 3 - A Study of Size and Species Limitations.* (1954).
127. Permal composites. <https://www.permali.co.uk/materials/composite/> accessed 29.9.2023..
128. CK Composites. <https://ckcomposites.com/insulam-densified-wood-laminate/> accessed 29.9.2023..
129. Stefanowski BK, Spear MJ, Curling SF & Pitman AJ. (2020) Properties of Lignia Modified Wood. in *Timber 2020* (2020).
130. Willemsen N. (2021) *Kebyony: Sustainability Report 2021.*
131. Emmerich L, Bollmus S & Militz H. (2019) Wood modification with DMDHEU (1,3-dimethylol-4,5-dihydroxyethyleneurea)—State of the art, recent research activities and future perspectives. *Wood Mater. Sci. Eng.* **14**, 3–18.
132. Kurkowiak K, Mayer AK, Emmerich L & Militz H. (2022) Investigations of the Chemical Distribution in Sorbitol and Citric Acid (SorCA) Treated Wood—Development of a Quality Control Method on the Basis of Electromagnetic Radiation. *Forests* **13**, 151.
133. Cai X, Riedl B, Zhang SY & Wan H. (2007) Effects of nanofillers on water resistance and dimensional stability of solid wood modified by melamine-urea-formaldehyde resin. *Wood Fiber Sci.* **39**, 307–318.
134. Yang T & Mei C. (2022) Effects of hemicellulose removal combined with polyethylene glycol impregnation on dimensional stability of wood. *Wood Mater. Sci. Eng.* **0**, 1–10.
135. Goli G, Negro F, Emmerich L & Militz H. (2022) Thermal and chemical modification of wood—a combined approach for exclusive, high-demanding performance products. *Wood Mater. Sci. Eng.* 1–9.
136. Kuka E, Cirule D, Andersone I, Andersons B, Kurnosova N, Verovkins A & Puke M. (2022) Environmental performance of combined treated wood. *Wood Mater. Sci. Eng.* **10**, 88-96.
137. Mantanis GI. (2017) Chemical Modification of Wood by Acetylation or Furfurylation: A Review of the Present Scaled-up Technologies. *BioResources* **12**, 4478–4489.

138. Papadopoulos AN & Hill CAS. (2003) The sorption of water vapour by anhydride modified softwood. *Wood Sci. Technol* **37**, 221–231.
139. Hill CAS, Kwon JH, Hale MDC, Ormondroyd GA, Suttie ED & Howard N. (2003) The Decay Resistance of Anhydride Modified Wood. in *The Third European Conference on Wood Modification*.
140. Hill CAS. (2009) Why does acetylation protect wood from microbiological attack? *Wood Mater. Sci. Eng.* **4**, 37–45.
141. Thybring EE. (2013) The decay resistance of modified wood influenced by moisture exclusion and swelling reduction. *Int. Biodeterior. Biodegrad.* **82**, 87–95.
142. Popescu CM, Hill CAS, Curling S, Ormondroyd G & Xie Y. (2014) The water vapour sorption behaviour of acetylated birch wood: How acetylation affects the sorption isotherm and accessible hydroxyl content. *J. Mater. Sci.* **49**, 2362–2371.
143. Hill CAS, Hale MD, Ormondroyd GA, Kwon JH & Forster SC. (2006) Decay resistance of anhydride-modified Corsican pine sapwood exposed to the brown rot fungus *Coniophora puteana*. *Holzforschung* **60**, 625–629.
144. Tullo AH. (2012) Making Wood Last Forever With Acetylation. *Chemical & Engineering News*.
145. Gibson S. (2016) Benefits of Acetylated Lumber. *Green Building News* <https://www.greenbuildingadvisor.com/article/the-rise-and-fall-of-a-miracle-wood>, accessed 29.07.2023.
146. Ogilvie S. (2021) *Trading update: Accsys Technologies PLC, Number 6627V, Released 16 April 2021, Accsys Technologies: London, UK.* (2021).
147. Willems W. (2022) Absolute and Universal Metric for the Degree of Thermal Conversion of Wood. in *10th European Conference on Wood Modification* 57–64.
148. Bhuiyan MTR, Hirai N & Sobue N. (2000) Changes of crystallinity in wood cellulose by heat treatment under dried and moist conditions. *J. Wood Sci.* **46**, 431–436.
149. Endo K, Obataya E, Zeniya N & Matsuo M. (2016) Effects of heating humidity on the physical properties of hydrothermally treated spruce wood. *Wood Sci. Technol.* **50**, 1161–1179.
150. Wentzel M, Altgen M & Militz H. (2018) Analyzing reversible changes in hygroscopicity of thermally modified eucalypt wood from open and closed reactor systems. *Wood Sci. Technol.* **52**, 889–907.
151. Hakkou M, Pétrissans M, El Bakali I, Gérardin P & Zoulalian A. (2005) Wettability changes and mass loss during heat treatment of wood. *Holzforschung* **59**, 35–37.
152. Grinins J, Andersons B, Biziks V, Andersone I & Dobele G. (2013) Analytical pyrolysis as an instrument to study the chemical transformations of hydrothermally modified wood. *J. Anal. Appl. Pyrolysis* **103**, 36–41.
153. Tjeerdsma BF, Boonstra M, Pizzi A, Tekely P & Militz H. (1998) Characterisation of thermally modified wood : molecular reasons for wood performance improvement. **56**, 149–153.
154. Pettersen R. (1984) The chemistry of solids. in *Chemical composition of wood* (ed. Rowell, R. M.) 57–126 American Chemical Society.
155. Hill C, Altgen M & Rautkari L. (2021) Thermal modification of wood—a review: chemical changes and hygroscopicity. *J. Mater. Sci.* **56**, 6581–6614.
156. Seborg RM, Tarkow H & Stamm AJ. (1953) Effect of heat upon the dimensional stabilisation of wood. *For. Prod. Res. Soc.* **3**,
157. Zhan T, Liu Z, Peng H, Jiang J, Zhang Y & Lyu J. (2021) Meta-analysis of anti-swelling efficiency (ASE) of heat-treated wood. *Eur. J. Wood Wood Prod.* 1–4
158. Candelier K, Thevenon M & Petrisans A. (2016) Control of wood thermal treatment and its effects on decay resistance : a review. *Ann. For. Sci.* 571–583.
159. Metsä-Kortelainen S & Viitanen H. (2009) Decay resistance of sapwood and heartwood of untreated and thermally modified Scots pine and Norway spruce compared with some other wood species. *Wood Mater. Sci. Eng.* **4**, 105–114.
160. Boonstra MJ, Van Acker J, Kegel E & Stevens M. (2007) Optimisation of a two-stage heat treatment process: Durability aspects. *Wood Sci. Technol.* **41**, 31–57.

161. Scheiding W, Ala-Viikari J & Tetri T. (2022) Thermal Wood Modification After 20 Years of Commercialisation: An Overview and the ThermoWood Story. in *10th European Conference on Wood Modification 17–28* (2022).
162. Welzbacher CR & Rapp AO. (2007) Durability of thermally modified timber from industrial-scale processes in different use classes: Results from laboratory and field tests. *Wood Mater. Sci. Eng.* **2**, 4–14.
163. Boonstra MJ, Van Acker J, Tjeerdma BF & Kegel E V. (2007) Strength properties of thermally modified softwoods and its relation to polymeric structural wood constituents. *Ann. For. Sci.* **64**, 679–690.
164. Yildiz S, Gezer ED & Yildiz UC. (2006) Mechanical and chemical behavior of spruce wood modified by heat. *Build. Environ.* **41**, 1762–1766.
165. Arnold M. (2010) Effect of moisture on the bending properties of thermally modified beech and spruce. *J. Mater. Sci.* **45**, 669–680.
166. Altgen M & Militz H. (2017) Thermally modified Scots pine and Norway spruce wood as substrate for coating systems. *J. Coatings Technol. Res.* **14**, 531–541.
167. Scheiding W. (2021) 20 Jahre Thermoholz. *Holzkurier*.
168. Homan WJ & Jorissen AJM. (2004) Wood modification developments. *Heron* **49**, 361–386.
169. Hamad SF, Farr N, Fei T, Shukor NF, Dean JS, Hayes SA, Foreman JP & Rodenburg C. (2019) Optimizing size and distribution of voids in phenolic resins through the choice of catalyst types. *J. Appl. Polym. Sci.* **136**, 1–10.
170. Gardziella A, Pilato LA & Knop A. (2000) *Phenolic Resins: Chemistry, Applications, Standardization, Safety and Ecology*. Springer-Verlag, Berlin Heidelberg.
171. Hussin MH, Abd Latif NH, Hamidon TS, Idris NN, Hashim R, Appaturi JN, Brosse N, Ziegler-Devin I, Chrusiel L, et al. (2022) Latest advancements in high-performance bio-based wood adhesives: A critical review. *J. Mater. Res. Technol.* **22**, 3909 - 3946.
172. Papadopoulou E & Chrissafis K. (2011) Thermal study of phenol-formaldehyde resin modified with cashew nut shell liquid. *Thermochim. Acta* **512**, 105–109.
173. Dunky M & Niemz P. (2002) *Holzwerkstoffe und Leime*. Springer, Berlin Heidelberg.
174. De Medeiros ES, Agnelli JAM, Joseph K, De Carvalho LH & Mattoso LHC. (2003) Curing behavior of a novolac-type phenolic resin analyzed by differential scanning calorimetry. *J. Appl. Polym. Sci.* **90**, 1678–1682.
175. So S & Rudin A. (1990) Analysis of the formation and curing reactions of resole phenolics. *J. Appl. Polym. Sci.* **41**, 205–232.
176. Deka M & Saikia CN. (2000) Chemical modification of wood with thermosetting resin: Effect on dimensional stability and strength property. *Bioresour. Technol.* **73**, 179–181.
177. Hosseinpourpia R, Adamopoulos S & Mai C. (2016) Dynamic vapour sorption of wood and holocellulose modified with thermosetting resins. *Wood Sci. Technol.* **50**, 165–178.
178. Turunen M, Alvilä L, Pakkanen TT & Rainio J. (2003) Modification of phenol-formaldehyde resole resins by lignin, starch, and urea. *J. Appl. Polym. Sci.* **88**, 582–588.
179. Tomita B & Hse C. (1998) Phenol — urea — formaldehyde (PUF) co-condensed wood adhesives. *Int. J. Adhes. Adhes.* **18**, 69–79.
180. Tomita B & Hse C-Y. (1992) Cocondensation of urea with methylolphenols in acidic conditions. *J. Polym. Sci. Part A Polym. Chem.* **30**, 1615–1624.
181. He G & Yan N. (2004) ¹³C NMR study on structure, composition and curing behavior of phenol-urea-formaldehyde resole resins. *Polymer (Guildf)*. **45**, 6813–6822.
182. Zhao C, Pizzi A & Garnier S. (1999) Fast advancement and hardening acceleration of low-condensation alkaline PF resins by esters and copolymerized urea. *J. Appl. Polym. Sci.* **74**, 359–378.
183. Kim MG, Amos LW & Barnes EE. (1990) Study of the Reaction Rates and Structures of a Phenol-Formaldehyde Resol Resin by Carbon-13 NMR and Gel Permeation Chromatography. *Ind. Eng. Chem. Res.* **29**, 2032–2037.
184. Myers GE, Christiansen AW, Geimer RL, Follensbee RA & Koutsky JA. (1991) Phenol–formaldehyde resin curing and bonding in steam-injection pressing. I. Resin synthesis, characterization, and cure behavior. *J. Appl. Polym. Sci.* **43**, 237–250.

185. Goodell B, Jellison J, Liu J, Daniel G, Paszczynski A, Fekete F, Krishnamurthy S, Jun L & Xu G. (1997) Low molecular weight chelators and phenolic compounds isolated from wood decay fungi and their role in the fungal biodegradation of wood. *J. Biotechnol.* **53**, 133-162.
186. Higuchi M, Nohno S & Morita M. (1999) Kinetics of the hydroxymethylation of phenol II: Values of rate parameters and results of simulation experiments. *J. Wood Sci.* **45**, 306-312.
187. Astarloa-Aierbe G, Echeverría JM, Martin MD & Mondragon I. (1998) Kinetics of phenolic resol resin formation by HPLC. 2. Barium hydroxide. *Polymer (Guildf).* **39**, 3467-3472.
188. Pasch H, Rode K, Ghahary R & Braun D. (1996) Matrix-assisted laser desorption/ionization mass spectrometry of synthetic polymers. **241**, 95-111.
189. Laborie MG, Salmén L, Frazier CE, Salmén L & A CEF. (2006) A morphological study of the wood / phenol-formaldehyde adhesive interphase. *J. Adhes. Sci. Technol.* **20**, 729-741.
190. He G & Yan N. (2005) Effect of wood species and molecular weight of phenolic resins on curing behavior and bonding development. *Holzforschung* **59**, 635-640.
191. Geimer RL, Follensbee RA, Christiansen AW, Koutsky JA & Myers GE. (1990) Resin characterization. *Cooperative Research Between University of Wisconsin--Madison and the USDA Forest Service, Forest Products Laboratory.*
192. He G, Riedl B & Ait-Kadi A. (2003) Model-free kinetics: Curing behavior of phenol formaldehyde resins by differential scanning calorimetry. *J. Appl. Polym. Sci.* **87**, 433-440.
193. Günzler H & Gremlich HU (2003) *IR-Spektroskopie: Eine Einführung.* Wiley, Weinheim.
194. Carotenuto G & Nicolais L. (1999) Kinetic study of phenolic resin cure by IR spectroscopy. *J. Appl. Polym. Sci.* **74**, 2703-2715.
195. Wang X, Chen X, Xie X, Yuan Z, Cai S & Li Y. (2019) Effect of phenol formaldehyde resin penetration on the quasi-static and dynamic mechanics of wood cellwalls using nanoindentation. *Nanomaterials* **9**,.
196. Akitt DJW & Mann M. (2000) *NMR and Chemistry*, London, CRC-Press.
197. Yelle DJ, Ralph J & Frihart CR. (2008) Characterization of nonderivatized plant cell walls using high-resolution solution-state NMR spectroscopy. *Magn. Reson. Chem.* **46**, 508-517.
198. Yelle DJ & Ralph J. (2016) Characterizing phenol-formaldehyde adhesive cure chemistry within the wood cell wall. *Int. J. Adhes. Adhes.* **70**, 26-36.
199. Panamgama LA & Pizzi A. (1995) A ¹³C-NMR analysis method for phenol-formaldehyde resin strength and formaldehyde emission. *J. Appl. Polym. Sci.* **55**, 1007-1015.
200. Grenier-Loustalot M-F, Larroque S, Grenier P & Bedel D. (1996) Phenolic resins: 3. Study of the reactivity of the initial monomers towards formaldehyde at constant pH, temperature and catalyst type. *Polymer (Guildf).* **37**, 939-953.
201. Wang J & Zhang YF. (2012) Chemical Structure and Curing Characteristics of Phenol Formaldehyde Resins Catalyzed with Calcium Oxide. *Polym. - Plast. Technol. Eng.* **51**, 1213-1217.
202. Grenier-Loustalot M-F, Larroque S, Grenier P, Leca J-P & Bedel D. (1994) Phenolic resins: 1. Mechanisms and kinetics of phenol and of the first polycondensates towards formaldehyde in solution. *Polymer (Guildf).* **35**, 3046-3054.
203. Grenier-Loustalot MF, Larroque S, Grenier P & Bedel D. (1996) Phenolic resins: 4. Self-condensation of methylolphenols in formaldehyde-free media. *Polymer (Guildf).* **37**, 955-964.
204. Astarloa-Aierbe G, Echeverría JM & Mondragon I. (1998) Kinetics of phenolic resol resin formation by HPLC. *Polymer (Guildf).* **40**, 5873-5878.
205. Nieh Lenoir & Sellers TJ. (1991) Performances of flakeboard bonded with three PF resins of different mole ratios and molecular weights. *Forest products journal (USA)* vol. v. 41 at (1991).
206. Christiansen AW & Gollob L. (1985) Differential Scanning Calorimetry of Phenol-Formaldehyde Resols. *J. Appl. Polym. Sci.* **30**, 827-835.
207. Grenier-Loustalot M-F, Larroque S, Grenier P, Leca J-P & Bedel D. (1994) Phenolic resins: 1. Mechanisms and kinetics of phenol and of the first polycondensates towards formaldehyde in solution. *Polymer (Guildf).* **35**, 3046-3054.

208. Pizzi A & Stephanou A. (1993) On the Chemistry, Behavior, and Cure Acceleration of Phenol-Formaldehyde Resins Under Very Alkaline Conditions. *J. Adhes. Sci.* **49**, 2157–2170.
209. Grenier-Loustalot M-F, Larroque S, Grande D & Grenier P. (1996) Phenolic resins: 2 . Influence of catalyst type on reaction mechanisms and kinetics. *Polymer (Guildf)*. **37**, 1363–1369.
210. Oldörp K & Miertzsch H. (1997) Untersuchungen zum Ersatz von Natriumhydroxid bei Phenolharzen durch Ammoniak. *Holz als Roh - und Werkst.* **55**, 97–102.
211. Chen Y, Fan D, Qin T & Chu F. (2014) Thermal degradation and stability of accelerated-curing phenol-formaldehyde resin. *BioResources* **9**, 4063–4075.
212. He G & Riedl B. (2004) Curing kinetics of phenol formaldehyde resin and wood-resin interactions in the presence of wood substrates. *Wood Sci. Technol.* **38**, 69–81.
213. He G & Yan N. (2005) Effect of wood on the curing behavior of commercial phenolic resin systems. *J. Appl. Polym. Sci.* **95**, 185–192.
214. Özparpucu M, Windeisen-Holzhauser E, Wegener G & Richter K. (2022) A new analytical approach to investigate the influence of wood extracts on the curing properties of phenol-resorcinol–formaldehyde (PRF) adhesives. *Wood Sci. Technol.* **56**, 349–365.
215. Roffael E. (2016) Significance of wood extractives for wood bonding. *Appl. Microbiol. Biotechnol.* **100**, 1589–1596.
216. Pizzi A, Mtsweni B & Parsons W. (1994) Wood-induced catalytic activation of PF adhesives autopolymerization vs. PF/wood covalent bonding. *J. Appl. Polym. Sci.* **52**, 1847–1856.
217. Pizzi A. (1990) A molecular mechanics approach to the adhesion of urea-formaldehyde resins to cellulose. Part 2. Amorphous vs. crystalline Cellulose I. *J. Adhes. Sci. Technol.* **4**, 589–595.
218. Pizzi A. (1990) A Molecular Mechanics Approach to the Adhesion of Urea-Formaldehyde Resins To Cellulose. Part 1. Crystalline Cellulose I. *J. Adhes. Sci. Technol.* **4**, 573–588.
219. Plaza NZ, Jakes JE, Frihart CR, Hunt CG, Yelle DJ, Lorenz LF, Heller WT, Pingali SV & Stone DS. (2019) Small-angle neutron scattering as a new tool to evaluate moisture-induced swelling in the nanostructure of chemically modified wood cell walls. *For. Prod. J.* **68**, 349–352.
220. Laborie MG. (2002) Investigation of the Wood-Phenol-Formaldehyde Adhesive Interphase Morphology. (Virginia Polytechnic Institute and State University, 2002).
221. Nishida M, Tanaka T, Miki T, Hayakawa Y & Kanayama K. (2017) Integrated analysis of solid-state NMR spectra and nuclear magnetic relaxation times for the phenol formaldehyde (PF) resin impregnation process into soft wood. *RSC Adv.* **7**, 54532–54541.
222. Nishida M, Tanaka T, Miki T, Hayakawa Y & Kanayama K. (2019) Integrated analysis of modified Japanese cypress using solid-state NMR spectra and nuclear magnetic relaxation times. *Cellulose* **26**, 3625–3642.
223. Sharma V, Yadav J, Kumar R, Tesarova D, Ekielski A & Mishra PK. (2020) On the rapid and non-destructive approach for wood identification using ATR-FTIR spectroscopy and chemometric methods. *Vib. Spectrosc.* **110**, 103097.
224. Johns WE & Niazi KA. (1980) Effect of pH and buffering capacity of wood on the relation time of urea formaldehyde resin. *Wood Fiber Sci.* **12**, 255–263.
225. Wang X, Huang Z, Cooper P, Zhang Y & Casilla R. (2010) The ability of wood to buffer highly acidic and alkaline adhesives. *Wood Fiber Sci.* **42**, 398–405.
226. Wojtasz-Mucha J, Hasani M & Theliander H. (2021) Dissolution of wood components during hot water extraction of birch. *Wood Sci. Technol.* **55**, 811–835.
227. Wise LE, Maxine M & D'Addieco AA. (1946) Chlorite holocellulose, its fractionation and bearing on summative wood analysis and on studies on the hemicelluloses. *Tech. Assoc. pulp Pap. Ind.* **29**, 210–218.
228. Kaar WE & Brink DL. (1991) Simplified analysis of acid soluble lignin. *J. Wood Chem. Technol.* **11**, 465–477.
229. Król P, Borysiuk P & Mamiński M. (2019) Comparison of methodologies for acid buffering capacity determination-empirical verification of models. *Appl. Sci.* **9**,

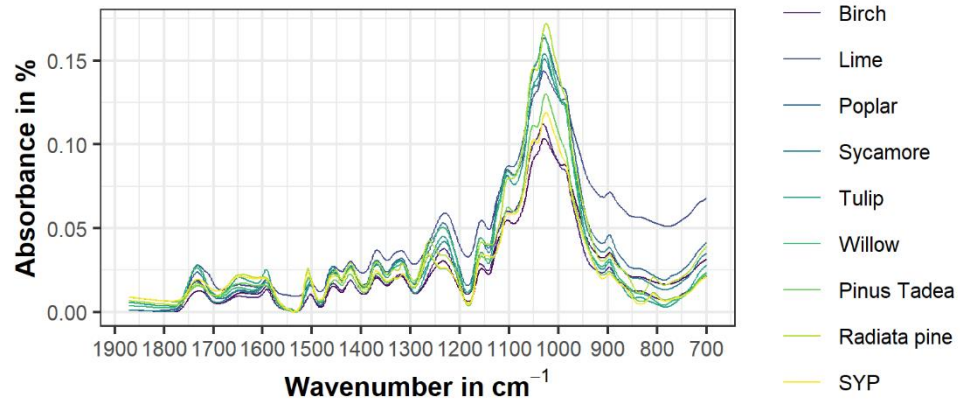
230. Król P, Toczyłowska-mamińska R & Mamiński M. (2017) A Critical Role for the Presence of Lignocellulosic Material in the Determination of Wood Buffering Capacity. **3813**.
231. Pandey KK. (1999) A Study of Chemical Structure of Soft and Hardwood and Wood Polymers by FTIR Spectroscopy. *J. Appl. Polym. Sci.* **71**, 1969–1975.
232. Sun JX, Mao FC, Sun XF & Sun RC. (2004) Comparative study of hemicelluloses isolated with alkaline peroxide from lignocellulosic materials. *J. Wood Chem. Technol.* **24**, 239–262.
233. Sills DL & Gossett JM. (2012) Using FTIR to predict saccharification from enzymatic hydrolysis of alkali-pretreated biomasses. *Biotechnol. Bioeng.* **109**, 353–362.
234. Kotilainen RA, Toivanen TJ & Alén RJ. (2000) FTIR monitoring of chemical changes in softwood during heating. *J. Wood Chem. Technol.* **20**, 307–320.
235. Bykov I. (2008) Characterization of Natural and Technical Lignins using FTIR Spectroscopy. *Msc Thesis at Lulea University of Technology, Lulea*
236. Liu CF, Xu F, Sun JX, Ren JL, Curling S, Sun RC, Fowler P & Baird MS. (2006) Physicochemical characterization of cellulose from perennial ryegrass leaves (*Lolium perenne*). *Carbohydr. Res.* **341**, 2677–2687.
237. Pandey KK & Pitman AJ. (2003) FTIR studies of the changes in wood chemistry following decay by brown-rot and white-rot fungi. *Int. Biodeterior. Biodegrad.* **52**, 151–160.
238. Lievens C, Mourant D, He M, Gunawan R, Li X & Li CZ. (2011) An FT-IR spectroscopic study of carbonyl functionalities in bio-oils. *Fuel* **90**, 3417–3423.
239. Hayasaka Y, Wilkinson KL, Elsey GM, Raunkjær M & Sefton MA. (2007) Identification of natural oak lactone precursors in extracts of American and French oak woods by liquid chromatography-tandem mass spectrometry. *J. Agric. Food Chem.* **55**, 9195–9201.
240. TAPPI T 435 - Hydrogen ion concentration (pH) of paper extracts (hot extraction method).
241. TAPPI T 509 - Hydrogen ion concentration (pH) of paper extracts (cold extraction method).
242. Elias R & Irle MA. (1996) The acidity of stored Sitka spruce chips. *Holz als Roh- und Werkst.* **54**, 65–68.
243. Geffert A, Geffertova J & Dudiak M. (2019) Direct method of measuring the pH value of wood. *Forests* **10**, 6–10.
244. TAPPI T 529 - Surface pH measurement of paper.
245. Xing C, Zhang SY & Deng J. (2004) Effect of wood acidity and catalyst on UF resin gel time. **58**, 408–412.
246. Giummarella N, Henriksson G, Salmén L & Lawoko M. (2017) On the effect of hemicellulose removal on cellulose-lignin interactions. *Nord. Pulp Pap. Res. J.* **32**, 542–549.
247. Pretsch E, Buehlmann P & Affolter C. (2000) *Structure Determination of Organic Compounds*. Springer, Berlin Heidelberg.
248. Qu C, Kishimoto T, Kishino M, Hamada M & Nakajima N. (2011) Heteronuclear single-quantum coherence nuclear magnetic resonance (HSQC NMR) characterization of acetylated fir (*Abies sachalinensis* MAST) wood regenerated from ionic liquid. *J. Agric. Food Chem.* **59**, 5382–5389.
249. Guo Z, Zeng S, Zhang Y, Lu X, Tian Y & Zheng B. (2015) The effects of ultra-high pressure on the structural, rheological and retrogradation properties of lotus seed starch. *Food Hydrocoll.* **44**, 285–291.
250. Chow S & Steiner PR. (1979) Comparisons of the cure of phenol-formaldehyde novolac and resol systems by differential scanning calorimetry. *J. Appl. Polym. Sci.* **23**, 1973–1985.
251. Behr G, Gellerich A, Bollmus S, Brinker S & Militz H. (2018) The influence of curing conditions on properties of melamine modified wood. *Eur. J. Wood Wood Prod.* **76**, 1263–1272.
252. Ozawa T. (1965) A New Method of Analyzing Thermogravimetric Data. *Bull. Chem. Soc. Jap.* **38**, 1881–1886.
253. Kissinger HE. (1957) Reaction Kinetics in Differential Thermal Analysis. *Anal. Chem.* **29**, 1702–1706.
254. He G & Riedl B. (2003) Phenol-urea-formaldehyde cocondensed resol resins: Their synthesis, curing kinetics, and network properties. *J. Polym. Sci. Part B Polym. Phys.* **41**, 1929–1938.
255. Wimmer R, Kläusler O & Niemz P. (2013) Water sorption mechanisms of commercial wood adhesive films. *Wood Sci. Technol.* **47**, 763–775.

256. Konnerth J, Stoeckel F, Mueller U & Gindl W. (2010) Elastic Properties of Adhesive Polymers. III. Adhesive Polymer Films Under Dry and Wet Conditions Characterized by Means of Nanoindentation. *J. Appl. Polym. Sci.* **118**, 1331–1334.
257. Wellen RMR & Canedo EL. (2014) On the Kissinger equation and the estimate of activation energies for non-isothermal cold crystallization of PET. *Polym. Test.* **40**, 33–38.
258. Pizzi A & Stephanou A. (1993) On the Chemistry, Behavior, and Cure Acceleration of Phenol-Formaldehyde Resins Under Very Alkaline Conditions. *J. Appl. Polym. Sci.* 2157–2170.
259. Poljanšek I & Krajnc M. (2005) Characterization of phenol-formaldehyde prepolymer resins by in line FT-IR spectroscopy. *Acta Chim. Slov.* **52**, 238–244.
260. Werstler DD. (1986) Quantitative ¹³C n.m.r. characterization of aqueous formaldehyde resins: 1. Phenol-formaldehyde resins. *Polymer (Guildf).* **27**, 750–756.
261. Park BD, Riedl B, Yoon Soo Kim & So WT. (2002) Effect of synthesis parameters on thermal behavior of phenol-formaldehyde resol resin. *J. Appl. Polym. Sci.* **83**, 1415–1424.
262. Urquhart AR. (1959) Sorption of water by cellulose and starch. *Recent Adv. Chem. Cellul. starch* 311–341.
263. Sander M, Lu Y & Pignatello JJ. (2005) A Thermodynamically Based Method to Quantify True Sorption Hysteresis. *J. Environ. Qual.* **34**, 1063–1072.
264. Hill CAS, Norton AJ & Newman G. (2010) The water vapour sorption properties of Sitka spruce determined using a dynamic vapour sorption apparatus. *Wood Sci. Technol.* **44**, 497–514.
265. Cheong IW, Shin JS, Kim JH & Lee SJ. (2004) Preparation of monodisperse melamine-formaldehyde microspheres via dispersed polycondensation. *Macromol. Res.* **12**, 225–232.
266. Shams MI, Yano H & Endou K. (2004) Compressive deformation of wood impregnated with low molecular weight phenol formaldehyde (PF) resin I: Effects of pressing pressure and pressure holding. *J. Wood Sci.* **50**, 337–342.
267. Ohmae K, Minato K & Norimoto M. (2002) The analysis of dimensional changes due to chemical treatments and water soaking for hinoki (*Chamaecyparis obtusa*) wood. *Holzforschung* **56**, 98–102.
268. Buchelt B, Dietrich T & Wagenführ A. (2012) Macroscopic and microscopic monitoring of swelling of beech wood after impregnation with furfuryl alcohol. *Eur. J. Wood Wood Prod.* **70**, 865–869.
269. Kupfernagel C, Spear M, Pitman A, Yelle D, Brown SP & Ormondroyd G. (2022) Cell wall diffusion of low molecular weight PUF resin studied by liquid- and solid-state NMR. in *18th Annual Meeting of the Northern European Network for Wood Science and Engineering (2022)*.
270. Thybring EE & Fredriksson M. (2023) Wood and Moisture. in *Springer Handbook of Wood Science and Technology (eds. Niemz P)*, Springer Nature, Switzerland.
271. Stamm JA. (1956) Dimensional Stabilization of Wood with Carbowaxes. *For. Prod. J.* **6**, 201–204.
272. Siebertz K, Bebbler D Van & Hochkirchen T. (2010) *Statistische Versuchsplanung*. Springer, Berlin Heidelberg.
273. Okhrimenko D V., Thomsen AB, Ceccato M, Johansson DB, Lybye D, Bechgaard K, Tougaard S & Stipp SLS. (2018) Impact of curing time on ageing and degradation of phenol-urea-formaldehyde binder. *Polym. Degrad. Stab.* **152**, 86–94.
274. Spear MJ, Dimitriou A, Binding T & Ormondroyd GA. (2016) Mild Thermal Modification to Add Value to UK Grown Larch: Monitoring Quality, Physical Properties and Benefits. in *Proceedings of the 59th International Convention of Society of Wood Science and Technology* 34–41 (2016).
275. Roffael E & Rauch W. (1974) Extraktstoffe in Eiche und ihr Einfluß auf die Verleimbarkeit mit alkalischen Phenol-Formaldehydharzen. *Holz als Roh- und Werkst.* **32**, 182–187.
276. Popvic M, Djiporovic-Momcilovic M, Budinski-Simendic J, Jovicic M & Gavrilovic-Grmusa I. (2013) The influence of wood extracts on the curing kinetics of urea-formaldehyde adhesive studied by iso-conversional method. *Pro Ligno* **9**, 153–163.
277. Van Loon LR & Glaus MA. (1997) Review of the kinetics of alkaline degradation of cellulose in view of its relevance for safety assessment of radioactive waste repositories. *J. Environ. Polym. Degrad.* **5**, 97–109.
278. Yelle DJ. (2017) Solution-state NMR analysis of hydroxymethylated resorcinol cured in the presence of crude milled-wood lignin from *Acer saccharum*. *J. Appl. Polym. Sci.* **134**,

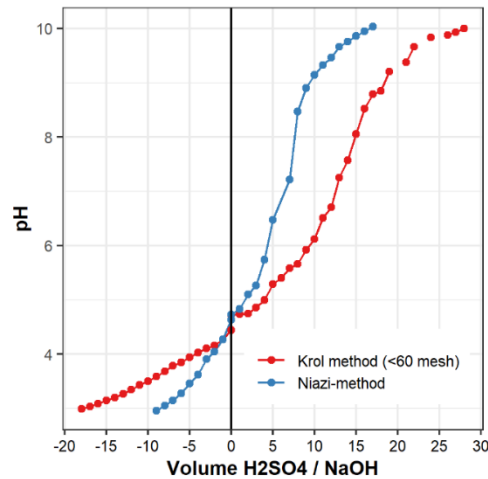
279. Kim H & Ralph J. (2010) Solution-state 2D NMR of ball-milled plant cell wall gels in DMSO-d₆/pyridine-d₅. *Org. Biomol. Chem.* **8**, 576–591.
280. Yelle DJ. (2023) Personal Communication.
281. Newman RH. (1992) Solid-State ¹³C NMR Spectroscopy of Multiphase Biomaterials. *Polym. Commun. Guildf.* **27**, 154–157.
282. Zumbulyadis N. (1983) Selective carbon excitation and the detection of spatial heterogeneity in cross-polarization magic-angle-spinning NMR. *J. Magn. Reson.* **53**, 486–494.
283. Tang HR, Wang YL & Belton PS. (2000) ¹³C CPMAS studies of plant cell wall materials and model systems using proton relaxation-induced spectral editing techniques. *Solid State Nucl. Magn. Reson.* **15**, 239–248.
284. Newman RH. (1992) Nuclear Magnetic Resonance Study of Spatial Relationships Between Chemical Components in Wood Cell Walls. *Holzforschung* **46**, 205–210.
285. Fung BM, Khitritin AK & Ermolaev K. (2000) An Improved Broadband Decoupling Sequence for Liquid Crystals and Solids. *J. Magn. Reson.* **142**, 97–101.
286. Metz G, Wu XL & Smith SO. (1994) Ramped-Amplitude Cross Polarization in Magic-Angle-Spinning NMR. *J. Magn. Reson. Ser. A* **110**, 219–227.
287. Frye JS. (1989) Comparison of inversion-recovery methods for measuring longitudinal relaxation rates. *Concepts Magn. Reson.* **1**, 27–33.
288. Torchia DA. (1978) The measurement of proton-enhanced carbon-13 T1 values by a method which suppresses artifacts. *J. Magn. Reson.* **30**, 613–616.
289. Kamke FA & Lee JN. (2007) Adhesive penetration in wood - A review. *Wood Fiber Sci.* **39**, 205–220.
290. Kupfernagel C, Spear MJ, Pitman AJ & Ormondroyd GA. (2023) Wood modification with phenol urea formaldehyde (PUF) resin: The influence of wood species selection on the dimensional stability. *Eur. J. Wood Wood Prod.* **81**, 5-19.
291. Newman RH & Hemmingson JA. (1990) Determination of the Degree of Cellulose Crystallinity in Wood by Carbon-13 Nuclear Magnetic Resonance Spectroscopy. *Holzforschung* **44**, 351–356.
292. Maunu SL. (2002) NMR studies of wood and wood products. *Prog. Nucl. Magn. Reson. Spectrosc.* **40**, 151–174.
293. Hult EL, Larsson PT & Iversen T. (2000) Comparative CP/MAS ¹³C-NMR study of cellulose structure in spruce wood and kraft pulp. *Cellulose* **7**, 35–55.
294. Argyropoulos DS & Morin FG. (1995) Probing the macromolecular structure of wood and pulps with proton spin-lattice relaxation time measurements in the solid state. *Wood Sci. Technol.* **29**, 19–30.
295. Schmidt RG & Frazier CE. (1998) ¹³C CP/MAS NMR as a direct probe of the wood-phenol formaldehyde adhesive bondline. *Wood Fiber Sci.* **30**, 250–258.
296. Jakes JE. (2019) Mechanism for Diffusion through Secondary Cell Walls in Lignocellulosic Biomass. *J. Phys. Chem. B* **123**, 4333–4339.
297. Kulasinski K, Guyer R, Derome D & Carmeliet J. (2015) Water Adsorption in Wood Microfibril-Hemicellulose System: Role of the Crystalline-Amorphous Interface. *Biomacromolecules* **16**, 2972–2978.
298. Terenzi C, Prakobna K, Berglund LA & Furó I. (2015) Nanostructural effects on polymer and water dynamics in cellulose biocomposites: 2H and 13C NMR relaxometry. *Biomacromolecules* **16**, 1506–1515.
299. Lignia Fire (2020) <https://www.residentialproductsonline.com/modified-wood-product-lignia-fire-achieves-30-minute-class-flame-spread-rating> (2020), accessed 5.1.2024.
300. Beckers E & Bongers HPM. (2003) Mechanical properties of acetylated solid wood treated on pilot plant scale Mechanical properties of acetylated solid wood treated on pilot plant scale.
301. Füchtner S, Brock-Nannestad T, Smeds A, Fredriksson M, Pilgård A & Thygesen LG. (2020) Hydrophobic and Hydrophilic Extractives in Norway Spruce and Kurile Larch and Their Role in Brown-Rot Degradation. *Front. Plant Sci.* **11**.
302. Vyazovkin S. (2020) Kissinger Method in Kinetics of Materials: Things to Beware and Be Aware of. *Molecules* **25**.

303. Vyazovkin S V & Lesnikovich AI. (1990) An approach to the solution of the inverse kinetic problem in the case of complex processes: Part 1. Methods employing a series of thermoanalytical curves. *Thermochim. Acta* **165**, 273–280.
304. Vyazovkin S & Sbirrazzuoli N. (1996) Mechanism and Kinetics of Epoxy–Amine Cure Studied by Differential Scanning Calorimetry. *Macromolecules* **29**, 1867–1873.
305. Digaitis R, Thybring EE, Thygesen LG & Fredriksson M. (2021) Targeted acetylation of wood: a tool for tuning wood-water interactions. *Cellulose* **28**, 8009–8025.
306. Arnould O, Capron M, Ramonda M, Laurans F, Alméras T, Pilate G & Clair B. (2022) Mechanical characterisation of the developing cell wall layers of tension wood fibres by Atomic Force Microscopy. *Peer Community J.* **2**,.
307. Konnerth J, Harper D, Lee SH, Rials TG & Gindl W. (2008) Adhesive penetration of wood cell walls investigated by scanning thermal microscopy (SThM). *Holzforschung* **62**, 91–98.
308. Kurkowiak K, Hentges D, Dumarçay S, Gérardin P & Militz H. (2022) Understanding the mode of action of sorbitol and citric acid (SorCA) in wood. *Wood Mater. Sci. Eng.* 1–9.
309. Wang Y, Azhar S, Lindström ME & Henriksson G. (2015) Stabilization of polysaccharides during alkaline pre-treatment of wood combined with enzyme-supported extractions in a biorefinery. *J. Wood Chem. Technol.* **35**, 91–101.
310. Curling SF, Fowler PA & Hill CAS. (2007) Development of a method for the production of hemicellulosic gels from Sitka spruce. *Carbohydr. Polym.* **69**, 673–677.
311. Slabohm M, Brischke C & Militz H. (2023) The durability of acetylated beech (*Fagus sylvatica* L.) laminated veneer lumber (LVL) against wood-destroying basidiomycetes. *Eur. J. Wood Wood Prod.* **81**, 911–921.
312. Neue Freileitungsmasten aus Furnierschichtholz – stabiler bei weniger Materialeinsatz. (2017) <https://biowerkstoffe.fnr.de/service/presse/pressearchiv/archiv-nachricht/neue-freileitungsmasten-aus-furnierschichtholz-stabiler-bei-weniger-materialeinsatz>, accessed 19.1.2024.
313. Karthäuser J, Biziks V, Frauendorf H, Mai C & Militz H. (2022) Vacuum Low-Temperature Microwave-Assisted Pyrolysis of Technical Lignins. *Polymers (Basel)*. **14**,.
314. Kellock M, Tuominen L, Widsten P, Treu A & Borrega M. (2023) Alkaline bark extract as impregnation solution for wood protection. in *Wood Science and Engineering 2023*.
315. Lignin-based resin (2017) <https://prefere.com/en/company/news/biopolymers-put-to-industrial-use-at-phenolic-resin-producer-prefere-resins>, accessed 20.1.2024.
316. Developing a lignin-based resin for plywood. (2020) <https://www.storaenso.com/en/newsroom/news/2020/6/developing-a-lignin-based-resin-for-plywood>, accessed 20.1.2024.
317. Karthäuser J, Biziks V, Frauendorf H, Hoffmann L, Raskop S, Roggatz D & Militz H. (2023) Substituting phenol in phenol–formaldehyde resins for wood modification by phenolic cleavage products from vacuum low-temperature microwave-assisted pyrolysis of softwood kraft lignin. *Cellulose* **30**, 7277–7293.
318. Militz H & Lande S. (2009) Challenges in wood modification technology on the way to practical applications. *Wood Mater. Sci. Eng.* **4**, 23–29.
319. Bongers F, Roberts M, Stebbins H & Rowell R. (2009) Introduction of Accoya® Wood on the Market – Technical Aspects. 301–309.

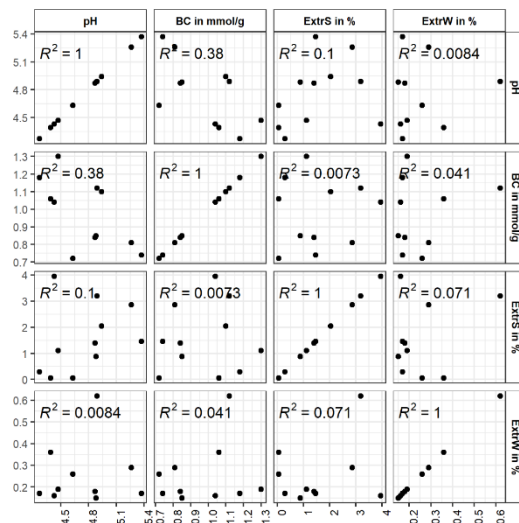
Appendix



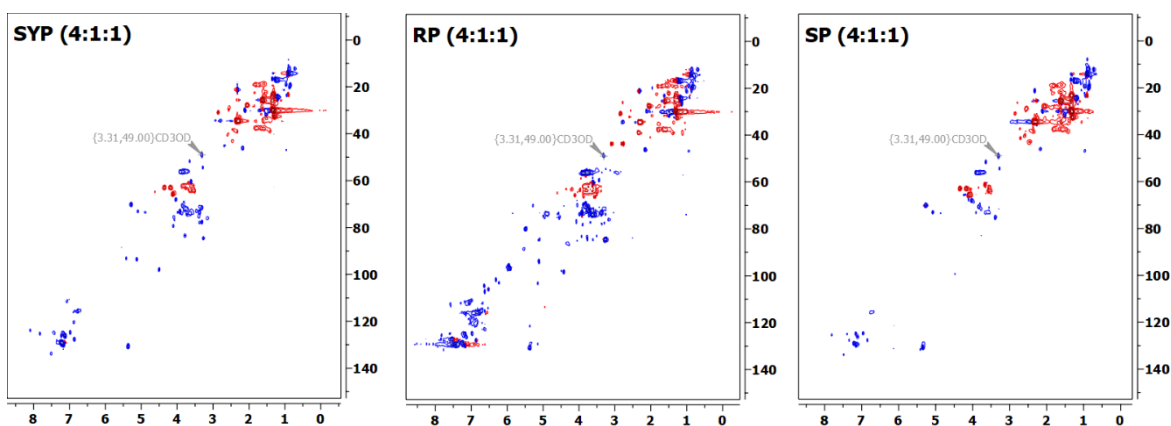
Appendix 1 FTIR-ATR spectra of all eleven unmodified timbers shown in absorbance mode. The conversion from reflectance to absorbance can be used for quantitative task, e.g., the development of partial least square models



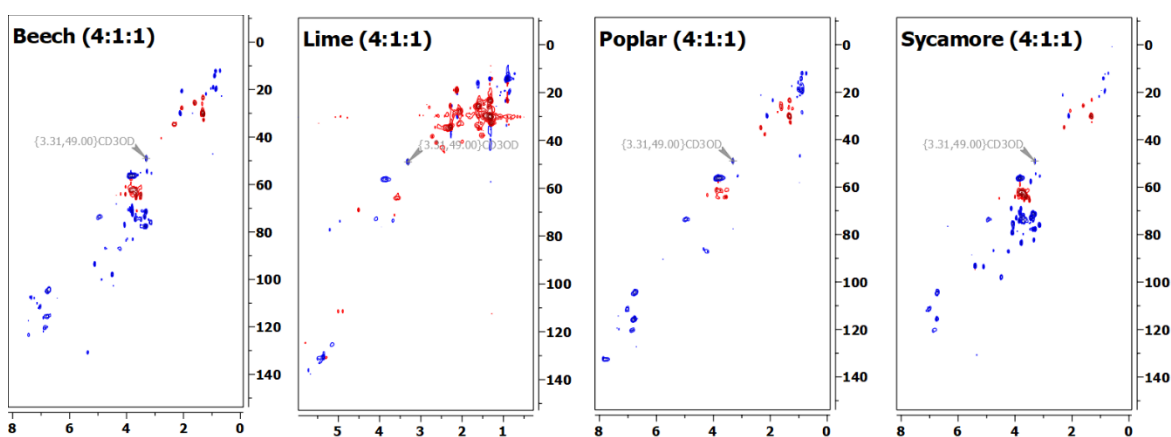
Appendix 2 Comparison of the titration curves obtained from in the hot-water extracts and the cold-water suspension of beech wood.



Appendix 3 Juxtaposition of extractives content (ExtrW and ExtrS) against pH value and alkaline buffer capacity. The missing correlation between pH, alkaline buffer capacity, ExtrS, and ExtrW content indicates that the extractives content has no influence in the alkaline buffering behaviour. Instead, the chemical structure of extractives seems to be crucial.



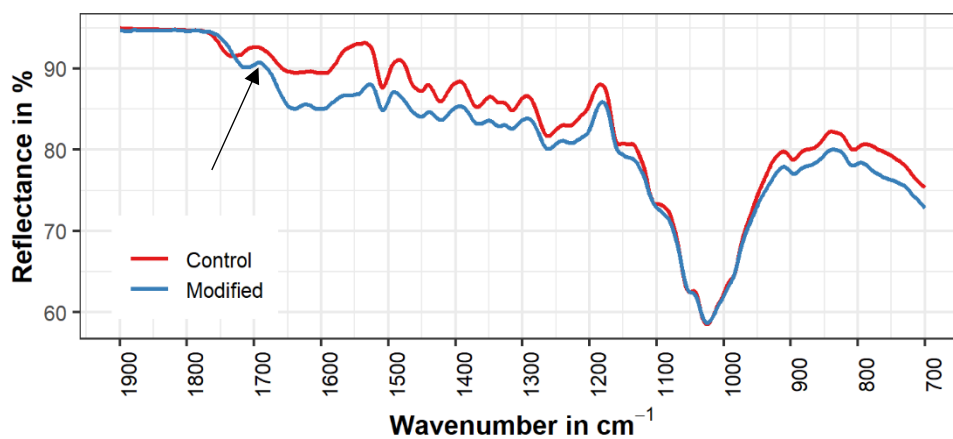
Appendix 4 ^1H - ^{13}C -Heteronuclear Single Quantum Coherence (HSQC) spectra of SYP, Radiata pine, and Scots pine solvent extractives (ExtrS). Similar spectra indicate a similar chemical composition.



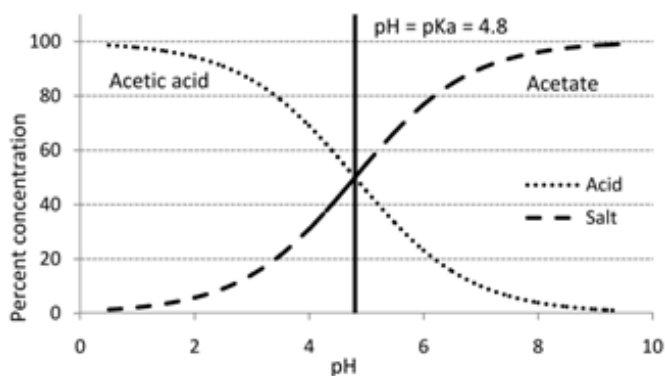
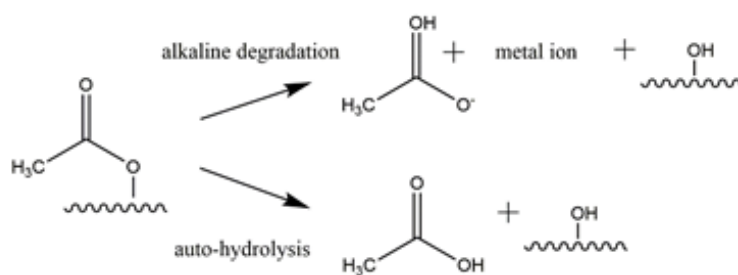
Appendix 5 ^1H - ^{13}C -Heteronuclear Single Quantum Coherence (HSQC) spectra of beech, lime, poplar, and sycamore solvent extractives (ExtrS). Dissimilar spectra indicate differences in the extractive fractions of hardwoods.

Appendix 6 Integrated peak areas of the uncured resin in the ^{13}C DEPTQ NMR spectrum. Peaks are normalised to the p-p methylene bridge signal at 41 ppm.

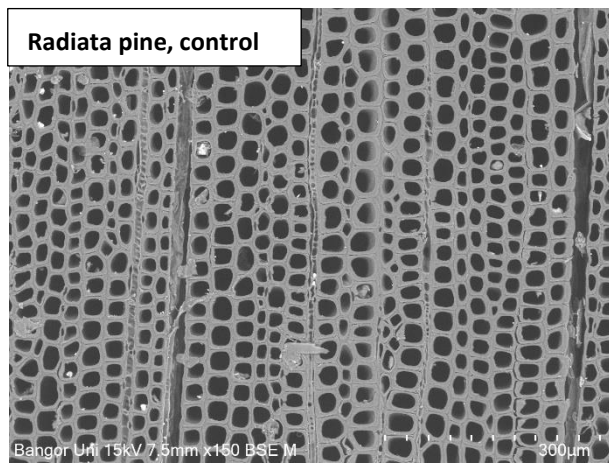
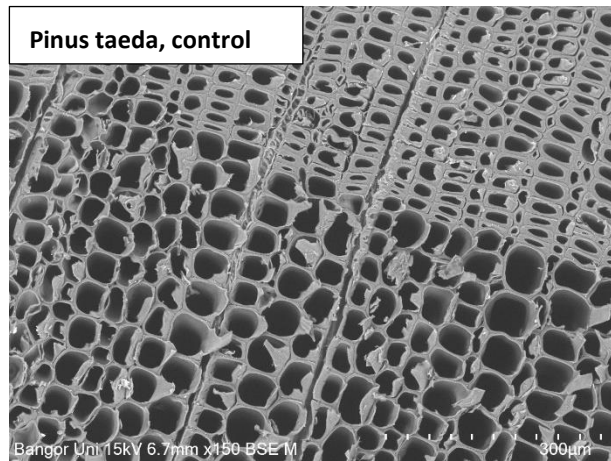
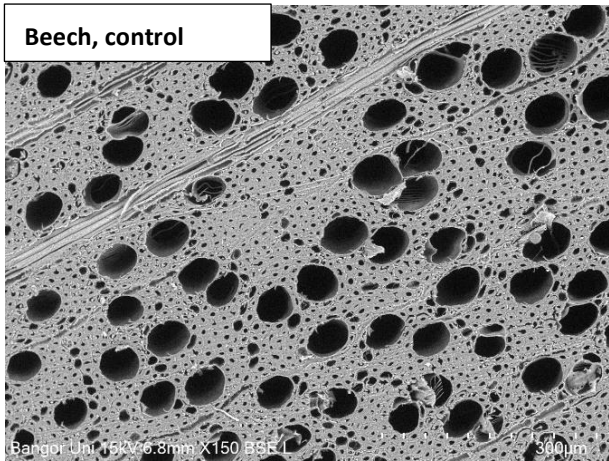
Chemical Shift Range in ppm	Normalized Peak Area
170.83 .. 169.92	-0.1
163.40 .. 162.29	0.78
161.75 .. 159.40	0.96
158.04 .. 150.58	1.32
135.49 .. 132.73	1.25
132.69 .. 126.43	-6.34
128.71 .. 128.14	0.32
126.17 .. 124.38	0.31
121.67 .. 120.62	-0.13
117.29 .. 115.98	-1.43
83.32 .. 82.67	0.03
72.61 .. 69.07	1.07
67.23 .. 66.15	0.88
65.83 .. 63.87	3.55
62.54 .. 59.96	5.72
50.43 .. 49.79	-0.11
41.57 .. 40.68	1
36.41 .. 35.35	0.88



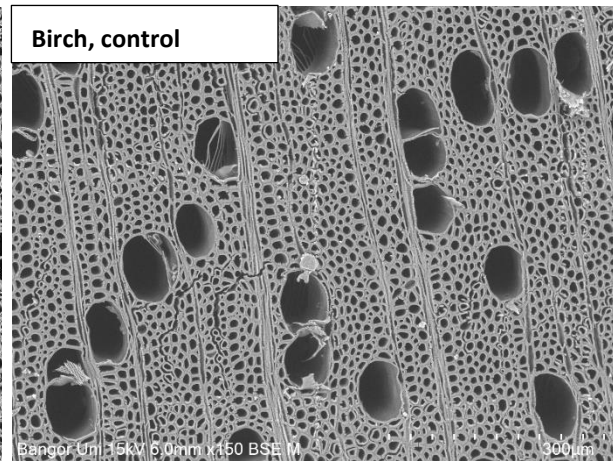
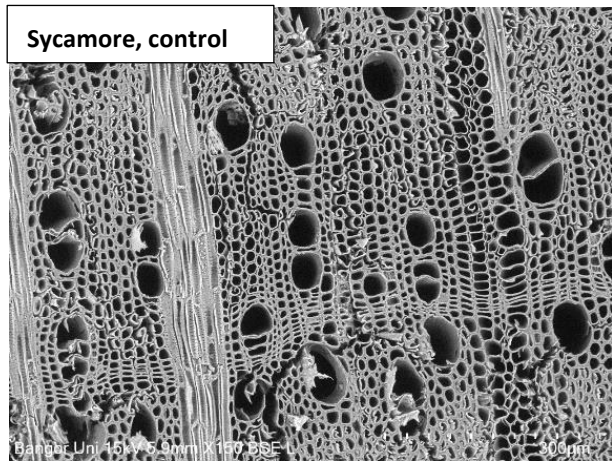
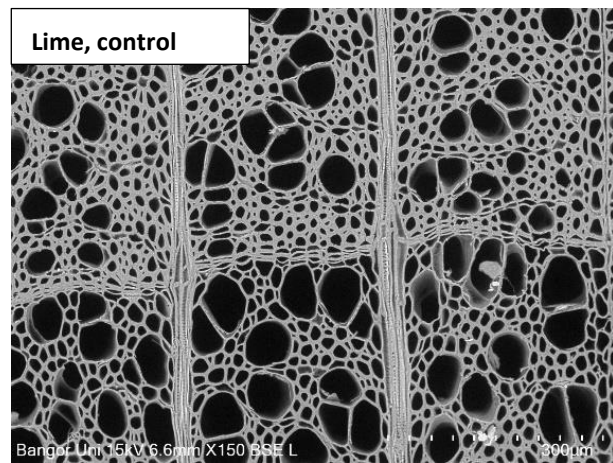
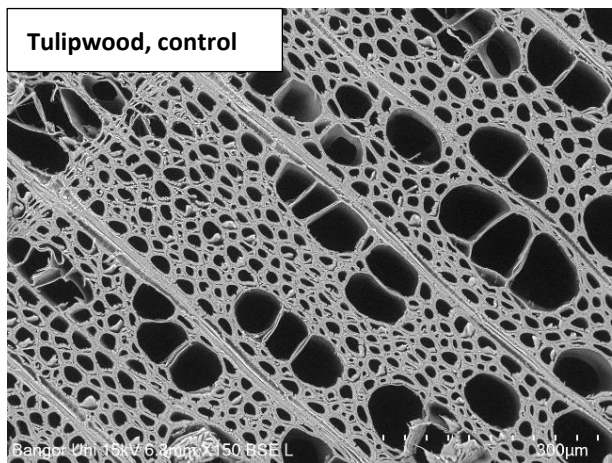
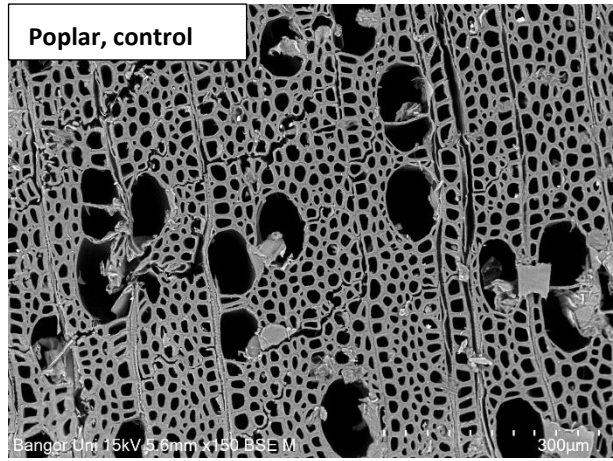
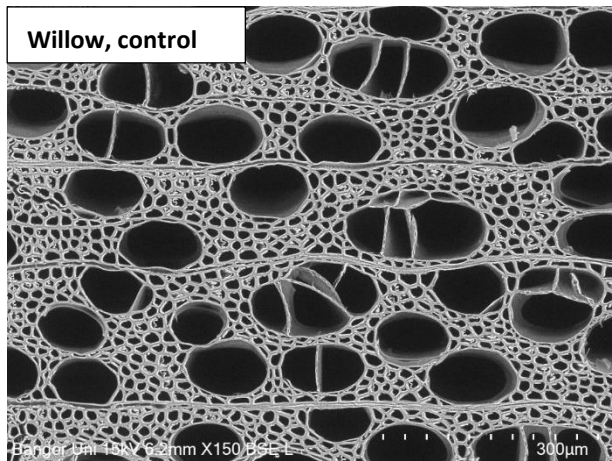
Appendix 7 FTIR-ATR spectrum of unmodified and modified Radiata pine wood. Shift of the carbonyl band to lower wavenumbers after modification. As a result of deacetylation, the carbonyl peak at 1730 cm^{-1} (indicated by arrow) shifts to lower wavenumbers after modification. This shift is observed in all timbers to a varying extent.



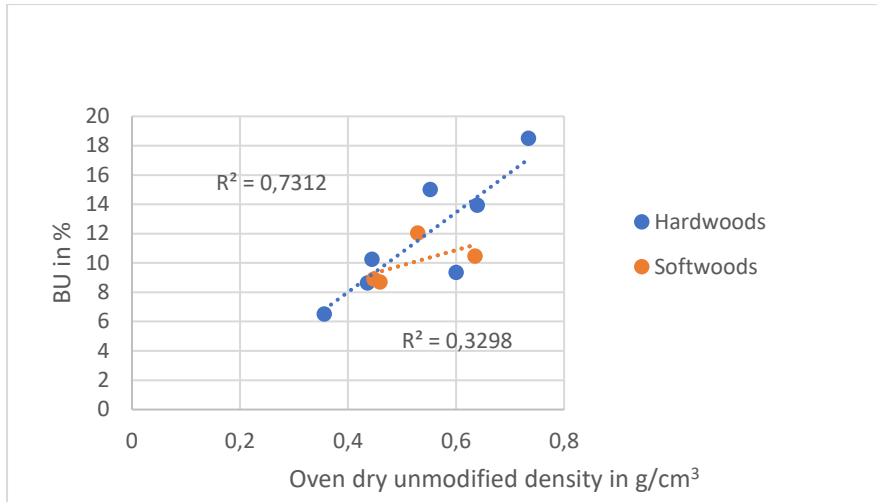
Appendix 8 (top) Deacetylation mechanism of O-acetyl groups in hemicelluloses in different pH environments. (bottom) equilibrium of acetic acid and acetate salt at different pH adopted from Patil (2012)⁵⁰.



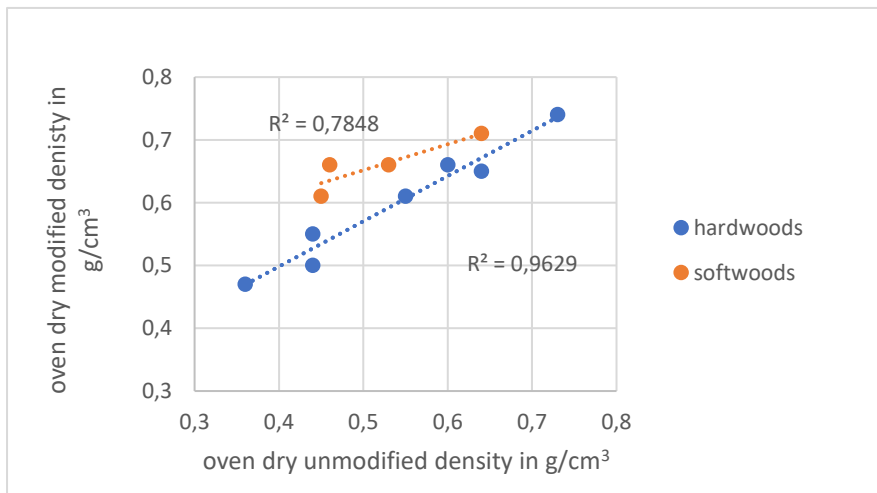
Appendix 9 (a) SEM images of unmodified timbers in the transverse section using the same magnification of 150x.



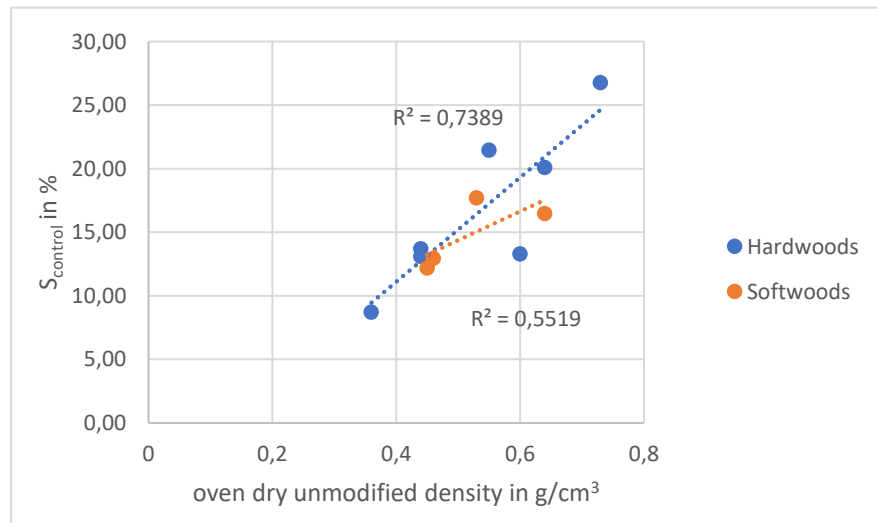
Appendix 9 SEM images of unmodified timbers in the transverse section using the same magnification of 150x.



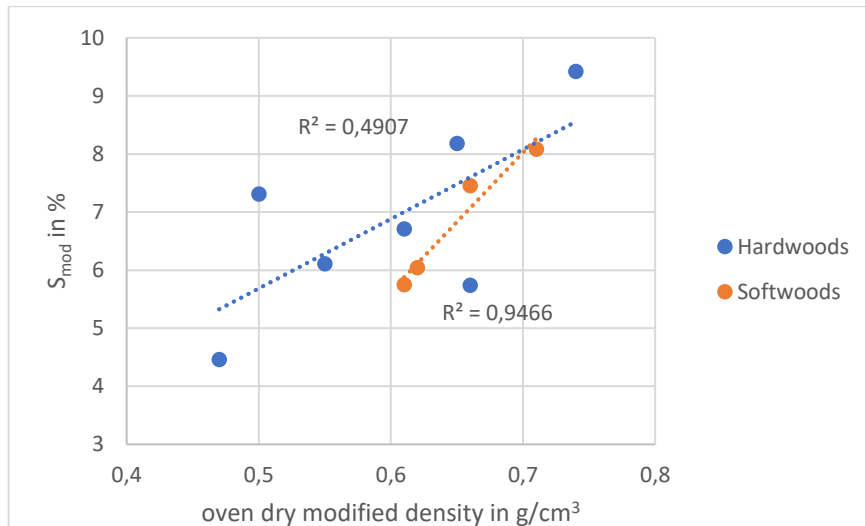
Appendix 10 Correlation between bulking coefficient (BU) and oven dry unmodified density in hardwoods and softwoods.



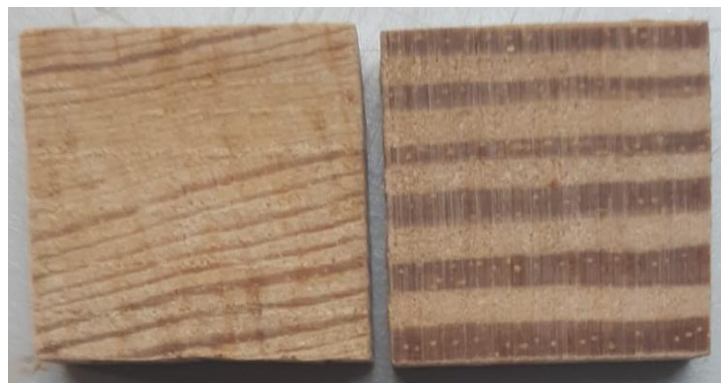
Appendix 11 Correlation between oven dry unmodified density and oven dry modified density in softwoods and hardwoods.



Appendix 12 Correlation between oven dry unmodified density and swelling coefficient of unmodified wood ($S_{control}$)



Appendix 13 Correlation between oven dry modified density and swelling coefficient of modified wood (S_{mod})



Appendix 14 Differences in annual ring width in SYP and Scots pine in this study. Scots pine (left) and SYP (right).

Appendix 15 Results of two-way ANOVA test showing the correlation between treating fluid, wood species, their interaction, and the swelling coefficient. Asterisks indicate statistical significance. The treating fluid has no significant effect on the swelling coefficient ($p > 0.05$).

	Df	Sum	Sq Mean	Sq F value	p-value
Treating_fluid	1	0	0.1	0.160	0.69004
Species	10	4809	480.9	579.372	< 2e-16 ***
Treating_fluid:Species	10	21	2.1	2.475	0.00823 **
Residuals	194	161	0.8		

Signif. codes: 0 '***' 0.001 '**' 0.01 '*' 0.05 '.' 0.1 ' ' 1

Appendix 16 Results of Tukey test showing the pairwise comparison of treating fluid within each species. P-values lower than 0.95 indicate a statically significant effect of the treating fluid on swelling coefficient after impregnation.

Test groups compared	diff	lwr	upr	p-value
In_water:Willow-In_resin:Willow	0.206739	-1.27826	1.691735	1
In_water:Poplar-In_resin:Poplar	-0.687	-2.17199	0.798001	0.986827
In_water:Tulipwood-In_resin:Tulipwood	0.903728	-0.62196	2.429417	0.856265
In_water:Radiata Pine-In_resin:Radiata Pine	-0.82186	-2.30686	0.663133	0.917768
In_water:Pinus taeda-In_resin:Pinus taeda	0.142302	-1.34269	1.627298	1
In_water:Scots Pine-In_resin:Scots Pine	0.292096	-1.15876	1.74295	1
In_water:Lime-In_resin:Lime	0.295274	-1.27005	1.860598	1
In_water:Sycamore-In_resin:Sycamore	1.448317	-0.07737	2.974006	0.086776
In_water:SYP-In_resin:SYP	-0.22376	-1.70875	1.26124	1
In_water: Birch-In_resin: Birch	-0.22483	-1.70983	1.260164	1
In_water:Beech-In_resin:Beech	-0.00592	-1.53161	1.519766	1

Appendix 17 – Results of two-way ANOVA test showing the effect of modification on the total swelling coefficient (bulking + swelling in water). Asterisks indicate statistical significance. Modified and unmodified groups have significantly different total swelling values ($p < 0.05$).

	Df	Sum Sq	Mean Sq	F value	p-value
Control_Modified	1	423	423.4	606.16	< 2e-16 ***
Species	10	4862	486.2	696.01	< 2e-16 ***
Control_Modified:Species	10	17	1.7	2.44	0.00922 **
Residuals	193	135	0.7		

Signif. codes: 0 '***' 0.001 '**' 0.01 '*' 0.05 '.' 0.1 ' ' 1

Appendix 18 Results of Tukey test showing the effect of modification on total swelling for every species. P-values lower than 0.95 indicate a statically significant effect of modification of modification on total swelling coefficient.

Test groups compared	diff	lwr	upr	p-value
control:Willow-modified:Willow	-2.55155	-3.91396	-1.18914	2.5E-08
control:Poplar-modified:Poplar	-3.48818	-4.85059	-2.12577	2.37E-13
control:Tulipwood-modified:Tulipwood	-2.79121	-4.19096	-1.39147	2.01E-09
control:Radiata Pine-modified:Radiata Pine	-2.96906	-4.33147	-1.60665	3.64E-11
control:Pinus taeda-modified:Pinus taeda	-2.31291	-3.67533	-0.9505	8.08E-07
control:Scots Pine-modified:Scots Pine	-2.70428	-4.06669	-1.34187	2.43E-09
control:Lime-modified:Lime	-1.43505	-2.83479	-0.0353	0.03737
control:Sycamore-modified:Sycamore	-2.22021	-3.61995	-0.82046	6.55E-06
control:SYP-modified:SYP	-2.92862	-4.29104	-1.56621	6.98E-11
control: Birch-modified: Birch	-3.12716	-4.48957	-1.76475	2.91E-12
control:Beech-modified:Beech	-3.48269	-4.88244	-2.08295	2.52E-13

Appendix 19 Total swelling (TS) compared with the swelling coefficient of unmodified wood ($S_{control}$). The difference between both values is between 1.25 – 3.49%.

Species	TS in %	$S_{control}$ in %	$\Delta(TS - S_{control})$ in %
Beech	11.26 (1.01)	26.76 (1.82)	2.89
Birch	16.59 (1.60)	20.09 (1.07)	3.13
Sycamore	16.98 (0.49)	13.28 (0.47)	2.36
Lime	22.71 (0.75)	21.46 (0.64)	1.25
Tulipwood	15.64 (0.98)	13.70 (0.59)	3.28
Poplar	23.22 (1.69)	13.10 (1.24)	3.49
Willow	29.65 (0.43)	8.71 (0.84)	2.55
SYP	15.17 (0.41)	16.46 (0.27)	2.92
Scots Pine	15.26 (0.42)	17.71 (0.12)	2.70
Pinus taeda	20.41 (0.44)	12.94 (0.64)	2.32
Radiata Pine	19.38 (0.50)	12.20 (0.53)	2.97

Appendix 20 Water uptake during second soak cycle (WU_2) including resin mass in the calculation. WU_s is higher in unmodified wood.

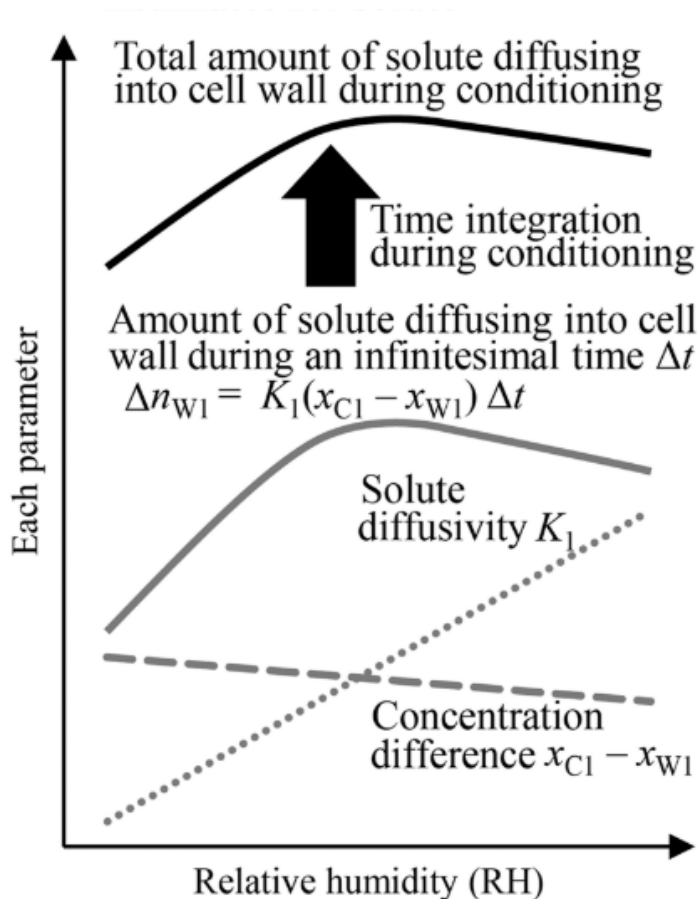
Species	WU2 in %	
	unmodified wood	modified wood
Willow	235.1 (11.25)	132.5 (5.92)
Poplar	191.7 (10.88)	122.1 (6.71)
Tulipwood	197.1 (3.38)	110.3 (1.64)
Radiata Pine	184.8 (3.73)	101.0 (1.14)
Pinus taeda	174.6 (12.20)	88.1 (5.06)
Scots Pine	153.5 (2.35)	82.0 (0.69)
Lime	149.2 (2.22)	91.8 (2.83)
Sycamore	123.0 (3.52)	81.6 (1.92)
SYP	116.2 (1.76)	75.6 (2.07)
Birch	112.5 (8.40)	88.5 (3.85)
Beech	100.6 (1.13)	67.9 (0.70)

Appendix 21 Water uptake excluding the mass of resin in the first soak cycle (WU_0) of modified and unmodified wood. WU_0 is higher in modified wood.

Species	WU 0 in %	
	unmodified wood	modified wood
Willow	229.1 (9.66)	246.8 (14.99)
Poplar	186.4 (19.32)	186.1 (16.46)
Tulipwood	196.6 (4.09)	204.9 (3.06)
Radiata Pine	183.3 (3.58)	205.0 (3.78)
Pinus taeda	175.9 (12.51)	192.0 (17.68)
Scots Pine	151.0 (1.58)	159.4 (1.74)
Lime	150.2 (2.87)	154.9 (6.82)
Sycamore	117.3 (4.77)	121.0 (5.86)
SYP	113.8 (2.01)	126.3 (4.11)
Birch	110.1 (8.79)	129.9 (8.72)
Beech	99.0 (0.97)	110.0 (1.40)

Appendix 22 Results of Tukey test showing the effect of modification on total mass loss for every species. P-values lower than 0.95 indicate a statically significant effect of modification on the total mass during water soaking.

Test groups compared	diff	lwr	upr	p-value
control:Willow-modified:Willow	-0.0904794	-0.3392308	0.15827195	0.99943328
control:Poplar-modified:Poplar	-0.0350763	-0.61845	0.54829734	1
control:Tulipwood-modified:Tulipwood	1.45994847	1.2111971	1.70869985	9.2149E-15
control:Radiata Pine-modified:Radiata Pine	0.94092228	0.67871531	1.20312925	9.6589E-15
control:Pinus taeda-modified:Pinus taeda	1.5313272	1.28257583	1.78007858	9.2149E-15
control:Scots Pine-modified:Scots Pine	0.6412605	0.39250913	0.89001188	2.2449E-13
control:Lime-modified:Lime	-0.0640576	-0.312809	0.18469373	0.99999789
control:Sycamore-modified:Sycamore	-0.1026007	-0.3664414	0.16123998	0.99853375
control:SYP-modified:SYP	0.30563015	0.05687878	0.55438153	0.00252389
control:Birch-modified:Birch	0.76084917	0.51209779	1.00960054	1.0814E-13
control:Beech-modified:Beech	0.36566945	0.11010171	0.62123719	0.00010411



Appendix 23 Comparative effects of mechanisms active during cell wall diffusion. The effect of resin mobility (solute diffusivity often) outweighs that of the concentration gradient. Adapted from Tanaka et al.⁹⁰.

Appendix 24 Results of Tukey test showing the pairwise comparison of resin concentrations within each species. P-values lower than 0.95 indicate a statically significant effect of the bulking coefficient (BU).

rowname	diff	lwr	upr	p adj
30%:Beech-20%:Beech	1.80893	0.6826564	2.9352036	0.0000698
40%:Beech-20%:Beech	2.5585856	1.432312	3.6848592	0.0000000
40%:Beech-20%:Beech	0.7496556	-0.376618	1.8759292	0.4660809
30%:Radiata pine-20%:Radiata pine	0.9651972	-0.191939	2.1223333	0.1794757
40%:Radiata pine-20%:Radiata pine	-0.3690487	-1.4953223	0.7572249	0.9800592
40%:Radiata pine-30%:Radiata pine	-1.3342459	-2.491382	-0.1771097	0.0120857
30%:Tulipwood-20%:Tulipwood	0.852624	-0.2736496	1.9788976	0.2911450
40%:Tulipwood-20%:Tulipwood	0.8651021	-0.2611715	1.9913757	0.2728783
40%:-:Tulipwood-30%:Tulipwood	0.0124781	-1.1137955	1.1387517	1.0000000

Appendix 25 Results of Tukey test showing the pairwise comparison of resin concentrations within each species. P-values lower than 0.95 indicate a statically significant effect of the swelling coefficient S_{mod2} .

rowname	diff	lwr	upr	p adj
30%:Beech-20%:Beech	-0.1538919	-0.8060875	0.4983038	0.9977695
40%:Beech-20%:Beech	-1.1013637	-1.7535593	-0.4491681	0.0000244
40%:Beech-20%:Beech	-0.9474718	-1.5996675	-0.2952762	0.0004537
30%:Radiata pine-20%:Radiata pine	0.4393632	-0.2307042	1.1094305	0.4869981
40%:Radiata pine-20%:Radiata pine	1.4265686	0.774373	2.0787643	0.0000000
40%:Radiata pine-30%:Radiata pine	0.9872055	0.3171381	1.6572728	0.0003553
30%:Tulipwood-20%:Tulipwood	-0.3585511	-1.0107467	0.2936446	0.7121748
40%:Tulipwood-20%:Tulipwood	-0.5229796	-1.1751752	0.129216	0.2217709
40%:-:Tulipwood-30%:Tulipwood	-0.1644285	-0.8166242	0.4877671	0.9964601

Appendix 26 Results of Tukey test showing the pairwise comparison of resin pH values within each species. P-values lower than 0.95 indicate a statically significant effect of the bulking coefficient BU.

rowname	diff	lwr	upr	p adj
9.45:Beech-9.16:Beech	-0.7974098	-1.5455504	-0.0492691	0.0261564
9.87:Beech-9.16:Beech	-2.0396592	-2.7877998	-1.2915185	0.0000000
9.87:Beech-9.45:Beech	-1.2422494	-1.99039	-0.4941088	0.0000135
9.45:Radiata Pine-9.16:Radiata Pine	-0.6151436	-1.3632842	0.1329971	0.2181393
9.87:Radiata Pine-9.16:Radiata Pine	-0.6901166	-1.4382573	0.058024	0.1002483
9.87:Radiata Pine-9.45:Radiata Pine	-0.0749731	-0.8231137	0.6731676	1.0000000
9.45:SYP-9.16:SYP	-0.3855037	-1.1336443	0.3626369	0.8539255
9.87:SYP-9.16:SYP	-1.0045574	-1.752698	-0.2564167	0.0010690
9.87:SYP-9.45:SYP	-0.6190537	-1.3671943	0.129087	0.2102386
9.45:Tulipwood-9.16:Tulipwood	0.2465567	-0.5469663	1.0400796	0.9963910
9.87:Tulipwood-9.16:Tulipwood	-0.0568573	-0.8049979	0.6912834	1.0000000
9.87:Tulipwood-9.45:Tulipwood	-0.3034139	-1.0969369	0.490109	0.9801900

Appendix 27 Results of Tukey test showing the pairwise comparison of resin pH values within each species. P-values lower than 0.95 indicate a statically significant effect of the swelling coefficient S_{mod2}

rowname	diff	lwr	upr	p adj
9.45:Beech-9.16:Beech	0.8914358	0.3209876	1.4618841	0.0000561
9.87:Beech-9.16:Beech	1.9563524	1.3859042	2.5268006	0.0000000
9.87:Beech-9.45:Beech	1.0649165	0.4944683	1.6353647	0.0000006
9.45:Radiata Pine-9.16:Radiata Pine	0.2076564	-0.3784234	0.7937362	0.9890716
9.87:Radiata Pine-9.16:Radiata Pine	1.3198181	0.7493699	1.8902663	0.0000000
9.87:Radiata Pine-9.45:Radiata Pine	1.1121617	0.5260819	1.6982415	0.0000004
9.45:SYP-9.16:SYP	0.4908732	-0.079575	1.0613214	0.1647344
9.87:SYP-9.16:SYP	1.3856242	0.7995444	1.971704	0.0000000
9.87:SYP-9.45:SYP	0.894751	0.3086712	1.4808309	0.0000929
9.45:Tulipwood-9.16:Tulipwood	-0.0257157	-0.6307674	0.579336	1.0000000
9.87:Tulipwood-9.16:Tulipwood	0.6990751	0.1286269	1.2695233	0.0045203
9.87:Tulipwood-9.45:Tulipwood	0.7247908	0.1197391	1.3298425	0.0062300

Appendix 28 Results of Tukey test showing the pairwise comparison of resin pH values within each species. P-values lower than 0.95 indicate a statically significant effect of the total mass loss ML_{total}

rowname	diff	lwr	upr	p adj
9.45:Beech-9.16:Beech	-0.377849	-0.5711732	-0.1845249	0.0000002
9.87:Beech-9.16:Beech	-1.3340337	-1.5224628	-1.1456046	0.0000000
9.87:Beech-9.45:Beech	-0.9561847	-1.1446137	-0.7677556	0.0000000
9.45:Radiata Pine-9.16:Radiata Pine	-0.4990071	-0.6874362	-0.310578	0.0000000
9.87:Radiata Pine-9.16:Radiata Pine	-1.8920523	-2.0853764	-1.6987281	0.0000000
9.87:Radiata Pine-9.45:Radiata Pine	-1.3930451	-1.5814742	-1.204616	0.0000000
9.16:SYP-9.45:Radiata Pine	1.0395407	0.8561373	1.2229441	0.0000000
9.45:SYP-9.45:Radiata Pine	0.8716367	0.6832076	1.0600658	0.0000000
9.87:SYP-9.45:Radiata Pine	0.0116602	-0.1717432	0.1950636	1.0000000
9.45:Tulipwood-9.16:Tulipwood	-0.0784916	-0.2669207	0.1099375	0.9622774
9.87:Tulipwood-9.16:Tulipwood	-1.5140806	-1.6974841	-1.3306772	0.0000000
9.87:Tulipwood-9.45:Tulipwood	-1.435589	-1.6240181	-1.24716	0.0000000

Appendix 29 Results of one-way ANOVA test showing the correlation between test group and the bulking coefficient BU. Asterisks indicate statistical significance. The BU differs significantly between test groups.

	Df	Sum	Sq	Mean	Sq	F	value	Pr(>F)	
Test_Group	8	24.25	3.0319	14.69	6.07E-12	***			
Residuals	64	13.21	0.2064						

Signif. codes:	0	'***'	0.001	'**'	0.01	'*'	0.05	.'	0.1

Appendix 30 Results of one-way ANOVA test showing the correlation between test group and the swelling coefficient S_{mod2} . Asterisks indicate statistical significance. S_{mod2} differs significantly between test groups.

	Df	Sum	Sq	Mean	Sq	F	value	Pr(>F)		
Test_Group	8	8.749	1.0936	6.621	6.14E-06	***				
Residuals	52	8.588	0.1652							

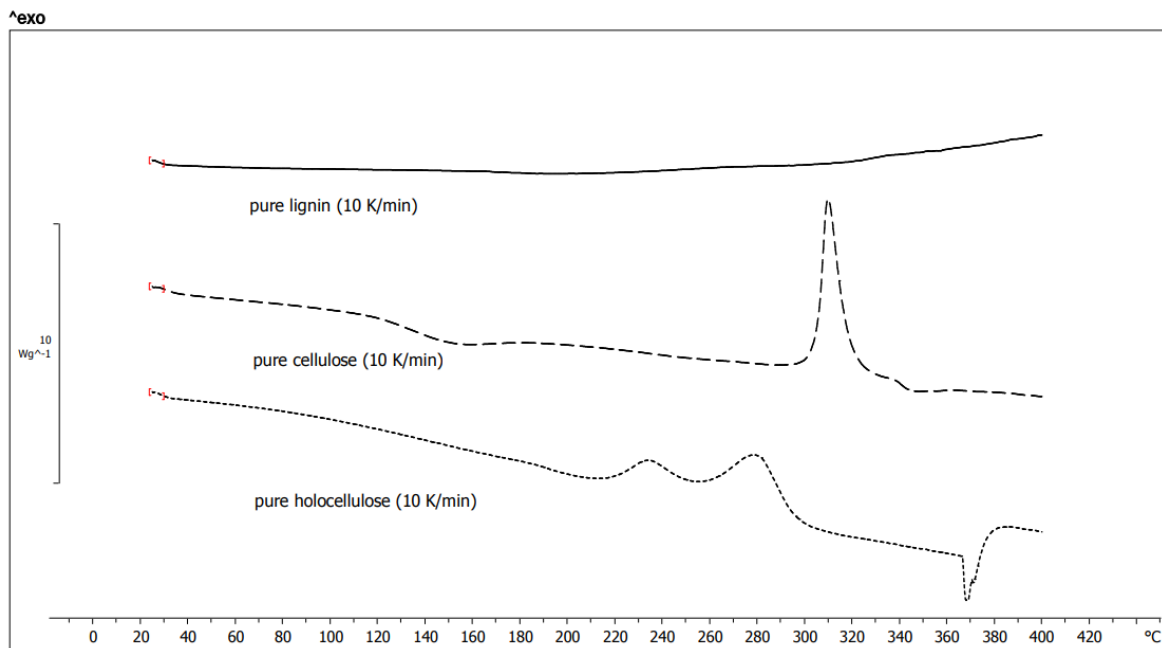
Signif.	codes:	0	'***'	0.001	'**'	0.01	'*'	0.05	'.'	0.1

Appendix 31 Results of Tukey test showing the pairwise comparison of test groups. P-values lower than 0.95 indicate a statically significant effect of the bulking coefficient BU.

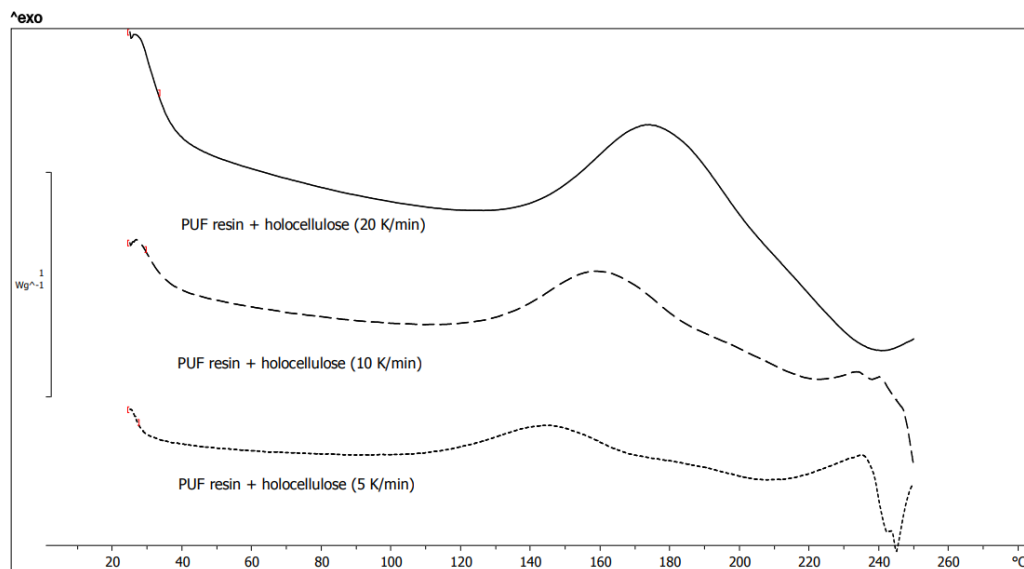
rowname	diff	lwr	upr	p adj
A-Control	0.8505634	0.0974191	1.6037076	0.0156515
B-Control	0.0207575	-0.6493575	0.6908725	1
C-Control	0.9269835	0.2568685	1.5970985	0.0011417
D-Control	0.7537181	-0.045112	1.5525482	0.0792977
E-Control	-0.5205482	-1.2392839	0.1981875	0.3431541
F-Control	1.2723587	0.6022437	1.9424737	2.42E-06
G-Control	1.0419591	0.3718441	1.712074	0.0001617
H-Control	1.0166713	0.3465564	1.6867863	0.0002511
B-A	-0.8298059	-1.5984805	-0.0611313	0.024879
C-A	0.0764201	-0.6922545	0.8450947	0.9999964
D-A	-0.0968452	-0.9799851	0.7862946	0.9999922
E-A	-1.3711116	-2.1825224	-0.5597007	3.226E-05
F-A	0.4217953	-0.3468793	1.1904699	0.7063967
G-A	0.1913957	-0.5772789	0.9600703	0.9965122
H-A	0.166108	-0.6025666	0.9347826	0.998713
C-B	0.906226	0.2187025	1.5937495	0.0023174
D-B	0.7329606	-0.0805281	1.5464494	0.1099165
E-B	-0.5413057	-1.2762992	0.1936878	0.3211555
F-B	1.2516012	0.5640778	1.9391247	6.456E-06
G-B	1.0212016	0.3336781	1.708725	0.0003624
H-B	0.9959139	0.3083904	1.6834373	0.0005509
D-C	-0.1732654	-0.9867541	0.6402234	0.9988399
E-C	-1.4475317	-2.1825252	-0.7125382	9.883E-07
F-C	0.3453752	-0.3421483	1.0328987	0.7943803
G-C	0.1149756	-0.5725479	0.802499	0.9998037
H-C	0.0896878	-0.5978356	0.7772113	0.9999702
E-D	-1.2742664	-2.1282516	-0.4202811	0.0003351
F-D	0.5186406	-0.2948482	1.3321293	0.5178031
G-D	0.2882409	-0.5252478	1.1017297	0.9660216
H-D	0.2629532	-0.5505355	1.0764419	0.9805421
F-E	1.7929069	1.0579134	2.5279004	2.291E-09
G-E	1.5625073	0.8275138	2.2975008	1.332E-07
H-E	1.5372196	0.8022261	2.2722131	2.075E-07
G-F	-0.2303996	-0.9179231	0.4571238	0.9756946
H-F	-0.2556874	-0.9432108	0.4318361	0.9549673
H-G	-0.0252877	-0.7128112	0.6622357	1

Appendix 32 Results of Tukey test showing the pairwise comparison of test groups. P-values lower than 0.95 indicate a statically significant effect of the swelling coefficient S_{mod2} .

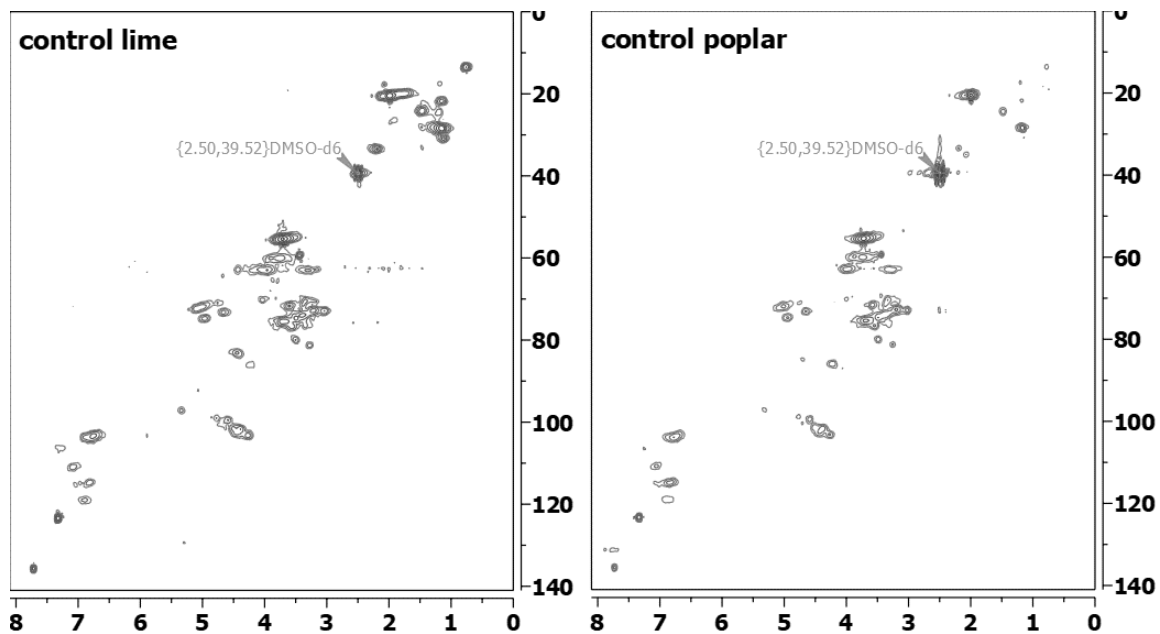
rowname	diff	lwr	upr	p adj
A-Control	-0.37241	-1.16264	0.417831	0.838675
B-Control	0.124076	-0.56901	0.81716	0.999643
C-Control	-0.51778	-1.15677	0.121212	0.202703
D-Control	-0.43109	-1.16458	0.302404	0.615625
E-Control	0.420047	-0.24267	1.082761	0.516614
F-Control	-0.49134	-1.15405	0.171378	0.306247
G-Control	0.173618	-0.4463	0.793531	0.991654
H-Control	-0.78599	-1.47907	-0.0929	0.015416
B-A	0.496482	-0.35237	1.345333	0.621679
C-A	-0.14537	-0.95066	0.659918	0.99962
D-A	-0.05868	-0.94083	0.823471	1
E-A	0.792453	-0.03179	1.616694	0.06833
F-A	-0.11893	-0.94317	0.70531	0.999929
G-A	0.546024	-0.24421	1.336261	0.398953
H-A	-0.41358	-1.26243	0.43527	0.812782
C-B	-0.64186	-1.35205	0.068344	0.106308
D-B	-0.55516	-1.35146	0.241129	0.386842
E-B	0.295971	-0.43565	1.027588	0.924127
F-B	-0.61541	-1.34703	0.116204	0.165502
G-B	0.049542	-0.64354	0.742625	1
H-B	-0.91006	-1.6693	-0.15083	0.008369
D-C	0.086692	-0.66299	0.836377	0.999987
E-C	0.937826	0.257231	1.618421	0.001367
F-C	0.026442	-0.65415	0.707037	1
G-C	0.691397	0.052405	1.330389	0.024723
H-C	-0.26821	-0.97841	0.441992	0.94786
E-D	0.851134	0.081129	1.621139	0.020047
F-D	-0.06025	-0.83025	0.709755	0.999999
G-D	0.604705	-0.12879	1.338196	0.184996
H-D	-0.3549	-1.15119	0.441393	0.875901
F-E	-0.91138	-1.6143	-0.20847	0.003171
G-E	-0.24643	-0.90914	0.416286	0.952213
H-E	-1.20603	-1.93765	-0.47442	7.04E-05
G-F	0.664955	0.00224	1.32767	0.048621
H-F	-0.29465	-1.02627	0.436967	0.925909
H-G	-0.9596	-1.65269	-0.26652	0.001275



Appendix 33 Thermogram of pure cellulose, holocellulose, and lignin isolated from tulipwood. DSC scans were performed between 20 - 400°C in high-pressure crucibles at a heating rate of 10 °C/min.

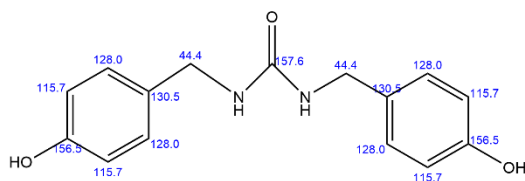


Appendix 34 DSC thermogram of holocellulose mixed with PUF resin at heating rates 5, 10, 20°C/min.

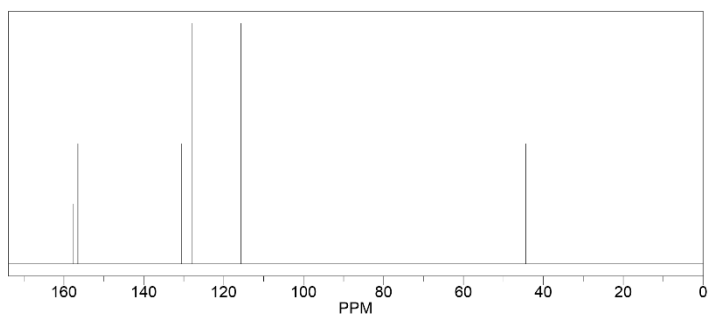


Appendix 35 ^1H - ^{13}C HSQC NMR spectrum of unmodified poplar and lime wood for reference.

ChemNMR ¹³C Estimation



Estimation quality is indicated by color: **good**, **medium**, **rough**

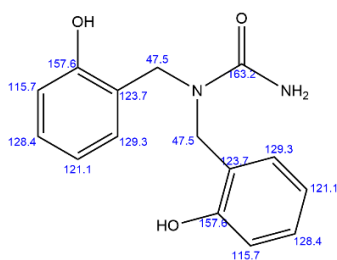


Protocol of the C-13 NMR Prediction: (Lib=S)

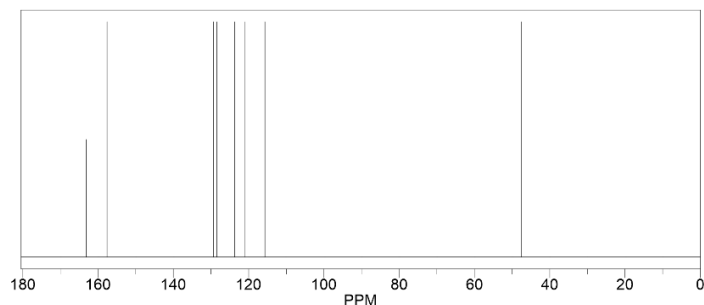
Node	Shift	Base + Inc.	Comment (ppm rel. to TMS)
C	156.5	128.5	1-benzene
		28.8	1 -O
		-2.0	1 -C-N
		1.2	general corrections
C	156.5	128.5	1-benzene
		28.8	1 -O
		-2.0	1 -C-N
		1.2	general corrections
C	130.5	128.5	1-benzene
		-7.4	1 -O
		13.9	1 -C-N
		-4.5	general corrections
C	130.5	128.5	1-benzene
		-7.4	1 -O
		13.9	1 -C-N
		-4.5	general corrections
CH	115.7	128.5	1-benzene
		-12.8	1 -O
		-0.2	1 -C-N
		0.2	general corrections
CH	115.7	128.5	1-benzene
		-12.8	1 -O
		-0.2	1 -C-N
		0.2	general corrections
CH	128.0	128.5	1-benzene
		1.4	1 -O
		-1.4	1 -C-N
		-0.5	general corrections
CH	128.0	128.5	1-benzene
		1.4	1 -O
		-1.4	1 -C-N
		-0.5	general corrections
CH	115.7	128.5	1-benzene
		-12.8	1 -O
		-0.2	1 -C-N
		0.2	general corrections
CH	115.7	128.5	1-benzene
		-12.8	1 -O
		-0.2	1 -C-N
		0.2	general corrections
CH	128.0	128.5	1-benzene
		1.4	1 -O
		-1.4	1 -C-N
		-0.5	general corrections
C	157.6	161.2	N-urea
		1.0	1 -C
		1.0	1 -C
		-5.6	general corrections
CH2	44.4	-2.3	aliphatic
		24.3	1 alpha -1:C*C*C*C*C*C*1
		28.3	1 alpha -N
		2.6	1 beta -C(=O)-N
		0.3	1 delta -C
		-8.8	general corrections
CH2	44.4	-2.3	aliphatic
		24.3	1 alpha -1:C*C*C*C*C*C*1
		28.3	1 alpha -N
		2.6	1 beta -C(=O)-N
		0.3	1 delta -C
		-8.8	general corrections

Appendix 36 Structure assigned to PUF_A, using the chemical prediction tool of Mestre Nova

ChemNMR ¹³C Estimation



Estimation quality is indicated by color: **good**, **medium**, **rough**

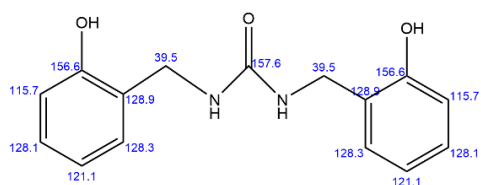


Protocol of the C-13 NMR Prediction: (Lib=S)

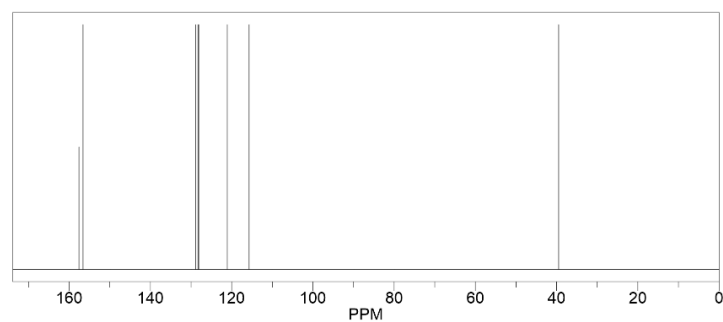
Node	Shift	Base + Inc.	Comment (ppm rel. to TMS)
C	157.6	128.5	1-benzene
		28.8	1 -O
		-0.4	1 -C-N-C
		0.7	general corrections
C	157.6	128.5	1-benzene
		28.8	1 -O
		-0.4	1 -C-N-C
		0.7	general corrections
C	123.7	128.5	1-benzene
		-12.8	1 -O
		8.7	1 -C-N-C
		-0.7	general corrections
C	123.7	128.5	1-benzene
		-12.8	1 -O
		8.7	1 -C-N-C
		-0.7	general corrections
CH	115.7	128.5	1-benzene
		-12.8	1 -O
		-0.2	1 -C-N-C
		0.2	general corrections
CH	115.7	128.5	1-benzene
		-12.8	1 -O
		-0.2	1 -C-N-C
		0.2	general corrections
CH	129.3	128.5	1-benzene
		1.4	1 -O
		-0.4	1 -C-N-C
		-0.2	general corrections
CH	129.3	128.5	1-benzene
		1.4	1 -O
		-0.4	1 -C-N-C
		-0.2	general corrections
CH	128.4	128.5	1-benzene
		1.4	1 -O
		-1.7	1 -C-N-C
		0.2	general corrections
CH	128.4	128.5	1-benzene
		1.4	1 -O
		-1.7	1 -C-N-C
		0.2	general corrections
CH	121.1	128.5	1-benzene
		-7.4	1 -O
		-0.2	1 -C-N-C
		0.2	general corrections
CH	121.1	128.5	1-benzene
		-7.4	1 -O
		-0.2	1 -C-N-C
		0.2	general corrections
C	163.2	161.2	N-urea
		2.0	2 -C
		-2.3	aliphatic
CH2	47.5	24.3	1 alpha -1:C*C*C*C*C*C*1
		28.3	1 alpha -N
		2.6	1 beta -C(=O)-N
		9.4	1 beta -C
		-2.6	1 gamma -1:C*C*C*C*C*C*1
		-6.2	1 gamma -O
		-6.0	general corrections
		-2.3	aliphatic
CH2	47.5	24.3	1 alpha -1:C*C*C*C*C*C*1
		28.3	1 alpha -N
		2.6	1 beta -C(=O)-N
		9.4	1 beta -C
		-2.6	1 gamma -1:C*C*C*C*C*C*1
		-6.2	1 gamma -O
		-6.0	general corrections
		-2.3	aliphatic

Appendix 37 Structure assigned to PUF_B using the chemical shift prediction tool of Mestre Nova

ChemNMR ¹³C Estimation



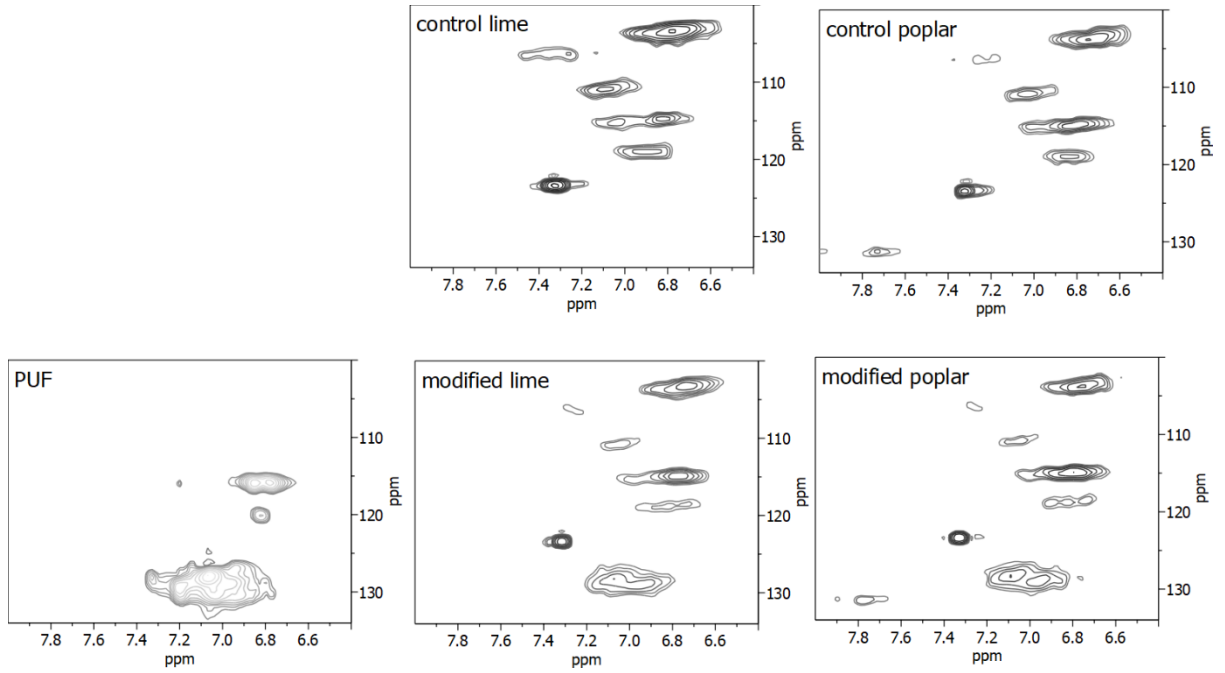
Estimation quality is indicated by color: **good**, **medium**, **rough**



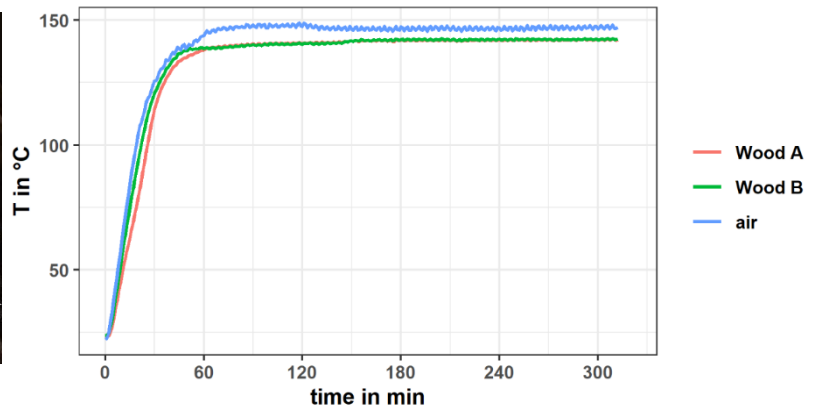
Protocol of the C-13 NMR Prediction: (Lib=S)

Node	Shift	Base + Inc.	Comment (ppm rel. to TMS)
C	156.6	128.5	1-benzene
		28.8	1 -O
		-1.4	1 -C-N
		0.7	general corrections
C	156.6	128.5	1-benzene
		28.8	1 -O
		-1.4	1 -C-N
		0.7	general corrections
C	128.9	128.5	1-benzene
		-12.8	1 -O
		13.9	1 -C-N
		-0.7	general corrections
C	128.9	128.5	1-benzene
		-12.8	1 -O
		13.9	1 -C-N
		-0.7	general corrections
CH	115.7	128.5	1-benzene
		-12.8	1 -O
		-0.2	1 -C-N
		0.2	general corrections
CH	128.3	128.5	1-benzene
		1.4	1 -O
		-1.4	1 -C-N
		-0.2	general corrections
CH	115.7	128.5	1-benzene
		-12.8	1 -O
		-0.2	1 -C-N
		0.2	general corrections
CH	128.3	128.5	1-benzene
		1.4	1 -O
		-1.4	1 -C-N
		-0.2	general corrections
CH	128.1	128.5	1-benzene
		1.4	1 -O
		-2.0	1 -C-N
		0.2	general corrections
CH	121.1	128.5	1-benzene
		-7.4	1 -O
		-0.2	1 -C-N
		0.2	general corrections
CH	128.1	128.5	1-benzene
		1.4	1 -O
		-2.0	1 -C-N
		0.2	general corrections
CH	121.1	128.5	1-benzene
		-7.4	1 -O
		-0.2	1 -C-N
		0.2	general corrections
C	157.6	161.2	N-urea
		1.0	1 -C
		1.0	1 -C
		-5.6	general corrections
CH2	39.5	-2.3	aliphatic
		24.3	1 alpha -1:C*C*C*C*C*1
		28.3	1 alpha -N
		2.6	1 beta -C(=O)-N
		-6.2	1 gamma -O
		0.3	1 delta -C
		-7.5	general corrections
CH2	39.5	-2.3	aliphatic
		24.3	1 alpha -1:C*C*C*C*C*1
		28.3	1 alpha -N
		2.6	1 beta -C(=O)-N
		-6.2	1 gamma -O
		0.3	1 delta -C
		-7.5	general corrections

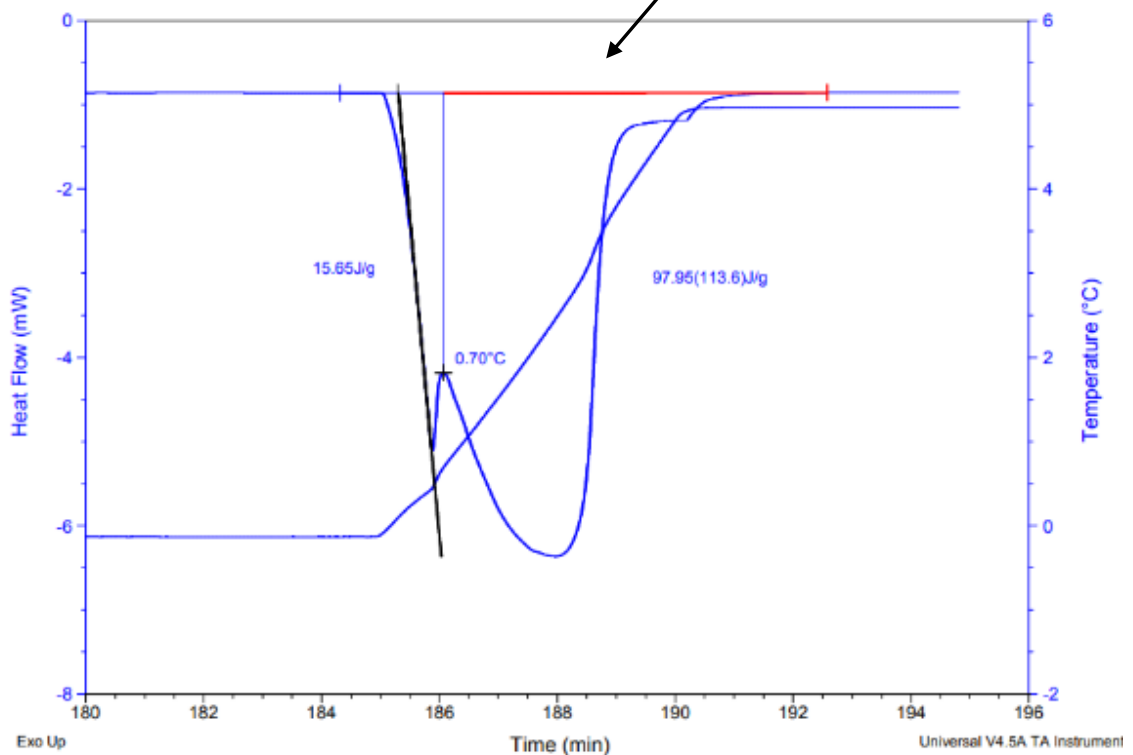
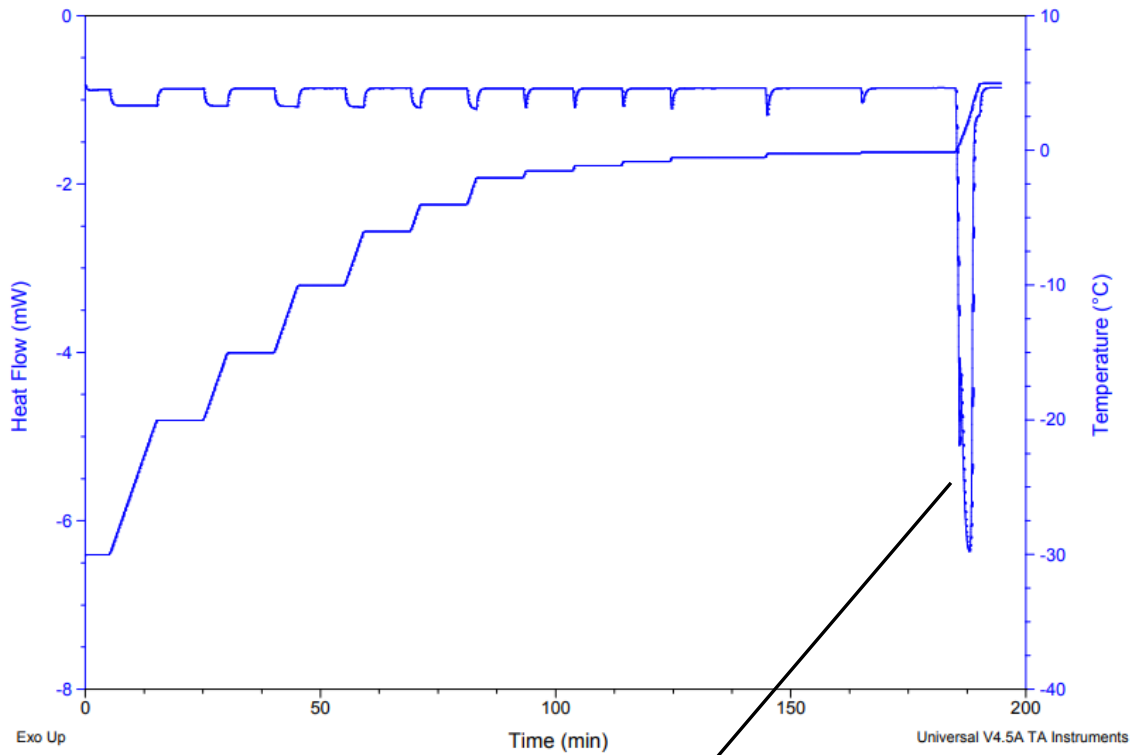
Appendix 38 Structure assigned to PUF_b using the chemical shift prediction tool of Mestre Nova



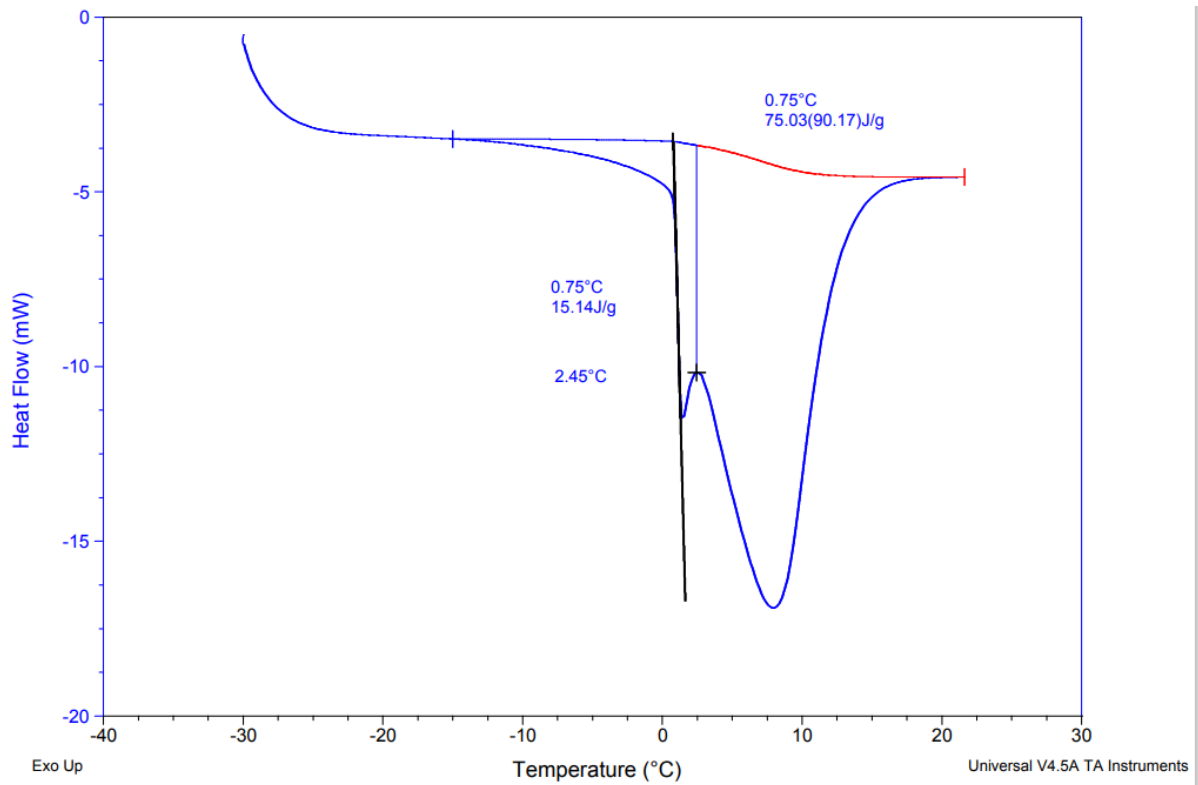
Appendix 39 Partial two dimensional ^1H - ^{13}C HSQC NMR spectrum of PUF resin (left), modified and unmodified lime (centre), and modified and unmodified poplar (right). $\text{PF}_{2/4}$ and PF_6 signals overlap with $\text{G}_{2/6}$ signal of wood. Novel signal indicating the presence of methylene bridges between G-lignin and PUF resin were not detected.



Appendix 40 (left) Thermocouples and wood samples used for the temperature measurement. (right) Temperature profiles during heat curing are similar for Wood A and B, despite slightly different moisture contents prior to cure.



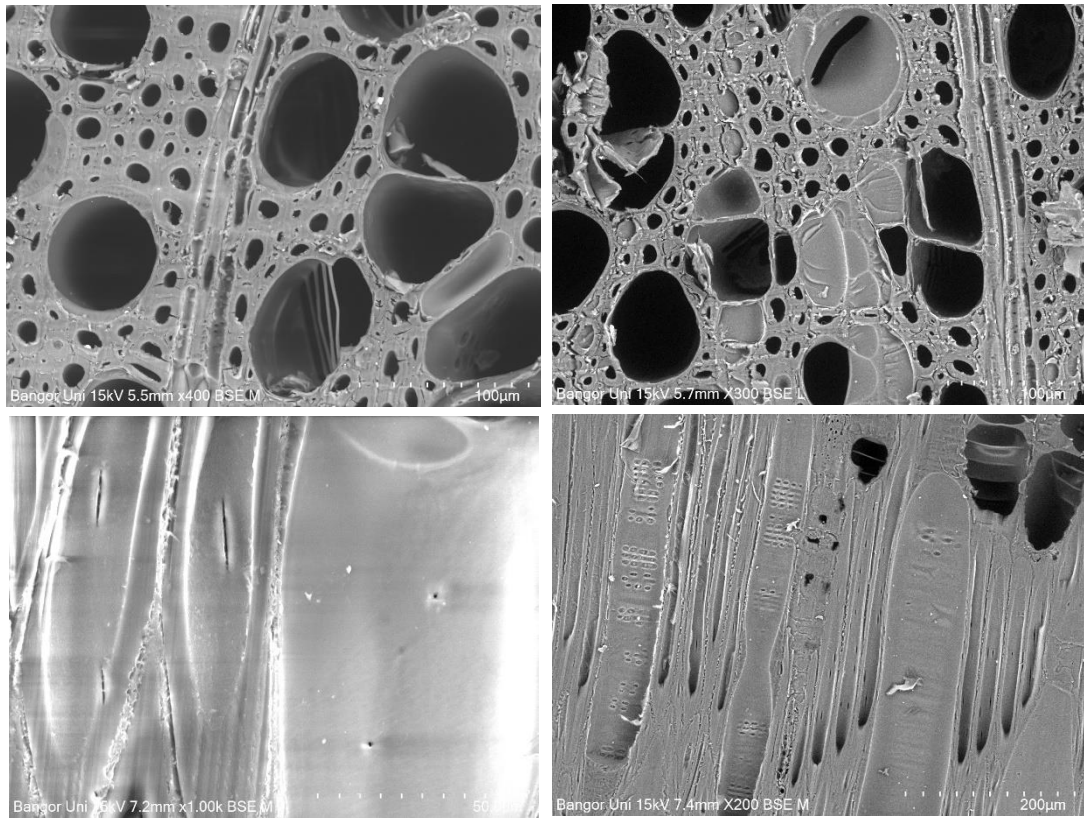
Appendix 41 Thermogram of the isothermal method. Example DSC scan of Wood A showing endothermic peaks related to each step. The inset shows the last step between -0.1°C and 5°C . The first peak was assigned to FBW in pores larger than 396 nm and the second peak was assigned to BW.



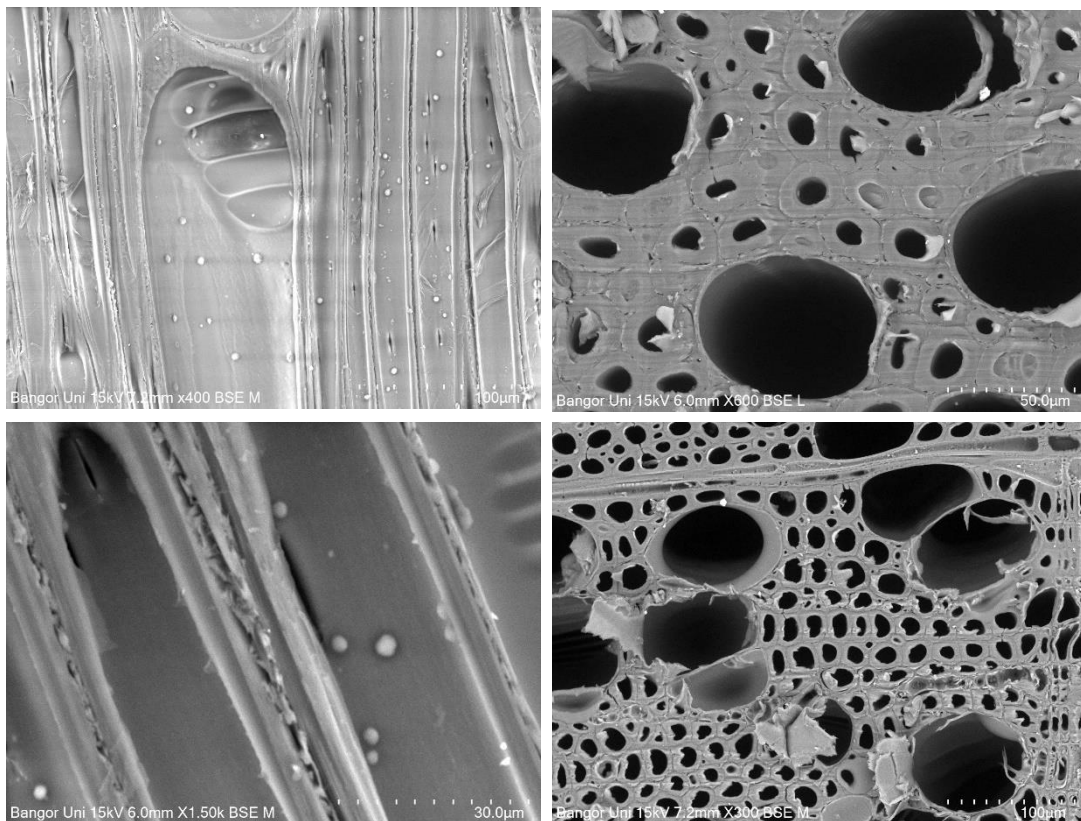
Appendix 42 Thermogram of the dynamic method. Example DSC scan of Wood A showing endothermic peaks related to melting of FBW and BW.

Appendix 43 The effect of different diffusion and drying conditions in Wood A and Wood B on their performance in ASE tests. ML1, ML2, ML3 – mass loss due to leaching in water during three cycles of soaking, WU1, WU2, WU3 – gravimetric water uptake during 3 cycles of soaking.

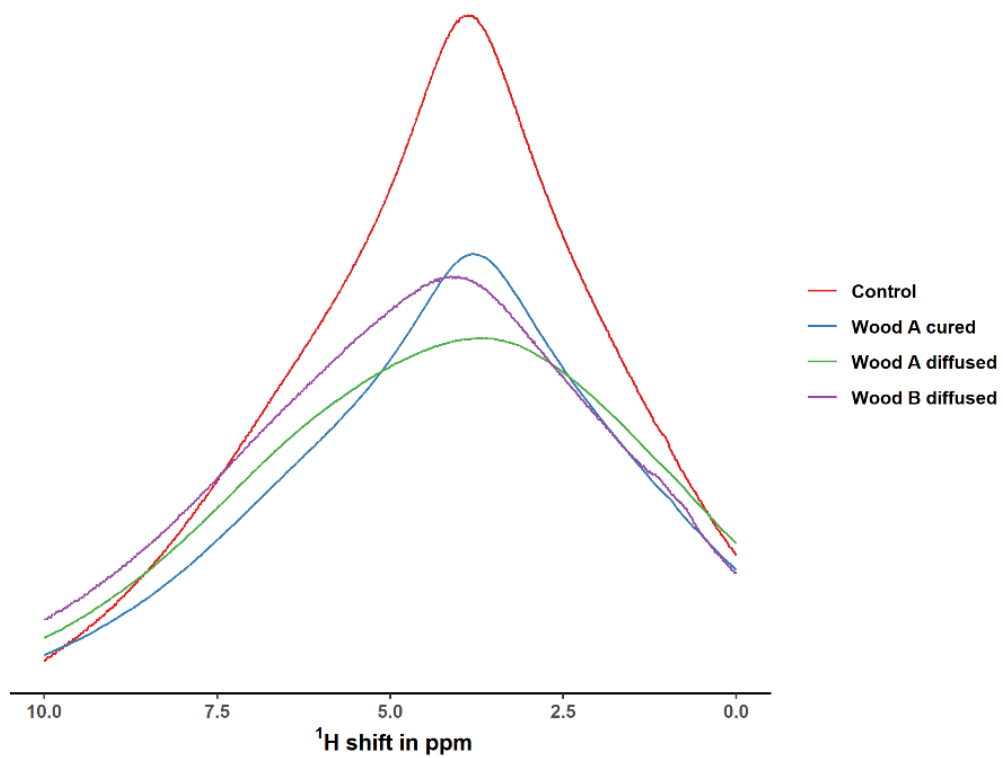
	ML1 in %	ML2 in %	ML3 in %	ML total in %	WU1 in %	WU2 in %	WU3 in %
A	-2.65 (0.08)	-1.08 (0.10)	-0.43 (0.08)	-4.11 (0.09)	98.32 (3.08)	102.00 (2.94)	105.14 (3.08)
B	-3.10 (0.17)	-1.09 (0.09)	-0.62 (0.12)	-4.75 (0.19)	97.28 (2.01)	102.17 (2.11)	104.59 (2.45)



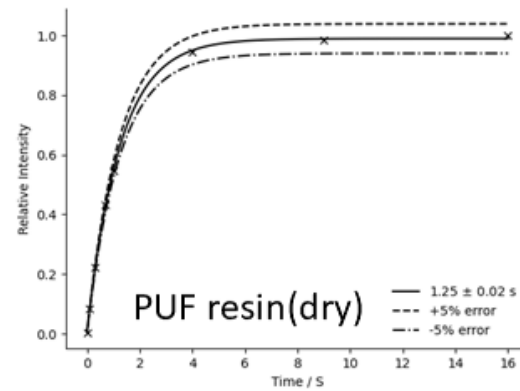
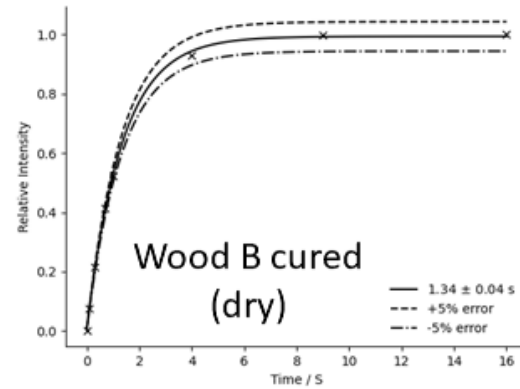
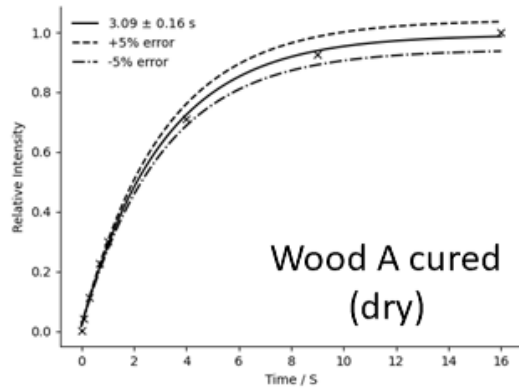
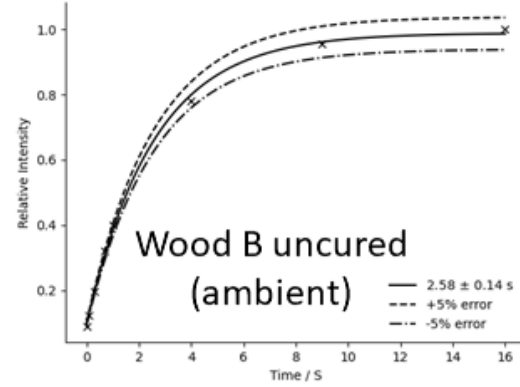
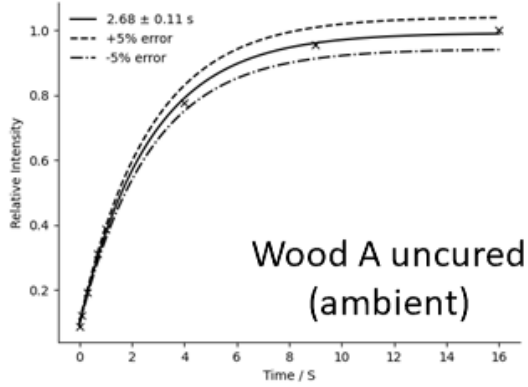
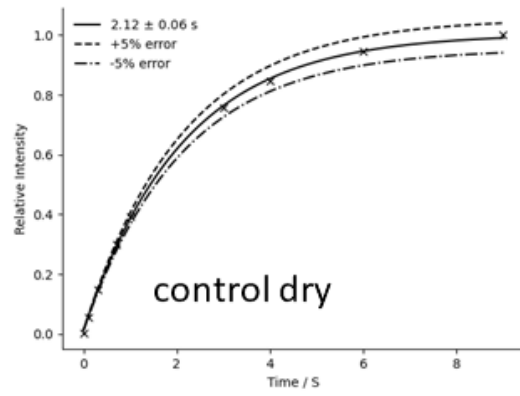
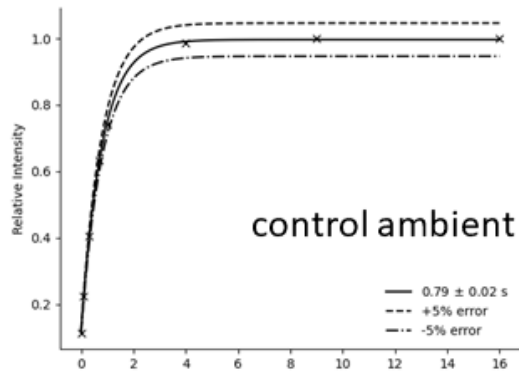
Appendix 44 Scanning electron microscopy images of Wood A in the cured state.



Appendix 45 Scanning electron microscopy images of Wood B in the cured state.



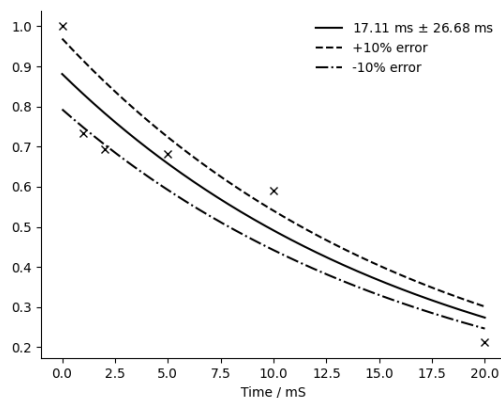
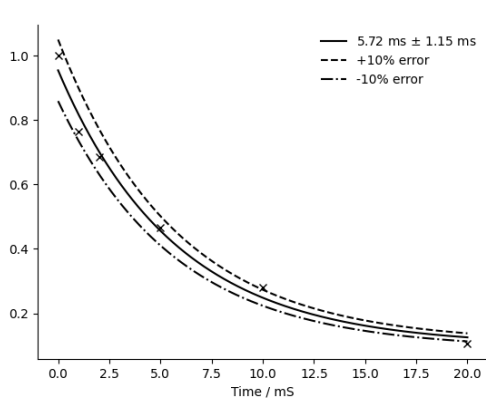
Appendix 46 ^1H (500 MHz) MAS (12.5 kHz) 1D NMR inversion recovery spectra of the unmodified control, Wood A and B after diffusion, and Wood A after heat curing.



Appendix 47 Plots of signal intensity against contact time for $T_1(^1H)$ in all samples.

Appendix 48 Numerical representation of the $T_{1\rho}$ relaxation times that were measured in this study.

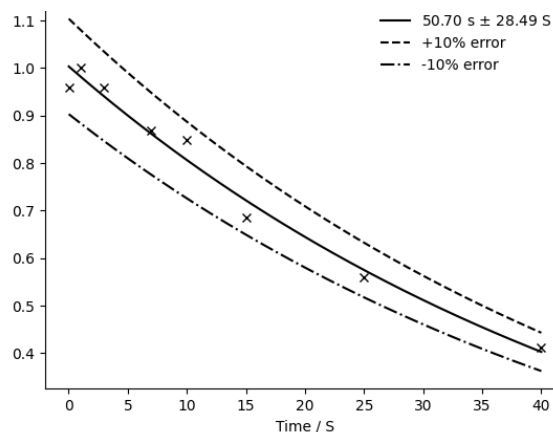
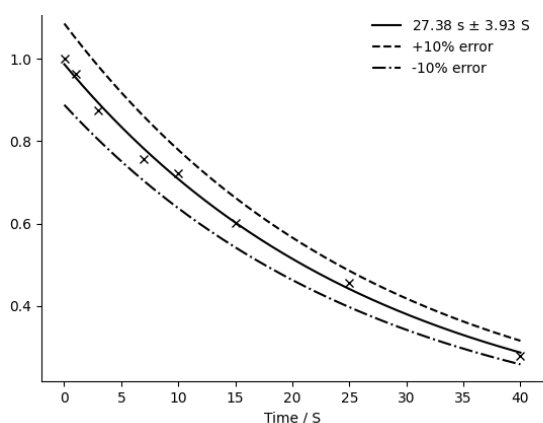
$\delta(^{13}\text{C}) / \text{ppm}$	group	state of wood	state of resin	$T_{1\rho}$ in ms	error in ms
21	A	ambient	uncured	2.4	0.8
21	A	dry	cured	2.5	0.9
21	B	ambient	uncured	2.0	0.3
21	B	dry	cured	5.0	1.5
21	Control	ambient	control	0.3	2.9
21	Control	dry	control	7.3	1.3
57	A	ambient	uncured	3.8	0.5
57	A	dry	cured	6.3	1.8
57	B	ambient	uncured	2.7	0.3
57	B	dry	cured	6.3	0.8
57	Control	ambient	control	5.6	0.5
57	Control	dry	control	6.9	0.5
65	A	ambient	uncured	3.7	0.5
65	A	dry	cured	8.3	0.9
65	B	ambient	uncured	2.6	0.4
65	B	dry	cured	7.1	1.0
65	Control	ambient	control	5.2	0.4
65	Control	dry	control	6.6	0.8
75	A	ambient	uncured	3.4	0.4
75	A	dry	cured	7.2	1.1
75	B	ambient	uncured	2.6	0.3
75	B	dry	cured	6.4	0.5
75	Control	ambient	control	5.4	0.4
75	Control	dry	control	5.8	0.6
84	A	ambient	uncured	3.4	0.5
84	A	dry	cured	5.5	0.8
84	B	ambient	uncured	2.6	0.2
84	B	dry	cured	6.6	0.6
84	Control	ambient	control	4.9	0.6
84	Control	dry	control	5.5	0.9
89	A	ambient	uncured	4.9	1.0
89	A	dry	cured	9.4	2.9
89	B	ambient	uncured	3.7	0.6
89	B	dry	cured	8.0	1.2
89	Control	ambient	control	4.9	1.1
89	Control	dry	control	11.0	9.9
106	A	ambient	uncured	3.8	0.2
106	A	dry	cured	8.2	0.9
106	B	ambient	uncured	2.9	0.3
106	B	dry	cured	6.9	0.7
106	Control	ambient	control	5.4	0.6
106	Control	dry	control	6.1	0.7
130	A	ambient	uncured	3.3	0.4
130	A	dry	cured	8.3	1.2
130	B	ambient	uncured	2.5	0.3
130	B	dry	cured	6.4	0.4
130	Control	ambient	control	2.4	1.5
130	Control	dry	control	6.2	1.0
161	A	ambient	uncured	2.9	0.7
161	A	dry	cured	6.1	0.9
161	B	ambient	uncured	1.7	0.2
161	B	dry	cured	6.4	0.2
161	Control	ambient	control	7.4	2.1
161	Control	dry	control	6.0	1.7



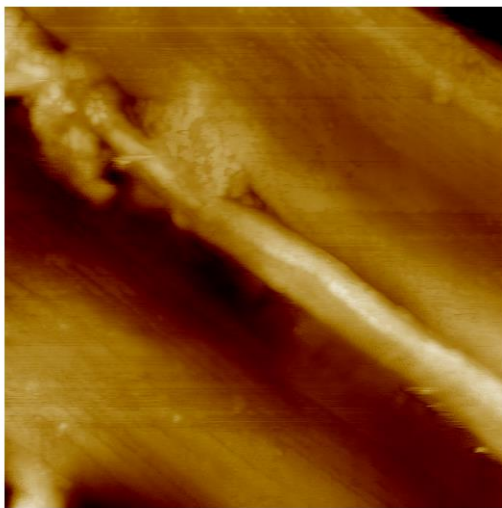
Appendix 49 An example plot of signal intensity against contact time for $T_{1\rho}$. The left plot shows an example of a good data fit for the 84 ppm peak in dry unmodified wood. The right plot shows an example of a poor data fit with a high error for the 89 ppm peak in dry unmodified wood.

Appendix 50 Numerical representation of the T₁ (¹³C) relaxation times that were measured in this study.

$\delta(^{13}\text{C}) / \text{ppm}$	group	state of wood	state of resin	T ₁ (¹³ C) in s	error in s
21	A	ambient	uncured	2.9	0.99
21	A	dry	cured	NA	NA
21	B	ambient	uncured	NA	NA
21	B	dry	cured	NA	NA
21	Control	ambient	control	3.98	0.63
21	Control	dry	control	14.07	6.85
57	A	ambient	uncured	2.81	0.4
57	A	dry	cured	NA	NA
57	B	ambient	uncured	0.83	0.34
57	B	dry	cured	1.05	0.23
57	Control	ambient	control	2.21	0.21
57	Control	dry	control	2.58	0.55
62	A	ambient	uncured	3.76	0.83
62	A	dry	cured	2.99	0.28
62	B	ambient	uncured	3.2	0.58
62	B	dry	cured	3.27	0.66
62	Control	ambient	control	2.84	0.61
62	Control	dry	control	3.3	0.9
75	A	ambient	uncured	10.56	2.42
75	A	dry	cured	20.27	7.82
75	B	ambient	uncured	13.07	1.91
75	B	dry	cured	14.87	2.76
75	Control	ambient	control	17.23	0.87
75	Control	dry	control	17.64	1.24
84	A	ambient	uncured	13.83	10.31
84	A	dry	cured	NA	NA
84	B	ambient	uncured	28.26	9.04
84	B	dry	cured	15.51	4.59
84	Control	ambient	control	27.38	3.93
84	Control	dry	control	20.48	2.12
89	A	ambient	uncured	2.19	3.85
89	A	dry	cured	NA	NA
89	B	ambient	uncured	NA	NA
89	B	dry	cured	NA	NA
89	Control	ambient	control	53.88	38.57
89	Control	dry	control	14.85	8.53

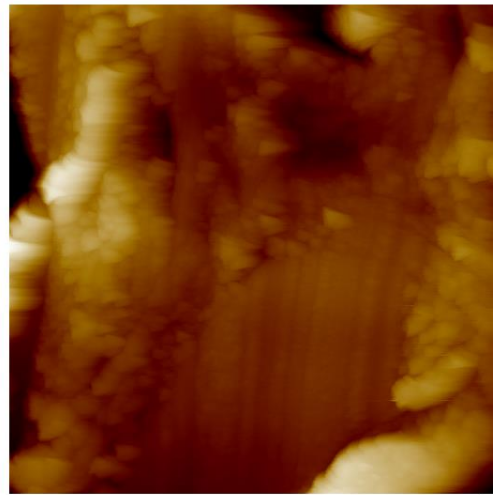


Appendix 51 An example plot of signal intensity against contact time for T₁ (¹³C). The left plot shows an example of a good data fit for the 84 ppm peak in ambient unmodified wood. The right plot shows an example of a poor data fit for the 89 ppm peak in ambient unmodified wood.



Height

2.0 μm



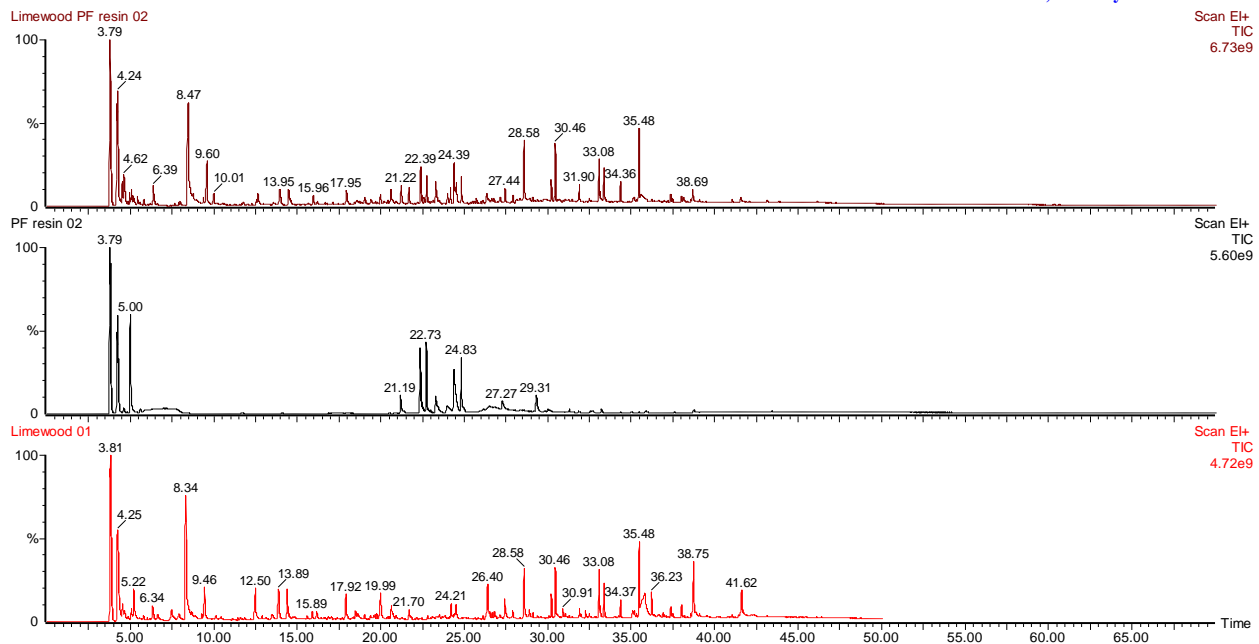
Height

2.0 μm

Appendix 52 Atomic force microscopy (AFM) images obtained for unmodified *Radiata* pine (left) and modified tulipwood (right) in tapping mode. Both images are showing the border of for adjacent cells with the middle lamella approximately in the centre of the image.

20220518 550 5s

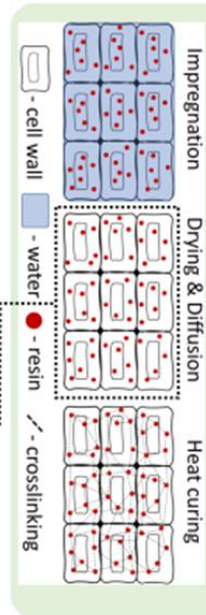
, 19-May-2022 + 11:20:13



Appendix 53 Pyrolysis gas chromatography (GC) mass spectroscopy (MS) showing the chromatogram of unmodified lime wood, pure PUF resin, and modified lime wood. The absence of new peaks in the modified lime wood indicates the absence of covalent bond between the resin and in the woo.

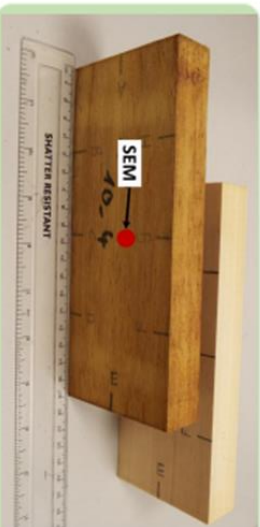
Modification Process

Wood modification with low molecular weight thermosetting resin is a promising technique that is suitable for upscaling. This modification aims at increasing the service life of low-quality timbers. The wood is impregnated with an aqueous resin, which contains phenolic and urea-based monomers. After a diffusion step, the resin has made its way into the cell walls, where a 3D network is created during a heat curing step at elevated temperatures.



How drying conditions can affect resin modified wood.

Carlo Kupfermangel¹, Morvenna Spear¹, Graham Ormondroyd¹ and Andrew Pitman²
¹BioComposites Centre, Bangor University, Gwynedd, UK
²BM TRADA, Buckinghamshire, UK



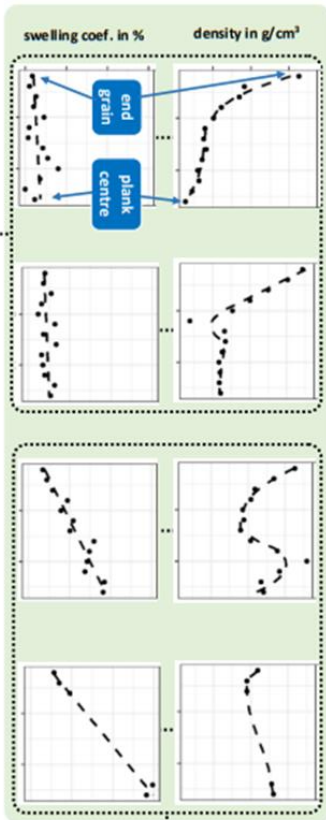
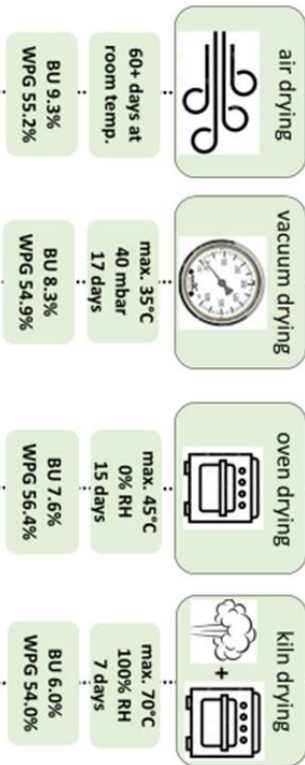
Sample Preparation

The sapwood of tulipwood (*Liriodendron tulipifera*) was cut to specimens with the dimensions 200 (l) x 70 (t) x 30 (t) mm³. These samples were impregnated with phenolic resin using a pressure vessel at 12 bar. The impregnated specimens were dried with 4 different methods (air, vacuum, oven, kiln) and subsequently heat cured at 150°C in a lab oven. The bulking coefficient (BU) and weight percentage gain (WPG) were determined in the large specimens. Afterwards, one quarter of each specimen was used to cut small samples with dimensions 20 (l) x 20 (t) x 5 (t) mm³, in which the density and swelling coefficient were determined in a transect along the longitudinal direction of the plank.

Conclusion

The drying method clearly has an influence on the BU and swelling coef. in modified wood. A longer drying time at lower (non-curing) temperatures seems to improve the BU and swelling coef. in air and vacuum dried wood, whereas the harsher drying regime in oven and kiln dried wood seems to have negative effect on these parameters.

Air and vacuum drying resulted in a density gradient across the length of the specimens, but the swelling coef. was uniform. The opposite trend may be observed in kiln dried wood. The SEM images show extensive resin accumulations in the cell lumens of kiln dried wood, which indicated that the resin failed to migrate into the cell wall. It appears beneficial to allow sufficient time for resin cell wall diffusion to occur in the drying process.



The density in the longitudinal direction of the plank is relatively constant, indicating uniform resin distribution. The swelling coef. increases towards the centre of the plank, indicating dissimilar resin cell wall penetration.

The density trend in the longitudinal direction of the plank has a gradient, indicating resin accumulation at the crosscut surface. The swelling coef. is uniform indicating similar resin cell wall penetration across the plank.

